2016

LATE EVENTS OF HUMAN METAPNEUMOVIRUS INFECTION: INSIGHTS INTO VIRAL SPREAD WITHIN THE RESPIRATORY EPITHELIUM

Farah El Najjar
University of Kentucky, farahelnajjar2585@gmail.com
Digital Object Identifier: http://dx.doi.org/10.13023/ETD.2016.009

STUDENT AGREEMENT:

I represent that my thesis or dissertation and abstract are my original work. Proper attribution has been given to all outside sources. I understand that I am solely responsible for obtaining any needed copyright permissions. I have obtained needed written permission statement(s) from the owner(s) of each third-party copyrighted matter to be included in my work, allowing electronic distribution (if such use is not permitted by the fair use doctrine) which will be submitted to UKnowledge as Additional File.

I hereby grant to The University of Kentucky and its agents the irrevocable, non-exclusive, and royalty-free license to archive and make accessible my work in whole or in part in all forms of media, now or hereafter known. I agree that the document mentioned above may be made available immediately for worldwide access unless an embargo applies.

I retain all other ownership rights to the copyright of my work. I also retain the right to use in future works (such as articles or books) all or part of my work. I understand that I am free to register the copyright to my work.

REVIEW, APPROVAL AND ACCEPTANCE

The document mentioned above has been reviewed and accepted by the student's advisor, on behalf of the advisory committee, and by the Director of Graduate Studies (DGS), on behalf of the program; we verify that this is the final, approved version of the student's thesis including all changes required by the advisory committee. The undersigned agree to abide by the statements above.

Farah El Najjar, Student

Dr. Rebecca E. Dutch, Major Professor

Dr. Michael D. Mendenhall, Director of Graduate Studies

LATE EVENTS OF HUMAN METAPNEUMOVIRUS INFECTION: INSIGHTS INTO VIRAL SPREAD WITHIN THE RESPIRATORY EPITHELIUM

DISSERTATION

A dissertation submitted in partial fulfillments of the
requirements for the degree of Doctor of Philosophy in the
College of Medicine
at the University of Kentucky

By
Farah El Najjar

Lexington, Kentucky

Director: Dr. Rebecca E Dutch, Professor of Biochemistry

Lexington, Kentucky

2016

ABSTRACT OF DISSERTATION

LATE EVENTS OF HUMAN METAPNEUMOVIRUS INFECTION: INSIGHTS INTO VIRAL SPREAD WITHIN THE RESPIRATORY EPITHELIUM

Human metapneumovirus (HMPV) is a leading cause of respiratory tract infections worldwide across all age groups, and is particularly devastating in the pediatric, elderly and immunocompromised populations. Despite its high prevalence and burden on human health, there are currently no treatments or vaccines against HMPV infections. HMPV is an enveloped virus that belongs to the paramyxovirus family. Paramyxoviruses in general form by assembly of virus components at the plasma membrane followed by budding and release of virus particles into the extracellular matrix to spread infection. The process of forming new virus particles requires complex interactions between viral and cellular components and the requirements for particle production differ substantially among paramyxoviruses. Several key aspects of the life cycle of HMPV remain unknown. The work presented here provides significant advances in understanding the mechanisms underlying assembly and spread of HMPV in human bronchial airway epithelial cells. We provide evidence that HMPV induces reorganization of the actin cytoskeleton and microtubules at late stages of infection leading to the formation of complex networks of branched filaments and intercellular extensions, structures that have not been previously reported for paramyxoviruses. Our results indicate a novel mode of HMPV spread directly from cell-to-cell across intercellular extensions. We identified an important role of actin and the Rho GTPases Rac1 and Cdc42 in direct cell-to-cell spread of HMPV. While roles for paramyxovirus matrix and fusion proteins in membrane deformation have been previously demonstrated for several paramyxoviruses, we show that the HMPV phosphoprotein (P) associates with actin and induces formation of membrane extensions, suggesting a role for the P protein in HMPV exit from the cell. Additionally, infection of differentiated, polarized human airway tissues showed that release of HMPV particles at the apical side is inefficient and revealed that spread of HMPV in these tissues can occur in the presence of neutralizing

antibodies. HMPV infection also resulted in reorganization of the actin cytoskeleton in these tissues mainly at the apical side. Collectively, the data provided in this dissertation reveal a novel mechanism by which HMPV uses the cytoskeleton for cell-to-cell transmission and provide critical insights into spread of respiratory viruses within the airway epithelium.

KEYWORDS: Paramyxovirus, Human metapneumovirus, respiratory epithelium, assembly, spread

Farah El Najjar

Student's Signature

January 21, 2016

Date

LATE EVENTS OF HUMAN METAPNEUMOVIRUS INFECTION: INSIGHTS INTO VIRAL SPREAD WITHIN THE RESPIRATORY EPITHELIUM

By

Farah El Najjar

Rebecca E. Dutch, Ph.D.
Director of Dissertation

Michael D. Mendenhall, Ph.D.
Director of Graduate Studies

January 21, 2016

Dedicated to
Jihad, Souhaila, Diana and Jad

ACKNOWLEDGMENTS

The work presented in this dissertation would not have been possible without the help, dedication and guidance of many people. First and foremost, I would like to express my deepest gratitude to Dr. Rebecca Dutch for the mentorship, encouragement and tremendous support she provided during my graduate studies at both the academic and personal levels. She is an exemplary role model; her excitement for science, amazing optimism and success will always be a great inspiration. Since I started my research studies, she has inspired me to ask challenging questions, seek my own ideas and develop into an independent thinker. My scientific accomplishments, writing abilities and presentation skills are all attributed to her commitment to provide excellent training to her students. Her integrity, patience and understanding coupled with her sincere concern about my future career and thoughtfulness towards my family's and my overall wellbeing, are all a reflection of her qualities that makes her a great mentor. Her impact on my scientific career and my personal life will be long-lasting.

I would also like to thank my dissertation committee: Dr. Udeni Balasuriya, Dr. Trever Creamer and Dr. Mathew Gentry. They are all remarkable scientists and I truly appreciate their valuable feedback, time and guidance. I would like to extend my thanks to my outside examiner Dr. Peter Nagy for his time and effort in reviewing this dissertation. I am also grateful to collaborators who provided reagents and expertise that helped to complete this work: Dr. Ursula Buchholz, Dr. John Williams, Dr. Raymond Pickels, Dr. Sagar Goyal and Dr. Jeff Esko.

A special thank you to Dr. Carole Moncman; her amazing microscopy skills and willingness to help have been invaluable in moving my dissertation work forward. Furthermore, I would like to thank her for providing advice and answering my random scientific questions. She has become and will continue to be a great mentor and friend.

In addition, I would like to thank all the faculty, postdoctoral fellows, research staff, and fellow graduate students in the department of Molecular and Cellular Biochemistry for providing a stimulating and nourishing working environment and for sharing reagents and equipment. Drs. Sidney Whiteheart, Craig Vander Kooi, Tianyan

Gao, Haining Zhu, Kevin Sarge, Doug Andres, Skip Waechter and Michael Mendenhall, thank you for the advice and guidance you provided during my graduate studies. I would also like to express my sincere thanks to Rachel Putty, Tonya Simon and Phil Dickson for their day-to-day assistance and support.

To current members of the Dutch lab, Dr. Nicolas Cifuentes, Edita Klimyte and Stacy Webb, thank you for the great times, for your support, friendship and for making the lab environment very enjoyable and collaborative. A special thanks to Stacy Smith for her help and for allowing the lab to run smoothly. You will all be missed. I would also like to thank former members of the lab, especially Dr. Cyril Masante, Dr. Andres Chang, Dr. Brent Hackett and Dr. Clint Smith for all the help they provided when I first joined the lab.

In addition to all the above individuals who have contributed immensely to my professional development, I would like to thank everyone who have made the time throughout my graduate studies a very enriching experience at the personal level. A heartfelt thank you to all my friends whose care, kindness and support helped in providing me a home away from home. Thank you for making this time an unforgettable experience.

Finally, this goes to my family for their tremendous encouragement, love and unconditional support. To my parents, Jihad and Souhaila, thank you for all the sacrifices you made that allowed me to pursue my career goals and for being a great source of motivation through all these years. To my siblings, Diana and Jad, thank you for always being there for me and for knowing how to cheer me up. You are the reason I stand here today.

TABLE OF CONTENTS

LIST OF TABLES

LIST OF FIGURES

CHAPTER 1: BACKGROUND AND INTRODUCTION

Portions of this chapter were adapted from: Paramyxovirus Glycoprotein Incorporation, Assembly and Budding: A Three Way Dance for Infectious Particle Production. Farah El Najjar, Anthony P. Schmitt and Rebecca Ellis Dutch. *Viruses* 2014, *6*(8), 3019-3054.

Paramyxoviruses: Classification and medical significance. The *Paramyxoviridae* is a family of enveloped viruses with negative strand, non-segmented RNA genomes that causes significant disease in humans and animals. Important human pathogens within this family include measles virus (MeV), mumps virus (MuV) and human respiratory syncytial virus (HRSV), which is the single largest cause of respiratory tract infections in the pediatric population [1]. In addition, several paramyxoviruses have recently been identified, including the respiratory pathogen human metapneumovirus (HMPV) and the deadly zoonotic Hendra (HeV) and Nipah (NiV) viruses [2-4]. Paramyxoviruses also lead to high burdens on agriculture and the global economy by infecting avian species (Newcastle disease virus (NDV) and avian metapneumovirus (AMPV) [5,6]), cattle (rinderpest virus), as well as pigs (NiV) [3] and horses (HeV) [4]. Based on morphological characteristics, sequence homology and protein function, paramyxoviruses are further classified into two subfamilies: the *Paramyxovirinae* and the *Pneumovirinae*.

Paramyxovirus particles (depicted in Figure 1.1) are pleomorphic in shape. For many family members, particles are primarily spherical, and range in size from 150 nm to 300 nm in diameter; however, a filamentous form predominates for some viruses such as HRSV and the parainfluenza viruses, and these particles can reach up to 10 μm in length [7-12]. The viral membrane of paramyxoviruses contains two major glycoproteins required for virus entry into target cells: the attachment protein (termed HN for hemagglutinin-neuraminidase, H for hemagglutinin, or G for glycoprotein, depending on the virus) and the fusion (F) protein. These glycoproteins are densely packed on the viral envelope and form spike layers as seen under cryo-electron microscopy [13,14]. A subset of paramyxoviruses have an additional surface glycoprotein, the small

hydrophobic (SH) protein whose function in the viral life cycle is less clear since it is dispensable for virus replication in vitro [15-19]. Inside the viral envelope, the RNA genome is encapsidated by the nucleocapsid proteins (N or NP), forming the flexible, loosely coiled nucleocapsid structure, termed ribonucleoprotein complex (RNP), to which the viral RNA-dependent RNA polymerase complexes, made of large polymerase (L) protein and phosphoprotein (P), are bound. The RNA genomes of paramyxoviruses are 15-19 kb in length and contain six to ten genes. As is the case for most negative-strand RNA viruses, association of the paramyxovirus RNP with the viral membrane is mediated by the matrix (M) protein.

Human metapneumovirus and its significance to human health. Human metapneumovirus (HMPV) is a major cause of acute upper and lower respiratory tract infections worldwide [12,20-25]. HMPV was originally identified in 2001 in the Netherlands in patients with symptoms similar to human respiratory syncytial virus (HRSV) infection [2]. Since its initial report, studies have shown that HMPV has been circulating in human populations for more than 50 years [26,27]. Two lineages, A and B, exist for HMPV and they are further subdivided into two sub-lineages, A1, A2, B1 and B2 [2]. A number of reports indicate that there are no differences in disease severity between the two lineages [28,29]. Virtually all children are exposed to the virus by the age of five [2,30]. However, the virus induces incomplete immunity and recurrent infections can occur throughout life [31], thus HMPV can infect all age groups. Severe disease associated with HMPV infection occurs in young children, elderly and immunocompromised individuals. Between 5 and 20% of hospitalization rates due to respiratory infections in young children are caused by HMPV and it is generally considered as the second or third leading cause of severe respiratory diseases in this age group [32,33]. HMPV is also a significant cause of morbidity and mortality in immunocompromised and elderly populations [31,34], and a recent report indicated that hospitalization rates for HMPV infection in older adults are similar to those of influenza infections [35].

The most common clinical presentations of HMPV infection in children include cough, fever, rhinitis, wheezing, and otitis media [36,37]. More severe infections can also occur and common complications include bronchiolitis, croup, asthma exacerbation, and pneumonia [37-43]. Elderly that require hospitalization due to HMPV infection present with bronchitis, pneumonia, COPD exacerbations, and congestive heart failure [44]. Though mainly restricted to the respiratory tract, a few reports have associated HMPV with infections in the central nervous system [45-47]. Currently, there are no specific antiviral treatments or vaccines for HMPV infections. Besides ribavirin and monoclonal antibodies to the virus that have marginal anti-HMPV activity, the only form of treatment is supportive.

Paramyxovirus assembly and budding. The process by which paramyxovirus particles are formed and released at the cell membrane involves a series of highly coordinated and organized events that eventually result in the production of fully infectious virus particles. Figure 1.2 depicts the general life cycle of paramyxoviruses, which culminates in newly synthesized virus particles being assembled and released into the extracellular matrix. Infection is initiated upon binding of the attachment protein to a cell surface receptor, followed by fusion of the viral membrane to a host cell membrane, a step promoted by the F protein. The viral genome is then released into the cytoplasm where all the steps of the replication cycle occur. Primary transcription of the negative sense RNA genome by the viral RNA-dependent RNA polymerase follows the "stop-start" model resulting in a gradient of mRNA abundance such that genes at the 3'end are transcribed in higher amounts than genes at the 5'end [1]. Replication of the full-length genome occurs only after accumulation of viral proteins and involves production of positive sense anti-genomes which act as templates for the synthesis of new negative-sense genomic RNA. Progeny genomes can then be used for further replication, for secondary transcription, or for incorporation into virus particles. The newly synthesized RNPs are then transported to selected sites at the plasma membrane where interaction with the viral integral membrane glycoproteins occurs, followed by membrane scission and release of virus particles. Incorporation of RNPs and envelope glycoproteins into infectious virus particles is a highly complex and coordinated process that requires

cooperation among the three main structural components of the virus: the surface glycoproteins, the RNPs and the matrix proteins. While the majority of paramyxoviruses fit with this overall model, studies on the molecular mechanisms involved in the assembly and budding of paramyxovirus particles revealed significant differences between members of this family.

Viral proteins involved in paramyxovirus particle production. The three key components in production of infectious paramyxovirus particles, the surface glycoproteins, the matrix proteins and the RNPs, must coalesce at the plasma membrane to initiate budding. Interactions among these three components are critical for glycoprotein incorporation and particle assembly. The matrix protein is generally considered the main driver of paramyxovirus assembly and can interact with both the glycoproteins and the core RNPs in an orderly manner. However, paramyxovirus surface glycoproteins are not simply bit players in this process, but instead can play important roles in directing the process of particle formation.

Matrix proteins as coordinators of paramyxovirus assembly and budding. The M protein, the most abundant protein in the virion, plays a fundamental role in paramyxovirus assembly through its ability to interact with multiple partners. M proteins can self-assemble, bind directly to cellular membranes, and interact with the RNP complex and the cytoplasmic tails of glycoproteins, thus allowing the RNP core to associate with a region at the plasma membrane where the surface glycoproteins are concentrated, which will become the budding site. The importance of M proteins for paramyxovirus particle production was originally shown in Sendai virus and measles virus, where mutations in the M gene encoding an unstable M protein was correlated with severe defects in infectious particle production [48-51]. Our understanding of the role of M protein in the process of paramyxovirus assembly was enhanced by studies involving virus-like particle formation (VLPs) and reverse genetics, as recombinant viruses with mutations or deletions in the M gene revealed the significance of the matrix protein in incorporation of other viral components and in viral budding. For example, deletion of the measles virus M protein led to an increase in cell-associated virus and the loss of co-localization of the surface glycoproteins with the RNPs [52]. A recent study by Mitra et

al. showed that infection with an M-null HRSV resulted in impairment of infectious particle release and alterations in the intracellular localization of the RNP complex as well as in the distribution of glycoproteins on the plasma membrane, further demonstrating the essential role of M in the assembly and budding of virus particles [53]. For many paramyxoviruses, including Sendai virus (SeV) [54,55], MeV [56,57], NiV [58,59], hPIV1 [60], and NDV [61], transient expression of M protein by itself is sufficient to promote budding of VLPs, indicating that the M protein of these viruses has the ability to efficiently associate with membranes, induce membrane curvature and promote scission. Although matrix proteins of different paramyxoviruses display similar functions, they vary greatly in length and amino acid sequences.

Despite the essential role of the M protein in paramyxovirus particle production, the mechanisms by which M regulates the assembly and budding processes vary among different members of the family. Unlike SeV, MeV, NDV, NiV and hPIV3, where the M protein is sufficient for VLP formation, other paramyxoviruses require interactions of M with the surface glycoproteins or with the RNP for particle formation, indicating that there are significant variations in the function of M and in the strategies that different family members employ for efficient particle production. Differences in the role of M in the assembly of paramyxoviruses were also demonstrated by electron cryo-tomography showing the 3D structures of virus particles. While the general ultrastructural model of paramyxoviruses depicts M protein as lining the inner leaflet of the viral envelope, recent cryo-tomography data show that this structure does not apply to all paramyxoviruses. For RSV, NDV and SeV, M forms a layer under the viral membrane only in a small percentage of virus particles. In the majority of particles, M was observed to be dissociated from the membrane and disassembled, potentially to allow the conformational changes of the F protein from the pre-fusion to the post-fusion form by releasing interactions with the F cytoplasmic tail [62-64]. A recent study revealed that for RSV the surface area of the virion membrane which is covered by M varies significantly depending on the morphology of the virus particle with the highest coverage (86%) detected in filamentous particles and the lowest (24%) in spherical viruses [65]. The arrangement of the surface proteins and the matrix proteins in the 3D structures of NDV and RSV suggest an interaction between these two viral components. In MeV, on the

other hand, M protein was not located under the viral membrane but was found to assemble on the RNP forming a bundled two-layer helical structure inside the virion [66]. These findings suggest significant mechanistic differences in the way M interacts with the RNPs and envelope proteins to assemble virus particles.

Interaction of ribonucleoprotein complex with glycoproteins and M. During replication, the newly synthesized genomic RNA is tightly wrapped with the nucleoprotein for protection from degradation, forming a helical RNP complex [67]. Encapsidation of RNA by N does not depend on specific nucleotide sequences, as expression of N in the absence of infection can result in the formation of nucleocapsid-like structures resulting from N non-specifically binding host-cell RNAs [55,60,68-70]. Prior to virus budding, newly synthesized RNPs must assemble with the surface glycoproteins and the M protein at the plasma membrane. While multiple copies of the RNA genome can be packaged within a single particle [64,65,71,72], incorporation of RNPs into virions is selective and depends on species homology between M and the nucleocapsid protein, genome length, and to a lesser extent on the polarity of the genome [73-75]. Targeting of RNPs to the plasma membrane assembly sites is primarily mediated by the M protein. M proteins of several paramyxoviruses, including SeV, MeV and PIV5, are known to interact with the nucleocapsid protein to mediate incorporation of the RNPs into virions [73,76,77]. Studies using recombinant viruses also demonstrated that deletions or mutations of the M gene can block RNP complex transport to the plasma membrane during infection, further supporting the important role of M protein in RNP inclusion into virus particles [53,57]. Within the *pneumovirinae* subfamily, association of M with the RNP can occur through interaction of M with the transcription elongation factor, M2-1 protein, which is also considered a component of the RNP complex [62,65,78]. M can also bind RNA directly or can bind to the large polymerase L protein [79,80]. In addition to interacting with M to facilitate their incorporation into virions, in some cases the paramyxovirus nucleocapsid proteins play a role in increasing efficiency of VLP budding [14,69]. Co-imunoprecipitation experiments showed that the fusion protein of NDV interacts with the NP protein in purified VLPs and not with the M protein, suggesting that interaction of F with NP may be involved in localization of NP at plasma membrane assembly sites [61]. In other cases, such as SeV, interaction of the M

protein with a viral glycoprotein is required for concentration of the RNPs at the plasma membrane and their subsequent assembly into particles [81].

Active role of glycoproteins in paramyxovirus particle formation. While the role of M proteins as organizers of paramyxovirus assembly has been well established, the important function of membrane proteins in the late phases of paramyxovirus infection has gradually become clearer. Surface glycoproteins of paramyxoviruses are well characterized for their significance in membrane fusion and viral entry; however, substantial evidence implicates an active role of these membrane glycoproteins in the end stages of the virus replication cycle (reviewed in [82,83]). Paramyxovirus glycoproteins can specify the location for viral budding through interactions with lipids, associate with the M protein to aid in assembly, and in some cases, interact with RNPs as part of virus assembly. For assembly of infectious particles, M must target the cytoplasmic RNPs to the budding site at the plasma membrane where the viral integral membrane glycoproteins are concentrated, thus paramyxovirus M proteins are suggested to bind membranes at areas enriched with the envelope proteins. Consistent with this view, the ultrastructure of NDV revealed that the M protein forms a grid-like array where the glycoproteins were densely packed [63]. In addition, an inner layer of membrane-bound M was associated with regular spacing of the pre-fusion F protein in RSV virions, further supporting an interaction between M and F [62]. Studies have demonstrated that membrane proteins interact with the matrix protein for a number of paramyxoviruses, and this interaction is needed to organize assembly and for the incorporation of glycoproteins into budding virus particles, but many differences exist between various members with respect to the contribution of this interaction to particle formation and the individual roles of the attachment and fusion proteins. For SeV, M can interact with both F and HN [84-86] but only the fusion protein is important for virus production and its function is as critical as that of M since alterations in F can attenuate virus production up to 70% [86-88]. Expression of glycoproteins was also shown to be important for budding of VLPs. Loo et al. have recently shown that while HMPV M interacts with both F and G proteins, expression of HMPV G facilitates formation of VLPs [10]. Specific interactions between M and HN of NDV have also been reported; however, this interaction does not have an effect on efficiency of VLP release [61]. Similar results were seen for MeV, NiV and

RSV, indicating that glycoproteins can enhance budding efficiency for only a subset of paramyxoviruses [56,58,59,89].

In addition to their contribution to the budding process, paramyxovirus glycoproteins are also implicated in assembly of other viral components. The fusion protein of RSV was shown to be responsible for incorporation of G and SH proteins into budded virions and for their co-localization with N at plasma membrane assembly sites; however, F deletion had no effect on M assembly into virions [89]. A key function for the fusion protein in SeV assembly was shown, as mutations in F altered cellular localization of both HN and M, although interaction of F with M was not affected [81]. These findings indicate that the paramyxovirus glycoproteins can play significant roles in the assembly and budding processes, but different paramyxoviruses utilize their glycoproteins differently.

Paramyxovirus surface glycoproteins contain short cytoplasmic tails which extend on the inner side of the plasma membrane. Several studies have demonstrated that the role of paramyxovirus glycoproteins in particle formation depends on their cytoplasmic tails, as these regions are required for glycoprotein incorporation into packaged particles and for glycoprotein interactions with M. Biochemical and co-localization studies revealed that M can interact with the cytoplasmic tail of the homotypic attachment proteins for RSV, HMPV, NDV and measles [10,61,90,91]. These finding are surprising for the pneumoviruses RSV and HMPV since G is dispensable for viral replication in vitro [92,93]. This suggests that while interaction of M with G is dispensable for virus production in these cases, the presence of G may contribute to optimal virus production manifested by an increase in HMPV VLP formation [10] and a role for G in SH incorporation into RSV particles [89]. For other paramyxoviruses, the cytoplasmic tail of F protein plays an important role in late stages of viral infection. The cytoplasmic tails of MuV and hPIV1 F proteins are involved in particle assembly [14,94]. For RSV, formation of viral filaments depends on the cytoplasmic tail of the fusion protein [89,95]. For measles virus, truncations in the cytoplasmic tails of F and H do not alter assembly of viral components at the cell membrane but do affect the incorporation of F, M and H into released particles [96]. Deletion of the cytoplasmic tail of measles virus F protein is

associated with increased cell-cell fusion, similar to what is seen for the MeV strain obtained from subacute sclerosing panencephalitis (SSPE) patients. It has been suggested that interaction of M with the cytoplasmic tails of F locks F in the pre-fusion conformation during the process of assembly; thus removal of the cytoplasmic tail, and loss of the M interaction domain, facilitates fusion [52,62,97]. The importance of the glycoprotein cytoplasmic tails for particle assembly appears to be a common feature of many RNA viruses, as truncations in the cytoplasmic tails of the glycoproteins hemagglutinin [98] (HA) and neuraminidase (NA) of influenza A virus or of the rhabdovirus G result in severe defects in particle formation [99,100].

Intracellular trafficking of paramyxovirus components. During paramyxovirus replication, the glycoproteins, matrix proteins and RNPs are synthesized at distinct sites in the cytoplasm and must be transported to the plasma membrane for coordinated assembly. The different viral components reach the plasma membrane by different mechanisms and interact with each other in an orderly manner either during trafficking or at the cell surface prior to packaging into virions. Paramyxovirus proteins are carried to the cellular plasma membranes by utilizing various cellular machineries including endocytic and exocytic pathways, in addition to vesicular trafficking and the cytoskeleton.

Trafficking of viral glycoproteins. Paramyxovirus glycoproteins are synthesized in the endoplasmic reticulum (ER) and traffic through the secretory pathway, and in some cases through endocytic pathways, to the plasma membrane. Proper trafficking is needed for incorporation into budding virions or induction of cell-cell fusion for direct cell-to-cell transmission of virus particles. For some paramyxoviruses, data indicate that the fusion and attachment proteins can interact following their synthesis in the ER, and thus are transported to the cell surface as a metastable protein complex. This has been suggested to occur for NDV, MeV and human parainfluenza viruses 2 and 3 [101-103]. Alternatively, the F protein and the attachment protein can traffic separately and only associate after reaching the plasma membrane, which is the case for HeV and NiV [104,105]. For PIV5, F and HN also associate at the cell surface but formation of the F-HN complex requires receptor binding [106]. During their synthesis in the ER,

glycoproteins must undergo proper folding and oligomerization prior to trafficking to the cell surface. Mutational analyses showed that mutations which interfere with proper folding or assembly of the final oligomeric structure of paramyxovirus glycoproteins generally result in their retention in the ER and prevent their transport through the exocytic pathway to the cell surface [107-110]. The contribution of the ectodomain in proper folding and stability of the trimeric fusion protein or the tetrameric attachment protein is well established, but substantial evidence also indicates an important role of the transmembrane domains and cytoplasmic tails in the oligomerization process and folding of the ectodomain [109,111-113]. Mutation of a TYTLE motif in the cytoplasmic tail of SeV F protein prevented its transport to the PM, and the protein was instead retained in the ER. This failure to traffic was hypothesized to be due to the failure of the F mutant to trimerize [81]. Similar findings were reported for the PIV5 HN protein, as deletion of the cytoplasmic tail prevented its assembly to an oligomer and transport to the cell surface [110]. In addition to their role in protein oligomerization, the cytoplasmic tails are thought to facilitate proper trafficking of glycoproteins to the cell surface by binding cellular factors that direct protein targeting to the plasma membrane and by harboring residues that facilitate interaction with negatively charged lipids at the plasma membrane. N-glycosylation can also be essential for the proper folding, stability, intracellular transport, and surface expression of the paramyxovirus glycoproteins. Removal of N-glycans from the glycoproteins of NDV, CDV, PIV5, SeV, HeV and NiV had a significant effect on their exocytic transport and surface expression [114-120]. However, removal of all three N-glycans did not affect transport of the RSV F protein to the cell surface indicating that the degree to which N-glycosylation influences proper folding and transport varies among paramyxovirus glycoproteins [121,122].

Trafficking of viral glycoproteins has been demonstrated to involve tyrosine-based and di-leucine motifs which are involved in protein trafficking in both secretory and endocytic pathways. Several paramyxovirus glycoproteins have endocytic signals and can undergo internalization following trafficking to the plasma membrane [123-127]. For instance, the cytoplasmic tails of NiV and HeV F proteins contain a tyrosine-based motif (YXXΦ), where X is any amino acid and Φ is a residue with a bulky hydrophobic side chain, that is required for internalization of the protein from the cell surface

[126,127]. PIV5 HN is internalized from the plasma membrane by clathrin-coated pits but its internalization depends on a single glutamic acid residue at the boundary between the transmembrane domain and the ectodomain [124,128]. Henipavirus fusion proteins are the only paramyxovirus glycoproteins that have an absolute dependence on endocytosis for proteolytic activation by cathepsin L [126,129-131]. With the exception of Henipaviruses, the relevance of endocytic signals in viral envelope glycoproteins is not yet well established. It has been proposed that down-regulation of attachment and fusion protein expression on the cell membrane may be a post-translational regulatory mechanism that plays an important role in viral pathogenicity through minimizing recognition of antigens on the infected cells by the immune system. Endocytic signals in viral glycoproteins can also affect efficiency of glycoprotein incorporation into virions and virus assembly. Mutation of the internalization signal in PIV5 HN has been shown to affect the incorporation of both F and HN into budded virions [132]. Interaction of the surface glycoproteins with the core matrix proteins may regulate expression of the paramyxovirus glycoproteins on the cell surface and decrease internalization of the glycoproteins, thus favoring their incorporation into assembled virus particles over endocytosis [52,97,133,134].

Intracellular transport of matrix proteins and ribonucleoproteins. Though originally synthesized in the cytoplasm, the matrix protein and the RNPs must subsequently translocate to viral budding sites at the plasma membrane; however, very little is currently known on the mechanisms underlying transport of these critical viral structural components. In the classical model for paramyxovirus assembly, the matrix protein is thought to interact with the RNP at the cell membrane to mediate its insertion into budding sites for the production of infectious virus particles. Substantial data, however, support an alternative model in which the matrix protein associates with the RNP complex in the cytoplasm prior to translocation to the plasma membrane. Data on both MeV and SeV suggest that the M protein binds to the RNP in the cytoplasm, and the two components are then co-transported to the plasma membrane [57,135]. Further support for an interaction of M with the RNP in the absence of membrane interactions was provided by the 3D structure of MeV particles, which showed that measles M protein

did not form a layer underneath the viral envelope, but instead associated with the RNPs to form a helical matrix-covered nucleocapsid structure inside the virion [66].

Data from live cell imaging revealed an important role of the host cytoskeleton in the trafficking of paramyxovirus RNP complexes. Filamentous RNPs of RSV show myosin-motor driven directional movement on the actin cytoskeleton [136]. In the case of SeV and MeV, RNPs are transported along microtubules using Rab11A containing vesicles, key regulators of trafficking within the recycling endosomal pathways and Golgi to the plasma membrane [137,138]. Rab11 endosomes are also part of the apical recycling endosome (ARE) pathway which controls apical transport of proteins in polarized cells, suggesting that this pathway may be particularly important in polarized cells. However, a requirement for Rab11A in assembly of SeV is observed in both polarized and non-polarized cells. In contrast, Rab11A dependent transport of measles RNPs is only critical for virus production in polarized epithelial cells and is not a general requirement for measles RNP trafficking. The Rab11-mediated recycling pathway is also important for budding of RSV particles from the apical surface [139]. In the course of RSV infection, the matrix protein localizes in cytoplasmic bodies containing the RNP complex proteins N, P, L, and M2-1, which are thought to be assembly bodies. Deletion of the matrix gene prevents the translocation of the viral RNP from the cytoplasmic inclusions to the cell surface suggesting that for RSV, trafficking of the RNPs depends on trafficking of M [53,140]. These findings indicate that large differences exist in the trafficking mechanisms of paramyxovirus RNPs. It is yet to be determined whether the Rab11 mediated pathway is utilized by other paramyxoviruses to transport the RNPs prior to assembly and if M is associated with the viral RNPs in the Rab11 containing endosomes to facilitate its trafficking. A recent study demonstrated that the incorporation of HIV1-Env protein into budding particles is dependent on the interaction of the Rab11-interacting proteins FIP1C/RCP and Rab14 with the cytoplasmic tail of the protein [141]. This raises the question of whether sorting of paramyxovirus glycoproteins to the plasma membrane can be mediated by components of the Rab11 pathway and this requires further investigation.

Although the entire replication cycle of paramyxoviruses occurs in the cytoplasm, the matrix proteins of HRSV, SeV, NDV and NiV have been shown to traffic through the nucleus early during virus infection. In the case of RSV, localization of M in the nucleus occurs through interaction of a nuclear localization signal (NLS) with the nuclear import receptor, importin β1, and its exit to the cytoplasm at later stages of infection is mediated by a nuclear export signal (NES) that directs Crm-1dependent nuclear export [142]. Nuclear-cytoplasmic trafficking of NiV M was also dependent on a NLS and a leucine-rich NES [143]. In contrast to both RSV and NiV, the matrix protein of NDV is present in the nucleus throughout infection, and recent studies indicate that NDV M localizes in the nucleolus primarily due to interaction with the nucleolar phosphoprotein B23 [144-149]. In all cases, trafficking of M to the nucleus and its localization there was necessary for later virus budding and efficient virus production. Although more studies are needed to clarify the biological function of M protein nuclear localization, it is proposed that M transits to the nucleus at early stages of infection to allow optimal transcription and translation of viral components, since the M protein of several paramyxoviruses has been shown to bind RNA directly and inhibit viral transcription [76,80]. Transition of M through the nucleus may also affect host transcription to enhance virus replication (similar to the matrix protein of vesicular stomatitis virus [150,151]) remove this?). The M protein of RSV has been shown to induce cell cycle arrest in lung epithelial cells by regulating p53 expression suggesting a role of M in influencing cellular transcriptional to control p53 levels [152].

Role of viral and cellular factors in paramyxovirus budding. Budding of enveloped viruses is a complex process that requires induction of membrane curvature followed by membrane scission and release of virus particles. Induction of membrane curvature and the final membrane fission event requires manipulation of the lipid-lipid interactions within cellular membranes, and is driven by interactions of viral proteins with membrane lipids in addition to viral-viral and viral-host protein interactions [153]. The mechanisms underlying budding of paramyxoviruses are still largely unknown, but it is evident that various paramyxoviruses exit infected cells using different mechanisms (reviewed in [82,83]). Budding of paramyxovirus particles is driven primarily by the matrix protein. The M protein binds membranes and homo-oligomerizes underneath the plasma

membrane to drive membrane deformation and promote the needed curvature. As previously mentioned, the M protein of a number of paramyxoviruses can induce formation of VLPs when expressed by itself [54]. In this case, self-association of M under the membrane may be sufficient to drive membrane deformation and outward budding of VLPs. It is equally possible that host proteins are recruited by M to the plasma membrane and thus the host machinery drives the membrane deformation and outward budding. One of the primary mechanisms involved in the release of nascent virus particles of many enveloped viruses, such as HIV-1, Ebola virus, and VSV requires a short stretch of amino acids in the matrix protein with a late budding function known as the "L" domain. These L domains, which vary among different viruses (P(T/S)AP, PPxY, YxxL), function by recruiting and interacting with cellular proteins of the endosomal sorting complex required for transport (ESCRT), which are part of the vacuolar protein sorting (VPS) pathway and are involved in promoting membrane fission steps that lead to the release of virus particles [154]. The paramyxoviruses PIV5 [69], NDV [149] and mumps virus [14] rely on the host ESCRT machinery during virus exit, as release of particles was inhibited by expression of a dominant negative VPS4A. Budding of PIV5, NDV and mumps virus is dependent on a FPIV-like motif in the M protein [14,149,155], which does not resemble canonical L-domain sequences, suggesting that these paramyxoviruses may utilize different components of the host ESCRT that can recognize and bind to a different amino acid sequence. There is increasing evidence that a growing number of viruses, including influenza virus and VSV, can bud from host cells independent of ESCRT machinery (reviewed in [153,156]). Budding of RSV [139], NiV [157], MeV [158], AMPV [159] and HMPV [160] has also been demonstrated to occur in an ESCRT-independent manner. The mechanisms used by ESCRT-independent viruses to bud from infected cells are still unknown for many of these viruses. Interestingly, budding and virus release of HRSV is dependent on Rab11-FIP2, and the Rab11 pathway was also shown to play a role in influenza virus production, suggesting that viruses may utilize the Rab11 endosomal pathway in a previously uncharacterized manner to achieve their exit from host cells [139,161].

Although M proteins are considered the driving force for budding of paramyxoviruses, increasing evidence demonstrates that the glycoproteins can also play a

role. Several paramyxovirus glycoproteins can induce VLP formation by themselves or must be present with the M protein for efficient VLP formation, indicating that surface glycoproteins in these cases are needed either to recruit M to assembly sites or to initiate budding. A major role of glycoproteins in paramyxovirus budding is well characterized for the SeV fusion protein. Sendai F induces VLP release when expressed alone in cells, and silencing of the F gene reduces virus production by 70% [86]. The ability of F to bud from the plasma membrane depends on a TYTLE motif in the cytoplasmic tail of the protein [81,162]. This suggests that the TYTLE motif may be needed to bind a cellular factor that facilitates budding. Sendai F also interacts with M in the ER and is responsible for carrying M to the plasma membrane. Interestingly, both proteins were found to contain amino acid sequences that resemble actin binding domains [54]. The host cytoskeleton has been shown to play an important role in the life cycle of several paramyxoviruses, and it is thought that cytoskeletal components are involved in paramyxovirus budding. Large amounts of actin were found associated with SeV particles and, interestingly, mutations of the actin binding domain in F resulted in a significant reduction in SeV VLP production, indicating that binding of SeV F protein to actin is important for budding of the virus. The requirement of the cytoplasmic tail domains of glycoproteins for budding of several paramyxoviruses may indicate that these domains are involved in binding cellular factors that usually are involved in exocytic pathways. Another significant role of paramyxovirus glycoproteins in paramyxovirus particle production is manifested in RSV production. Short filament-like structures containing F and G were seen in cells infected with M-null virus suggesting that RSV glycoproteins are capable of deforming the cell membrane and initiating bud formation [53]. Clustering of glycoproteins in lipid raft microdomains may create a pulling force on the plasma membrane and thus induce an initial membrane deformation that is further elongated by oligomerization of the matrix protein [62]. These observations suggest that the glycoproteins of paramyxoviruses can actively contribute to the budding process leading to virus egress from infected cells.

Current models for paramyxovirus assembly. Fundamental differences exist among the different family members in the mechanisms that underlie coordinated targeting to the assembly site, and three different models for paramyxovirus assembly can at present be

deduced (Figure 1.3). What factors determine which mechanism is employed by specific paramyxoviruses for completion of their life cycle are not currently known. It may be possible however that some members can employ more than one assembly mechanism either simultaneously or at different times during infection depending on cellular factors or in vivo conditions. In the first model, the fusion and attachment proteins interact following their synthesis in the ER and are co-transported to the plasma membrane as a complex. The matrix protein associates with the RNP in the cytoplasm and carries it to the plasma membrane where it assembles with surface glycoproteins. This model can be deduced mainly from studies done on MeV. Alternatively, the fusion and attachment proteins can traffic separately to the cell surface. In some cases, like SeV (model 2), the fusion protein can bind the matrix protein in the ER, and the two are transported as a complex to the plasma membrane where they create a nucleation site for assembly. Incorporation of the attachment protein likely occurs though interactions with M or with F. The RNP can traffic by itself to the assembly site and is packaged within particles upon binding to M or one of the glycoproteins. Studies of RSV suggest a third model of paramyxovirus assembly, where the formation of an assembly complex containing F, M and the RNP core occurs in inclusion bodies in the cytoplasm, with a role of the cytoplasmic tail of F in targeting M-RNP to assembly sites.

The actin cytoskeleton and its importance in viral infection.

***Overview of the actin cytoskeleton*.** Actin was first isolated in 1887 from muscle tissues as a coagulating factor [163], but it was not until 1940 that filamentous actin was observed and "actin" was given its name . The actin cytoskeleton is involved in pivotal functions in the cell from controlling cell shape and motility to organelle distribution, transport of cargo within the cells and intercellular communication. Actin exists in two forms in the cell: monomeric globular actin (G-actin) and polymeric filamentous actin (F-actin). Monomeric G-actin is a 43-KD protein that is highly conserved in eukaryotic cells from yeasts to humans and is often considered the most abundant protein in non-muscle cells. The atomic structure of G-actin contains two main domains and two subdomains that form two prominent clefts: a large nucleotide-binding cleft and a hydrophobic cleft that mediates interactions of actin with most actin binding proteins (ABPs) [164-166].

Three isoforms of G-actin that differ only by few amino acids mainly at the N-terminus of the protein are expressed in mammalian tissues: α-actin in muscle tissues, β- and γ-actin in non-muscle and muscle tissues [167]. Actin is in a dynamic state between its monomeric and filamentous forms with actin monomers assembling and disassembling at a continuous basis. Actin is an ATPase and the transition between the two states is controlled primarily by ATP hydrolysis and ions (K^+, Mg^{2+}). Assembly of actin filaments from G-actin occurs in two steps, an initial lag phase involving nucleation and formation of ATP-bound G-actin dimers and trimers followed by a rapid polymerization phase, ATP hydrolysis and dissociation of phosphate. The resulting actin filament is flexible, consists of two strands of parallel actin monomers with a right-handed helical twist and two ends that are dynamically different: a fast growing (+) barbed end to which ATP-bound G-actin is spontaneously added and a pointed (-) end where ADP-actin monomers dissociate and the filament shortens [168]. This process of actin polymerization/depolymerization known as actin filament treadmilling is tightly controlled by other cellular factors that are involved in regulating actin dynamics in the cell: ABPs and the Rho-family GTPases, in particular Cdc42, Rac and Rho [169-172].

ABPs are a family of proteins that can bind G-actin, F-actin or both and are involved in regulating actin filament nucleation, elongation, capping, crosslinking, severing, depolymerization and actin-associated motor activity (myosins). Polymerization of actin filaments is initiated when actin monomers are stabilized by an initiation complex. The first initiation complex to be identified and the most studied is the Arp2/3 complex, which consists of seven proteins including the actin related proteins Arp2, Arp3 and ARPC-1. By itself, the Arp2/3 complex has low polymerization-stimulating activity [173], but this activity is activated through interaction with Nucleation Promoting Factors (NPFs) such as members of the Wiskott–Aldrich syndrome protein (WASP)/WAVE family and WASP-interacting proteins (WIPs) [174-176]. NPFs, in addition to Arp2/3 biding motif, also have WH2 domain(s) that allow binding to monomeric actin, thus NPFs recruit actin and induce a conformational change in Arp2/3 to activate its nucleating activity [177,178]. In addition to the Arp2/3 complex, other actin nucleating factors include formins and tandem-monomer-binding nucleators [179]. Following

nucleation, filament elongation and stabilization is mediated by other ABPs such as profilin, cortactin, tropomyosin and the Ena/VASP family. In addition, once actin filaments are formed, a number of F-actin binding proteins can mediate the formation of more complex structures. Crosslinking proteins including fascins, fimbrins and spectrins promote formation of actin networks such as the cortical actin underlying the plasma membrane [180-182]. Actin filaments can also bundle with other proteins to form parallel or anti-parallel filaments [183]. Actin filaments are also subject to further branching by actin-nucleating protein. For example, when activated by NPFs, Arp2/3 can form a branched network from the side of an existing actin filament and proteins known as "capping proteins", such as gelsolin, can block the branching filament at the (+) barbed end, thus resulting in short, rigid branched networks that form entangled meshworks. However, in the absence of capping proteins, branched actin filaments can grow longer and form parallel or anti-parallel bundles [184]. Myosin motor proteins can bind actin and move unidirectionally along the actin filaments with some myosins (I or V) moving toward the barbed end and the cell periphery and others like myosin VI or IXb move to the cell center. Actin filaments can be disassembeled and depolymerized by the action of proteins such as ADF/cofilin and gelsolin [185,186]. These different configurations of F-actin are integrated in the cell to form four main structures: sheet-like structures containing branched and crosslinked actin networks (lamellipodia, ruffles and blebs), structures containing tight parallel actin bundles (filopodia and microvilli), contractile antiparallel bundles (stress fibers) and crosslinked networks (cortical actin directly linked to the plasma membrane by integral and peripheral membrane proteins). Stress fibers are essential for mediating attachment to the substratum and providing mechanical strength, lamellipodia comprise the leading edge of migrating cells while filopodia contain receptors for signaling as well as adhesion molecules.

The organization of the actin cytoskeleton in a cell is highly dynamic and it is mainly regulated by signaling proteins of the Rho GPTase family. More than 20 Rho GTPases regulate actin organization and rearrangement in the cell, but the most extensively studied ones include Rac1, Cdc42 and RhoA [187]. Rho GTPases are monomeric, low molecular weight proteins that act as molecular switches as they cycle

between a GTP-bound active form to a GDP-bound inactive form. Rho GTPases are strictly controlled by three sets of proteins: Guanine nucleotide exchange factors (GEFs) that catalyze GDP to GTP exchange, guanine nucleotide-dissociation inhibitors (GDIs) which prevents GDP to GTP exchange and Rho activation by binding the GDP-bound Rho and GTPase activating proteins (GAPs) that activate intrinsic GTPase hydrolysis activity. Rho GTPases regulate signaling pathways linking membrane receptors to the actin cytoskeleton. In their active GTP-bound form, Rho GTPases act by binding and activating actin nucleators. A large number of proteins that interact with Cdc42 and Rac1 contain a short amino acid motif (around 18 residues) that is known as the Cdc42/Rac1 Interactive Binding (CRIB) motif. Binding of Rho GTPases to their direct downstream effectors result in activation and membrane recruitment of the effector protein. Figure 1.4 summarizes the signaling pathways activated by the Rho GTPases Cdc42, RhoA and Rac [188]. Cdc42 can directly bind and activate the NPFs WASP and WAVE, thus activating the Arp2/3 complex downstream. Cdc42 also activate the formin mDia and DAAM1 as well as the p21 activating kinase (PAK). Activation of Cdc42 through these pathways result in formation of protrusive filopodia [189,190]. Similar to Cdc42, Rac1 also activates WASP and Arp2/3, PAK and the formins FMNL1 and FHOD1, mainly inducing membrane ruffling and lamellipodia as well as adhesion signaling [191-193] . Activation of RhoA in general results in cellular effects which opposes those induced by Cdc42 and Rac1. RhoA activates the formins mDia and DAAM1 as well as Rho associated kinase (ROCK) and cofilin downstream, leading to formation of stress fibers and focal adhesions. In addition, RhoA activates ROCK/myosin light chain (MLC) pathway leading to acto-myosin contractility and integrin adhesion. Thus, activation of these pathways in response to various upstream signals results in time and space-dependent remolding of the actin cytoskeleton which is essential to may cellular processes including migration, division and membrane trafficking.

Viruses and the actin cytoskeleton. Due to the important roles of the actin cytoskeleton in maintaining a plethora of cellular processes, it is perhaps not surprising that viruses have evolved various ways to manipulate the structure and function of the actin cytoskeleton to establish successful infection. The first reports linking virus infection

with an effect on the actin cytoskeleton were described in the 1970s with the identification of transforming viruses Rous sarcoma virus [194], Simian virus [195] and adenoviruses [196] where virus infection resulted in cell rounding, loss of contact inhibition, disruption of stress fibers and increase in cortical rigidity. Today, a large number of studies support an important role of actin at different stages of the viral life cycle from entry and replication to assembly and egress.

Virus infection of a host cell begins with attachment of a virus particle to the cell surface, and some viruses can induce alterations in the actin cytoskeleton at this step, even prior to entry. A process known as "virus surfing" have been described where some viruses, including retroviruses, papillomaviruses, herpesviruses, dengue virus and others, can bind cell surface receptors or extracellular matrix components and move along the plasma membrane by actin-driven motion [197-201] . In some cases, such as herpes simplex virus-1 (HSV-1) and dengue, interaction of virus with a cell surface receptor activates downstream signaling including Rac1 and Cdc42, inducing formation of filopodia and virus surfing on these structures. Following attachment, viruses have to overcome the plasma membrane and the three-dimensional network of cortical actin underneath to gain access to the cell. For viruses that take advantage of endocytosis to enter the cell, cortical actin does not create a barrier. However, studies have shown that actin filament dynamics and actin-associated signaling play an important role in entry of those viruses indicating the involvement of the actin cytoskeleton in endocytic virus entry [202-206] . The role of actin in entry of viruses that enter though membrane fusion is still not well understood. For paramyxoviruses, it has been shown that disruption of actin filaments reduces entry and cell-cell fusion and syncytia formation by RSV [207]. In addition, previous work in our lab indicated a role of Rac1 and Cdc42 in syncytia formation induced by HeV and PIV5 and a role for actin dynamics in fusion pore formation by PIV5 [208,209]. A role for actin has also been associated with replication of negative strand RNA viruses including the paramyxoviruses HRSV and canine distemper virus, although no clear mechanism has been described [210,211]. The actin cytoskeleton is also involved in later stages of the infection cycle and viruses mostly utilize the scaffolding and force-generating function of actin for particle assembly, release and spread. Recent studies revealed an important role of the actin cytoskeleton in

the trafficking of paramyxovirus RNP complexes. Filamentous RNPs of RSV show myosin-motor driven directional movement on the actin cytoskeleton [212]. In addition, actin was shown to be involved in co-transport of M-RNP complexes of measles virus to the cell surface [213], indicating role of actin in paramyxovirus assembly. Several reports also implicate a role of the actin cytoskeleton in last step of virus infection: exit and spread. Actin was shown to play a role in budding of several viruses including influenza virus, HIV-1 and the paramyxoviruses RSV, Sendai virus and measles virus [207,213-215]. In addition, a number of viruses has been shown to manipulate the actin cytoskeleton in fascinating ways to mediate their exit from the cell and spread from cell-to-cell. Viruses of different families including HIV-1, herpes simplex virus (HSV) and rotavirus can induce formation of actin extensions to disseminate infection over long distances [216-218]. These viruses were shown to encode proteins that manipulate the actin cytoskeleton by different mechanisms. HIV-1 Nef protein modulates PAK2 activity [219] while alphavirus US3 kinase binds and phosphorylates PAK1 and PAK2 [220]. Actin manipulation by rotavirus involves two proteins NSP4 that inactivates cofilin and VP4 that associates with actin [218,221]. Vaccinia virus represents another example of an extensive manipulation of the actin cytoskeleton where the virus can modulate the three Rho GTPases Cdc42, Rac1 and RhoA by different mechanisms to promote direct cell-to-cell spread of virus particles [222].

A role of the actin cytoskeleton at different steps of the infection cycle has been described for a large number of viruses to this date. Although viruses do not usually encode actin cytoskeleton components, they encode proteins that can modulate actin-associated signaling or actin-modulating proteins directly to manipulate actin structures in the cell. However, for paramyxoviruses little is known about virus interactions with the actin cytoskeleton and the specific roles of actin during infection.

Dissertation overview

The dissertation focuses on understanding the mechanisms involved in the formation and spread of HMPV particles. As a recently discovered virus, several aspects of the life cycle of HMPV are not well understood. Previous work in our laboratory and others has provided important information on early stages of HMPV infection involving

mechanisms of viral membrane fusion and HMPV binding to the cell surface. However, the late stages of infection by which the different virus components assemble and exit the cell as infectious virus particles have not been thoroughly investigated and only a few reports have provided information on the late stages of HMPV infection. Similar to other paramyxoviruses, HMPV M was shown to be required for budding of virus particles [160]. In addition, both F and M are needed for production of VLPs suggesting an important role for these two proteins in the assembly and budding steps of HMPV infection [10], and budding occurs in an ESCRT independent manner [160]. However, most of these studies were done in non-respiratory cells, which do not represent the best model for studying HMPV infection. To gain better insight about the infection cycle of HMPV, I initially performed imaging analysis on human bronchial epithelial cells (BEAS-2B) infected with HMPV and identified structures including branched filamentous networks of budding viral filaments and long intercellular extensions, structures that have not been described for other paramyxoviruses. Thus, my dissertation work focused on investigating the mechanisms underlying the formation of these structures and their functional significance for HMPV infection with my major hypothesis being that viral and cellular factors contribute to the formation of unique structures that are needed for HMPV assembly and spread. My results indicate that the actin cytoskeleton plays an important role in the budding of branched filamentous networks, in the formation and elongation of intercellular extensions and in production of HMPV particles, while microtubules contributed to elongation of cellular extensions but not in formation of branched filaments. Further studies indicated a role of intercellular extensions in direct cell-to-cell spread of virus particles, which in contrast to cell-free HMPV infection, does not depend on heparan sulfate and can evade neutralizing antibodies. This work suggested several possible models for spread of HMPV infection in a monolayer of human bronchial epithelial cells that differ from the models available for paramyxovirus assembly and spread. In addition, I also performed studies of HMPV infection in a human airway epithelium (HAE) model that closely resembles the airway epithelium. Results from these studies revealed important insights in the mode of spread of HMPV within airway tissues. HMPV infection was concentrated at the apical side of tissues, which is in accordance to its localized infection in the respiratory tract. However,

in contrast to several other respiratory paramyxoviruses, release of HMPV particles at the apical side was inefficient. Furthermore, the actin cytoskeleton was involved in HMPV spread in HAE. We also identified a novel role for HMPV P, and for a paramyxovirus P protein, in membrane deformation at late stages of infection. These findings reveal novel features of late steps of HMPV replication and represent a step forward in our understanding of the mechanisms by which this respiratory pathogen can spread infection from cell-to-cell. We hypothesize that HMPV activates signaling pathways associated with the actin cytoskeleton to promote efficient spread within the human airway epithelium. Further investigation of the late stages of infection involving HMPV interaction with the actin cytoskeleton could contribute to the knowledge that is required for moving forward toward developing anti-HMPV treatments.

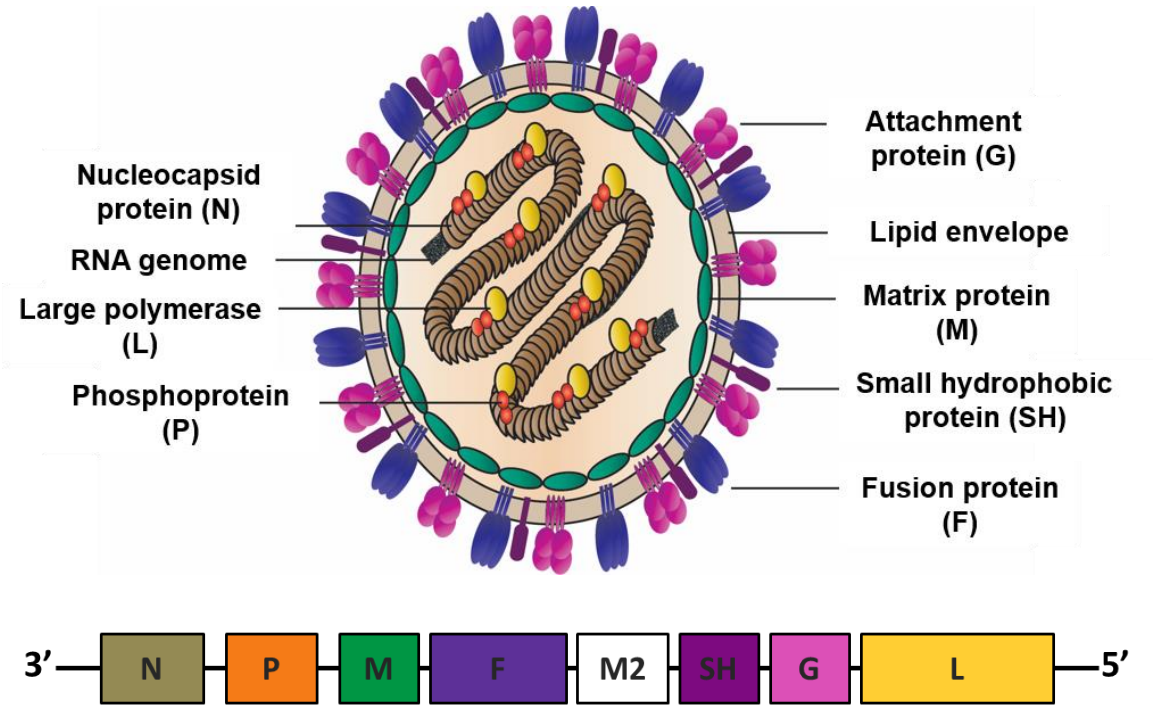

Figure 1.1 Schematic of a paramyxovirus particle.

The viral envelope, containing two main surface glycoproteins: fusion protein (purple) and attachment protein (magenta), surrounds the single stranded RNA genome (gray) which is encapsidated by the nucleocapsid protein (brown) and bound by phosphoprotein (orange) and the large polymerase protein (yellow). Underlying the membrane is a layer of matrix proteins (green). Some paramyxoviruses have an additional surface protein termed the small hydrophobic protein (SH). The RNA genome with the sequence of genes from the 3'end to the 5' end is depicted.

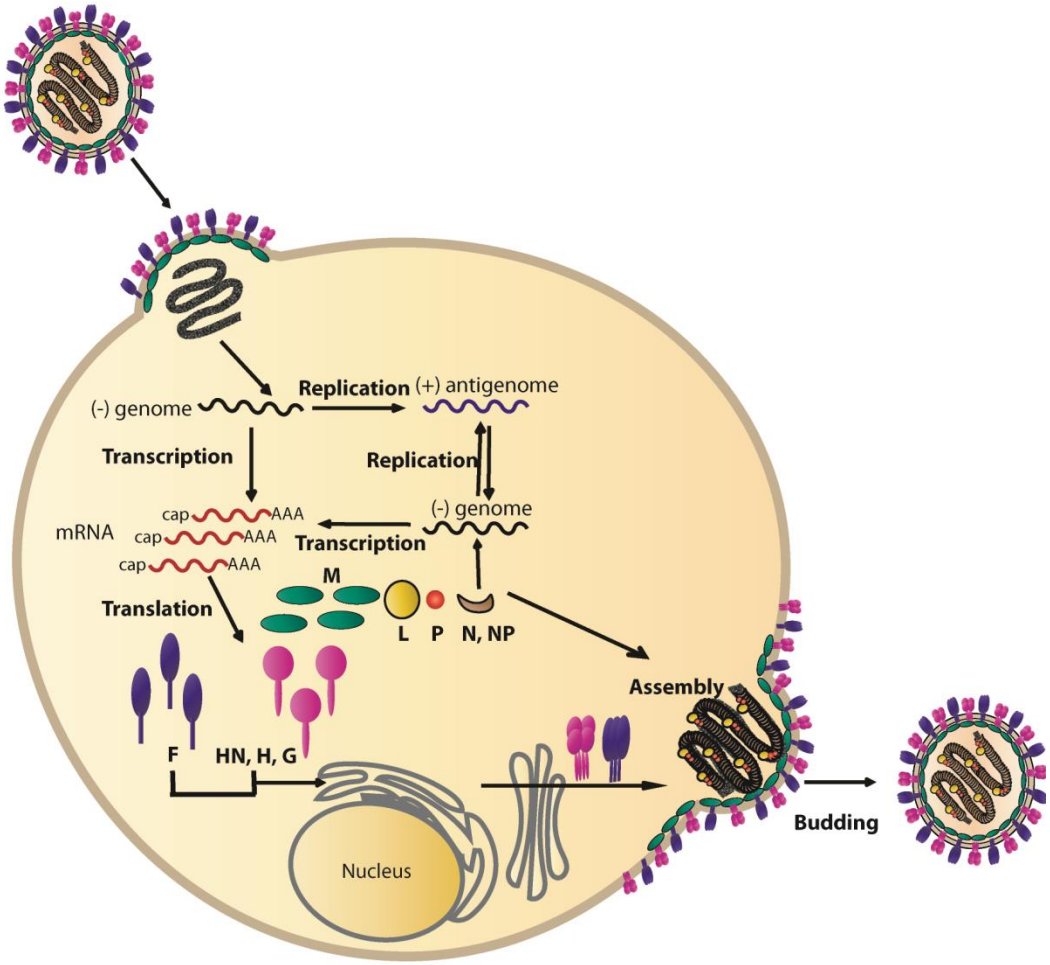

Figure 1.2. Schematic illustration of the life cycle of paramyxoviruses.

Transcription and replication of the viral genome occurs in the cytoplasm by the action of the viral RNA-dependent RNA polymerase. The newly synthesized viral components translocate to discrete sites at the infected cell plasma membrane where assembly and budding of infectious virus particles occur. For details, refer to text.

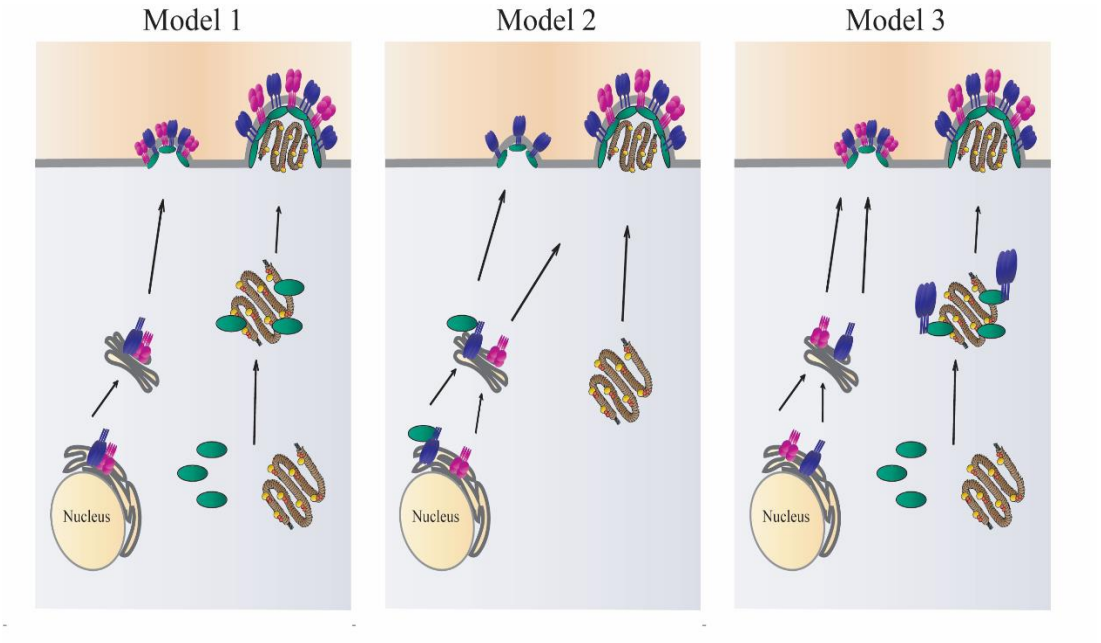

Figure 1.3. Models of paramyxovirus assembly.

Model 1: F protein and attachment protein are co-transported to the plasma membrane, and M associates with the RNP in the cytoplasm and carries it to the plasma membrane. Model 2: F protein and the attachment protein traffic separately to the cell surface, the RNP traffic by itself to assembly sites and is packaged within particles upon binding to M or one of the glycoproteins. Model 3: an assembly complex of F, M and the RNP core form in the cytoplasm and traffic to assembly sites. F protein shown in purple, attachment protein in magenta, M protein in green and the RNP complex in brown.

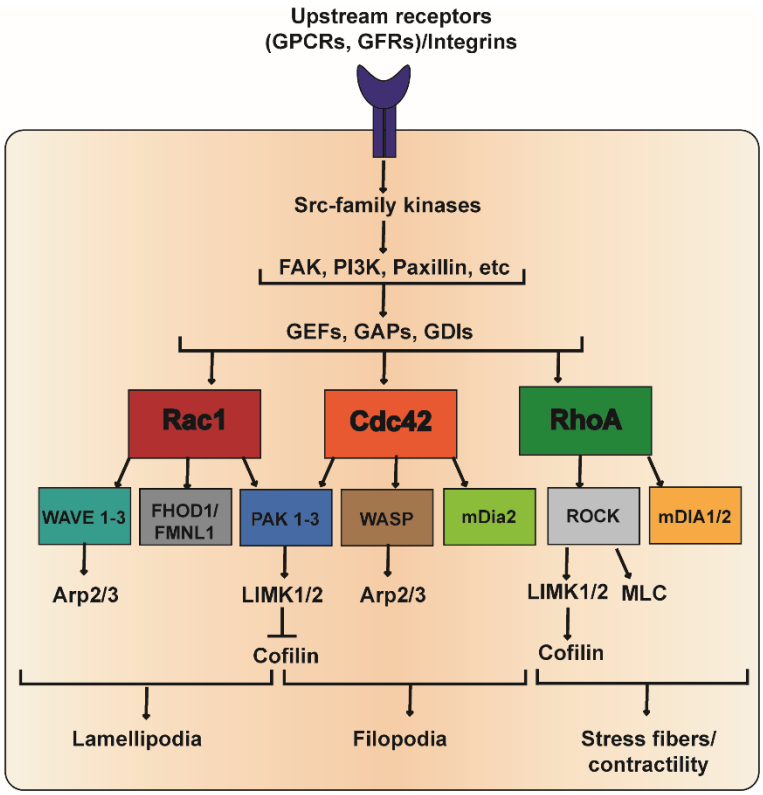

Figure 1.4. Rho-family GTPase signaling regulates actin dynamics.

Upstream signaling pathways modulate guanine nucleotide exchange factors (GEFs), GTPase-activating proteins (GAPs) and guanine nucleotide dissociation inhibitors (GDIs) which in turn regulate activity of Rac1, Cdc42 and RhoA. Rac1 activates WAVE/Arp2/3, the formins FHOD1 and FMNL1 and PAK/LIMK to promote lamellipodia formation. Cdc42 activates WASP/Arp2/3, PAK/LIMK and the formin mDia that contribute to filopodia formation. RhoA activates ROCK/LIMK, ROCK/MLC and mDIA1/2 to promote stress fiber formation and contractility.

CHAPTER 2: MATERIALS AND METHODS

Cell lines. BEAS-2B cells, obtained from ATCC, were grown in Bronchial Epithelial Cell Growth Medium (BEGM) containing all the recommended supplements (Lonza). 16HBE cells [223], kindly provided by Dieter C. Gruenert, University of California, San Francisco, were grown in Minimum Essential Medium w/ Earle's salt (Invitrogen) plus 10% fetal bovine serum (FBS) and 2mM L-glutamine (Invitrogen). A549 cells were maintained in Roswell Park Memorial Institute medium (RPMI; Lonza) supplemented with 10% FBS. COS-7 cells and Vero cells were grown in Dulbecco's modified Eagle's medium (DMEM; Gibco) supplemented with 10% FBS. CHO-K1 and pgsA745 cells, obtained from ATCC, and pgsD677, (provided by Jeff Esko, University of California, San Diego, CA) were grown in HyClone Ham's F-12, Kaighn's modification medium (Thermo Scientific, Waltham, MA) supplemented with 10% FBS.

Plasmids, antibodies and reagents. A codon optimized HMPV N gene in pCAGGS was kindly provided by Ursula J. Buchholz, (NIAID). The coding sequence for HMPV M was synthesized in a puc57 vector (Genetech, Arcade, NY) and subcloned into pCAGGS. Full length cDNA for HMPV P was amplified by RT-PCR from RNA isolated from HMPV CAN97-83 and cloned into pCAGGS. Antibodies for HMPV N protein (ab94801), P protein (ab94803) and F protein (ab94800) were obtained from ABCAM. A polyclonal antibody against the avian metapneumovirus C M protein, kindly provided by Sagar M. Goyal (University of Minnesota, Minneapolis, MN), which has been shown to cross-react with HMPV M, was used to detect HMPV M protein [160]. Filamentous actin was detected using phalloidin, and the antibody for tubulin was purchased from the Proteintech group (66031). A monoclonal Ab 12CA5 to the HA tag was obtained from Roche. Secondary antibodies conjugated with Fluorescein isothiocyanate (FITC) or Tetramethylrhodamine (TRITC) were obtained from Jackson ImmunoResearch. Drugs for disruption of the actin cytoskeleton or microtubules were purchased as indicated: cytochalasin D (C8273; Sigma), latrunculin A (428021; Calbiochem), jasplakinolide (sc-202191; Santa Cruz), paclitaxel (580556; Calbiochem), nocodazole (487928;

Calbiochem), rhosin (555460; Calbiochem), NSC 23766 (sc-204823; Santa Cruz), ML 141 (4266; Tocris), wiskostatin (681660; Calbiochem), and CK-666 (SML0006, Sigma).

Transient transfections. HMPV proteins N, P, F, M, SH-HA and SH-HA were transiently expressed using the mammalian expression vector pCAGGS [224]. Cells were transiently transfected with the plasmid DNA using lipofectmaine plus according to the manufacturer's protocol (Invitrogen, Carlsbad, CA).

Virus propagation and titer determination. HMPV and recombinant, green fluorescent protein (GFP)-expressing HMPV (rgHMPV) strain CAN97-83 (genotype group A2), kindly provided by Peter L. Collins and Ursula J. Buchholz (NIAID), were propagated in Vero cells or LLC-MK2. Cells were infected at a multiplicity of infection (MOI) of 0.02, incubated at 37ºC with Opti-MEM supplemented with 200mM of L-glutamine and 0.3µg/ml of L-1-Tosylamide-2-phenylethyl chloromethyl ketone (TPCK) trypsin with the trypsin replenished every day. After a period of 4-6 days, cells and media were collected and centrifuged at 2500 rpm for 15 minutes at 4 ºC on a Sorvall RT7 tabletop centrifuge. The supernatant was then subjected to centrifugation on a 20% sucrose cushion for 2 hours and a half hours at 135,000 x g 4°C using a SW28 swinging bucket rotor on a Beckman Optima L90-K ultracentrifuge. The pellet was resuspended in Opti-MEM and left at 4°C overnight. Aliquots of the samples were made the next morning and stored at -80°C. Titers of rgHMPV were determined by performing serial dilutions of the virus samples on a 96-well plate, incubation for 24 hours followed by counting the number of GFP positive cells. For determination of titers of non-GFP expressing HMPV, virus samples were subjected to serial dilution, 100µl of virus was added to LLC-MK2 cells, incubated at 37ºC for 1 hour followed by overlay with Opti-MEM containing 0.75% metylcellulose. After 4-5 days, cells were fixed in 10% formalin, incubated with anti-HMPV F antibody followed by a peroxidase-conjugated secondary antibody. Peroxidase substrate was added and plaques were then counted. To determine cell-associated virus titers, cells were scraped, 1x sucrose phosphoglycerate was added followed by three freeze-thaw cycles. For determination of titers of released virus, cell culture media was collected, centrifuged at 2,500 rpm for 15 min at 4°C on a Sorvall RT7 tabletop

centrifuge followed by centrifugation on a 20% sucrose cushion at 135,000 x g and 4°C for 2 hours and 30 minutes using a sw41 swinging bucket rotor on a Beckman ultracentrifuge

HMPV purification by sucrose density gradient centrifugation for mass spectrometry analysis. BEAS-2B cells were mock infected or infected with HMPV and virus propagation was performed as described above. Cell culture media was collected and centrifuged at 2500 rpm for 15 minutes on a Sorvall RT7 tabletop centrifuge. The supernatant was then subjected to centrifugation on a 20% sucrose cushion for 2 and a half hours at 135000 x g, 4°C using a SW28 swinging bucket rotor on a Beckman Optima L90-K ultracentrifuge. Virus pellets were then resuspended in 1x Tris-sodium-EDTA (TNE) buffer, layered onto a 30%-45%-60% (weight/volume) discontinuous sucrose gradient and centrifuged at 35000rpm for 90 minutes at 4ºC. The band containing the virus at the 30%-45% interface was collected and centrifuged on a 30% to 60% continuous sucrose gradient for 18 hours at 35000rpm and 4ºC. The virus-containing band was pelleted on a 20% sucrose cushion. The pellet was resuspended in 1x TNE buffer and centrifuged at 400 x g for 10 minutes using an Amicon Ultra Filter Unit 100 000 to get rid of low molecular weight contaminants. The ultrapure virus was then subjected to mass spectrometric analysis. Analysis was also done on virus propagated in COS-7 cells and purified as mentioned above.

Mass spectrometry for detection of HMPV-associated cellular proteins. Mass spectrometry analysis was performed by Jing Chen**.** The virus solution was denatured with 8M urea and subjected to dithiothreitol reduction and iodoacetamide alkylation. The sample was then diluted to a 2M final concertation of urea and digested in-solution with trypsin. The tryptic peptides were subjected to shot-gun proteomics analysis as previously described [225]. LC-MS/MS analysis was performed using an LTQ-Orbitrap mass spectrometer (Thermo Fisher Scientific, Waltham, MA) coupled with an Eksigent Nanoflex cHiPLC™ system (Eksigent, Dublin, CA) through a nano-electrospray ionization source. The peptide samples were separated with a reversed phase cHiPLC column (75 μm x 150 mm) at a flow rate of 300 nL/min. Mobile phase A was water with

0.1% (*v*/*v*) formic acid while B was acetonitrile with 0.1% (*v*/*v*) formic acid. A 50 min gradient condition was applied: initial 3% mobile phase B was increased linearly to 40% in 24 min and further to 85% and 95% for 5 min each before it was decreased to 3% and re-equilibrated. The mass analysis method consisted of one segment with eight scan events. The 1st scan event was an Orbitrap MS scan (300-1800 m/z) with 60,000 resolution for parent ions followed by data dependent MS/MS for fragmentation of the 7 most intense ions with collision induced dissociation (CID) method. For identifying host proteins in purified HMPV particles, the LC-MS/MS data were submitted to a local mascot server for MS/MS protein identification via Proteome Discoverer (version 1.3, Thermo Fisher Scientific, Waltham, MA) against Homo sapiens (human) taxonomy subset of Swissprot database. Typical parameters used in the MASCOT MS/MS ion search were: trypsin digest with maximum of two miscleavages, cysteine carbamidomethylation, methionine oxidation, a maximum of 10 ppm MS error tolerance, and a maximum of 0.8 Da MS/MS error tolerance. A decoy database was built and searched. Filter settings that determine false discovery rates (FDR) are used to distribute the confidence indicators for the peptide matches. Peptide matches that pass the filter associated with the strict FDR (with target setting of 0.01) are assigned as high confidence. For MS/MS ion search, proteins with two or more high confidence peptides were considered unambiguous identifications without manual inspection. Proteins identified with one high confidence peptide were manually inspected and confirmed.

Immunofluorescence and confocal microscopy. Cells grown in 6-well plates or 35 mm dishes containing coverslips were infected with HMPV and at various times post infection, cells were washed in phosphate buffer saline (PBS) and fixed in 4% paraformaldehyde for 15 minutes at room temperature. Cells were then permeabilized in 1% Triton X-100 for 15 minutes at 4°C followed by blocking in 1% normal goat serum and incubation with the corresponding primary antibody overnight at 4°C. The following day, cells were washed with 0.05% tween-PBS, secondary antibodies were added, and cells were incubated at 4°C for one hour. Coverslips were then mounted on glass slides using Vectashield mounting media (Vectorlabs, Burlingame, CA). Pictures were taken using a Nikon 1A confocal microscope and analyzed with the NIS-Elements software.

All images were processed in Adobe Photoshop, with equivalent adjustments made to all panels.

Immunostaining for Stochastic Optical Reconstruction Microscopy (STORM). BEAS-2B cells grown in glass bottom 35mm dishes were fixed in 3% paraformaldehyde for 15 minutes followed by reduction in 0.1% sodium borohydride (NaBH4) for 7 minutes at room temperature. Cells were then washed three times with PBS, five minutes per wash while shaking, and permeabilized in 0.2% Triton X-100 for 15 minutes prior to blocking in 10% NGS/0.05% Triton for 90 minutes at room temperature. Primary antibodies diluted in 5% NGS/0.05% Triton were then added and incubated for 60 minutes followed by washing five times in 1%NGS/0.05% Triton and incubation with the secondary antibody for 30 minutes. Washes using 1%NGS/0.05% Triton was then performed for five times followed by post fixation in 3% PFA for 10 minutes, three washes with PBS and two washes with distilled water. Cells were stored at 4°C until imaging using a Nikon Super Resolution Microscope N-STORM and image processing was performed using NIS-elements software.

Co-culture assay for direct cell-to-cell-spread of HMPV. BEAS-2B cells were infected with rgHMPV at an M.O.I. of 1 for 48 hours and then incubated with 7μM of cell tracker orange CMRA (Life Technologies, # C34551) for 30 minutes at 37ºC, 5% CO2. Cells were then washed 5 times with PBS to remove any bound virus particles, lifted up with trypsin and added to uninfected BEAS-2B target cells at a ratio of 1:1.Neutralizing antibodies, DS7 and 54G10, were then added and cells incubated for additional 24 hours. Afterwards, cells were collected, fixed in 1% formaldehyde and analyzed by flow cytometry. Direct cell-to-cell spread was defined as the percentage of GFP-only positive cells normalized to percentage of double positive (GFP/cell tracker CMRA orange) donor cells. To test the role of heparan sulfate in direct cell-to-cell spread of HMPV, BEAS-2B donor cells were infected and stained with cell tracker orange CMRA as mentioned above and incubated with CHO, pgsD677 or pgsA745 cells at a ratio of 1:1 and co-cultured for 24 hours.

Flow Cytometry Analysis. For determination of percentage of target cells infected in the coculture assay, cells were fixed in 1% formaldehyde diluted in PBS with 50mM EDTA, and analyzed with a BD FACSCalibur (BD, Franklin Lakes, NJ). Expression of GFP and cell tracker CMRA orange of at least 50,000 cells was determined and data analysis was performed using BDFACS software (BD Biosciences). The percentage of GFP-expressing cells was normalized to percentage of double positive donor cells in each condition followed by normalization to control samples.

Infection of Human Airway Epithelium (HAE) tissues. Human tracheal bronchial differentiated airway (Epiairway) tissues were purchased from MatTek (Ashland, MA) and maintained in 5ml of AIR-100 media at 37°C for one week prior to infection, with the media changed and apical surface washed with 0.9% NaCl every other day to remove mucus. Prior to infection, the apical surface was washed three times with 200µl of HBS buffer supplemented with 75 µg/ml of lysophosphatidylcholine, each wash for 10 minutes, and 1 ml of HBS was added to basolateral side and left for 30 minutes. Tissues were then infected at the apical or basolateral side with HMPV or rgHMPV for 2 hours at 37°C while shaking every 15 minutes. Tissues were then washed once with HBS and incubated in 5ml of media containing 0.5 µg/ml TPCK-trypsin at 37°C. Images were taken daily using a 5x objective of a Zeiss Axiovert 100 microscope. For determination of percent infection, tissues were washed once with PBS, followed by a wash in 7 mM EDTA and incubation in trypsin for 15 minutes at room temperature. Cells were collected with DMEM, filtered through a 70 µM nylon mesh and centrifuged at 200g for 5 min. Cells were then resuspended in a 1% formaldehyde fixation solution and the percentage of GFP positive cells was determined by fluorescence-activated cell sorting (FACS) analysis. To prepare tissues for immunofluorescence, tissues were fixed in 4% PFA for 20 minutes at room temperature, removed from the plastic wells, embedded in Optimal Cutting Temperature (OCT) and frozen on dry ice prior to sectioning using a microtome cryostat. Sections were permeabilized in 0.5% Triton for 15 minutes at room temperature and processed for immunofluorescence as described above.

Cell shedding. Cell shedding at the apical surface of HAE was quantified by determining the amount of dsDNA using the Quant-It PicoGreen dsDNA kit (Invitrogen). Apical surfaces of HAE were washed with 150 µl of Opti-MEM for one hour at 37°C. Washes were then stored at –80°C until analysis. Samples were diluted 5-fold in 1x Tris-EDTA buffer, reagent was added following the manufacturer's instructions using a 96-well plate format and fluorescent intensity was measured on a SpectraMax Gemini XPS plate reader (Molecular Devices). The concentration of dsDNA for each sample was calculated based on fluorescence of a titrated dsDNA standard.

Western blot analysis for virus protein detection. Cells were lysed in 2x sodium dodecyl sulfate (SDS) loading buffer and homogenized using cell Qiashredders (QIAGEN # 79656) following the manufacturer's protocol. Lysates were then boiled for 10 minutes, loaded onto a 10% SDS-polyacrylamide gel, and proteins were transferred onto a polyvinyl difluoride (PVDF) membrane. Membranes were blocked in 5% nonfat milk in TBST and incubated with the indicated primary antibody followed by IRDye680-conjugated goat anti-rabbit antibody or IRDye800-conjugated goat anti-mouse antibody. Membranes were visualized using Odyssey infrared imagining system (Li-Cor Biotechnology, Lincoln, NE) and band intensities were quantified using ImageQuant TL (GE Healthcare, Piscataway, NJ).

Stellaris Fluorescent in situ hybridization (FISH) for viral RNA detection. 48 DNA probes targeting the HMPV vRNA genome between nt 1-5467 were obtained from BioSearch Technologies (Novato, CA) and designed using the software provided by the company. Each probe is 20 nt long and linked at the 3'end to Quasar 570 fluorophore. BEAS-2B cells grown in 8-well chamber slides were infected with HMPV at an MOI of 1. 24, 48 and 72 h.p.i, cells were fixed for 10 min with 4% PFA and then permeabilized overnight with 70% ethanol at 4°C. The next day cells were washed once with 2X SSC-10% formamide buffer, and then incubated overnight at 25°C in hybridization buffer (4X SSC, 1X Denhardt's solution, 150 µg/mL ssDNA, 2mM EDTA, 50% formamide in DEPC treated water) containing the probes at a concentration of 2.5 mM. After 24 hrs,

cells were washed two times for 20 min with 2X SSC-10% formamide buffer and slides were then mounted using Vectashield mounting media.

Proximity ligation assay (PLA). BEAS-2B cells grown on 10mm coverslips were mock infected or infected with HMPV at an M.O.I. of 2 and 24 h.p.i., cells were fixed with 4% PFA and permeabilized with 1% Trition X-100-PBS. Cells were then incubated in blocking solution at 37ºC for 2 hours. A mouse primary antibody for HMPV P and a rabbit beta actin antibody were added and incubated overnight at 4ºC. Proximity ligation assay was then performed using Duolink In Situ red mouse/rabbit kit (Sigma, DUO92101). PLA probes diluted 1:5 were added and cells were incubated for 1 hour at 37ºC in a humidified chamber and processed for ligation for additional 30 minutes at 37ºC. Cells were then washed twice, polymerase was added and DNA was amplified with a florescent substrate for 100 minutes at 37ºC. Coverslips were then mounted on glass slides using Vectashield and images were taken on a Nikon A1 confocal laser microscope. Images were processed and analyzed for total florescent intensity using BlobFinder software.

Electron microscopy on HAE. Mock or HMPV infected HAE were fixed in 2% PFA and & 1.25% glutaraldehyde overnight at 4 ºC. Tissues were then post-fixed in 1% osmium oxide followed by dehydration in graded ethanols. Resins were then added 2x and allowed to polymerize at 60ºC overnight. Araldite resins were used to tissues. Sections were then cut and cells were examined using a Hitachi 7100 transmission electron microscope.

Metabolic labeling and immunoprecipitation. Eighteen to twenty-four hours post-transfection, cells were starved in cysteine- and methionine- deficient DMEM media for 45 minutes followed by labeling in Tran^{35}S-label (100 μCi/ml; Perkin Elmer, Waltham, Massachusetts). To determine total expression of proteins, cells were labeled for the indicated time at 37°C and lysed immediately. Cells were then washed and lysed in radioimmunoprecipitation assay (RIPA) lysis buffer (100 mM Tris-HCl ,pH 7.4, 150 mM NaCl, 0.1% SDS, 1% Triton X-100, 1% deoxycholic acid) containing 0.15 M NaCl and

supplemented with protease inhibitors. Lysates were then clarified by centrifugation at 136,000xg for 15 minutes at 4°C and supernatants were immunoprecipitated with anti-peptide sera to the F protein or monoclonal Ab 12CA5 to the HA tag and protein-A conjugated sepharose beads. Immunoprecipitated proteins were analyzed on 10% sodium dodecyl sulfate-polyacrylamide gel electrophoresis (SDS-PAGE) and visualized using the Typhoon imaging system (Amersham Biosciences/GE Healthcare Life Sciences, New Jersey). ImageQuant TL (GE Healthcare, Piscataway, NJ) was used to determine band densitometry.

Cell permeability test. COS-7 or Vero cells were transfected using Fugene 6. The day after transfection, cells were starved in Cys-Met-DMEM in the presence or absence of 500 μg/ml hygromycin B (Sigma) for 45 min. Cells were subsequently labeled with Tran^{35}S for 1, 2, or 3 h in the presence or absence of 500 μg/ml hygromycin B. After being labeled, the indicated proteins were immunoprecipitated as described above.

Cell cytotoxicity test. Vero or COS-7 cells were plated in a 96-well plate to allow processing of quadruplicate samples. The following day, cells were transfected with HMPV F, SH-HA, or HA-SH (empty vector as the control). The next day, cells were washed and a mix of 80 μl of Opti-MEM and 20 μl of cell titer solution was added according to the manufacturer's instructions (Promega, Madison, WI). The absorbance of each well was measured every 10 min using μQuant (Bio-Tek Instruments Inc., Winooski, VT) until the optical density (OD) reached 1.0.

Cell tracker staining. COS-7 cells were transfected using Fugene 6. Twenty-four hours posttransfection, cells were washed once with PBS and incubated with 10 μM CellTracker green 5-chloromethylfluorescein diacetate (CMFDA) (Molecular Probes) in prewarmed culture medium for 45 min at 37°C. After incubation, the staining solution was removed and the cells were washed once with culture medium and incubated for an additional 30 min at 37°C. Cells were then washed with PBS, fixed with 3.7% formaldehyde for 15 min at room temperature, and processed for immunofluorescence as

described below. A secondary goat anti-mouse antibody conjugated with tetramethyl rhodamine isocyanate (TRITC) was used to detect HA-tagged HMPV SH protein.

CHAPTER 3: HMPV INDUCES REMODELING OF THE ACTIN CYTOSKELETON FOR DIRECT CELL-TO-CELL SPREAD OF VIRUS PARTICLES

Introduction

Human metapnemovirus (HMPV) is a major cause of acute upper and lower respiratory tract infections worldwide [12,21-25]. HMPV was originally identified in 2001 in patients with symptoms similar to human respiratory syncytial virus (HRSV) infection [2]. Since its initial report, studies have shown that HMPV has been circulating in human populations for more than 50 years [26,27]. Between 5 and 20% of hospitalization rates due to respiratory infections in young children are caused by HMPV and it is generally considered as the second or third cause of severe respiratory diseases in this age group [32,33]. HMPV is also a significant cause of morbidity and mortality in immunocompromised and elderly populations [31,34] and a recent report indicated that hospitalization rates for HMPV infection in older adults are similar to those of influenza infections [35] . Clinical presentation of HMPV infection can range from cough, fever, rhinitis and wheezing to more severe infections including bronchiolitis, croup, asthma exacerbation, and pneumonia, and disease severity may be increased by co-infection with other respiratory pathogens [37-43]. Currently, there are no specific antiviral treatments or vaccines for HMPV infections, and ribavirin and monoclonal antibodies to the virus have been shown to have marginal anti-HMPV activity, so the only form of treatment is supportive [226,227].

HMPV is a member of the Paramyxoviridae family, genus *Pneumovirinae,* which includes enveloped viruses with a negative sense, single stranded RNA genomes. HMPV particles, similar to other paramyxoviruses, are highly pleomorphic in shape with both spherical and filamentous morphologies reported [2,12,34]. The HMPV genome is approximately 13,000 nucleotides in length and encodes for three surface glycoproteins: the fusion protein (F), the attachment protein (G), and the small hydrophobic protein (SH) that are densely packed on the viral envelope; a matrix protein (M), and five proteins that are associated with the RNA genome: nucleocapsid protein (N),

phosphoprotein (P), large polymerase protein (L), M2-1 and M2-2 proteins. Paramyxovirus infection is initiated upon fusion of the viral membrane with a host cell membrane, which is driven primarily by the F protein [228,229]. The entire replication cycle occurs in the cell cytoplasm and the newly synthesized virus components are transported to specific sites at the plasma membrane where assembly occurs followed by release of progeny virions from the infected cell into the extracellular matrix to spread infection [82,230,231]. Studies on the molecular aspects of HMPV infection over the past decade resulted in a better understanding of the mechanisms of entry and fusion of this pneumovirus [232-234]. However, the late stages in the replication cycle during which viral components assemble and exit the cell are not well understood. Efficient production of infectious particles involves coalescence of internal viral components including the viral genome, its associated proteins and the M protein with the integral membrane surface glycoproteins. The HMPV M protein, similar to other paramyxovirus M proteins, has been shown to play an essential role in production of virus particles and virus spread [160]. In addition, it has been demonstrated that formation of HMPV virus like particles (VLPs) occurs following co-expression of the F and M proteins, with the G protein enhancing this process, thus indicating an important role of these protein in the HMPV assembly process [10,233]. Assembly is followed by membrane budding and a scission process that allows release of particles into the extracellular matrix and spread of infection. Several enveloped viruses, including HIV and Ebola virus, and some paramyxoviruses such as mumps virus, parainfluenza virus 5 and Newcastle disease virus, utilize components of the endosomal sorting complex required for transport (ESCRT) pathway to exit the cell [14,69,154,235]. However, HMPV and a number of other viruses, including influenza virus, RSV and measles virus, bud in an ESCRT independent manner [139,158,236,237]. Several reports indicated an important role of the actin cytoskeleton and microtubules in assembly and budding of paramyxovirus particles. Sendai virus and measles virus utilize microtubules to transport their ribonucleoproteins (RNPs) to the cell surface [137,138], and release of human parainfluenza virus 3 is dependent on microtubules [238]. The actin cytoskeleton was also shown to play an important role in assembly and budding of measles virus, Sendai virus, and RSV

[136,213,239]. The role of actin in Sendai virus budding was recently revealed where it was shown that M protein induces remodeling of both β- and γ-actin [239]

Although release and subsequent entry of free virus particles into a new target cell is considered the primary route of infection for enveloped viruses, a substantial body of evidence indicates that spread of a number of viruses can occur directly from cell-to-cell without diffusion through the extracellular environment. Viruses that can move directly for cell to cell include hepatitis C virus, rabies virus and several members of the herpesvirus, retrovirus, poxvirus families [216,240-249]. The mechanisms by which these viruses subvert cellular processes for cell-to-cell spread can vary substantially; however, one of the main mechanisms involved is manipulation of the cell cytoskeleton [197,218,250-252]. For paramyxoviruses, cell-to-cell spread of viruses independent of particle release occurs for measles virus across neuronal synapses and fusion pores in epithelial cells and for RSV through syncytia formation [253-257]. Recently, it was reported that influenza A virus and the paramyxovirus parainfluenza virus 5 (PIV5) can also spread directly between cells in a neutralizing antibody independent manner [258].

In this study, we sought to characterize the late steps of HMPV infection in human bronchial epithelial cells and to identify host factors critical to this stage of the replication cycle. We demonstrate that HMPV infection results in remodeling of the cell cytoskeleton leading to the formation of extensive branched networks of cell-associated virus filaments and stimulation of intercellular extensions where the major viral structural proteins and viral RNA localize. Our results indicate that active actin dynamics are critical for the formation of these structures since treatment of cells with actin depolymerizing or stabilizing drugs or targeted inhibition of the major regulators of actin dynamics, the Rho GTPases Rac1, Cdc42 and RhoA, decreased the formation of branched viral filamentous networks and intercellular extensions. We also show that microtubules play a role in elongation of intercellular extensions. Studies of HMPV spread in a co-culture assay revealed a novel mode of direct cell-to-cell spread of HMPV which, in contrast to cell-free infection, is independent of neutralizing antibodies and does not require heparan sulfate. Analysis of the involvement of the cell cytoskeleton in

direct cell-to-cell spread of HMPV showed a major role for an intact actin cytoskeleton, Cdc42, Rac1 and microtubules in HMPV spread in the co-culture assay, thus supporting the association of intercellular extensions and branched viral filamentous networks with enhanced intercellular spread. These results provide evidence for a novel mechanism by which HMPV utilizes the cell cytoskeleton for direct cell-to-cell spread.

Results

HMPV buds primarily as cell-associated filamentous networks

Production of paramyxovirus particles is generally a multistep process that occurs in the cytoplasm of an infected cell and culminates in the assembly of virus components at the plasma membrane followed by budding and release of infectious virus particles [82,230]. HMPV lacking the envelope proteins G and SH, has been shown to be infectious in vitro and in vivo [16,93] indicating that assembly of infectious HMPV particles does not require G and SH proteins. To investigate the late stages of the replication cycle of HMPV, we determined the cellular localization of the main viral structural proteins in human bronchial epithelial cells, BEAS-2B: the N and P proteins, which are bound to the viral genome and are part of the ribonucleoprotein (RNP) complex, the internal protein M, and the envelope F protein. By 18 h.p.i., viral proteins were primarily at the plasma membrane and in filaments protruding from the plasma membrane (white arrowheads, Figure 3.1A). In addition, P protein can be seen in discrete cytoplasmic structures or inclusion bodies (Figure 3.1A, 18 hpi, inset). Inclusion body formation has been associated with infection of a number of negative sense RNA viruses. The precise role of inclusion bodies in paramyxovirus infection is not well understood; however, some studies indicate the presence of RNA genome in these bodies suggesting that these are sites of active RNA replication [259-261]. Several respiratory viruses, including influenza virus, RSV and PIV3 form filaments at the plasma [9,262,263], and it was recently shown that HMPV VLPs bud as filamentous structures in LLC-MK2 cells [10]. However, interestingly, by 24 h.p.i., viral proteins were seen primarily in cell-associated branched filaments (red arrowhead, Figure 3.1A) that formed an extensive filamentous network between cells as infection progressed to 48 h.p.i. (Figure 3.1B). Viral proteins also localized in extensions that ran between infected cells, which we

termed intercellular extensions (Fig 3.1A. white arrows). These extensions were seen extending from opposite sides of a cell, indicating that they are not retraction fibers. Filaments containing viral proteins were also seen projecting from these intercellular extensions. Staining with the plasma membrane marker wheat germ agglutinin (WGA) showed that both intercellular extensions (arrow) and filaments (inset) are extensions of the plasma membrane (Figure 3.1C). To clearly differentiate between filaments and intercellular extensions, we measured the diameter of these–structures using ImageJ analysis tool. Intercellular extensions were thicker, ranging from 850 nm to 1840 nm, with an average diameter of 1.1 µm compared to 0.47 µm for the filaments with a range 252 nm to 660 nm (Figure 3.1D).

To further examine the structure of the filaments and intercellular extensions, super-resolution microscopy was performed using a STORM (Stochastic Optical Reconstruction Microscopy) imaging system. A cellular extension is seen protruding from the cell body (Figure 3.1E, arrow) with M and N localized throughout the length of the extension. M and N also localized in branched filaments protruding from the cell body and the cellular extension. An organized localization of M and N is seen within the filaments, with the N protein observed in the core of the filament surrounded by the M protein (Figure 3.1E, inset). Filamentous structures budding at the surface of cells infected with influenza virus and RSV were shown to be consistent with virus particles having a filamentous morphology termed viral filaments [262] . Thus, the organized localization of M and N in the branched filaments revealed by STORM suggests that these structures are associated with filamentous budding HMPV. Determination of HMPV titers at different hours post-infection showed that titers of cell-associated virus were 0.5 – 1 log higher than those of released virus particles throughout the infection period in BEAS-2B cells, indicating that HMPV is primarily cell associated (Figure 1E). Previous studies of HMPV infection in LLC-MK2 cells indicated that the virus was mainly cell-associated and that budding particles were filamentous [264,265]. However, the extensive branched networks and intercellular extensions visualized during HMPV infection in a more physiologically relevant model of human bronchial epithelial cells represent a new paradigm for paramyxoviruses.

Cell-associated branched HMPV filaments are actin based

Several respiratory viruses, including influenza virus, RSV and parainfluenza virus 2, form filaments at the plasma membrane; however very little is currently known about the mechanisms by which filamentous viruses assemble and their relevance to virus pathogenesis [9,95,262,266-268]. The process of virus budding depends on both viral products and cellular factors. Our results indicate that HMPV infection results in the formation of more complex filamentous structures at late stages of infection, but the factors responsible for their formation are unknown.

Change in the shape of the plasma membrane is regulated by the cell cortex which is composed mainly of F-actin, thus induction of membrane extensions should require reorganization of the cortical F-actin. In addition, recent studies indicate a role of microtubules in regulating the structure of cortical F-actin further contributing to plasma membrane dynamics [269]. Viruses can manipulate the cell cytoskeleton in fascinating ways at different stages of the replication cycle and a number of viruses, including retroviruses and alphaviruses, has been reported to induce formation of actin- or tubulin-based cellular extensions during their exit from the cell [270,271]. For paramyxoviruses, a role of actin has been described in the release of measles virus, RSV and Sendai virus, and microtubules were involved in release of PIV3 [136,138,207,213,238,239,264]. To determine the contribution of the cell cytoskeleton to the formation of the cell-associated branched filaments and intercellular extensions, infected BEAS-2B cells were co-stained for viral proteins and F-actin or tubulin. Both tubulin and F-actin co-localized with HMPV N (as well as with M, P and F (data not shown)) in budding viral filamentous networks (Figure 3.2A, inset). Tubulin and F-actin were also present in intercellular extensions (Figure 3.2A, arrows). The staining for N and F-actin was more intense in the intercellular extensions and branched filaments than in the cell body, while that of tubulin was faint in these structures. In addition, high resolution microscopy showed localization of actin (green) in a viral filament budding from the cell body (Figure 3.2B arrow) as well as in the branched filaments along with viral proteins M and P (red), respectively (Figure 3.2B arrowhead) indicating the close association of F-actin with the budding

structures in HMPV-infected cells. This is in contrast to what has been reported for RSV since F-actin was excluded from the viral filaments in RSV infected cells [272]. To further investigate if the formation of HMPV filamentous networks was dependent on actin or microtubules, cells were infected for 2 hours and then treated with either DMSO or with inhibitors of actin or microtubule dynamics until fixation at 24 h.p.i. Disruption or stabilization of microtubule polymerization using nocodazole or paclitaxel, respectively, did not prevent the formation of branching HMPV filamentous networks indicating that microtubule dynamics are not required for budding of cell-associated filamentous HMPV (Figure. 3.3A, arrows). In contrast, disruption of actin polymerization using cytochalasin D or latrunculin A or treatment of cells with jasplakinolide to stabilize actin filaments resulted in loss of the extensive filamentous HMPV networks seen in DMSO control treated cells (arrow), indicating an important role of active actin dynamics in the budding of the complex filamentous networks (Figure 3.3A). However, filaments containing HMPV N were seen in cells treated with cytochalasinD, latrunculinA and jasplakinolide (Figure 3.3A, arrowheads). Upon disruption of actin polymerization (cytochalasinD or latrunculinA), the filaments were smaller than in control DMSO cells, but they were in close proximity with intracellular actin (Figure 3.3A, cytochalasinD, inset). In cells treated with jasplakinolide, there was colocalization of N and F-actin in filamentous structures that were also different than those seen in control cells. The HMPV M, P and F proteins were seen in similar filaments upon inhibition of actin dynamics (data not shown). To obtain a quantitative measurement of the effect of the different inhibitors on the formation of branched filaments, we performed Scholl analysis on infected cells. This method of image quantitation is commonly used to measure the complexity of dendritic branching in neurons by creating concentric circles around the cell body and determining the number of intersections at a defined distance from the center of the cell body [273]. Consistent with the microscopic images, disruption of microtubules did not affect level of filamentous branching, whereas inhibition of actin dynamics prevented branching of filamentous networks (Figure 3.3B). STORM imaging showed intracellular filaments containing N and M in cells treated with cytochalasinD and the localization of N and M in these filaments resemble that of control cells (Figure 3.1E) with the N protein on the inside and M on the outside (Figure 3.3C). These

filaments can deform the plasma membrane since WGA staining showed deformation of the plasma membrane coinciding with budding filaments (Figure 3.3D). These observations indicate that assembly of HMPV into initial filamentous structures is driven primarily by viral proteins or other host factors but does not require actin polymerization. However, actin polymerization is required for efficient budding of HMPV filamentous networks from the plasma membrane.

A role actin in HMPV infection cycle was further supported by the detection of large amounts of actin in ultrapurified HMPV particles by mass spectrometry (Table 1). Briefly, HMPV was propagated in BEAS-2B cells, cell culture media containing released virus particles was then collected, purified by discontinuous and continuous sucrose gradients and analyzed by LC-MS/MS. To confirm that the cellular proteins detected in the purified HMPV particles are specific and are not contaminants from released exosomes, we performed the same purification steps on media collected from uninfected cells. As seen in Table 2, mostly keratin was detected in supernatants collected from mock infected cells and actin was present in very small amounts (total number of peptides is 2). However, actin was detected in high amounts in purified HMPV (more than 20 peptides). In addition, several other actin associated proteins, including actinin and myosin were present in purified HMPV further supporting the involvement of actin in the formation of HMPV particles. Tubulin, vimentin and other cytoskeleton associated proteins were also found suggesting their involvement in HMPV replication (Table 1).

HMPV-induced elongation of intercellular extensions requires active actin and microtubule dynamics

Intercellular extensions have been identified as a means of intercellular communication in different cell types and research over the past decade has provided important information on their nature and function [274,275]. These cellular structures, sometimes termed cytonemes or tunneling nanotubes depending on their function and composition, are–membrane bridges that contain actin, and in some cell types also microtubules. It has been previously demonstrated that primary human bronchial

epithelial cells can form bridges between individual cells. These bridges were found to contain both F-actin and microtubules, and varied greatly in their length (range 50 µm - 1 mm) and diameter (1 µm - 20 µm) [276]. Our results demonstrate that both F-actin and tubulin were detected in intercellular extensions containing HMPV proteins and staining with the plasma membrane marker wheat germ agglutinin showed that they are extensions of the plasma membrane (Figure 3.2A, Figure 3.3C). To determine whether the intercellular extensions observed in HMPV-infected BEAS-2B cells are induced or altered by HMPV infection, mock infected cells were stained for F-actin. Intercellular extensions were seen in uninfected cells (Figure 3.4A); however, the percentage of cells with intercellular extensions significantly increased upon HMPV infection indicating that these cellular structures exist in non-infected cells but HMPV infection induce their formation (Figure 3.4B). In addition, quantification of the length of the intercellular extensions showed that while extensions in uninfected cells averaged 40 µm, the majority of extensions in HMPV-infected cells were longer, with the average length in HMPV-infected cells of 80 µm, double that in uninfected cells (40 µm) (Figure 3.4C). To investigate the role of actin and microtubules in the formation of these intercellular extensions in HMPV-infected BEAS-2B cells, inhibitors of cytoskeleton dynamics were added 2 hours after infection and left on cells until fixation at 24 h.p.i.. The formation of intercellular extensions was not blocked by addition of nocodazole or paclitaxel indicating that microtubule dynamics are not required for the formation of intercellular extensions (Figure 3.4D and 3.4E, arrows). Inhibition of actin polymerization by cytochalasin D and stabilization of actin by jasplakinolide significantly reduced formation of intercellular extensions in infected cells (Figure 3.4E). Figure 3.4D shows the majority of cells treated with actin drugs lacking intercellular extensions. Thus, even though both tubulin and F-actin are present in intercellular extensions, only actin polymerization is essential for intercellular extension formation Collectively, these results indicate that HMPV can induce actin reorganization to induce elongation of intercellular extensions and that the formation of intercellular extensions seen in HMPV-infected cells depends on actin polymerization.

Rho GTPases involved in actin remodeling are involved in the formation of actin-based structures induced by HMPV infection

The actin cytoskeleton is highly dynamic and is under the control of complex signaling pathways involving three main Rho family GTPases, Cdc42, Rac1 and RhoA. Activation of Cdc42, Rac1 and RhoA results in formation of protrusive filopodia, lamellipodia and stress fibers, respectively [277,278]. To address the role of these signaling pathways in the co-opting of the actin cytoskeleton during HMPV infection, we utilized cell permeable, targeted inhibitors for these GTPases and assessed the effects on the budding of branched filamentous networks and on formation of intercellular extensions. DMSO or inhibitors were added to cells 2 h.p.i. and 22 hours later, cells were fixed and stained for F-actin to visualize changes in the actin cytoskeleton and N protein. Inhibition of Cdc42 (ML141) resulted in a dramatic loss of filamentous structures at the cell periphery compared to control cells and N was mostly cytosolic with faint staining in the cellular extension (Figure 3.5A, ML-141 arrowhead). In cells that were treated with the Rac1 inhibitor (NSC-23766), N was localized in intercellular extensions, and short filaments were seen protruding from the main extension (Figure 3.5A, NSC-23766, arrow). Upon inhibition of RhoA, N had a punctate localization pattern in the intercellular extension (Figure 3.5A, rhosin arrowhead) and in some cells, short branched filaments were seen (Figure 3.5A, rhosin arrowhead). These observations indicate that inhibition of the three GTPases did not prevent intercellular extension formation, contrary to what we saw with disruption of actin dynamics (Figure 3.3); however inhibition of all three Rho GTPases resulted in a significant decrease in the percentage of infected cells with extensions compared to DMSO treated cells, with inhibition of Cdc42 and Rac1 having a higher effect than RhoA inhibition (Figure 3.5B). This suggests that induction of these extensions in HMPV-infected cells involves activation of the Rho family GTPases signaling pathways that control actin dynamics in the cell. In addition, inhibition of RhoA and Rac1 resulted in partial budding of filaments whereas inhibition of Ccdc42 drastically decreased formation of branched filaments (Figure 3.5A). Equivalent to what was seen in microscopic imaging, inhibition of all Rho GTPases resulted in decrease in the degree of branching compared to control cells (Figure 3.5C). The highest level of inhibition was seen for Cdc42 followed by RhoA and Rac1. Thus, these results indicate

that formation of HMPV branched filamentous networks and induction of intercellular extensions involves signaling pathways mediated by Cdc42, RhoA and Rac1, although to varying extents. Cdc42 is essential for the formation of not only the filamentous networks but also budding of HMPV filaments suggesting an important role of Cdc42 in assembly. Rac1 is involved in the branching of filamentous networks but is not required for the assembly of filaments since short filamentous structures were observed in cells treated with the Rac1 inhibitor (Figure 3.5A, arrow, NSC-23766). Both Cdc42 and Rac1 are critical for induction of intercellular extensions which is consistent with their role in promoting actin polymerization required for extension formation. Treatment of cells with the RhoA/C inhibitor rhosin led to decrease in branching of filaments and reduction in extension length thus indicating a role of this GTPase in HMPV-induced actin remodeling. In addition, the effects of Rho GTPase inhibition on filament assembly is different from that of inhibition of actin polymerization indicating that actin by itself is not required for the assembly of HMPV filaments but rather other effectors of signaling related to regulation of actin dynamics are involved. Proteomic analysis of ultrapurified HMPV particles indicated the presence of Cdc42 and RhoA (Table 1) further suggesting their importance for the HMPV replication cycle. Our results thus suggest that coordination of activation of the three Rho GTPases, Rac1, Cdc42 and RhoA is involved in actin cytoskeleton rearrangement induced by HMPV to induce formation of intercellular extensions and budding of filamentous networks.

Intercellular extensions play a role in direct cell-to-cell spread of HMPV particles

Our data above indicate that HMPV infection results in elongation of existing intercellular extensions in BEAS-2B cells (Figure 3.4). To assess if these extensions are generally associated with HMPV infection or are specific for BEAS-2B cells, other cell types including 16HBEs (human bronchial epithelial cells), A549 cells and Vero cells were infected and cells were immunostained for the HMPV N protein and F-actin. Figure 3.6A shows that intercellular extensions containing HMPV viral proteins exist in these different cell types, indicating that utilization of these structures during HMPV infection is not restricted to BEAS-2B cells. The filamentous network of branching filaments was also seen in 16HBE cells (Figure 3.6A arrowhead) suggesting that formation of these structures may be common to human bronchial epithelial cells. In addition, extensions

were seen in live BEAS-2B cells extending from an infected cell to an uninfected cell (Figure 3.6B) confirming that they are not artifacts of immunofluorescence processing and that they are associated with live infection of HMPV. As seen in Figure 3.6B, extensions from infected cells are not always directed to the closest neighboring cells but can extend over long distances to reach another cell. Our results indicated that they can reach over 300 μm in length (Figure 3.4). Several viruses have been shown to induce the formation of cellular extensions as a mechanism of direct cell-to-cell spread of virus particles [197,216,250,251,258,279]. To determine the potential role of intercellular extensions on transmission of virus particles, we tested virus spread in the presence of a viscous methyl cellulose overlay media to prevent diffusion of cell-free virus particles. Cells were infected with a GFP-expressing HMPV (rgHMPV) and two hours later, infection media was removed and replaced with regular media or media with 1% methylcellulose and spread was monitored for a period of 5 days. HMPV spread, seen as GFP expressing cells (Figure 3.6C), occurred in the presence of methyl cellulose suggesting that HMPV can spread even when diffusion of released virus particles is compromised.

To verify that HMPV can spread directly from cell-to-cell, we developed a co-culture assay (Figure 3.7A). Cells were infected with rgHMPV (M.O.I. 2) for 48 hours and then stained with 7μM of the cell tracker orange CMRA dye for 30 minutes before lifting with trypsin. The infected donor cells were then added to unstained target cells at a ratio of 1:1 and 24 hours post co-culture, cells were collected and analyzed by flow cytometry. GFP-only positive cells represented the newly infected target cells. To test direct cell-to-cell spread of HMPV, cells were co-cultured in the presence of two neutralizing antibodies, DS7 and 54G10 targeted against the fusion protein. These antibodies have been shown to inhibit infection by cell-free HMPV particles [280,281]. Consistent with this, pre-incubation of HMPV with DS7 or 54G10 prior to addition to cells significantly inhibited cell-free infection of HMPV up to 90% (Figure 3.7B). However, inhibition of HMPV infection by the neutralizing antibodies was only approximately 60% under co-culture conditions, indicating that HMPV can spread in the presence of either DS7 or 54G10 and has a neutralizing antibody-independent mechanism

of infection. This finding is consistent with direct cell-to-cell spread of HMPV virus particles.

Previous work in our laboratory demonstrated that binding and entry of HMPV requires expression of heparan sulfate on the surface of target cells [232]. To determine whether spread of HMPV in the co-culture assay was dependent on heparan sulfate, we utilized CHO cells derivatives, psgD677 and pgsA745. pgsD677 cells lack N-acetylglucosaminyl- and glucuronosyl-transferase enzymes and are thus incapable of synthesizing heparan sulfate. pgsA745 cells lack all glycosaminoglycans (GAGs) due to mutation in the xylosyltransferase gene [282,283]. Consistent with previous studies, cell-free HMPV infection requires heparan sulfate (Figure 3.7C). However, HMPV efficiently infected target cells that lack heparan sulfate under co-culture conditions. These data combined with the results from the neutralizing antibodies strongly indicate that HMPV has two modes of infection: cell-free infection that is blocked by neutralizing antibodies and ~~is~~ requires binding to heparan sulfate moieties, and cell-to-cell infection that is neutralizing antibody- and heparan sulfate independent.

Intercellular extensions can transfer cellular components between cells including cytoplasmic materials, organelles, membrane proteins and signaling molecules [274,275,284]. To verify that the GFP expression in target cells was not due to passive diffusion of soluble GFP from infected donor cells to target cells, we performed the co-culture assay in the presence of cycloheximide to inhibit new protein translation and synthesis. Addition of cycloheximide diminished GFP expression in target cells indicating that active protein synthesis is required (Figure 3.7E).

We next determined the effect of the different cytoskeletal drugs, which interfered with the elongation of these extensions, on spread of HMPV in the presence of neutralizing antibodies. Infected donor cells were pretreated for one hour with the specific drug prior to incubation with naïve target cells and DS7 antibody was used for neutralization of released virus particles. Manipulation of microtubule dynamics by nocodazole or paclitaxel reduced intercellular spread of HMPV. Disruption of actin

polymerization with cytochalasin D, which dramatically decreased formation of intercellular extensions (Figure 3.4), resulted in a significant decrease in spread of HMPV (Figure 3.7D). Actin stabilization with jasplakinolide also led to a decrease in HMPV intercellular spread but to a lower extent. Interestingly, inhibition of both Rac1 (NSC-7366) and Cdc42 (ML-141) significantly reduced cell-to-cell of HMPV; however, inhibition of RhoA with the inhibitor rhosin did not influence intercellular spread of HMPV (Figure 3.7D). Thus, our results indicate that inhibition of actin polymerization, Cdc42 and Rac1, which result in significant decrease in the formation of intercellular extensions, also decrease intercellular spread of HMPV, indicating a role of the extensions in cell-to-cell of HMPV.

To further examine the role of intercellular extensions in HMPV spread, FISH for detection of viral RNA was performed. Viral RNA was detected in discrete cytoplasmic structures (Figure 3.8 arrowhead) that resemble the inclusion bodies where HMPV P localized (Figure 3.1A). Inclusion bodies have been detected for several paramyxoviruses and are thought to be sites of active RNA replication[259,285]. The detection of HMPV RNA in these structures further supports this hypothesis for paramyxovirus RNA replication. Viral RNA was detected in intercellular extensions in cells infected with rgHMPV (Figure 3.8 arrow). Interestingly, structures similar to replication bodies were seen in the extensions suggesting that they can be transported across intercellular extensions between cells (Figure 3.8 arrowhead). The localization of the main HMPV structural proteins N, P, M and F and of viral RNA in intercellular extensions provides additional evidence for the involvement of extensions in HMPV spread. Interestingly, structures similar to replication bodies were seen in the extensions suggesting that they can be transported across.

Discussion

As a recently discovered virus [2], several aspects of HMPV replication cycle are poorly understood. In this study we reveal two distinct features of late stages of HMPV infection that constitute a new paradigm for paramyxovirus assembly and egress from the cell. Similar to other respiratory viruses, we show that HMPV can form filamentous

structures at the surface of infected cells, however, the filamentous structures induced by HMPV are more complex than what has been previously reported for respiratory viruses, to date, where a complex network of branched filaments formed in infected cells that contained all major virus components. The budding of these structures was largely dependent on actin polymerization and on actin associated signaling involving Rho GTPases Cdc42, Rac1 and RhoA. In addition, we show a novel mode of HMPV transmission from cell-to-cell across intercellular extensions that occurs independent of heparan sulfate and neutralizing antibodies.

Formation of filamentous virus particles has been reported for several respiratory viruses including RSV and influenza virus [262,266-268]; however how these structures are assembled and their significance for viral infectivity is not well understood. For influenza viruses, the filamentous morphology of the virus depends on actin polymerization as disruption of actin largely inhibits formation of filamentous viruses [262]. Conversely, for RSV actin and tubulin were not required for assembly of viral filaments, but actin was involved in anchoring the filaments to the cell surface and for virus replication [286]. HMPV has been shown to form filaments in infected LLC-MK2 cells [10,264]. Here we show that HMPV assembles into a complex network of branched filaments at the surface of BEAS-2B cells (Figure 3.1A) and these structures were also seen in 16HBE cells (Figure 3.7A) indicating that these are specific features of HMPV infection in bronchial epithelial cells. Budding of the filamentous networks was dependent on actin polymerization and not on microtubules (Figure 3.3A); however the initial assembly of a filamentous structure that can deform membranes does not require intact actin (Figure 3.3B,C). HMPV M has been shown to self-assemble into higher order structures, forming flexible helical filaments upon binding to lipids, and it is thought that the dimer subunits of M can associate through different side-by-side interactions which influence that curvature of the matrix arrays and thus virus morphogenesis [287]. In addition, HMPV P protein can form tetramers [288]; thus it possible that self-oligomerization and assembly of viral proteins can drive the formation of filamentous structures that constitute assembly intermediates and that polymerization of actin is needed to further drive the assembly and budding of the extensive branched filaments.

However, as actin was seen in close proximity with the filaments (Figure 3.3 inset), actin may be playing an accessory role. Interestingly, our results indicate that the Rho GTPases involved in controlling actin dynamics and structure in the cell, Cdc42, Rac1 and RhoA play an important role in the production of branched filaments (Figure 3.5). Cdc42 is required for the assembly of filaments since inhibition of Cdc42 abolished formation of filaments in HMPV infected cells. Short filamentous structures were seen in cells treated with inhibitors of Rac1 and RhoA (Figure 3.5A) and inhibition of these two GTPases decreased filamentous branching (Figure 3.5B) indicating a role in promoting further budding of the filaments but not necessarily in the initial assembly. One of the common downstream effectors of Rac1 and Cdc42 is the Arp2/3 initiation complex which activates actin polymerization as well as formation of branched actin filaments. Inhibition of Arp2/3 also decreased formation of branched filaments and localization of HMPV N was mainly intracellular, similar to Cdc42 inhibition (Figure 3.5A). Cdc42 activates Arp2/3 via WASP, so a role of WASP still needs to be determined. Taken together, these results indicate that assembly of HMPV filamentous intermediates does not depend on actin polymerization but rather on actin-associated signaling regulated mainly by Cdc42, and budding of branched filaments requires actin polymerization, Rac1 and RhoA. Rho GTPases have been shown to be involved at different stages of the infection cycle of several viruses and both RhoA and Rac1 were shown to be involved in the formation of filamentous RSV particles, suggesting that both of these pneumoviruses may utilize similar cellular pathways during virus assembly and egress [263,272]. RhoA had a role in localization of RSV F to discrete locations at the plasma membrane and it had been previously demonstrated that localization of F at the cell surface is required for assembly of RSV filaments and for coalescence of other viral components indicating an important role of RhoA in cellular localization of F and F in filament assembly [95]. Rho GTPases have a large number of downstream targets, thus it remains to be investigated how the different Rho GTPases are affecting HMPV proteins and how they regulate the assembly and budding process of HMPV filamentous branches.

The formation of cell-associated branched networks in HMPV infected cells raises questions about their importance for HMPV infection. First, it remains to be determined whether HMPV buds and is released from the cell in the form of this complex networks of filaments. Budding in this form may provide stability of virus particles as they exit the cell and are released into the extracellular matrix. Electron microscopic images of purified HMPV show pleomorphic particles with both mostly spherical morphology and also filamentous forms [289]. Thus, whether the filamentous morphology is maintained after release of virus particles from BEAS-2B cells is not known. Recent electron tomography images of the closely related RSV show that the position of M protein under the plasma membrane drives the filamentous morphology of the particles but as some of the virus gets released, M no longer forms a layer under the plasma membrane and the filamentous form is lost [62]. In addition, since branched filaments were seen in human bronchial epithelial cells and not in other cell types (Figures 3.1 and 3.7) indicates the effect of cell origin on virus assembly, and thus the relevance of this form of branched HMPV filaments for infection in the airway epithelium remains to be addressed.

An increasing number of reports show that some enveloped viruses can transmit from cell-to-cell, and between hosts, in novel ways beyond release of individual virus particles into the extracellular matrix [245,250,257,258,279,290-293]. Viral induction or modification of cellular structures to allow cell-to-cell spread is an intriguing theme of several recent studies, and our work supports a model where HMPV infection induces intercellular extensions that are key elements in direct cell-to-cell spread of this respiratory virus. For paramyxoviruses, cell-to-cell spread of viruses independent of particle release occurs for measles virus across neuronal synapses and fusion pores in epithelial cells and for RSV through syncytia formation [253-257]. Recently, intercellular spread independent of neutralizing antibodies was reported for PIV5 [258]. These studies indicate that mechanisms of paramyxovirus spread can vary greatly and shift the more generally accepted mode of spread by single particle release to more complex models. Direct cell-to-cell transmission of virus particles overcomes the rate limiting step of diffusion of particles across the extracellular space and also provides a means by which particles can be transferred in a way that evades the immune response. Our data from the

co-culture assay indicate that HMPV particles can spread in a neutralizing antibody independent manner, and that spread is dependent on formation of intercellular extensions (Figure 3.7). Disruption of actin polymerization or influencing HMPV-induced elongation of intercellular extensions by Cdc42 and Rac1 inhibition decreased intercellular spread of HMPV (Figure 3.7B) indicating the involvement of these cellular structures in intercellular spread of HMPV. Formation of plasma membrane extensions by actin polymerization is driven mainly by activation of Rac1 and Cdc42 and their downstream effectors, and several viruses, including vaccinia virus and pseudorabies virus, induce actin-based cellular extensions by activating these signaling pathways [176,220]; however this is the first report of a paramyxovirus that depends on Rho GTPase signaling to induce actin-based cellular extensions for intercellular spread. Inhibition of RhoA did not affect cell-to-cell spread of HMPV relative to control cells. The effect of RhoA on HMPV cell-to-cell spread could be related to other effects of RhoA signaling on cell migration or cell-cell adhesion. In addition, the role of RhoA signaling in regulating actin dynamics is highly complex and involves several downstream effectors, including the actin binding proteins formins, cofilin as well as the ezrin/radixin/moesin (ERM) proteins that are the main regulators of the cell cortex by linking the cortical actin to the plasma membrane. In addition, RhoA contributes to membrane blebbing and can also alter microtubule dynamics [294,295]. Cofilin-1 and ERM proteins were detected in purified HMPV particles (Table 1), potentially indicating further the involvement of rhoA mediated signaling in HMPV infection. In addition, microtubules played an important role in HMPV spread (Figure 3.7D). For several RNA viruses, microtubules are involved in transport of the RNP complex to assembly sites at the plasma membrane [138], but this remains to be investigated for HMPV.

Several models currently exist for direct cell-to-cell spread of virus particles across cellular extensions [271]. Our results show that intercellular spread of HMPV does not depend on heparan sulfate and can evade neutralizing antibodies (Figure 3.7). In addition, vRNA rich structures that resemble inclusion bodies were seen traveling along the intercellular extension (Figure 3.8). This raises the possibility of whether intercellular spread of HMPV may not involve transfer of whole virus particles, but just the viral RNP complex. Intercellular spread independent of infectious particle production was suggested

for measles virus in epithelial cells and in neurons. Whether this can also occur with HMPV requires further investigation.

Collectively, our results show that HMPV infection involves manipulation of the actin cytoskeleton and actin-associated signaling resulting in the induction of two different structures, an extensive network of budding branched filaments and intercellular extensions that represent novel features for paramyxovirus assembly and spread.

*FISH experiments were performed by Nicolas Cifuentes and mass spectrometric analysis was done by Jing Chen.

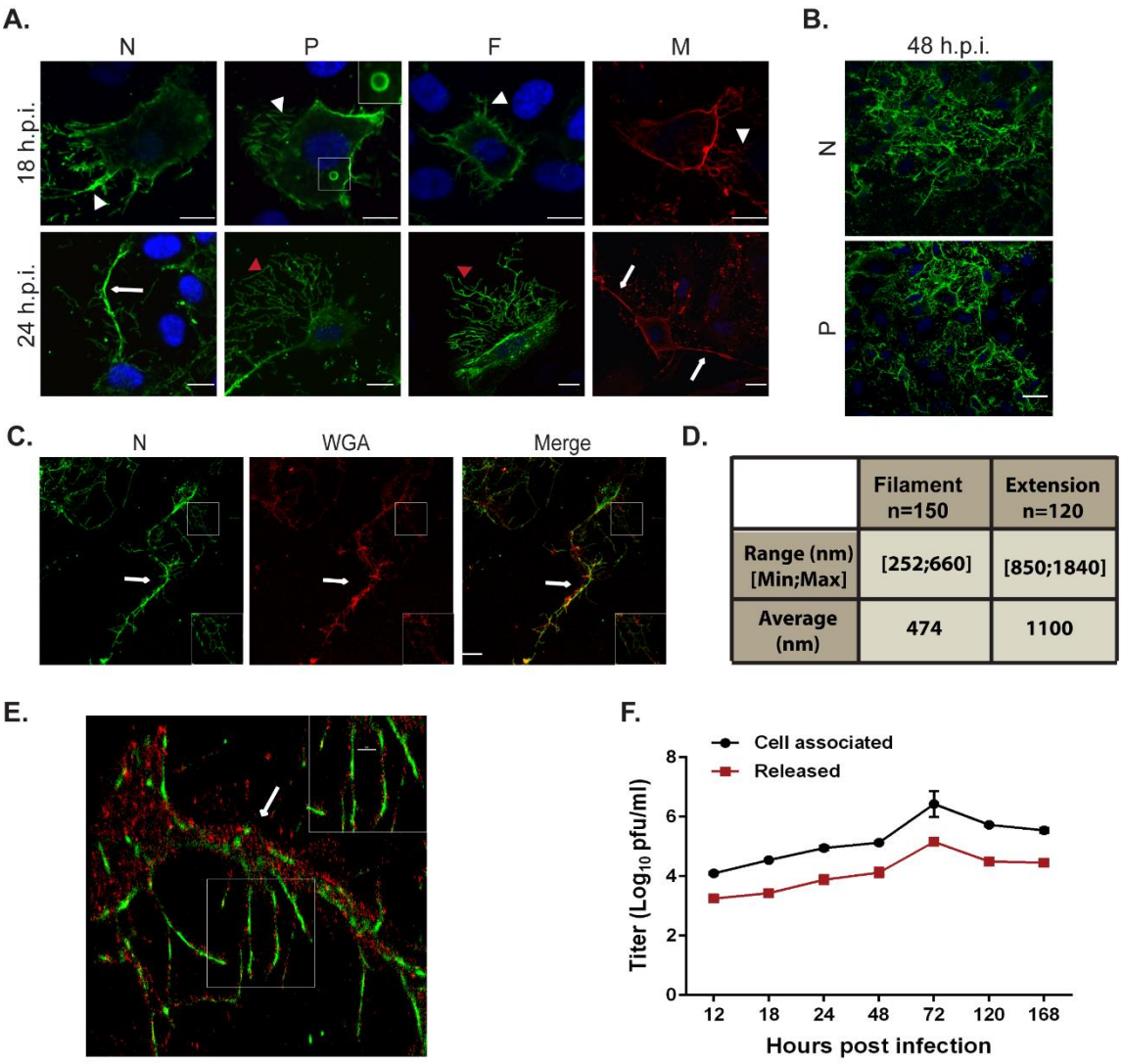

Figure 3.1. HMPV infection in BEAS-2B cells results in the formation of branched filamentous networks and intercellular extensions.

A) and B) Human bronchial epithelial airway cells, BEAS-2B, were infected with HMPV and at 24 h.p.i. (hours post infection) or 48 h.p.i., cells were fixed and processed for immunofluorescence staining. Images were taken using a Nikon CLSM. White arrows indicate intercellular extensions, red arrowheads indicate branched viral filaments and white arrowhead indicate viral filaments. . C) BEAS-2B cells were infected with HMPV at M/O.I. of 3 and at 24 h.p.i, cells were fixed and stained with the plasma membrane marker wheat germagglutinin or incubated with antibody for N. D) Cells were infected with HMPV for 24h, processed for Stochastic Optical Reconstruction Microscopy

(STORM) and stained with an anti-N antibody (green) and an anti-M antibody (red). Inset shows filaments with a central core of N protein surrounded by matrix protein. E) BEAS-2B cells were infected with rgHMPV at M.O.I. of 1 and at different times post infection, cells or culture media were collected and virus titers determined.

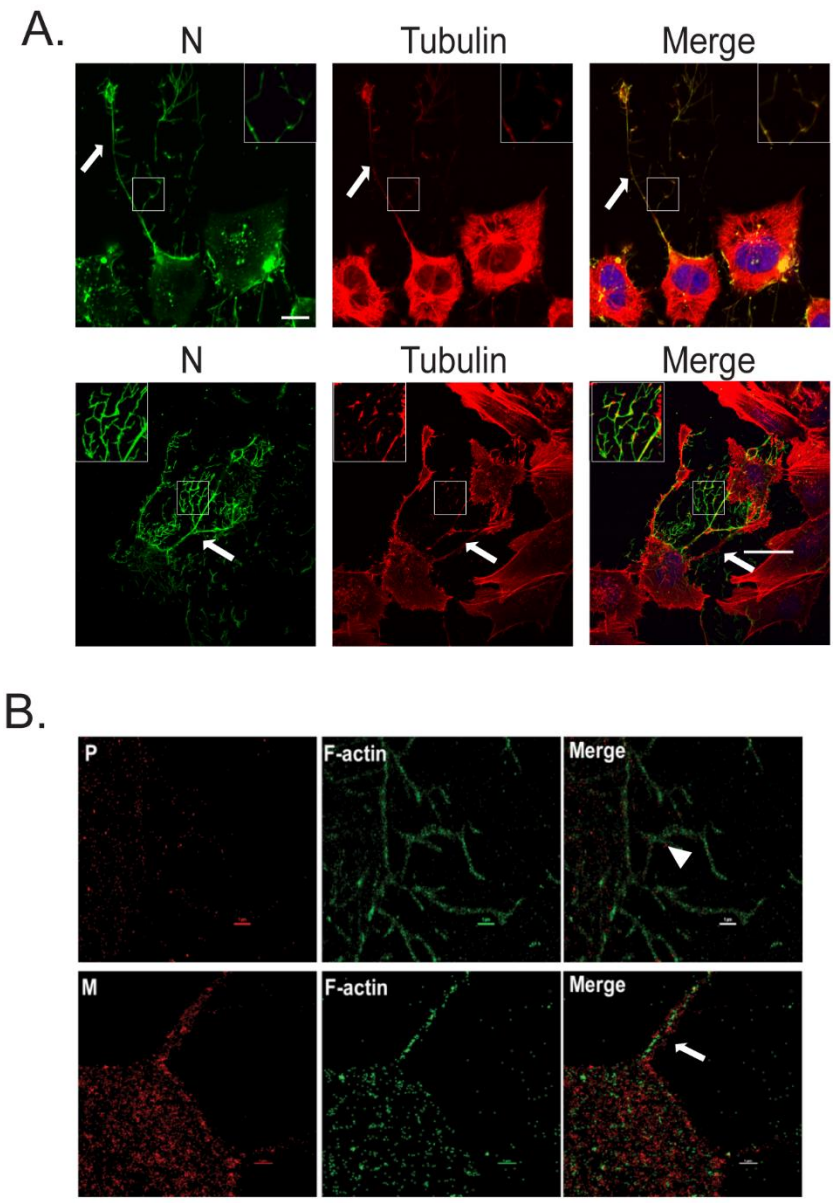

Figure 3.2. Actin and tubulin are present in intercellular extensions and branched filamentous networks.

A) BEAS-2B were infected with HMPV and 24 h.p.i. cells were fixed and stained for HMPV N, tubulin or F-actin. Inset shows colocalization of actin and tubulin with N in branched filaments. Arrows indicate intercellular extensions and insets show branched filaments. Scale bar = 50µm. B) Cells were infected with HMPV for 24h, processed for Stochastic Optical Reconstruction Microscopy (STORM) and stained with an anti-P or

anti-M antibody (red) and phalloidin (red). Arrow shows filament and arrowhead shows branched filaments.

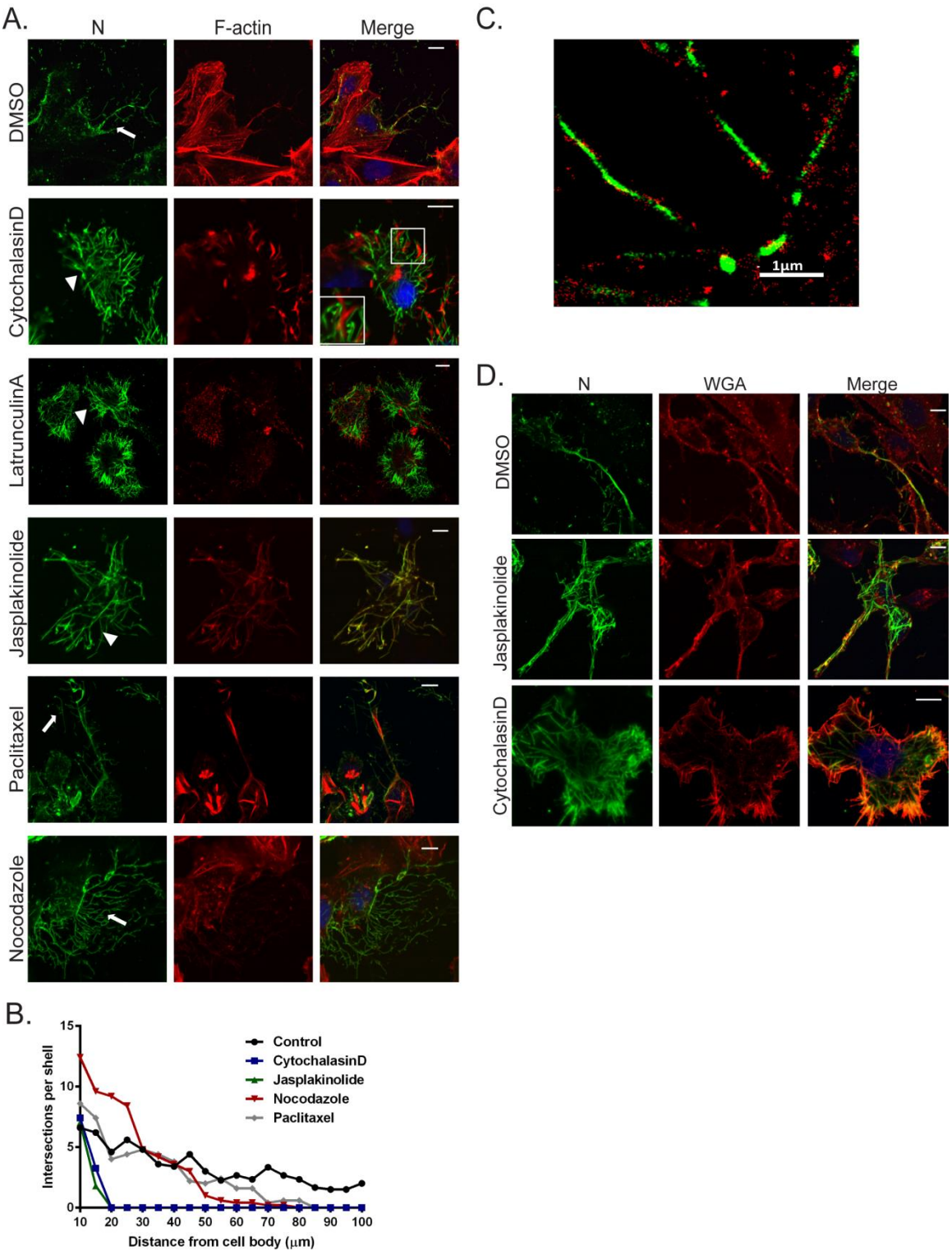

Figure 3.3. Actin and microtubules have different roles in formation of branched filamentous networks and intercellular extensions.

A) BEAS-2B, were infected with HMPV and 2 h.p.i. DMSO vehicle or drugs were added and cells were incubated for additional 22 hours. Cells were then fixed and processed for immunofluorescence staining. Arrows indicate branched filamentous network and arrowhead indicates viral filaments. . B) Cells were infected with HMPV for 2 hours and treated with cytochalasin D. 24 h.p.i. cells were processed for Stochastic Optical Reconstruction Microscopy (STORM) and stained with an anti-N antibody (green) and an anti-M antibody (red). C) BEAS-2B cells were infected with HMPV and drugs were added 2 h.p.i. and 24 h.p.i, cells were fixed and stained with the plasma membrane marker wheat germagglutinin (WGA) and antibody for N. Scale bars = 10μm.

Table 1: Protreomic Analysis of Purified HMPV Particles

Description, Human Protein	# Peptides
Actin, cytoplasmic 1 OS=Homo sapiens GN=ACTB PE=1 SV=1 - [ACTB_HUMAN]	28
Actin, cytoplasmic 2 OS=Homo sapiens GN=ACTG1 PE=1 SV=1 - [ACTG_HUMAN]	28
Annexin A2 OS=Homo sapiens GN=ANXA2 PE=1 SV=2 - [ANXA2_HUMAN]	23
POTE ankyrin domain family member E OS=Homo sapiens GN=POTEE PE=1 SV=3 - [POTEE_HUMAN]	11
Tubulin beta chain OS=Homo sapiens GN=TUBB PE=1 SV=2 - [TBB5_HUMAN]	26
Tubulin beta-2C chain OS=Homo sapiens GN=TUBB2C PE=1 SV=1 - [TBB2C_HUMAN]	25
Integrin beta-1 OS=Homo sapiens GN=ITGB1 PE=1 SV=2 - [ITB1_HUMAN]	29
Glyceraldehyde-3-phosphate dehydrogenase OS=Homo sapiens GN=GAPDH PE=1 SV=3 - [G3P_HUMAN]	19
Tubulin alpha-1B chain OS=Homo sapiens GN=TUBA1B PE=1 SV=1 - [TBA1B_HUMAN]	21
Tubulin beta-4 chain OS=Homo sapiens GN=TUBB4 PE=1 SV=2 - [TBB4_HUMAN]	22
Tubulin alpha-1C chain OS=Homo sapiens GN=TUBA1C PE=1 SV=1 - [TBA1C_HUMAN]	21
Tubulin beta-2B chain OS=Homo sapiens GN=TUBB2B PE=1 SV=1 - [TBB2B_HUMAN]	21
Tubulin beta-2A chain OS=Homo sapiens GN=TUBB2A PE=1 SV=1 - [TBB2A_HUMAN]	20
Putative annexin A2-like protein OS=Homo sapiens GN=ANXA2P2 PE=5 SV=2 - [AXA2L_HUMAN]	13
HLA class I histocompatibility antigen, A-1 alpha chain OS=Homo sapiens GN=HLA-A PE=1 SV=1 - [1A01_HUMAN]	11
HLA class I histocompatibility antigen, A-3 alpha chain OS=Homo sapiens GN=HLA-A PE=1 SV=2 - [1A03_HUMAN]	11
HLA class I histocompatibility antigen, A-11 alpha chain OS=Homo sapiens GN=HLA-A PE=1 SV=1 - [1A11_HUMAN]	11
HLA class I histocompatibility antigen, A-36 alpha chain OS=Homo sapiens GN=HLA-A PE=1 SV=1 - [1A36_HUMAN]	11
HLA class I histocompatibility antigen, B-57 alpha chain OS=Homo sapiens GN=HLA-B PE=1 SV=1 - [1B57_HUMAN]	11
HLA class I histocompatibility antigen, B-58 alpha chain OS=Homo sapiens GN=HLA-B PE=2 SV=1 - [1B58_HUMAN]	11
Actin, alpha cardiac muscle 1 OS=Homo sapiens GN=ACTC1 PE=1 SV=1 - [ACTC_HUMAN]	19
Tubulin alpha-1A chain OS=Homo sapiens GN=TUBA1A PE=1 SV=1 - [TBA1A_HUMAN]	20
Actin, alpha skeletal muscle OS=Homo sapiens GN=ACTA1 PE=1 SV=1 - [ACTS_HUMAN]	18
HLA class I histocompatibility antigen, A-24 alpha chain OS=Homo sapiens GN=HLA-A PE=1 SV=2 - [1A24_HUMAN]	12
HLA class I histocompatibility antigen, B-15 alpha chain OS=Homo sapiens GN=HLA-B PE=1 SV=2 - [1B15_HUMAN]	11
HLA class I histocompatibility antigen, B-46 alpha chain OS=Homo sapiens GN=HLA-B PE=2 SV=1 - [1B46_HUMAN]	10
HLA class I histocompatibility antigen, B-56 alpha chain OS=Homo sapiens GN=HLA-B PE=2 SV=1 - [1B56_HUMAN]	10
HLA class I histocompatibility antigen, B-53 alpha chain OS=Homo sapiens GN=HLA-B PE=1 SV=1 - [1B53_HUMAN]	10
HLA class I histocompatibility antigen, B-35 alpha chain OS=Homo sapiens GN=HLA-B PE=1 SV=1 - [1B35_HUMAN]	10
Actin, aortic smooth muscle OS=Homo sapiens GN=ACTA2 PE=1 SV=1 - [ACTA_HUMAN]	17
Pyruvate kinase isozymes M1/M2 OS=Homo sapiens GN=PKM2 PE=1 SV=4 - [KPYM_HUMAN]	15
4F2 cell-surface antigen heavy chain OS=Homo sapiens GN=SLC3A2 PE=1 SV=3 - [4F2_HUMAN]	16
Actin, gamma-enteric smooth muscle OS=Homo sapiens GN=ACTG2 PE=1 SV=1 - [ACTH_HUMAN]	16
Tubulin beta-3 chain OS=Homo sapiens GN=TUBB3 PE=1 SV=2 - [TBB3_HUMAN]	15
Sodium/potassium-transporting ATPase subunit alpha-1 OS=Homo sapiens GN=ATP1A1 PE=1 SV=1 - [AT1A1_HUMAN]	24
HLA class I histocompatibility antigen, A-23 alpha chain OS=Homo sapiens GN=HLA-A PE=1 SV=1 - [1A23_HUMAN]	11

Tubulin alpha-4A chain OS=Homo sapiens GN=TUBA4A PE=1 SV=1 - [TBA4A_HUMAN]	14
HLA class I histocompatibility antigen, B-59 alpha chain OS=Homo sapiens GN=HLA-B PE=2 SV=1 - [1B59_HUMAN]	9
HLA class I histocompatibility antigen, B-54 alpha chain OS=Homo sapiens GN=HLA-B PE=2 SV=1 - [1B54_HUMAN]	9
HLA class I histocompatibility antigen, B-55 alpha chain OS=Homo sapiens GN=HLA-B PE=1 SV=1 - [1B55_HUMAN]	9
HLA class I histocompatibility antigen, Cw-12 alpha chain OS=Homo sapiens GN=HLA-C PE=1 SV=2 - [1C12_HUMAN]	7
HLA class I histocompatibility antigen, B-51 alpha chain OS=Homo sapiens GN=HLA-B PE=1 SV=1 - [1B51_HUMAN]	8
HLA class I histocompatibility antigen, B-52 alpha chain OS=Homo sapiens GN=HLA-B PE=2 SV=1 - [1B52_HUMAN]	9
HLA class I histocompatibility antigen, B-78 alpha chain OS=Homo sapiens GN=HLA-B PE=2 SV=1 - [1B78_HUMAN]	8
HLA class I histocompatibility antigen, A-30 alpha chain OS=Homo sapiens GN=HLA-A PE=1 SV=2 - [1A30_HUMAN]	8
Integrin alpha-3 OS=Homo sapiens GN=ITGA3 PE=1 SV=4 - [ITA3_HUMAN]	22
HLA class I histocompatibility antigen, Cw-16 alpha chain OS=Homo sapiens GN=HLA-C PE=2 SV=1 - [1C16_HUMAN]	6
HLA class I histocompatibility antigen, Cw-17 alpha chain OS=Homo sapiens GN=HLA-C PE=1 SV=1 - [1C17_HUMAN]	4
Tubulin alpha-3C/D chain OS=Homo sapiens GN=TUBA3C PE=1 SV=3 - [TBA3C_HUMAN]	14
Tubulin alpha-8 chain OS=Homo sapiens GN=TUBA8 PE=1 SV=1 - [TBA8_HUMAN]	10
Alpha-enolase OS=Homo sapiens GN=ENO1 PE=1 SV=2 - [ENOA_HUMAN]	15
Tubulin alpha-3E chain OS=Homo sapiens GN=TUBA3E PE=1 SV=2 - [TBA3E_HUMAN]	11
HLA class I histocompatibility antigen, B-49 alpha chain OS=Homo sapiens GN=HLA-B PE=2 SV=2 - [1B49_HUMAN]	10
HLA class I histocompatibility antigen, B-50 alpha chain OS=Homo sapiens GN=HLA-B PE=2 SV=1 - [1B50_HUMAN]	10
HLA class I histocompatibility antigen, A-2 alpha chain OS=Homo sapiens GN=HLA-A PE=1 SV=1 - [1A02_HUMAN]	6
HLA class I histocompatibility antigen, A-32 alpha chain OS=Homo sapiens GN=HLA-A PE=2 SV=2 - [1A32_HUMAN]	6
HLA class I histocompatibility antigen, A-74 alpha chain OS=Homo sapiens GN=HLA-A PE=1 SV=1 - [1A74_HUMAN]	6
POTE ankyrin domain family member F OS=Homo sapiens GN=POTEF PE=1 SV=2 - [POTEF_HUMAN]	9
Annexin A6 OS=Homo sapiens GN=ANXA6 PE=1 SV=3 - [ANXA6_HUMAN]	16
HLA class I histocompatibility antigen, B-45 alpha chain OS=Homo sapiens GN=HLA-B PE=2 SV=1 - [1B45_HUMAN]	10
Annexin A1 OS=Homo sapiens GN=ANXA1 PE=1 SV=2 - [ANXA1_HUMAN]	9
Putative HLA class I histocompatibility antigen, alpha chain H OS=Homo sapiens GN=HLA-H PE=5 SV=2 - [HLAH_HUMAN]	7
HLA class I histocompatibility antigen, A-29 alpha chain OS=Homo sapiens GN=HLA-A PE=2 SV=2 - [1A29_HUMAN]	6
Beta-actin-like protein 2 OS=Homo sapiens GN=ACTBL2 PE=1 SV=2 - [ACTBL_HUMAN]	10
HLA class I histocompatibility antigen, B-82 alpha chain OS=Homo sapiens GN=HLA-B PE=2 SV=1 - [1B82_HUMAN]	9
Sodium/potassium-transporting ATPase subunit alpha-3 OS=Homo sapiens GN=ATP1A3 PE=1 SV=3 - [AT1A3_HUMAN]	12
HLA class I histocompatibility antigen, A-25 alpha chain OS=Homo sapiens GN=HLA-A PE=2 SV=1 - [1A25_HUMAN]	5
HLA class I histocompatibility antigen, A-26 alpha chain OS=Homo sapiens GN=HLA-A PE=1 SV=2 - [1A26_HUMAN]	5
HLA class I histocompatibility antigen, A-31 alpha chain OS=Homo sapiens GN=HLA-A PE=2 SV=2 - [1A31_HUMAN]	5
HLA class I histocompatibility antigen, A-34 alpha chain OS=Homo sapiens GN=HLA-A PE=1 SV=1 - [1A34_HUMAN]	5
HLA class I histocompatibility antigen, A-43 alpha chain OS=Homo sapiens GN=HLA-A PE=2 SV=1 - [1A43_HUMAN]	5
HLA class I histocompatibility antigen, A-66 alpha chain OS=Homo sapiens GN=HLA-A PE=1 SV=1 - [1A66_HUMAN]	5
HLA class I histocompatibility antigen, A-68 alpha chain OS=Homo sapiens GN=HLA-A PE=1	5

SV=4 - [1A68_HUMAN]	
HLA class I histocompatibility antigen, A-69 alpha chain OS=Homo sapiens GN=HLA-A PE=1 SV=2 - [1A69_HUMAN]	5
HLA class I histocompatibility antigen, Cw-4 alpha chain OS=Homo sapiens GN=HLA-C PE=1 SV=1 - [1C04_HUMAN]	5
Erythrocyte band 7 integral membrane protein OS=Homo sapiens GN=STOM PE=1 SV=3 - [STOM_HUMAN]	7
Putative beta-actin-like protein 3 OS=Homo sapiens GN=POTEKP PE=5 SV=1 - [ACTBM_HUMAN]	5
HLA class I histocompatibility antigen, B-13 alpha chain OS=Homo sapiens GN=HLA-B PE=2 SV=1 - [1B13_HUMAN]	9
HLA class I histocompatibility antigen, B-38 alpha chain OS=Homo sapiens GN=HLA-B PE=2 SV=1 - [1B38_HUMAN]	7
HLA class I histocompatibility antigen, B-27 alpha chain OS=Homo sapiens GN=HLA-B PE=1 SV=2 - [1B27_HUMAN]	7
HLA class I histocompatibility antigen, B-37 alpha chain OS=Homo sapiens GN=HLA-B PE=2 SV=1 - [1B37_HUMAN]	8
HLA class I histocompatibility antigen, B-39 alpha chain OS=Homo sapiens GN=HLA-B PE=2 SV=1 - [1B39_HUMAN]	7
HLA class I histocompatibility antigen, B-40 alpha chain OS=Homo sapiens GN=HLA-B PE=1 SV=1 - [1B40_HUMAN]	8
HLA class I histocompatibility antigen, B-47 alpha chain OS=Homo sapiens GN=HLA-B PE=2 SV=1 - [1B47_HUMAN]	9
HLA class I histocompatibility antigen, B-67 alpha chain OS=Homo sapiens GN=HLA-B PE=1 SV=1 - [1B67_HUMAN]	7
Sodium/potassium-transporting ATPase subunit alpha-2 OS=Homo sapiens GN=ATP1A2 PE=1 SV=1 - [AT1A2_HUMAN]	10
Tubulin beta-6 chain OS=Homo sapiens GN=TUBB6 PE=1 SV=1 - [TBB6_HUMAN]	14
HLA class I histocompatibility antigen, A-33 alpha chain OS=Homo sapiens GN=HLA-A PE=1 SV=3 - [1A33_HUMAN]	3
HLA class I histocompatibility antigen, B-44 alpha chain OS=Homo sapiens GN=HLA-B PE=1 SV=1 - [1B44_HUMAN]	9
HLA class I histocompatibility antigen, Cw-14 alpha chain OS=Homo sapiens GN=HLA-C PE=2 SV=2 - [1C14_HUMAN]	4
HLA class I histocompatibility antigen, Cw-15 alpha chain OS=Homo sapiens GN=HLA-C PE=1 SV=1 - [1C15_HUMAN]	6
Myosin-9 OS=Homo sapiens GN=MYH9 PE=1 SV=4 - [MYH9_HUMAN]	13
HLA class I histocompatibility antigen, B-7 alpha chain OS=Homo sapiens GN=HLA-B PE=1 SV=3 - [1B07_HUMAN]	5
HLA class I histocompatibility antigen, B-8 alpha chain OS=Homo sapiens GN=HLA-B PE=1 SV=1 - [1B08_HUMAN]	5
HLA class I histocompatibility antigen, B-14 alpha chain OS=Homo sapiens GN=HLA-B PE=1 SV=1 - [1B14_HUMAN]	5
HLA class I histocompatibility antigen, B-18 alpha chain OS=Homo sapiens GN=HLA-B PE=1 SV=1 - [1B18_HUMAN]	5
HLA class I histocompatibility antigen, B-41 alpha chain OS=Homo sapiens GN=HLA-B PE=1 SV=1 - [1B41_HUMAN]	6
HLA class I histocompatibility antigen, B-42 alpha chain OS=Homo sapiens GN=HLA-B PE=1 SV=1 - [1B42_HUMAN]	5
HLA class I histocompatibility antigen, Cw-7 alpha chain OS=Homo sapiens GN=HLA-C PE=1 SV=3 - [1C07_HUMAN]	5
Guanine nucleotide-binding protein G(I)/G(S)/G(T) subunit beta-1 OS=Homo sapiens GN=GNB1 PE=1 SV=3 - [GBB1_HUMAN]	12
HLA class I histocompatibility antigen, B-48 alpha chain OS=Homo sapiens GN=HLA-B PE=1 SV=1 - [1B48_HUMAN]	5
HLA class I histocompatibility antigen, B-81 alpha chain OS=Homo sapiens GN=HLA-B PE=2 SV=1 - [1B81_HUMAN]	4
HLA class I histocompatibility antigen, Cw-5 alpha chain OS=Homo sapiens GN=HLA-C PE=2 SV=1 - [1C05_HUMAN]	4
HLA class I histocompatibility antigen, Cw-8 alpha chain OS=Homo sapiens GN=HLA-C PE=2 SV=1 - [1C08_HUMAN]	4
HLA class I histocompatibility antigen, Cw-6 alpha chain OS=Homo sapiens GN=HLA-C PE=1 SV=2 - [1C06_HUMAN]	5
Alpha-actinin-4 OS=Homo sapiens GN=ACTN4 PE=1 SV=2 - [ACTN4_HUMAN]	7
Alpha-actinin-1 OS=Homo sapiens GN=ACTN1 PE=1 SV=2 - [ACTN1_HUMAN]	7
Clathrin heavy chain 1 OS=Homo sapiens GN=CLTC PE=1 SV=5 - [CLH1_HUMAN]	5

Elongation factor 1-alpha 1 OS=Homo sapiens GN=EEF1A1 PE=1 SV=1 - [EF1A1_HUMAN]	12
Putative elongation factor 1-alpha-like 3 OS=Homo sapiens GN=EEF1AL3 PE=5 SV=1 - [EF1A3_HUMAN]	12
HLA class I histocompatibility antigen, B-73 alpha chain OS=Homo sapiens GN=HLA-B PE=1 SV=1 - [1B73_HUMAN]	3
Tubulin beta-8 chain OS=Homo sapiens GN=TUBB8 PE=1 SV=2 - [TBB8_HUMAN]	10
Cofilin-1 OS=Homo sapiens GN=CFL1 PE=1 SV=3 - [COF1_HUMAN]	5
Fructose-bisphosphate aldolase A OS=Homo sapiens GN=ALDOA PE=1 SV=2 - [ALDOA_HUMAN]	10
Annexin A5 OS=Homo sapiens GN=ANXA5 PE=1 SV=2 - [ANXA5_HUMAN]	7
HLA class I histocompatibility antigen, alpha chain F OS=Homo sapiens GN=HLA-F PE=2 SV=2 - [HLAF_HUMAN]	4
L-lactate dehydrogenase A chain OS=Homo sapiens GN=LDHA PE=1 SV=2 - [LDHA_HUMAN]	7
Guanine nucleotide-binding protein G(i) subunit alpha-2 OS=Homo sapiens GN=GNAI2 PE=1 SV=3 - [GNAI2_HUMAN]	10
HLA class I histocompatibility antigen, A-80 alpha chain OS=Homo sapiens GN=HLA-A PE=2 SV=1 - [1A80_HUMAN]	6
Putative tubulin-like protein alpha-4B OS=Homo sapiens GN=TUBA4B PE=5 SV=2 - [TBA4B_HUMAN]	1
Tubulin beta-8 chain B OS=Homo sapiens PE=1 SV=1 - [TBB8B_HUMAN]	9
Thy-1 membrane glycoprotein OS=Homo sapiens GN=THY1 PE=1 SV=2 - [THY1_HUMAN]	4
Guanine nucleotide-binding protein G(I)/G(S)/G(T) subunit beta-2 OS=Homo sapiens GN=GNB2 PE=1 SV=3 - [GBB2_HUMAN]	12
Triosephosphate isomerase OS=Homo sapiens GN=TPI1 PE=1 SV=2 - [TPIS_HUMAN]	7
Protein S100-A10 OS=Homo sapiens GN=S100A10 PE=1 SV=2 - [S10AA_HUMAN]	4
Beta-2-microglobulin OS=Homo sapiens GN=B2M PE=1 SV=1 - [B2MG_HUMAN]	5
Heat shock protein HSP 90-alpha OS=Homo sapiens GN=HSP90AA1 PE=1 SV=5 - [HS90A_HUMAN]	7
Heat shock cognate 71 kDa protein OS=Homo sapiens GN=HSPA8 PE=1 SV=1 - [HSP7C_HUMAN]	9
Histone H4 OS=Homo sapiens GN=HIST1H4A PE=1 SV=2 - [H4_HUMAN]	5
Heat shock protein HSP 90-beta OS=Homo sapiens GN=HSP90AB1 PE=1 SV=4 - [HS90B_HUMAN]	10
14-3-3 protein zeta/delta OS=Homo sapiens GN=YWHAZ PE=1 SV=1 - [1433Z_HUMAN]	4
Putative tubulin beta-4q chain OS=Homo sapiens GN=TUBB4Q PE=5 SV=1 - [TBB4Q_HUMAN]	7
Histone H2A type 1-B/E OS=Homo sapiens GN=HIST1H2AB PE=1 SV=2 - [H2A1B_HUMAN]	2
Histone H2A type 1-C OS=Homo sapiens GN=HIST1H2AC PE=1 SV=3 - [H2A1C_HUMAN]	2
Histone H2A type 1-D OS=Homo sapiens GN=HIST1H2AD PE=1 SV=2 - [H2A1D_HUMAN]	2
Histone H2A type 1-H OS=Homo sapiens GN=HIST1H2AH PE=1 SV=3 - [H2A1H_HUMAN]	2
Histone H2A type 1-J OS=Homo sapiens GN=HIST1H2AJ PE=1 SV=3 - [H2A1J_HUMAN]	2
Histone H2A type 1 OS=Homo sapiens GN=HIST1H2AG PE=1 SV=2 - [H2A1_HUMAN]	2
Histone H2A type 2-A OS=Homo sapiens GN=HIST2H2AA3 PE=1 SV=3 - [H2A2A_HUMAN]	2
Histone H2A type 2-C OS=Homo sapiens GN=HIST2H2AC PE=1 SV=4 - [H2A2C_HUMAN]	2
Histone H2A type 3 OS=Homo sapiens GN=HIST3H2A PE=1 SV=3 - [H2A3_HUMAN]	2
Histone H2A.J OS=Homo sapiens GN=H2AFJ PE=1 SV=1 - [H2AJ_HUMAN]	2
Protein S100-A11 OS=Homo sapiens GN=S100A11 PE=1 SV=2 - [S10AB_HUMAN]	2
Fatty acid synthase OS=Homo sapiens GN=FASN PE=1 SV=3 - [FAS_HUMAN]	12
5'-nucleotidase OS=Homo sapiens GN=NT5E PE=1 SV=1 - [5NTD_HUMAN]	6
Histone H2B type 1-H OS=Homo sapiens GN=HIST1H2BH PE=1 SV=3 - [H2B1H_HUMAN]	2
Histone H2B type 1-O OS=Homo sapiens GN=HIST1H2BO PE=1 SV=3 - [H2B1O_HUMAN]	2
Histone H2B type 2-F OS=Homo sapiens GN=HIST2H2BF PE=1 SV=3 - [H2B2F_HUMAN]	2
Histone H2B type 1-B OS=Homo sapiens GN=HIST1H2BB PE=1 SV=2 - [H2B1B_HUMAN]	2
Histone H2B type 1-C/E/F/G/I OS=Homo sapiens GN=HIST1H2BC PE=1 SV=4 - [H2B1C_HUMAN]	2
Histone H2B type 1-D OS=Homo sapiens GN=HIST1H2BD PE=1 SV=2 - [H2B1D_HUMAN]	2

Histone H2B type 1-J OS=Homo sapiens GN=HIST1H2BJ PE=1 SV=3 - [H2B1J_HUMAN]	2
Histone H2B type 1-K OS=Homo sapiens GN=HIST1H2BK PE=1 SV=3 - [H2B1K_HUMAN]	2
Histone H2B type 1-L OS=Homo sapiens GN=HIST1H2BL PE=1 SV=3 - [H2B1L_HUMAN]	2
Histone H2B type 1-M OS=Homo sapiens GN=HIST1H2BM PE=1 SV=3 - [H2B1M_HUMAN]	2
Histone H2B type 1-N OS=Homo sapiens GN=HIST1H2BN PE=1 SV=3 - [H2B1N_HUMAN]	2
Histone H2B type 2-E OS=Homo sapiens GN=HIST2H2BE PE=1 SV=3 - [H2B2E_HUMAN]	2
Histone H2B type 3-B OS=Homo sapiens GN=HIST3H2BB PE=1 SV=3 - [H2B3B_HUMAN]	2
Histone H2B type F-S OS=Homo sapiens GN=H2BFS PE=1 SV=2 - [H2BFS_HUMAN]	2
78 kDa glucose-regulated protein OS=Homo sapiens GN=HSPA5 PE=1 SV=2 - [GRP78_HUMAN]	7
Brain acid soluble protein 1 OS=Homo sapiens GN=BASP1 PE=1 SV=2 - [BASP1_HUMAN]	5
Transgelin-2 OS=Homo sapiens GN=TAGLN2 PE=1 SV=3 - [TAGL2_HUMAN]	2
Elongation factor 1-alpha 2 OS=Homo sapiens GN=EEF1A2 PE=1 SV=1 - [EF1A2_HUMAN]	6
Solute carrier family 2, facilitated glucose transporter member 1 OS=Homo sapiens GN=SLC2A1 PE=1 SV=2 - [GTR1_HUMAN]	6
Myosin light polypeptide 6 OS=Homo sapiens GN=MYL6 PE=1 SV=2 - [MYL6_HUMAN]	4
Keratin, type II cytoskeletal 1 OS=Homo sapiens GN=KRT1 PE=1 SV=6 - [K2C1_HUMAN]	6
Ras-related protein Rab-10 OS=Homo sapiens GN=RAB10 PE=1 SV=1 - [RAB10_HUMAN]	3
HLA class I histocompatibility antigen, Cw-2 alpha chain OS=Homo sapiens GN=HLA-C PE=1 SV=1 - [1C02_HUMAN]	3
Putative tubulin beta chain-like protein ENSP00000290377 OS=Homo sapiens PE=5 SV=2 - [YI016_HUMAN]	5
Peptidyl-prolyl cis-trans isomerase A OS=Homo sapiens GN=PPIA PE=1 SV=2 - [PPIA_HUMAN]	8
Ezrin OS=Homo sapiens GN=EZR PE=1 SV=4 - [EZRI_HUMAN]	5
Moesin OS=Homo sapiens GN=MSN PE=1 SV=3 - [MOES_HUMAN]	7
Radixin OS=Homo sapiens GN=RDX PE=1 SV=1 - [RADI_HUMAN]	5
Elongation factor 2 OS=Homo sapiens GN=EEF2 PE=1 SV=4 - [EF2_HUMAN]	4
HLA class I histocompatibility antigen, Cw-18 alpha chain OS=Homo sapiens GN=HLA-C PE=2 SV=1 - [1C18_HUMAN]	4
Galectin-1 OS=Homo sapiens GN=LGALS1 PE=1 SV=2 - [LEG1_HUMAN]	3
Integrin alpha-5 OS=Homo sapiens GN=ITGA5 PE=1 SV=2 - [ITA5_HUMAN]	2
Keratin, type II cytoskeletal 2 epidermal OS=Homo sapiens GN=KRT2 PE=1 SV=2 - [K22E_HUMAN]	2
HLA class I histocompatibility antigen, Cw-3 alpha chain OS=Homo sapiens GN=HLA-C PE=1 SV=2 - [1C03_HUMAN]	2
Chloride intracellular channel protein 1 OS=Homo sapiens GN=CLIC1 PE=1 SV=4 - [CLIC1_HUMAN]	2
L-lactate dehydrogenase A-like 6B OS=Homo sapiens GN=LDHAL6B PE=1 SV=3 - [LDH6B_HUMAN]	1
Transforming protein RhoA OS=Homo sapiens GN=RHOA PE=1 SV=1 - [RHOA_HUMAN]	5
Rho-related GTP-binding protein RhoC OS=Homo sapiens GN=RHOC PE=1 SV=1 - [RHOC_HUMAN]	3
Myosin-11 OS=Homo sapiens GN=MYH11 PE=1 SV=3 - [MYH11_HUMAN]	2
Sodium/potassium-transporting ATPase subunit alpha-4 OS=Homo sapiens GN=ATP1A4 PE=1 SV=3 - [AT1A4_HUMAN]	6
Guanine nucleotide-binding protein G(s) subunit alpha isoforms XLas OS=Homo sapiens GN=GNAS PE=1 SV=2 - [GNAS1_HUMAN]	3
Guanine nucleotide-binding protein G(s) subunit alpha isoforms short OS=Homo sapiens GN=GNAS PE=1 SV=1 - [GNAS2_HUMAN]	3
Potassium-transporting ATPase alpha chain 1 OS=Homo sapiens GN=ATP4A PE=2 SV=5 - [ATP4A_HUMAN]	3
Histone H3.1 OS=Homo sapiens GN=HIST1H3A PE=1 SV=2 - [H31_HUMAN]	2
Myosin-Ib OS=Homo sapiens GN=MYO1B PE=1 SV=3 - [MYO1B_HUMAN]	1
14-3-3 protein epsilon OS=Homo sapiens GN=YWHAE PE=1 SV=1 - [1433E_HUMAN]	2
HLA class I histocompatibility antigen, alpha chain E OS=Homo sapiens GN=HLA-E PE=1 SV=3 - [HLAE_HUMAN]	2
Large neutral amino acids transporter small subunit 1 OS=Homo sapiens GN=SLC7A5 PE=1	1

SV=2 - [LAT1_HUMAN]	
Serine/threonine-protein phosphatase PP1-beta catalytic subunit OS=Homo sapiens GN=PPP1CB PE=1 SV=3 - [PP1B_HUMAN]	2
Serine/threonine-protein phosphatase PP1-gamma catalytic subunit OS=Homo sapiens GN=PPP1CC PE=1 SV=1 - [PP1G_HUMAN]	2
Serine/threonine-protein phosphatase PP1-alpha catalytic subunit OS=Homo sapiens GN=PPP1CA PE=1 SV=1 - [PP1A_HUMAN]	2
Ras-related protein Rab-1A OS=Homo sapiens GN=RAB1A PE=1 SV=3 - [RAB1A_HUMAN]	2
Ras-related protein Rab-35 OS=Homo sapiens GN=RAB35 PE=1 SV=1 - [RAB35_HUMAN]	2
Ras-related protein Rab-8B OS=Homo sapiens GN=RAB8B PE=1 SV=2 - [RAB8B_HUMAN]	2
Ras-related protein Rab-15 OS=Homo sapiens GN=RAB15 PE=1 SV=1 - [RAB15_HUMAN]	2
Ras-related protein Rab-8A OS=Homo sapiens GN=RAB8A PE=1 SV=1 - [RAB8A_HUMAN]	2
Ras-related protein Rab-1B OS=Homo sapiens GN=RAB1B PE=1 SV=1 - [RAB1B_HUMAN]	2
Putative Ras-related protein Rab-1C OS=Homo sapiens GN=RAB1C PE=5 SV=2 - [RAB1C_HUMAN]	2
Alpha-actinin-2 OS=Homo sapiens GN=ACTN2 PE=1 SV=1 - [ACTN2_HUMAN]	2
Macrophage migration inhibitory factor OS=Homo sapiens GN=MIF PE=1 SV=4 - [MIF_HUMAN]	2
Intercellular adhesion molecule 1 OS=Homo sapiens GN=ICAM1 PE=1 SV=2 - [ICAM1_HUMAN]	2
14-3-3 protein beta/alpha OS=Homo sapiens GN=YWHAB PE=1 SV=3 - [1433B_HUMAN]	4
Alpha-actinin-3 OS=Homo sapiens GN=ACTN3 PE=1 SV=2 - [ACTN3_HUMAN]	1
Calmodulin OS=Homo sapiens GN=CALM1 PE=1 SV=2 - [CALM_HUMAN]	2
Myristoylated alanine-rich C-kinase substrate OS=Homo sapiens GN=MARCKS PE=1 SV=4 - [MARCS_HUMAN]	2
Cofilin-2 OS=Homo sapiens GN=CFL2 PE=1 SV=1 - [COF2_HUMAN]	2
Guanine nucleotide-binding protein G(i) subunit alpha-1 OS=Homo sapiens GN=GNAI1 PE=1 SV=2 - [GNAI1_HUMAN]	3
Guanine nucleotide-binding protein G(k) subunit alpha OS=Homo sapiens GN=GNAI3 PE=1 SV=3 - [GNAI3_HUMAN]	2
Guanine nucleotide-binding protein G(t) subunit alpha-1 OS=Homo sapiens GN=GNAT1 PE=1 SV=5 - [GNAT1_HUMAN]	2
Guanine nucleotide-binding protein G(t) subunit alpha-2 OS=Homo sapiens GN=GNAT2 PE=1 SV=4 - [GNAT2_HUMAN]	2
Guanine nucleotide-binding protein G(t) subunit alpha-3 OS=Homo sapiens GN=GNAT3 PE=2 SV=2 - [GNAT3_HUMAN]	2
Keratin, type I cytoskeletal 10 OS=Homo sapiens GN=KRT10 PE=1 SV=6 - [K1C10_HUMAN]	1
Myosin light chain 6B OS=Homo sapiens GN=MYL6B PE=1 SV=1 - [MYL6B_HUMAN]	2
Heat shock-related 70 kDa protein 2 OS=Homo sapiens GN=HSPA2 PE=1 SV=1 - [HSP72_HUMAN]	4
Ubiquitin-like protein ISG15 OS=Homo sapiens GN=ISG15 PE=1 SV=5 - [ISG15_HUMAN]	2
Tubulin beta-1 chain OS=Homo sapiens GN=TUBB1 PE=1 SV=1 - [TBB1_HUMAN]	4
Peroxiredoxin-1 OS=Homo sapiens GN=PRDX1 PE=1 SV=1 - [PRDX1_HUMAN]	4
Endoplasmin OS=Homo sapiens GN=HSP90B1 PE=1 SV=1 - [ENPL_HUMAN]	1
Sodium/potassium-transporting ATPase subunit beta-1 OS=Homo sapiens GN=ATP1B1 PE=1 SV=1 - [AT1B1_HUMAN]	3
CD9 antigen OS=Homo sapiens GN=CD9 PE=1 SV=4 - [CD9_HUMAN]	2
Proteasome activator complex subunit 1 OS=Homo sapiens GN=PSME1 PE=1 SV=1 - [PSME1_HUMAN]	1
14-3-3 protein gamma OS=Homo sapiens GN=YWHAG PE=1 SV=2 - [1433G_HUMAN]	3
Guanine nucleotide-binding protein subunit alpha-12 OS=Homo sapiens GN=GNA12 PE=1 SV=4 - [GNA12_HUMAN]	1
Guanine nucleotide-binding protein subunit alpha-13 OS=Homo sapiens GN=GNA13 PE=1 SV=2 - [GNA13_HUMAN]	1
Guanine nucleotide-binding protein G(olf) subunit alpha OS=Homo sapiens GN=GNAL PE=1 SV=1 - [GNAL_HUMAN]	1
Guanine nucleotide-binding protein G(o) subunit alpha OS=Homo sapiens GN=GNAO1 PE=1 SV=4 - [GNAO_HUMAN]	1
Putative heat shock protein HSP 90-alpha A4 OS=Homo sapiens GN=HSP90AA4P PE=5 SV=1 - [HS904_HUMAN]	1

Heat shock 70 kDa protein 6 OS=Homo sapiens GN=HSPA6 PE=1 SV=2 - [HSP76_HUMAN]	2
Heat shock 70 kDa protein 1A/1B OS=Homo sapiens GN=HSPA1A PE=1 SV=5 - [HSP71_HUMAN]	2
Heat shock 70 kDa protein 1-like OS=Homo sapiens GN=HSPA1L PE=1 SV=2 - [HS71L_HUMAN]	2
Putative heat shock 70 kDa protein 7 OS=Homo sapiens GN=HSPA7 PE=5 SV=2 - [HSP77_HUMAN]	2
Ras-related protein Rab-37 OS=Homo sapiens GN=RAB37 PE=1 SV=3 - [RAB37_HUMAN]	1
Ras-related protein Rab-33B OS=Homo sapiens GN=RAB33B PE=1 SV=1 - [RB33B_HUMAN]	1
Ras-related protein Rab-12 OS=Homo sapiens GN=RAB12 PE=1 SV=3 - [RAB12_HUMAN]	1
Ras-related protein Rab-14 OS=Homo sapiens GN=RAB14 PE=1 SV=4 - [RAB14_HUMAN]	1
Ras-related protein Rab-30 OS=Homo sapiens GN=RAB30 PE=1 SV=2 - [RAB30_HUMAN]	1
Ras-related protein Rab-3A OS=Homo sapiens GN=RAB3A PE=1 SV=1 - [RAB3A_HUMAN]	1
Ras-related protein Rab-3B OS=Homo sapiens GN=RAB3B PE=1 SV=2 - [RAB3B_HUMAN]	1
Ras-related protein Rab-3C OS=Homo sapiens GN=RAB3C PE=2 SV=1 - [RAB3C_HUMAN]	1
Ras-related protein Rab-3D OS=Homo sapiens GN=RAB3D PE=1 SV=1 - [RAB3D_HUMAN]	1
Ras-related protein Rab-43 OS=Homo sapiens GN=RAB43 PE=1 SV=1 - [RAB43_HUMAN]	1
Ras-related protein Rab-4A OS=Homo sapiens GN=RAB4A PE=1 SV=2 - [RAB4A_HUMAN]	1
Ras-related protein Rab-4B OS=Homo sapiens GN=RAB4B PE=1 SV=1 - [RAB4B_HUMAN]	1
Ras-related protein Rab-39B OS=Homo sapiens GN=RAB39B PE=1 SV=1 - [RB39B_HUMAN]	1
Putative Rab-43-like protein ENSP00000330714 OS=Homo sapiens PE=5 SV=3 - [RB43L_HUMAN]	1
Ras-related protein Rab-6A OS=Homo sapiens GN=RAB6A PE=1 SV=3 - [RAB6A_HUMAN]	1
Ras-related protein Rab-6B OS=Homo sapiens GN=RAB6B PE=1 SV=1 - [RAB6B_HUMAN]	1
Ras-related protein Rab-39A OS=Homo sapiens GN=RAB39 PE=2 SV=2 - [RB39A_HUMAN]	1
Eukaryotic initiation factor 4A-I OS=Homo sapiens GN=EIF4A1 PE=1 SV=1 - [IF4A1_HUMAN]	3
Eukaryotic initiation factor 4A-II OS=Homo sapiens GN=EIF4A2 PE=1 SV=2 - [IF4A2_HUMAN]	3
Lysosome-associated membrane glycoprotein 1 OS=Homo sapiens GN=LAMP1 PE=1 SV=3 - [LAMP1_HUMAN]	1
EGF-like repeat and discoidin I-like domain-containing protein 3 OS=Homo sapiens GN=EDIL3 PE=1 SV=1 - [EDIL3_HUMAN]	1
Voltage-dependent anion-selective channel protein 1 OS=Homo sapiens GN=VDAC1 PE=1 SV=2 - [VDAC1_HUMAN]	2
Rho-related GTP-binding protein RhoB OS=Homo sapiens GN=RHOB PE=1 SV=1 - [RHOB_HUMAN]	1
Sodium/potassium-transporting ATPase subunit beta-3 OS=Homo sapiens GN=ATP1B3 PE=1 SV=1 - [AT1B3_HUMAN]	2
Thioredoxin OS=Homo sapiens GN=TXN PE=1 SV=3 - [THIO_HUMAN]	1
Heat shock protein beta-1 OS=Homo sapiens GN=HSPB1 PE=1 SV=2 - [HSPB1_HUMAN]	2
Clathrin heavy chain 2 OS=Homo sapiens GN=CLTCL1 PE=1 SV=2 - [CLH2_HUMAN]	1
Basigin OS=Homo sapiens GN=BSG PE=1 SV=2 - [BASI_HUMAN]	2
Phosphoglycerate mutase 1 OS=Homo sapiens GN=PGAM1 PE=1 SV=2 - [PGAM1_HUMAN]	2
Histone H2A type 1-A OS=Homo sapiens GN=HIST1H2AA PE=1 SV=3 - [H2A1A_HUMAN]	1
Histone H2A type 2-B OS=Homo sapiens GN=HIST2H2AB PE=1 SV=3 - [H2A2B_HUMAN]	1
Histone H2A.V OS=Homo sapiens GN=H2AFV PE=1 SV=3 - [H2AV_HUMAN]	1
Histone H2A.x OS=Homo sapiens GN=H2AFX PE=1 SV=2 - [H2AX_HUMAN]	1
Histone H2A.Z OS=Homo sapiens GN=H2AFZ PE=1 SV=2 - [H2AZ_HUMAN]	1
Guanine nucleotide-binding protein subunit beta-4 OS=Homo sapiens GN=GNB4 PE=1 SV=3 - [GBB4_HUMAN]	5
14-3-3 protein sigma OS=Homo sapiens GN=SFN PE=1 SV=1 - [1433S_HUMAN]	3
Fructose-bisphosphate aldolase C OS=Homo sapiens GN=ALDOC PE=1 SV=2 - [ALDOC_HUMAN]	1
Stonin-2 OS=Homo sapiens GN=STON2 PE=1 SV=1 - [STON2_HUMAN]	1
Tubulin alpha chain-like 3 OS=Homo sapiens GN=TUBAL3 PE=1 SV=2 - [TBAL3_HUMAN]	3

Proteasome subunit alpha type-6 OS=Homo sapiens GN=PSMA6 PE=1 SV=1 - [PSA6_HUMAN]	1
Profilin-1 OS=Homo sapiens GN=PFN1 PE=1 SV=2 - [PROF1_HUMAN]	5
Pyruvate kinase isozymes R/L OS=Homo sapiens GN=PKLR PE=1 SV=2 - [KPYR_HUMAN]	1
Keratin, type II cytoskeletal 6B OS=Homo sapiens GN=KRT6B PE=1 SV=5 - [K2C6B_HUMAN]	1
ADP-ribosylation factor 3 OS=Homo sapiens GN=ARF3 PE=1 SV=2 - [ARF3_HUMAN]	1
ADP-ribosylation factor 1 OS=Homo sapiens GN=ARF1 PE=1 SV=2 - [ARF1_HUMAN]	1
Phosphoglycerate kinase 1 OS=Homo sapiens GN=PGK1 PE=1 SV=3 - [PGK1_HUMAN]	4
Vimentin OS=Homo sapiens GN=VIM PE=1 SV=4 - [VIME_HUMAN]	2
Rho GDP-dissociation inhibitor 1 OS=Homo sapiens GN=ARHGDIA PE=1 SV=3 - [GDIR1_HUMAN]	2
Protein disulfide-isomerase A3 OS=Homo sapiens GN=PDIA3 PE=1 SV=4 - [PDIA3_HUMAN]	2
Myosin-10 OS=Homo sapiens GN=MYH10 PE=1 SV=3 - [MYH10_HUMAN]	3
D-3-phosphoglycerate dehydrogenase OS=Homo sapiens GN=PHGDH PE=1 SV=4 - [SERA_HUMAN]	1
CD151 antigen OS=Homo sapiens GN=CD151 PE=1 SV=3 - [CD151_HUMAN]	1
Probable phosphoglycerate mutase 4 OS=Homo sapiens GN=PGAM4 PE=1 SV=1 - [PGAM4_HUMAN]	1
Phosphoglycerate mutase 2 OS=Homo sapiens GN=PGAM2 PE=1 SV=3 - [PGAM2_HUMAN]	1
Importin subunit beta-1 OS=Homo sapiens GN=KPNB1 PE=1 SV=2 - [IMB1_HUMAN]	1
Charged multivesicular body protein 4b OS=Homo sapiens GN=CHMP4B PE=1 SV=1 - [CHM4B_HUMAN]	1
Filamin-A OS=Homo sapiens GN=FLNA PE=1 SV=4 - [FLNA_HUMAN]	1
Ras-related protein Rab-13 OS=Homo sapiens GN=RAB13 PE=1 SV=1 - [RAB13_HUMAN]	1
Leukocyte surface antigen CD47 OS=Homo sapiens GN=CD47 PE=1 SV=1 - [CD47_HUMAN]	1
Potassium-transporting ATPase alpha chain 2 OS=Homo sapiens GN=ATP12A PE=2 SV=3 - [AT12A_HUMAN]	3
Ubiquitin OS=Homo sapiens GN=RPS27A PE=1 SV=1 - [UBIQ_HUMAN]	1
Putative heat shock protein HSP 90-alpha A2 OS=Homo sapiens GN=HSP90AA2 PE=1 SV=2 - [HS902_HUMAN]	1
Putative heat shock protein HSP 90-beta 2 OS=Homo sapiens GN=HSP90AB2P PE=1 SV=2 - [H90B2_HUMAN]	2
GTP-binding nuclear protein Ran OS=Homo sapiens GN=RAN PE=1 SV=3 - [RAN_HUMAN]	1
CD97 antigen OS=Homo sapiens GN=CD97 PE=1 SV=4 - [CD97_HUMAN]	1
Myosin-Ic OS=Homo sapiens GN=MYO1C PE=1 SV=3 - [MYO1C_HUMAN]	3
Histone H3.1t OS=Homo sapiens GN=HIST3H3 PE=1 SV=3 - [H31T_HUMAN]	1
Histone H3.2 OS=Homo sapiens GN=HIST2H3A PE=1 SV=3 - [H32_HUMAN]	1
Histone H3.3 OS=Homo sapiens GN=H3F3A PE=1 SV=2 - [H33_HUMAN]	1
Histone H3.3C OS=Homo sapiens GN=H3F3C PE=1 SV=3 - [H3C_HUMAN]	1
Guanine nucleotide-binding protein G(I)/G(S)/G(O) subunit gamma-12 OS=Homo sapiens GN=GNG12 PE=1 SV=3 - [GBG12_HUMAN]	2
Ras GTPase-activating-like protein IQGAP1 OS=Homo sapiens GN=IQGAP1 PE=1 SV=1 - [IQGA1_HUMAN]	4
HLA class I histocompatibility antigen, alpha chain G OS=Homo sapiens GN=HLA-G PE=1 SV=1 - [HLAG_HUMAN]	1
L-lactate dehydrogenase B chain OS=Homo sapiens GN=LDHB PE=1 SV=2 - [LDHB_HUMAN]	1
L-lactate dehydrogenase A-like 6A OS=Homo sapiens GN=LDHAL6A PE=2 SV=1 - [LDH6A_HUMAN]	1
L-lactate dehydrogenase C chain OS=Homo sapiens GN=LDHC PE=2 SV=4 - [LDHC_HUMAN]	2
Dynactin subunit 1 OS=Homo sapiens GN=DCTN1 PE=1 SV=3 - [DCTN1_HUMAN]	1
Acetyl-CoA acetyltransferase, cytosolic OS=Homo sapiens GN=ACAT2 PE=1 SV=2 - [THIC_HUMAN]	1
Phosphoglycerate kinase 2 OS=Homo sapiens GN=PGK2 PE=1 SV=3 - [PGK2_HUMAN]	1
Gamma-enolase OS=Homo sapiens GN=ENO2 PE=1 SV=3 - [ENOG_HUMAN]	1
Monocarboxylate transporter 4 OS=Homo sapiens GN=SLC16A3 PE=1 SV=1 - [MOT4_HUMAN]	1
Myosin-14 OS=Homo sapiens GN=MYH14 PE=1 SV=1 - [MYH14_HUMAN]	2

Myosin-13 OS=Homo sapiens GN=MYH13 PE=1 SV=1 - [MYH13_HUMAN]	1
Myosin-1 OS=Homo sapiens GN=MYH1 PE=1 SV=3 - [MYH1_HUMAN]	1
Myosin-2 OS=Homo sapiens GN=MYH2 PE=1 SV=1 - [MYH2_HUMAN]	1
Myosin-3 OS=Homo sapiens GN=MYH3 PE=1 SV=3 - [MYH3_HUMAN]	1
Myosin-4 OS=Homo sapiens GN=MYH4 PE=1 SV=2 - [MYH4_HUMAN]	1
Myosin-6 OS=Homo sapiens GN=MYH6 PE=1 SV=4 - [MYH6_HUMAN]	1
Myosin-7B OS=Homo sapiens GN=MYH7B PE=2 SV=2 - [MYH7B_HUMAN]	1
Myosin-7 OS=Homo sapiens GN=MYH7 PE=1 SV=5 - [MYH7_HUMAN]	1
Myosin-8 OS=Homo sapiens GN=MYH8 PE=1 SV=3 - [MYH8_HUMAN]	1
Protein NDRG1 OS=Homo sapiens GN=NDRG1 PE=1 SV=1 - [NDRG1_HUMAN]	1
CD44 antigen OS=Homo sapiens GN=CD44 PE=1 SV=2 - [CD44_HUMAN]	1
Neuroplastin OS=Homo sapiens GN=NPTN PE=1 SV=1 - [NPTN_HUMAN]	1
Destrin OS=Homo sapiens GN=DSTN PE=1 SV=3 - [DEST_HUMAN]	1
Solute carrier family 2, facilitated glucose transporter member 14 OS=Homo sapiens GN=SLC2A14 PE=2 SV=1 - [GTR14_HUMAN]	1
Solute carrier family 2, facilitated glucose transporter member 3 OS=Homo sapiens GN=SLC2A3 PE=1 SV=1 - [GTR3_HUMAN]	1
Ras-related C3 botulinum toxin substrate 1 OS=Homo sapiens GN=RAC1 PE=1 SV=1 - [RAC1_HUMAN]	2
Syntenin-1 OS=Homo sapiens GN=SDCBP PE=1 SV=1 - [SDCB1_HUMAN]	1
Histone H2B type 1-A OS=Homo sapiens GN=HIST1H2BA PE=1 SV=3 - [H2B1A_HUMAN]	1
Class E basic helix-loop-helix protein 41 OS=Homo sapiens GN=BHLHE41 PE=2 SV=1 - [BHE41_HUMAN]	1
Guanine nucleotide-binding protein G(I)/G(S)/G(T) subunit beta-3 OS=Homo sapiens GN=GNB3 PE=1 SV=1 - [GBB3_HUMAN]	3
Inositol 1,4,5-triphosphate receptor-interacting protein-like 1 OS=Homo sapiens GN=ITPRIPL1 PE=1 SV=1 - [IPIL1_HUMAN]	1
Myosin light chain 3 OS=Homo sapiens GN=MYL3 PE=1 SV=3 - [MYL3_HUMAN]	1
Ras-related C3 botulinum toxin substrate 2 OS=Homo sapiens GN=RAC2 PE=1 SV=1 - [RAC2_HUMAN]	1
Rho-related GTP-binding protein RhoG OS=Homo sapiens GN=RHOG PE=1 SV=1 - [RHOG_HUMAN]	1
Ras-related C3 botulinum toxin substrate 3 OS=Homo sapiens GN=RAC3 PE=1 SV=1 - [RAC3_HUMAN]	1
Cell division control protein 42 homolog OS=Homo sapiens GN=CDC42 PE=1 SV=1 - [CDC42_HUMAN]	1
Rho-related GTP-binding protein RhoJ OS=Homo sapiens GN=RHOJ PE=1 SV=1 - [RHOJ_HUMAN]	1
Rho-related GTP-binding protein RhoQ OS=Homo sapiens GN=RHOQ PE=1 SV=2 - [RHOQ_HUMAN]	1
Ras-related protein Rap-1A OS=Homo sapiens GN=RAP1A PE=1 SV=1 - [RAP1A_HUMAN]	2
Ras-related protein Rap-1b OS=Homo sapiens GN=RAP1B PE=1 SV=1 - [RAP1B_HUMAN]	2
Neutral amino acid transporter B(0) OS=Homo sapiens GN=SLC1A5 PE=1 SV=2 - [AAAT_HUMAN]	1
14-3-3 protein theta OS=Homo sapiens GN=YWHAQ PE=1 SV=1 - [1433T_HUMAN]	2
14-3-3 protein eta OS=Homo sapiens GN=YWHAH PE=1 SV=4 - [1433F_HUMAN]	2
Cysteine and glycine-rich protein 1 OS=Homo sapiens GN=CSRP1 PE=1 SV=3 - [CSRP1_HUMAN]	1
Myosin light chain 1/3, skeletal muscle isoform OS=Homo sapiens GN=MYL1 PE=1 SV=3 - [MYL1_HUMAN]	2
Eukaryotic initiation factor 4A-III OS=Homo sapiens GN=EIF4A3 PE=1 SV=4 - [IF4A3_HUMAN]	1
Zinc finger protein 638 OS=Homo sapiens GN=ZNF638 PE=1 SV=2 - [ZN638_HUMAN]	2
Exportin-2 OS=Homo sapiens GN=CSE1L PE=1 SV=3 - [XPO2_HUMAN]	1
Ubiquinone biosynthesis monooxygenase COQ6 OS=Homo sapiens GN=COQ6 PE=1 SV=2 - [COQ6_HUMAN]	1
Serine/threonine-protein kinase Nek10 OS=Homo sapiens GN=NEK10 PE=2 SV=2 - [NEK10_HUMAN]	2
Probable Xaa-Pro aminopeptidase 3 OS=Homo sapiens GN=XPNPEP3 PE=1 SV=1 -	1

[XPP3_HUMAN]	
Transmembrane channel-like protein 1 OS=Homo sapiens GN=TMC1 PE=1 SV=2 - [TMC1_HUMAN]	1
Leucine-rich repeat-containing protein 40 OS=Homo sapiens GN=LRRC40 PE=1 SV=1 - [LRC40_HUMAN]	1
Lactadherin OS=Homo sapiens GN=MFGE8 PE=1 SV=2 - [MFGM_HUMAN]	3
Calnexin OS=Homo sapiens GN=CANX PE=1 SV=2 - [CALX_HUMAN]	2
Neuroblast differentiation-associated protein AHNAK OS=Homo sapiens GN=AHNAK PE=1 SV=2 - [AHNK_HUMAN]	1
Glyceraldehyde-3-phosphate dehydrogenase, testis-specific OS=Homo sapiens GN=GAPDHS PE=1 SV=2 - [G3PT_HUMAN]	1
Cytochrome P450 2J2 OS=Homo sapiens GN=CYP2J2 PE=1 SV=2 - [CP2J2_HUMAN]	1
Golgi-specific brefeldin A-resistance guanine nucleotide exchange factor 1 OS=Homo sapiens GN=GBF1 PE=1 SV=2 - [GBF1_HUMAN]	1
Troponin I, cardiac muscle OS=Homo sapiens GN=TNNI3 PE=1 SV=3 - [TNNI3_HUMAN]	1
WD repeat-containing protein 33 OS=Homo sapiens GN=WDR33 PE=1 SV=2 - [WDR33_HUMAN]	1
Troponin I, fast skeletal muscle OS=Homo sapiens GN=TNNI2 PE=1 SV=2 - [TNNI2_HUMAN]	1
WD repeat-containing protein 92 OS=Homo sapiens GN=WDR92 PE=1 SV=1 - [WDR92_HUMAN]	1
WD repeat-containing protein 46 OS=Homo sapiens GN=WDR46 PE=1 SV=2 - [WDR46_HUMAN]	1
RasGAP-activating-like protein 1 OS=Homo sapiens GN=RASAL1 PE=1 SV=2 - [RASL1_HUMAN]	1
Guanine nucleotide-binding protein G(I)/G(S)/G(O) subunit gamma-5 OS=Homo sapiens GN=GNG5 PE=1 SV=3 - [GBG5_HUMAN]	1
CD59 glycoprotein OS=Homo sapiens GN=CD59 PE=1 SV=1 - [CD59_HUMAN]	1
Glucosamine--fructose-6-phosphate aminotransferase [isomerizing] 2 OS=Homo sapiens GN=GFPT2 PE=1 SV=3 - [GFPT2_HUMAN]	1
Fumarylacetoacetate hydrolase domain-containing protein 1 OS=Homo sapiens GN=FAHD1 PE=1 SV=2 - [FAHD1_HUMAN]	1
Tropomyosin alpha-3 chain OS=Homo sapiens GN=TPM3 PE=1 SV=1 - [TPM3_HUMAN]	2
Tropomyosin alpha-4 chain OS=Homo sapiens GN=TPM4 PE=1 SV=3 - [TPM4_HUMAN]	2
Myosin-Ia OS=Homo sapiens GN=MYO1A PE=1 SV=1 - [MYO1A_HUMAN]	1
Tropomyosin alpha-1 chain OS=Homo sapiens GN=TPM1 PE=1 SV=2 - [TPM1_HUMAN]	1
Tropomyosin beta chain OS=Homo sapiens GN=TPM2 PE=1 SV=1 - [TPM2_HUMAN]	1
17-beta-hydroxysteroid dehydrogenase type 6 OS=Homo sapiens GN=HSD17B6 PE=1 SV=1 - [H17B6_HUMAN]	1
Ras-related protein Rap-1b-like protein OS=Homo sapiens PE=2 SV=1 - [RP1BL_HUMAN]	1
Prospero homeobox protein 2 OS=Homo sapiens GN=PROX2 PE=2 SV=2 - [PROX2_HUMAN]	1
Putative upstream-binding factor 1-like protein 1 OS=Homo sapiens GN=UBTFL1 PE=5 SV=1 - [UBFL1_HUMAN]	1
G2 and S phase-expressed protein 1 OS=Homo sapiens GN=GTSE1 PE=1 SV=2 - [GTSE1_HUMAN]	2
Inversin OS=Homo sapiens GN=INVS PE=1 SV=2 - [INVS_HUMAN]	1
Zinc finger protein 782 OS=Homo sapiens GN=ZNF782 PE=2 SV=1 - [ZN782_HUMAN]	1
Eukaryotic translation initiation factor 3 subunit C OS=Homo sapiens GN=EIF3C PE=1 SV=1 - [EIF3C_HUMAN]	1
DnaJ homolog subfamily C member 25 OS=Homo sapiens GN=DNAJC25 PE=2 SV=1 - [DJC25_HUMAN]	1
Coiled-coil domain-containing protein 28A OS=Homo sapiens GN=CCDC28A PE=1 SV=1 - [CC28A_HUMAN]	1
Cytochrome P450 27C1 OS=Homo sapiens GN=CYP27C1 PE=2 SV=1 - [C27C1_HUMAN]	1
Cell division control protein 6 homolog OS=Homo sapiens GN=CDC6 PE=1 SV=1 - [CDC6_HUMAN]	1
Proto-oncogene serine/threonine-protein kinase mos OS=Homo sapiens GN=MOS PE=1 SV=1 - [MOS_HUMAN]	1
Ribonucleases P/MRP protein subunit POP1 OS=Homo sapiens GN=POP1 PE=1 SV=2 - [POP1_HUMAN]	1
Titin OS=Homo sapiens GN=TTN PE=1 SV=2 - [TITIN_HUMAN]	3

DNA excision repair protein ERCC-8 OS=Homo sapiens GN=ERCC8 PE=1 SV=1 - [ERCC8_HUMAN]	1
Acetyl-CoA acetyltransferase, mitochondrial OS=Homo sapiens GN=ACAT1 PE=1 SV=1 - [THIL_HUMAN]	1
UPF0027 protein C22orf28 OS=Homo sapiens GN=C22orf28 PE=1 SV=1 - [CV028_HUMAN]	1
THO complex subunit 3 OS=Homo sapiens GN=THOC3 PE=1 SV=1 - [THOC3_HUMAN]	1
Pleiotropic regulator 1 OS=Homo sapiens GN=PLRG1 PE=1 SV=1 - [PLRG1_HUMAN]	1
WD repeat-containing protein 5B OS=Homo sapiens GN=WDR5B PE=2 SV=1 - [WDR5B_HUMAN]	1
Coiled-coil domain-containing protein 63 OS=Homo sapiens GN=CCDC63 PE=1 SV=1 - [CCD63_HUMAN]	1
Leishmanolysin-like peptidase OS=Homo sapiens GN=LMLN PE=2 SV=1 - [LMLN_HUMAN]	1
WD repeat-containing protein 86 OS=Homo sapiens GN=WDR86 PE=5 SV=2 - [WDR86_HUMAN]	1

Table 2: Proteomic Analysis of Exosomes Purified from Mock Infected Cells

Description, Human Proteins	# Peptides
Keratin, type II cytoskeletal 1 OS=Homo sapiens GN=KRT1 PE=1 SV=6 - [K2C1_HUMAN]	48
Keratin, type I cytoskeletal 9 OS=Homo sapiens GN=KRT9 PE=1 SV=3 - [K1C9_HUMAN]	45
Keratin, type I cytoskeletal 10 OS=Homo sapiens GN=KRT10 PE=1 SV=6 - [K1C10_HUMAN]	38
Keratin, type II cytoskeletal 2 epidermal OS=Homo sapiens GN=KRT2 PE=1 SV=2 - [K22E_HUMAN]	33
Keratin, type II cytoskeletal 6A OS=Homo sapiens GN=KRT6A PE=1 SV=3 - [K2C6A_HUMAN]	31
Keratin, type II cytoskeletal 6C OS=Homo sapiens GN=KRT6C PE=1 SV=3 - [K2C6C_HUMAN]	30
Keratin, type II cytoskeletal 6B OS=Homo sapiens GN=KRT6B PE=1 SV=5 - [K2C6B_HUMAN]	30
Keratin, type I cytoskeletal 14 OS=Homo sapiens GN=KRT14 PE=1 SV=4 - [K1C14_HUMAN]	35
Keratin, type I cytoskeletal 16 OS=Homo sapiens GN=KRT16 PE=1 SV=4 - [K1C16_HUMAN]	32
Keratin, type II cytoskeletal 5 OS=Homo sapiens GN=KRT5 PE=1 SV=3 - [K2C5_HUMAN]	29
Keratin, type I cytoskeletal 17 OS=Homo sapiens GN=KRT17 PE=1 SV=2 - [K1C17_HUMAN]	25
Hornerin OS=Homo sapiens GN=HRNR PE=1 SV=2 - [HORN_HUMAN]	8
Keratin, type II cytoskeletal 75 OS=Homo sapiens GN=KRT75 PE=1 SV=2 - [K2C75_HUMAN]	11
Desmoplakin OS=Homo sapiens GN=DSP PE=1 SV=3 - [DESP_HUMAN]	10
Keratin, type II cytoskeletal 2 oral OS=Homo sapiens GN=KRT76 PE=1 SV=2 - [K22O_HUMAN]	10
Protein S100-A9 OS=Homo sapiens GN=S100A9 PE=1 SV=1 - [S10A9_HUMAN]	8
Keratin, type I cytoskeletal 15 OS=Homo sapiens GN=KRT15 PE=1 SV=3 - [K1C15_HUMAN]	9
Keratin, type II cytoskeletal 3 OS=Homo sapiens GN=KRT3 PE=1 SV=3 - [K2C3_HUMAN]	9
Keratin, type I cytoskeletal 13 OS=Homo sapiens GN=KRT13 PE=1 SV=4 - [K1C13_HUMAN]	6
Keratin, type II cytoskeletal 8 OS=Homo sapiens GN=KRT8 PE=1 SV=7 - [K2C8_HUMAN]	5
Protein S100-A7 OS=Homo sapiens GN=S100A7 PE=1 SV=4 - [S10A7_HUMAN]	4
Keratin, type II cytoskeletal 1b OS=Homo sapiens GN=KRT77 PE=2 SV=3 - [K2C1B_HUMAN]	5
Keratin, type I cytoskeletal 19 OS=Homo sapiens GN=KRT19 PE=1 SV=4 - [K1C19_HUMAN]	7
Keratin, type I cytoskeletal 28 OS=Homo sapiens GN=KRT28 PE=1 SV=2 - [K1C28_HUMAN]	4
Keratin, type II cytoskeletal 72 OS=Homo sapiens GN=KRT72 PE=1 SV=2 - [K2C72_HUMAN]	3
Keratin, type II cytoskeletal 79 OS=Homo sapiens GN=KRT79 PE=1 SV=2 - [K2C79_HUMAN]	6
Protein S100-A8 OS=Homo sapiens GN=S100A8 PE=1 SV=1 - [S10A8_HUMAN]	4
Keratin, type II cytoskeletal 4 OS=Homo sapiens GN=KRT4 PE=1 SV=4 - [K2C4_HUMAN]	4
Calmodulin-like protein 5 OS=Homo sapiens GN=CALML5 PE=1 SV=2 - [CALL5_HUMAN]	3
Keratin, type II cytoskeletal 7 OS=Homo sapiens GN=KRT7 PE=1 SV=5 - [K2C7_HUMAN]	6
Keratin, type I cytoskeletal 25 OS=Homo sapiens GN=KRT25 PE=1 SV=1 - [K1C25_HUMAN]	2
Keratin, type I cytoskeletal 27 OS=Homo sapiens GN=KRT27 PE=1 SV=2 - [K1C27_HUMAN]	2
Annexin A2 OS=Homo sapiens GN=ANXA2 PE=1 SV=2 - [ANXA2_HUMAN]	4
Glyceraldehyde-3-phosphate dehydrogenase OS=Homo sapiens GN=GAPDH PE=1 SV=3 - [G3P_HUMAN]	3
Keratin, type I cytoskeletal 20 OS=Homo sapiens GN=KRT20 PE=1 SV=1 - [K1C20_HUMAN]	3
Keratin, type II cytoskeletal 73 OS=Homo sapiens GN=KRT73 PE=1 SV=1 - [K2C73_HUMAN]	5
Keratin, type II cytoskeletal 74 OS=Homo sapiens GN=KRT74 PE=1 SV=2 - [K2C74_HUMAN]	4
Desmoglein-1 OS=Homo sapiens GN=DSG1 PE=1 SV=2 - [DSG1_HUMAN]	4
Protein S100-A7A OS=Homo sapiens GN=S100A7A PE=1 SV=3 - [S1A7A_HUMAN]	2
Junction plakoglobin OS=Homo sapiens GN=JUP PE=1 SV=3 - [PLAK_HUMAN]	3
Fatty acid-binding protein, epidermal OS=Homo sapiens GN=FABP5 PE=1 SV=3 - [FABP5_HUMAN]	2
Keratin, type II cuticular Hb4 OS=Homo sapiens GN=KRT84 PE=2 SV=2 - [KRT84_HUMAN]	3
Keratin, type I cytoskeletal 24 OS=Homo sapiens GN=KRT24 PE=1 SV=1 - [K1C24_HUMAN]	2
Putative annexin A2-like protein OS=Homo sapiens GN=ANXA2P2 PE=5 SV=2 - [AXA2L_HUMAN]	3
Actin, cytoplasmic 1 OS=Homo sapiens GN=ACTB PE=1 SV=1 - [ACTB_HUMAN]	2

Actin, cytoplasmic 2 OS=Homo sapiens GN=ACTG1 PE=1 SV=1 - [ACTG_HUMAN]	2
Keratin, type I cytoskeletal 12 OS=Homo sapiens GN=KRT12 PE=1 SV=1 - [K1C12_HUMAN]	2
Glial fibrillary acidic protein OS=Homo sapiens GN=GFAP PE=1 SV=1 - [GFAP_HUMAN]	1
Keratin, type II cytoskeletal 80 OS=Homo sapiens GN=KRT80 PE=1 SV=2 - [K2C80_HUMAN]	2
Keratinocyte proline-rich protein OS=Homo sapiens GN=KPRP PE=1 SV=1 - [KPRP_HUMAN]	3
Neurofilament heavy polypeptide OS=Homo sapiens GN=NEFH PE=1 SV=4 - [NFH_HUMAN]	2
Keratin, type I cytoskeletal 26 OS=Homo sapiens GN=KRT26 PE=1 SV=2 - [K1C26_HUMAN]	1
Keratin, type II cytoskeletal 71 OS=Homo sapiens GN=KRT71 PE=1 SV=3 - [K2C71_HUMAN]	2
Filaggrin-2 OS=Homo sapiens GN=FLG2 PE=1 SV=1 - [FILA2_HUMAN]	1
Keratin, type II cytoskeletal 78 OS=Homo sapiens GN=KRT78 PE=2 SV=2 - [K2C78_HUMAN]	2
Keratin, type I cytoskeletal 23 OS=Homo sapiens GN=KRT23 PE=1 SV=2 - [K1C23_HUMAN]	1
Keratin-like protein KRT222 OS=Homo sapiens GN=KRT222 PE=2 SV=1 - [KT222_HUMAN]	1
Cathepsin D OS=Homo sapiens GN=CTSD PE=1 SV=1 - [CATD_HUMAN]	1
Protein S100-A11 OS=Homo sapiens GN=S100A11 PE=1 SV=2 - [S10AB_HUMAN]	1
Actin, alpha skeletal muscle OS=Homo sapiens GN=ACTA1 PE=1 SV=1 - [ACTS_HUMAN]	1
Actin, gamma-enteric smooth muscle OS=Homo sapiens GN=ACTG2 PE=1 SV=1 - [ACTH_HUMAN]	1
Actin, alpha cardiac muscle 1 OS=Homo sapiens GN=ACTC1 PE=1 SV=1 - [ACTC_HUMAN]	1
Actin, aortic smooth muscle OS=Homo sapiens GN=ACTA2 PE=1 SV=1 - [ACTA_HUMAN]	1
POTE ankyrin domain family member I OS=Homo sapiens GN=POTEI PE=3 SV=1 - [POTEI_HUMAN]	1
POTE ankyrin domain family member F OS=Homo sapiens GN=POTEF PE=1 SV=2 - [POTEF_HUMAN]	1
POTE ankyrin domain family member E OS=Homo sapiens GN=POTEE PE=1 SV=3 - [POTEE_HUMAN]	1
Alpha-enolase OS=Homo sapiens GN=ENO1 PE=1 SV=2 - [ENOA_HUMAN]	1
Beta-enolase OS=Homo sapiens GN=ENO3 PE=1 SV=5 - [ENOB_HUMAN]	1
Gamma-enolase OS=Homo sapiens GN=ENO2 PE=1 SV=3 - [ENOG_HUMAN]	1
Arginase-1 OS=Homo sapiens GN=ARG1 PE=1 SV=2 - [ARGI1_HUMAN]	2
Microtubule-associated protein 1B OS=Homo sapiens GN=MAP1B PE=1 SV=2 - [MAP1B_HUMAN]	2
Keratin, type I cytoskeletal 18 OS=Homo sapiens GN=KRT18 PE=1 SV=2 - [K1C18_HUMAN]	1
Keratin, type I cuticular Ha7 OS=Homo sapiens GN=KRT37 PE=2 SV=3 - [KRT37_HUMAN]	1
Keratin, type I cuticular Ha3-II OS=Homo sapiens GN=KRT33B PE=2 SV=3 - [KT33B_HUMAN]	1
Keratin, type I cuticular Ha6 OS=Homo sapiens GN=KRT36 PE=1 SV=1 - [KRT36_HUMAN]	1
Keratin, type I cuticular Ha8 OS=Homo sapiens GN=KRT38 PE=2 SV=3 - [KRT38_HUMAN]	1
Keratin, type I cuticular Ha1 OS=Homo sapiens GN=KRT31 PE=2 SV=3 - [K1H1_HUMAN]	1
Keratin, type I cuticular Ha5 OS=Homo sapiens GN=KRT35 PE=2 SV=5 - [KRT35_HUMAN]	1
Keratin, type I cuticular Ha2 OS=Homo sapiens GN=KRT32 PE=1 SV=3 - [K1H2_HUMAN]	1
Peroxiredoxin-1 OS=Homo sapiens GN=PRDX1 PE=1 SV=1 - [PRDX1_HUMAN]	1
Peroxiredoxin-2 OS=Homo sapiens GN=PRDX2 PE=1 SV=5 - [PRDX2_HUMAN]	1
Calmodulin-regulated spectrin-associated protein 2 OS=Homo sapiens GN=CAMSAP2 PE=1 SV=3 - [CAMP2_HUMAN]	1
Arf-GAP with SH3 domain, ANK repeat and PH domain-containing protein 2 OS=Homo sapiens GN=ASAP2 PE=1 SV=3 - [ASAP2_HUMAN]	1
Transmembrane and coiled-coil domain-containing protein 6 OS=Homo sapiens GN=TMCO6 PE=2 SV=2 - [TMCO6_HUMAN]	1
Transcription factor 15 OS=Homo sapiens GN=TCF15 PE=2 SV=3 - [TCF15_HUMAN]	1
DnaJ homolog subfamily C member 15 OS=Homo sapiens GN=DNAJC15 PE=1 SV=2 - [DJC15_HUMAN]	1
Plasminogen activator inhibitor 2 OS=Homo sapiens GN=SERPINB2 PE=1 SV=2 - [PAI2_HUMAN]	1
Cyclin-dependent kinase 7 OS=Homo sapiens GN=CDK7 PE=1 SV=1 - [CDK7_HUMAN]	1
Bifunctional ATP-dependent dihydroxyacetone kinase/FAD-AMP lyase (cyclizing) OS=Homo sapiens GN=DAK PE=1 SV=2 - [DHAK_HUMAN]	1
Zinc finger protein 878 OS=Homo sapiens GN=ZNF878 PE=3 SV=2 - [ZN878_HUMAN]	1
ETS homologous factor OS=Homo sapiens GN=EHF PE=2 SV=1 - [EHF_HUMAN]	1

FCH and double SH3 domains protein 2 OS=Homo sapiens GN=FCHSD2 PE=1 SV=3 - [FCSD2_HUMAN]	1
Amiloride-sensitive sodium channel subunit delta OS=Homo sapiens GN=SCNN1D PE=1 SV=2 - [SCNND_HUMAN]	1
Serpin B3 OS=Homo sapiens GN=SERPINB3 PE=1 SV=2 - [SPB3_HUMAN]	2
Serpin B4 OS=Homo sapiens GN=SERPINB4 PE=1 SV=2 - [SPB4_HUMAN]	1
Nesprin-2 OS=Homo sapiens GN=SYNE2 PE=1 SV=3 - [SYNE2_HUMAN]	1
AF4/FMR2 family member 4 OS=Homo sapiens GN=AFF4 PE=1 SV=1 - [AFF4_HUMAN]	1

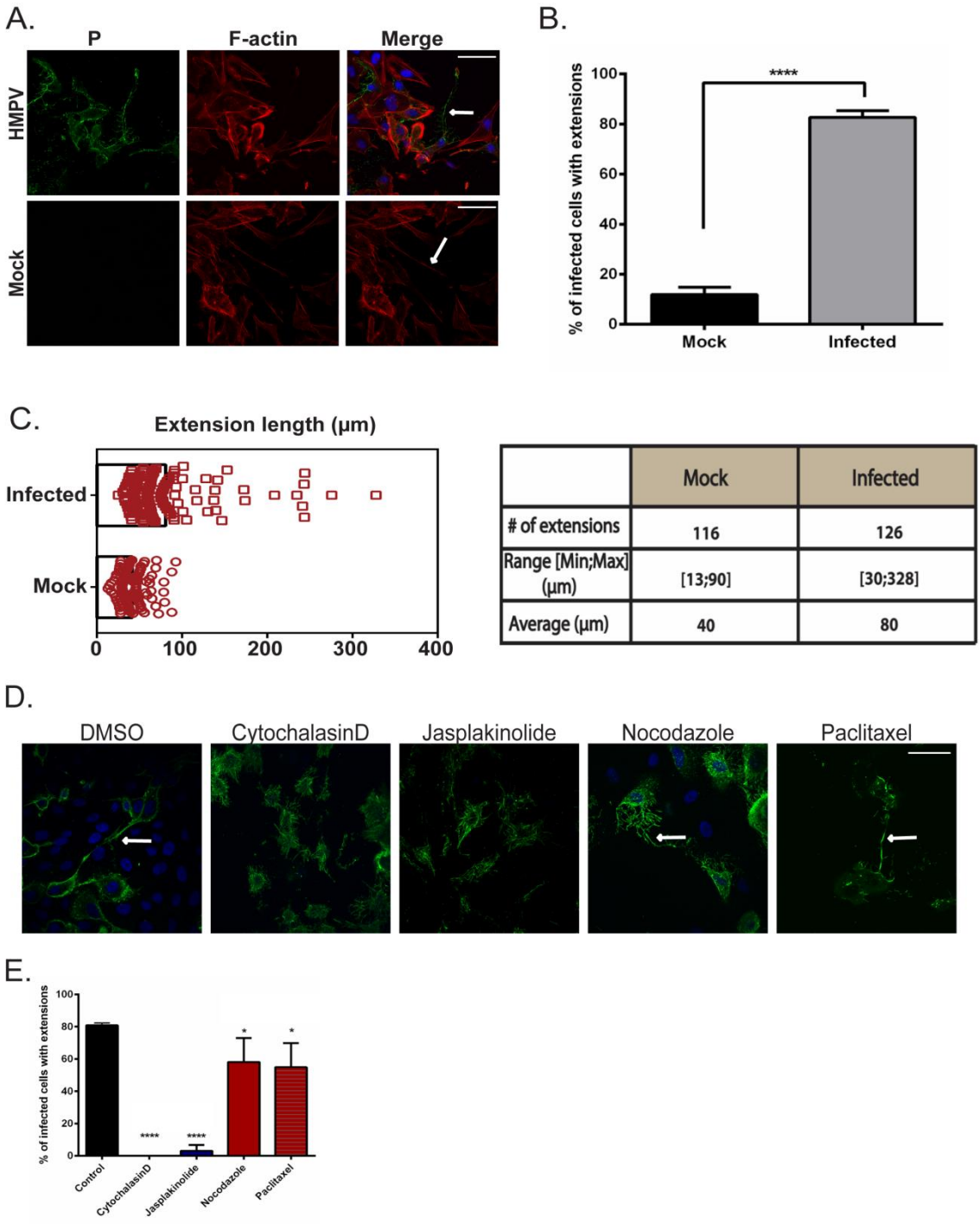

	Mock	Infected
# of extensions	116	126
Range [Min;Max] (µm)	[13;90]	[30;328]
Average (µm)	40	80

Figure 3.4. HMPV-induced elongation of intercellular extensions involves both actin and microtubules

A) BEAS-2B were mock infected or infected with HMPV and 24 h.p.i. cells were fixed and stained for HMPV N or F-actin. Arrows indicate intercellular extensions. B) BEAS-2B, were either mock infected or infected with HMPV and 24 h.p.i. cells were fixed and processed for immunofluorescence staining. Images were taken and extension length for 100 cells was determined using image J analysis tool. C) Cells were infected with HMPV for 2 hours and incubated with DMSO or the indicated drug. 24 h.p.i., cells were processed for imaging. D and E) Images were analyzed using image J analysis tool and the percentage of cells with extensions was determined.

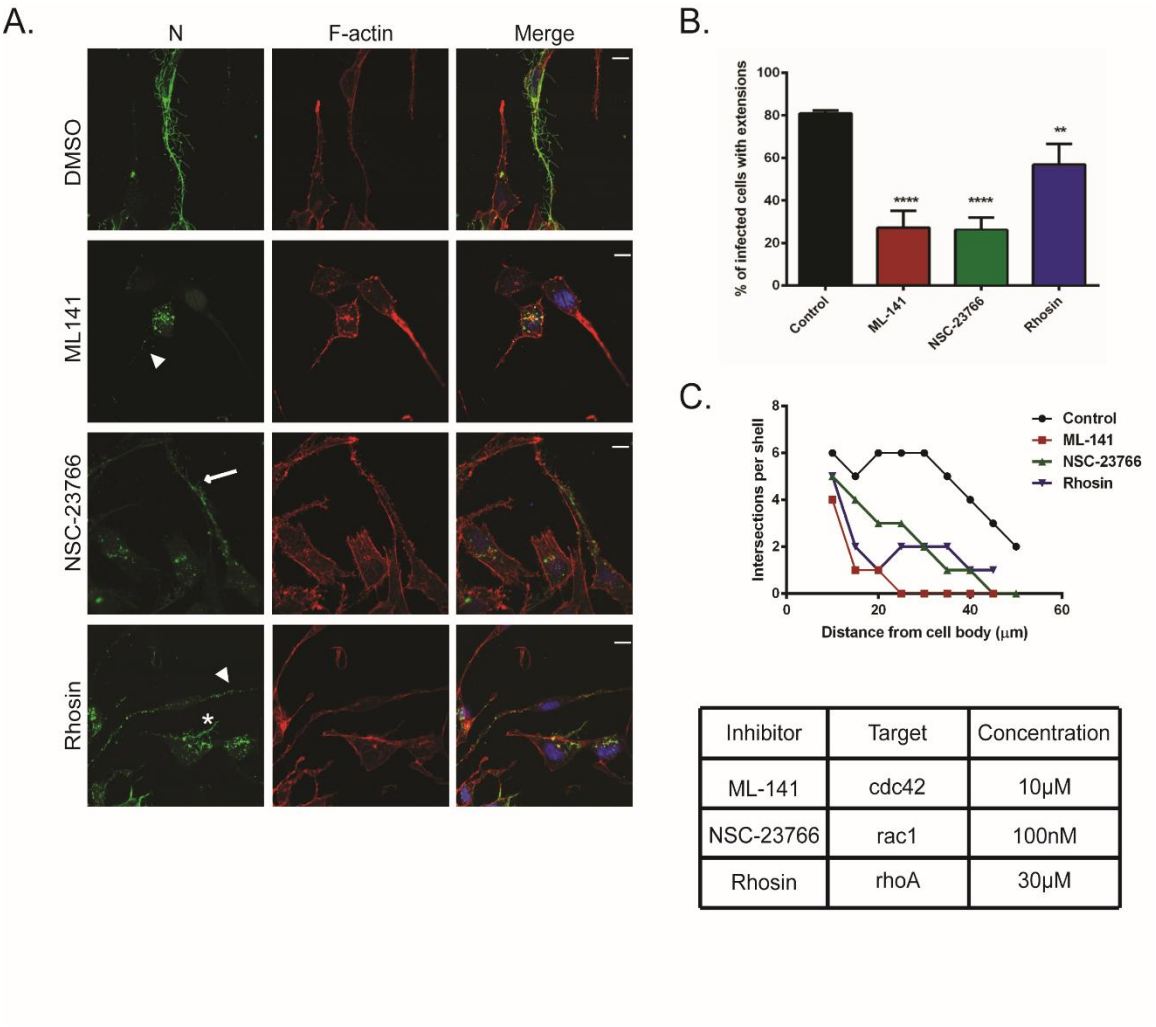

Inhibitor	Target	Concentration
ML-141	cdc42	10μM
NSC-23766	rac1	100nM
Rhosin	rhoA	30μM

Figure 3.5. Actin cytoskeleton rearrangement induced by HMPV infection involve signaling mediated by cdc42, rac1 and rhoA GTPases.

A) Cells were infected with HMPV and drugs added 2 hours later. 24 h.p.i. cells were fixed and stained for HMPV N or F-actin. Arrows indicate intercellular extensions. Images were then processed using neuron j analysis tool for determination of percentage of infected cells with extensions (B) or degree of branching (C). Statistical analysis was done using One-ay ANOVA, **p<0.01, ***p<0.001.

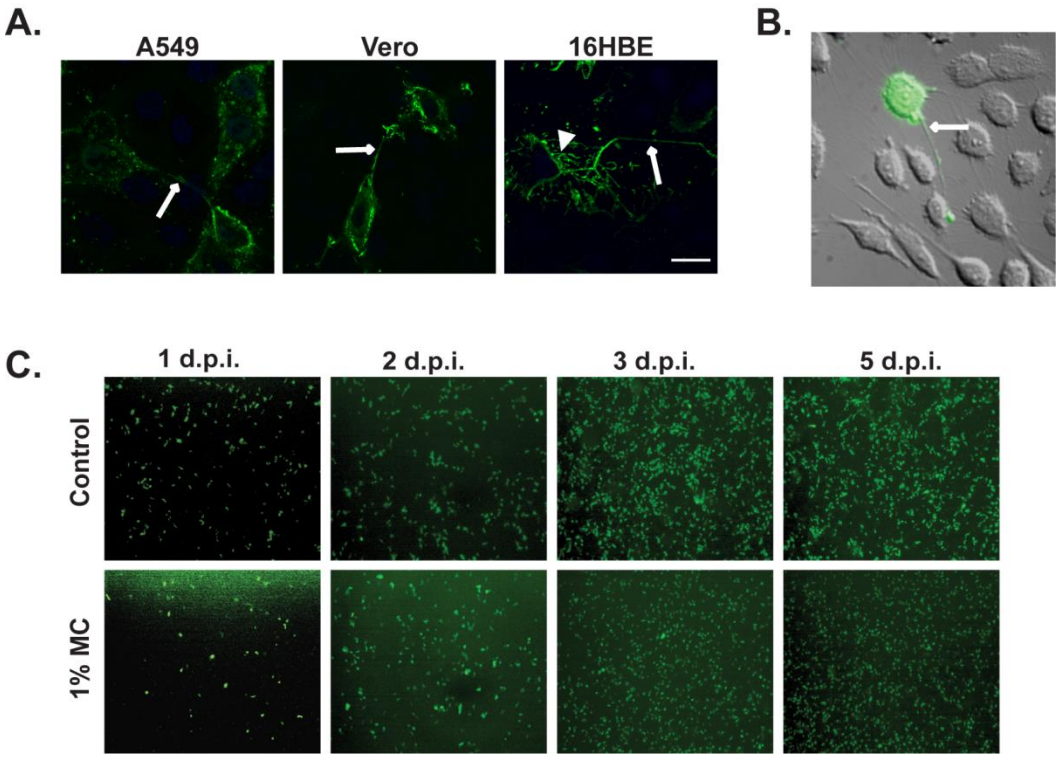

Figure 3.6. Intercellular extensions exist in live cells and HMPV can spread in the presence of methylcellulose.

A) A549, Vero or 16HBE cells were infected with HMPV and 24 h.p.i., cells were fixed and stained for N protein. Arrows indicate intercellular extensions and arrowhead shows branched filaments. Scale bar = 20 µm. B) BEAS-2B cells were infected with rgHMPV and 24 h.p.i. live cells were imaged on Axiovert100 microscope. Arrow shows intercellular extension. C) BEAS-2B cells were infected with rgHMPV at an M.O.I. of 1 and 2 hours later, infection media was removed and replaced with regular media or media containing 1% methylcellulose (MC). Images were taken every 24 hours for 5 days

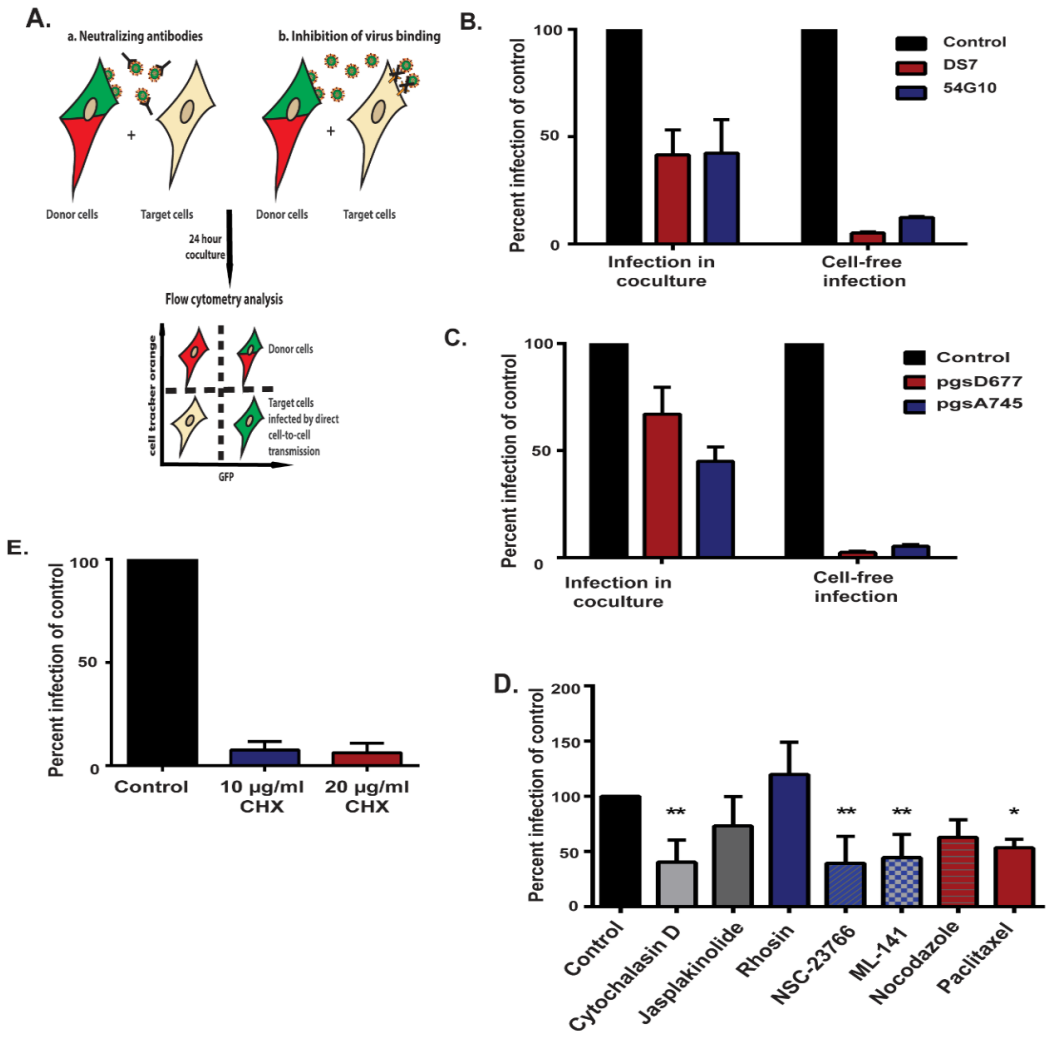

Figure 3.7. HMPV can spread directly from cell-to-cell.

A) Schematic of the coculure assay. BEAS-2B cells were infected with rgHMPV at an M.O.I. of 2 and 48 h.p.i., cells were stained with cell tracker CMRA orange dye for 30 minutes. Infected donor cells were then collected and incubated with naïve target cells at a ratio of 1:1. To study direct cell transmission, assay was done in the presence of neutralizing antibodies (B) or using target cells that lack heparan sulfate binding factor for HMPV infection (C) 24 hours post coculture cells were collected and analyzed by flow cytometry. (D) Donor cells were treated with the indicated inhibitor 1 hour prior to coculture and maintained in the media for 24 hours. Cells were collected and analyzed by

flow cytometry. (E) Cyclohexamide was added to cells either 2 hours post infection by cell-free particles or directly following coculture. 24 hours later, cells were collected and analyzed by flow cytometry. Error bars indicate mean ± standard deviation. Statistical analysis was done using ANOVA, *$p<0.05$, **$p<0.01$.

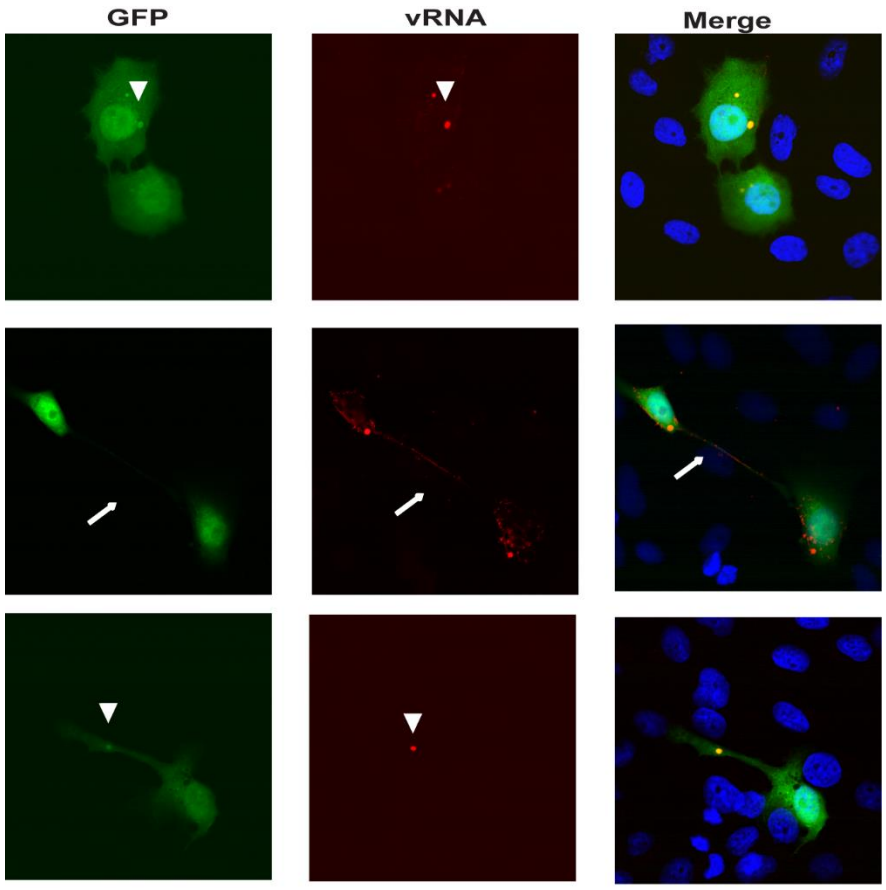

Figure 3.8. HMPVvRNA is present in intercellular extensions.

72 hours post infection with rgHMPV, cells were fixed in 70% ethanol and incubated with the FISH probes targeting viral RNA overnight. Cells were then washed with 2xSCC buffer and mounted with vectashield. Arrow indicates intercellular extension and arrowhead shows replication body.

CHAPTER 4: HMPV INFECTION IN A HUMAN AIRWAY EPITHELIUM MODEL

Introduction

Human metapneumovirus (HMPV) is a respiratory pathogen of the *Paramyxoviridae* family that was first isolated in 2001 in the Netherlands [2]. Today, HMPV is considered the second or third most common cause of hospitalization in children following respiratory pathogen behind human respiratory virus (RSV) [41] and causes respiratory tract disease worldwide [12,21-24,296]. The most common symptoms caused by HMPV include cough, fever, rhinitis and wheezing [38]. More severe infections occur mainly in infants, elderly and immunocompromised patients, resulting in bronchiolitis, croup and pneumonia. A few reports have associated HMPV with infections in the central nervous system [45-47]; however, studies of HMPV infection in small animal models and nonhuman primates show that HMPV infects the upper and lower respiratory tract, with no evidence for dissemination of infection to internal organs, thus indicating a primary tropism of HMPV for the respiratory epithelium [226,297,298]. HMPV was shown to infect airway epithelial cells from nasal tissues to the bronchioles, and viral replication occurred mainly in ciliated epithelial cells in macaques [297-300]. Progress of infection is associated with disruption to the architecture of the epithelium, sloughing of cells, loss of ciliation and lung inflammation [297-299,301]. The airway epithelium functions as an important line of defense against respiratory pathogens due to the ability of epithelial cells to create a permeability barrier at the mucosal surface, elicit innate immune recognition, and release cytokines, chemokines, mucus and a variety of antimicrobial substances. Epithelial cells are a specialized cell type characterized by their polarized plasma membrane which is divided into two discrete domains, the apical domain and the basolateral domain, established by the sorting of proteins and lipids in the trans golgi network or secretory pathways and recycling endosomes [302]. In addition, these cells form special cell-cell junctions including gap junctions, desmosomes and the apical junction complex made up of tight junctions and adherens junctions that are critical for epithelial barrier function [303]. The mechanisms that contribute to the polarized nature and the permeability barrier function of epithelial cells can influence virus infections and viruses in turn have evolved different mechanisms for manipulating

these pathways during infection. Several paramyxoviruses utilize epithelial surfaces as important replication sites and studies of these viruses in polarized cells revealed important information about different aspects of the viral life cycle and mechanisms of pathogenesis [139,304-306]. Very little is currently known about the characteristics of HMPV infection in polarized human respiratory epithelial cells. We utilized a model of well-differentiated, polarized and pseudostratified human airway epithelium (HAE) to study HMPV infection and spread. Our results show that HMPV infection in HAE cultures is short-lived, does not result in decrease in transepithelial electric resistance (TEER) but was associated with enhanced cell shedding from the apical side. Viral structural proteins localize to the apical surface of the airway epithelium; however budding of virus particles at this side is inefficient. Interestingly, addition of neutralizing antibodies at the apical surface of HAE cultures did not inhibit spread of HMPV. In addition, infection of HAE tissues by HMPV resulted in reorganization of the cortical apical actin network and disruption of actin polymerization inhibited spread of infection, thus supporting a role of actin cytoskeleton in HMPV infection and spread in polarized epithelial cells. Collectively, our data provide novel insights into budding and spread of HMPV in HAE cultures and indicates a novel role of the actin cytoskeleton in HMPV infection in these tissues.

Results

HMPV infection at the apical side of polarized human airway epithelial tissues is associated with cell shedding and inefficient particle release

To examine HMPV infection in polarized epithelial cells, we obtained a model of highly differentiated, pseudostratified cultures of human-derived tracheal/bronchial epithelial cells that resemble the mucociliary phenotype and functions of the human airway epithelium with moving cilia and mucus production. HAE cultures (depicted in Figure 4.1A) obtained from Mattek Corporation were received and maintained for one week prior to conducting the infection studies while changing media at the basolateral side and washing the mucus on the apical side every other day. We first determined whether HMPV can infect the apical side or basolateral side of the HAE tissues. Cultures were inoculated with a recombinant GFP-expressing HMPV (rgHMPV) at a multiplicity

of infection (M.O.I.) of 3 at either surface for 2 hours, washed and incubated for different hours post infection to monitor spread of infection. Trypsin was added to media on the basolateral side and replenished every other day. Images were taken every 24 hours using a florescence microscope to detect GFP expression as an indication of rgHMPV infection. Figure 4.1B shows that inoculation of the virus from the apical side resulted in productive HMPV infection, whereas no infection was seen when the virus was added to the basolateral side. This suggests that at least one receptor(s) used by HMPV for entry, which has not been identified yet, exists at the apical side of the human airway epithelium. As a control for virus infection in HAE cultures, we infected tissues with GFP-expressing parainfluenza virus 5 (rgPIV5) at M.O.I. of 3 and monitored progress of infection. Infection by rgPIV5 was more productive than HMPV and persisted for a longer period of time (Figure 4.1C) indicating significant differences between these two viruses. For cultures that were infected with HMPV at the apical side, an increase of GFP expression was seen as infection progressed from 24 hours post infection (h.p.i.) to 48 h.p.i. indicating spread of HMPV infection. However, at day 3 post infection, there was decrease in GFP expression and the decrease persisted to 7 days post infection (Fig 4.1B). This suggested that GFP-positive HMPV infected epithelial cells were being lost from the epithelium. To test this possibility, we quantified shedding of cells at the apical side by determining the amount of dsDNA that was present in the apical washes at different days post infection in both uninfected and HMPV-infected tissues. Shedding of cells was seen in both tissues and the pattern of shedding was the same suggesting that this is an intrinsic characteristic of these tissues; however, at 3 day post infection shedding of cells was significantly increased in tissues infected with HMPV (Figure 4.1D), which would correlate with decrease in GFP-positive cells in HAE tissues at this timepoint. The increase in shedding of cells in mock-infected tissues at 3 d.p.i. could be related to our experimental setup and handling of the tissues. An increase in shedding of ciliated cells from the airway epithelium was recently reported for RSV and was shown to be induced by the nonstructural protein NS2 [307]. HMPV lacks nonstructural proteins NS1/NS2 that are present in RSV particles suggesting that these two related viruses may utilize different ways for inducing shedding of infected cells that would contribute to airway obstruction which is a symptom of both viral infections.

To test whether the increased sloughing of cells upon HMPV infection resulted in disruption to the epithelium cultures, we examined changes in the ultrastructure of mock-infected and HMPV-infected tissues using transmission electron microscopy. Briefly, 48 hours after infection, tissues were fixed in glutaraldehyde/osmium oxide, dehydrated in ethanol to preserve the luminal surface and embedded in epoxy resins. Following overnight polymerization, sections were cut and tissues were examined using a transmission electron microscope. The architecture of the tissues showed pseudostratification with cilia on the apical surface (Figure 4.1E, arrow). No major differences were observed in the structure of tissues suggesting that HMPV infection, which peaked at 48 h.p.i. in HAE did not result in major cytopathology in these tissues (Figure 4.1E).

Assembly and budding of paramyxoviruses in polarized cells depends primarily on polarized sorting of viral envelope glycoproteins or the matrix protein (M) [308-312]. HMPV particles contain three envelope glycoproteins, fusion protein (F), attachment protein (G) and small hydrophobic protein (SH), an internal matrix protein (M) and proteins of the polymerase complex, large polymerase (L), polymerase cofactor phosphoprotein (P) and the RNA-encapsidating nucleocapsid protein (N). We determined location of M, N and F in HAE cultures at 24 h.p.i..HMPV F, M and N all localized to the apical side of the epithelium (Figure 4.2A arrows). Epithelial cell cultures are composed of different types of epithelial cells including ciliated and nonciliated cells in addition to mucus producing cells that face the apical surface as well as intermediate and basal cells at the basolateral side. HMPV was shown to preferentially infect ciliated cells in macaques [298] . To verify that HMPV infects ciliated cells in HAE, cultures were infected with HMPV and 24 hours later, tissues were fixed, frozen and cryosectioned. Immunofluorescence was then performed using antibodies for HMPV N protein and sentan (also termed sntn), a structural protein of apical cilia. HMPV N was located in cells that express the sntn protein indicating that HMPV infects ciliated epithelial cells in HAE (Figure 4.2B arrow), however N was also detected in cells that

didn't express sntn protein (Figure 4.2B arrowhead) suggesting that infection of non-ciliated cells can also occur.

The localization of HMPV M, N and F at the apical side suggests that budding of HMPV particles takes place at this surface of the epithelium. To determine titers of HMPV released at the apical surface, 150 µl of media was added on this side at different times post infection, incubated at 37ºC for 1 hour and flash frozen to preserve virus particles. Titers were then determined on LLCMK2 cells. We could not detect infectious HMPV particles at the apical side prior to 72 h.p.i. and virus titers were low at this time point, with an average of less than 1.5 $\log_{10}$ pfu/ml (Figure 4.2C). The low titers suggest that if HMPV particle release occurred at the apical side prior to 3 days post infection, it was below our detection limits in the plaque assay. As detection of very low amounts of virus may require a more sensitive assay, RT-PCR for the HMPV M gene was utilized, and low levels of the HMPV genome at the apical side at 24 and 48 h.p.i. was detected (Figure 4.2D). These results indicate that despite accumulation of HMPV structural proteins at the apical side of HAE, HMPV particles are released with low efficiency at the apical surface.

HMPV spread in HAE can occur independent of neutralizing antibodies

Our results above indicate that HMPV particles are released from the apical side of HAE cultures at low levels and we were unable to detect released particles prior to 3 days post infection; however rgHMPV spread was most evident from 24 to 48 h.p.i. (Figure 4.1B). Several respiratory paramyxoviruses have been studied in HAE cultures and results from these studies indicated significant differences between different family members; however, for these viruses including RSV, Sendai virus and measles virus, particles were efficiently released at either the apical side [313-315]. The low amounts of HMPV particles released at the apical side, in contrast to the efficient spread observed, suggests HMPV spread within HAE tissue may occur horizontally, i.e. directly from cell to cell without virus release and reentry. To test this interesting possibility, we analyzed HMPV spread in the presence of neutralizing antibodies. Tissues were infected with rgHMPV for 2 hours, washed and 100 µl of media alone or media containing neutralizing

antibodies was added to the apical side and spread was monitored while replenishing the antibodies every 24 hours. Two neutralizing antibodies, DS7 and 54G10, which target the fusion protein, were used. These antibodies have been shown to inhibit cell-free infection of HMPV in vitro [280,281]. Pre-incubation of HMPV with either DS7 or 54G10 antibodies before inoculation at the apical side showed a major decrease in infection (Figure 4.3A) indicating that these antibodies can neutralize cell-free HMPV infection in HAE tissues. Interestingly, spread of HMPV in these tissues was not inhibited in the presence of neutralizing antibodies (Figure 4.3B) suggesting that HMPV has a neutralizing antibody independent mode of transmission in airway epithelial tissues.

HMPV infection induces remodeling of the cytoskeleton in HAE cultures

The ability of epithelial cells to establish and maintain cell-cell junctions and polarity depends in large part on the organization of the actin cytoskeleton and actin-associated signaling [316-318]. Actin in epithelial cells has a distinct organization that depends on interactions of actin with the cell junctions. The highly organized distribution of actin at the apical and lateral membranes of polarized epithelial cells often creates a barrier for the entry or exit of viruses that replicate at epithelial surfaces and viruses have evolved different mechanisms to manipulate the actin cytoskeleton in epithelial cells to establish infection [319]. Recent studies show that infection of both Sendai virus and RSV in polarized epithelial cells results in remodeling of the actin cytoskeleton [239,320]. For Sendai virus, reorganization of actin was associated with efficient release of virus particles and for RSV, actin remodeling induced disruption of apical junctional complexes. We have shown that HMPV infection in BEAS-2B cells leads to rearrangement of the actin cytoskeleton. In addition actin was present in large amounts in HMPV particles and played an important role in intercellular spread of HMPV and also contributed to release of virus particles. To determine the role of the actin cytoskeleton in HMPV infection in polarized epithelial cells, we infected HAE cultures with HMPV and 2 hours post infection, cytochalasin D and latrunculin A, drugs that disrupt polymerization of actin, were added to media at the basolateral side and infection was evaluated 48 hours later. Whereas initial infection was established in tissues that were treated with cytochalasin D and latrunculin A, spread of rgHMPV in these tissues was decreased compared to control DMSO treated HAE (Figure 4.4A), thus indicating that

an intact actin cytoskeleton plays an important role in spread of HMPV in the airway epithelium.

We next examined the effect of HMPV infection on the structure of the actin cytoskeleton in HAE. Tissues were either mock infected or infected with HMPV and 24 or 72 hours later, tissues were fixed and processed for immunofluorescence using phallodin to detect filamentous actin and antibodies for HMPV proteins to distinguish infected cells. In polarized epithelial cells, cortical actin filaments in association with tight and adherens junctions form an actin belt at the apical membrane which provides support between the subapical membrane and the junctional complex. In addition, filamentous actin, usually in conjunction with myosin I, is also present along the lateral membranes between tight junctions [318]. A normal organization of the actin cytoskeleton can be seen in mock infected tissues at both 24 and 72 hours post infection showing the terminal actin belt at the apical side (Figure 4.4B white arrow) and actin filaments along the lateral membrane (Figure 4.4B white arrowhead). However, tissues infected with HMPV exhibited a marked disruption of the apical actin belt (Figure 4.4B red arrow) mainly at sites where viral proteins localized. In addition, alterations in F-actin structure can be also observed at the lateral membrane (Figure 4.4B red arrowhead) in HMPV infected tissues. This reorganization of the actin cytoskeleton was seen at 24 h.p.i. and persisted to 72 h.p.i. indicating that HMPV induced alterations to the actin cytoskeleton occurred throughout this time (Figure 4.4B). Since the actin cytoskeleton plays a major role in establishment and stability of cell-cell junctions in polarized cells, we determined whether the changes in the organization of F-actin in HAE tissues upon HMPV infection were associated with disruption of the apical junction complex and loss of epithelial barrier function. Tissues were either mock infected or infected with HMPV and at different hours post infection, transepithelial electric resistance (TEER) was measured using a volt-ohm meter. Despite slight decrease in TEER in HMPV infected tissues compared to mock infected cultures during the first three days of infection, HAE cultures that were infected with HMPV maintain high TEER. In addition, epithelial resistance remains constant during the 7 day period of HMPV infection indicating functional tight junctions. Thus, these results indicate that HMPV infection in HAE

depends on an intact actin cytoskeleton for efficient spread and induces remodeling of the actin cytoskeleton organization but does not affect the epithelial barrier function.

Discussion

HMPV is an important human respiratory virus that causes upper and lower respiratory tract diseases ranging from cough and rhinorrhea to bronchiolitis and pneumonia. Several animal models have been used to study HMPV infection, including, mice, ferrets, cotton rats as well as nonhuman primates [298,299,321,322], and results from these studies have shown that HMPV infects primarily airway epithelial cells. Since its initial discovery in 2001, most experiments modeling HMPV infection have been done in non-polarized and non-respiratory cell types that do not represent the best physiological model to mimic HMPV infection in the airway epithelium. Thus, very little is currently understood about the interaction of HMPV with the airway epithelium. In this study, we utilized well differentiated, polarized human-derived bronchial/tracheal epithelial cells (HAE) that closely resemble the authentic human airway to study late stages of HMPV infection involving budding and spread. We show that HMPV infects the apical surface of HAE cultures, resulting in limited infection that is associated with an increase in cell shedding at day 3 post infection but does not efficiently release virus particles at the apical surface. In addition, HMPV infection in HAE resulted in remodeling of the actin cytoskeleton at the apical side within 24 hours post infection without significant effects on the architecture of the infected tissues or epithelial barrier function.

Evidence from experimental HMPV infection in macaques indicated that virus replication is short lived and restricted to airway tissues [298]. In that study, it was shown that HMPV excretion peaks two days following infection and that infected cells are lost from the epithelium starting 5 days post infection. Our data show similar observations with HMPV infection in HAE tissues. Infection was limited with the highest level of GFP expression detected 48 h.p.i. followed by decrease in GFP-expressing cells from days 3 to 7 post infection (Figure 4.1A). The decrease in GFP expression at 3 d.p.i. was associated with significant increase in cell shedding compared to mock infected tissues indicating an

enhanced loss of GFP-positive infected cells (Figure 4.1B). Detection of cells at the apical side in both mock and HMPV infected tissues is likely related to turnover of apical epithelial cells in HAE cultures. Shedding of cells in association with virus infection in HAE models has been shown for other respiratory viruses including PIV3, RSV and influenza virus [307,323,324]. Recently, it has been shown that sloughing of cells in RSV infected HAE was induced by the NS2 protein [307]. However, shedding of cells was significantly higher than non-infected tissues from days 3 to 7 after initial infection. This is in contrast to what we see for HMPV in that the pattern of shedding of cells is the same in mock and HMPV infected tissues but is enhanced with infection suggesting differences in the mechanisms by which these two viruses induce clearance of cells from HAE. In addition, our results show that HMPV does not induce changes in TEER during the course of infection for 7 days (Figure 4.4C) indicating that the epithelial barrier function is not disrupted, in contrast to what was recently reported for RSV [320]. Decrease in TEER during RSV infection was correlated with disruption of the apical junctional complex and is associated with changes in the actin cytoskeleton. Interestingly, HMPV induced alterations in the actin cytoskeleton that were manifested in disruption of apical actin belt at sites where HMPV proteins localized as well as changes in actin filaments at the lateral membranes (Figure 4.4B). The apical actin belts between adjacent cells interact with each other through the apical junctional complexes and studies have shown that changes in the cortical actin organization in epithelial tissues can alter the structure of tight junctions and barrier function [325,326]. Our results show that HMPV induced alteration to apical actin organization did not result in disruption of barrier function (Figure 4.4C), thus it remains to be determined if the alterations in actin organization during HMPV infection affect apical junction complex formation.

HAE models have been used to study several respiratory paramyxoviruses including PIV3, PIV5, RSV and Sendai virus [313-315,323]. Results from these studies showed that virus particles of these different family members bud preferentially from the apical side consistent with localized infection in the lungs. Interestingly however, our results show that although HMPV proteins M, F and N accumulate at the apical surface at 24 h.p.i., infectious particles could not be detected until 3 d.p.i. (Figure 2C). RT-PCR

revealed the presence of HMPV RNA genomes at 24 and 48 h.p.i. in apical washes of HAE (Figure 4.2D), indicating that the amount of particles released at these time points is below our detection limit in the plaque assay. In addition, the low titers of released HMPV at 3 d.p.i. (Figure 4.2C) show that release of HMPV at the apical side of HAE is not efficient. The inefficient release of HMPV particles at the apical side at 24 and 48 hours post infection, however, was coupled with an increase in virus spread from 24 to 48 hours (Figure 4.1B). Interestingly, detection of HMPV shedding in adults experimentally challenged with HMPV infection was shown to occur starting 4 days after infection and peaked at day 8-9 d.p.i. [327], which is later than most paramyxoviruses [328,329]. These observations raise important questions about the spread of HMPV within the airway epithelium. Our results show that HMPV can spread in HAE even in the presence of neutralizing antibodies (Figure 4.3B) and that spread requires cytoskeletal dynamics (Figure 4.4A). Spread of respiratory viruses within the epithelium is primarily thought to occur by release of virus particles at the apical side followed by reinfection of neighboring cells. However, alternative mechanisms of spread have been shown to occur for different viruses, including measles virus and herpes simplex virus (HSV), that involve either budding of viruses at the intercellular space between apical junction complexes or intercellular spread of viral genomes without extracellular particle release [257,330].

Collectively, our results suggest three possible models for HMPV spread in the airway epithelium. We have shown that HMPV release can occur at the apical face, although it is inefficient, indicating that at least some HMPV spread in the airway may result from particles budding out form the apical side which then re-infect neighboring cells (Figure 4.5, model 1). Examination of infected tissues using transmission electron microscopy allowed visualization of virus-like bodies in aggregates released at the apical side infected tissue but not in mock tissues, suggesting that HMPV release does not involve single particles but complexes of several virions, consistent with our observation of large networks of branched filaments in BEAS-2B cells (Figure 3.1A). Release of particles in this form may help stabilize viruses for transmission from host-to-host. The second model (Figure 4.5C model 2) posits spread of virus at the intercellular space

between cell-cell junctions. Changes in the apical actin belt at 24 and 72 h.p.i. indicate that these are not induced only by initial infection but persist during the infection process. It is possible that HMPV particles are released into the intercellular space where they gain access to a receptor there and this binding process may induce downstream signaling leading to changes in actin organization. In this case, virus infection would spread from cell-to-cell within the epithelium without release of particles at the luminal space, decreasing access by neutralizing antibodies difficult. In addition, this model would be consistent with the increase in GFP positive cells from 24 to 48 h.p.i. and the low amounts of HMPV genomes that were detected at these time points. One other alternative mode of spread of HMPV in HAE is the passage of particles between apical junction complexes (Figure 4.5 model 3), which would allow spread without release of extracellular particles and thus evade neutralizing antibodies. Figure 4.5 B shows a virus-like body at an intercellular junction. Several respiratory viruses use components of the apical junction complex as their receptors [257,331,332]. Due to the tight connection between the actin cytoskeleton and proteins of tight junctions or adherens junction, binding to these proteins can induce changes in actin that were seen in HMPV infection at the apical and lateral membranes. Furthermore, it has been shown that disruption of actin polymerization in epithelial tissues results in endocytosis of proteins of the apical junction complexes [325]. Thus, it is possible that HMPV utilizes a component of these cell-cell junction complexes for entry and inhibition of actin polymerization in HAE cultures led to internalization of that receptor and thus spread of HMPV was inhibited. How viruses transmit from cell to cell is determined by the location of the receptor in the polarized epithelium, thus identification of HMPV receptor will help uncover the mechanism of HMPV spread within the airway tissues and this requires further investigation.

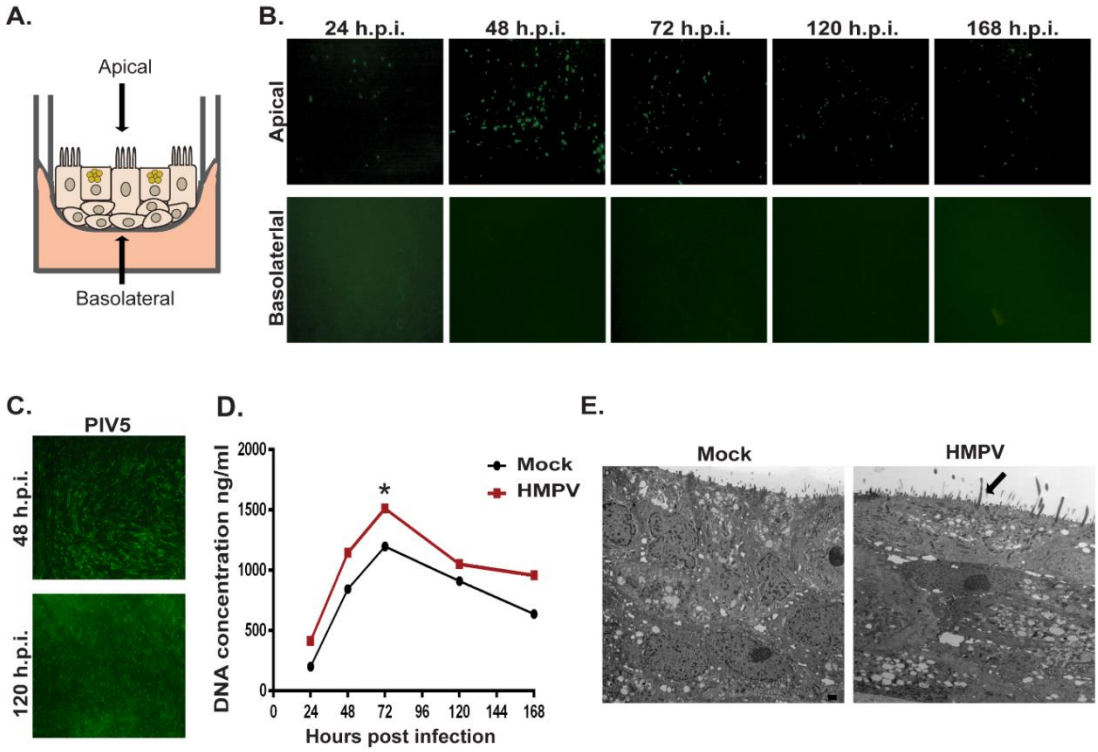

Figure 4.1. HMPV infection in polarized human airway epithelial cells (HAE).

A) Schematic of HAE. B) HAE tissues were washed three times with 75µg/ml of lysophosphatidylcholine (LPC) in hepes buffer saline (HBS) at the apical side or HBS only at the basolateral side. rgHMPV was then inoculated at either side at a multiplicity of infection (M.O.I.) of 3. 24 hours later, tissues were analyzed for GFP expression using a florescence microscope and pictures were taken at the indicated hours post infection. C) HAE were infected with rgPIV5 and images were taken at 48 and 120 h.p.i. D) To detect shedding of epithelial cells at the apical side of HAE, 150 µl of Opti-MEM media was added to apical surface at different hours post infection in mock- or HMPV- infected tissues followed by incubation at 37ºC for 1 hour. Apical washes were then analyzed for the amount of dsDNA. Statistical analysis was performed using one-way Anova. * indicates $p<0.01$. E) 48 hours post infection, HAE cultures were fixed and processed for imaging on a transmission electron microscope. Scale bar, 1µm.

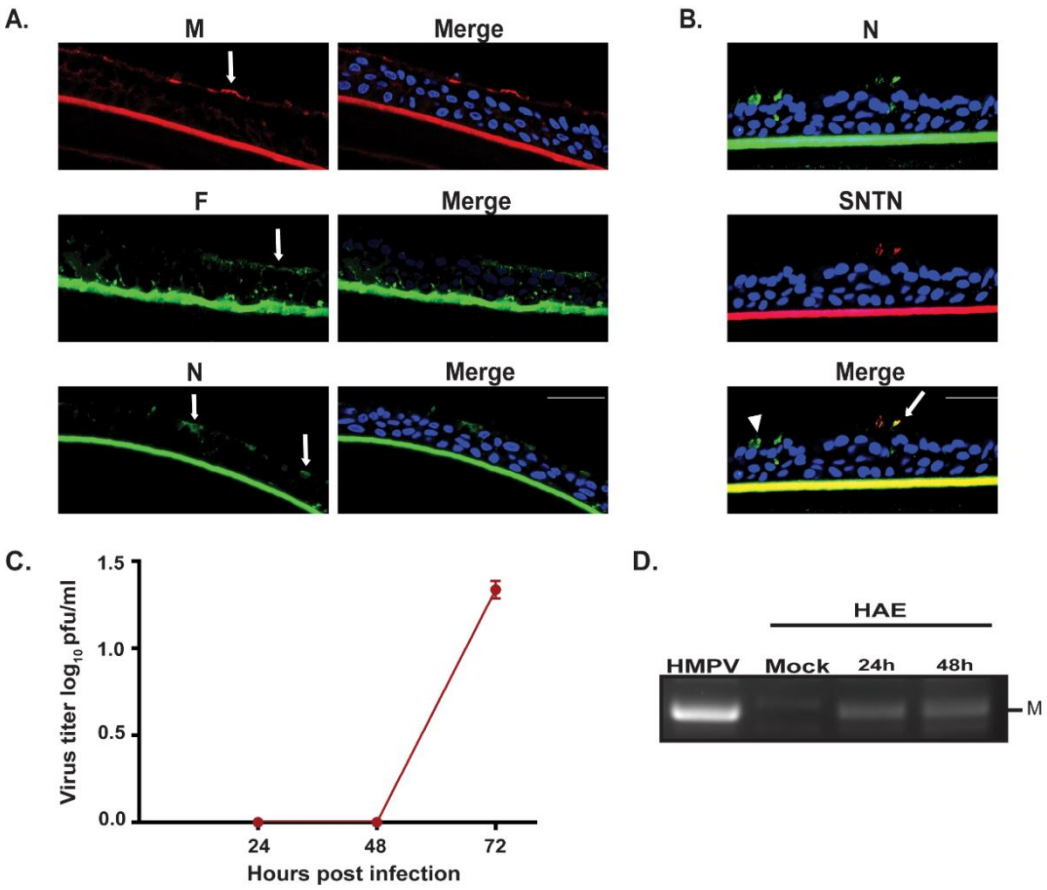

Figure 4.2. HMPV infection at apical surface of HAE is associated with inefficient virus release.

A) HAE tissues were infected with HMPV at an M.O.I. of 3 and 24 hours later, cultures were fixed in 4 % paraformaldehyde followed by embedding in OCT. Tissues were frozen, cryosectioned and processed for immunofluorescence staining with antibodies for the indicated viral protein. Images were taken on a confocal microscope. Arrows indicate protein localization at the apical side. Green line is autofluorescence from membrane. B) 24 hours post infection, HAE were fixed, embedded and cryosections were stained for HMPV N and SNTN. Arrow indicates colocalization of N with SNTN in ciliated cells and arrowhead indicates non-ciliated cell expressing N. C) To determine titers of rgHMPV released at the apical surface, 150µl of media was added to apical side and titers were determined. D) RNA extraction was performed on apical washes of HAE

followed by reverse transcriptase-PCR using primers for HMPV M. Scale bars, 50 μm. Error bars represent mean ±standard deviation of two independent experiments.

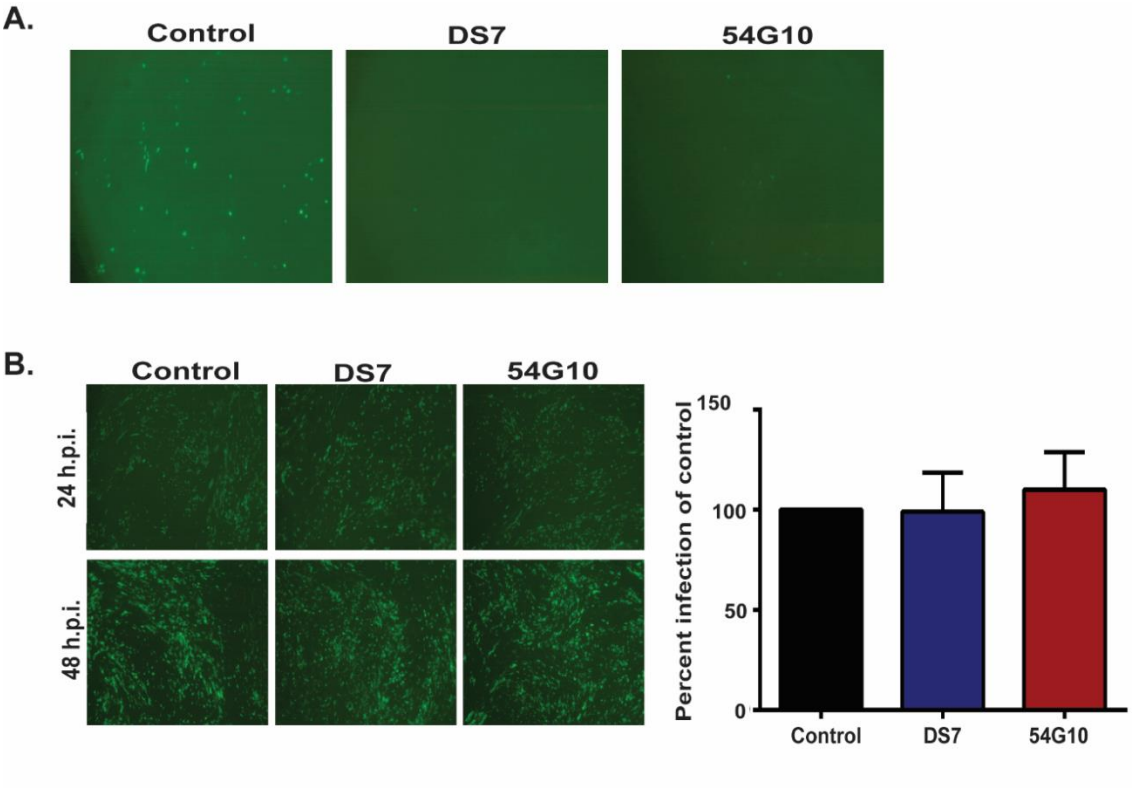

Figure 4.3. HMPV can spread in the presence of neutralizing antibodies in HAE.

A) Infection media with rgHMPV at M.O.I. of 3 was preincubated in the absence or presence of neutralizing antibodies DS7 (10µg/ml) and 54G10 (0.4µg/ml) for 1 hour at 37ºC while rotating every 15 minutes. HMPV was then inoculated at apical side and incubated for 2 hours. Infection media was then removed, apical surface washed once and images were taken on a florescence microscope 24 hours later. B) HAE tissues were infected with HMPV for 2 hours followed by addition of 100µl of control media or media containing the indicated antibody DS (10µg/ml) and 54G10 (0.4µg/ml). Images were taken every 24 hours to monitor spread of rgHMPV and media with antibodies was replenished every 24 hours. Cells were then collected with trypsin and analyzed with flow cytometry to determine percentage of GFP positive cells. Error bars represent mean ±standard deviation of two independent experiments. One-way ANOVA, non-significant.

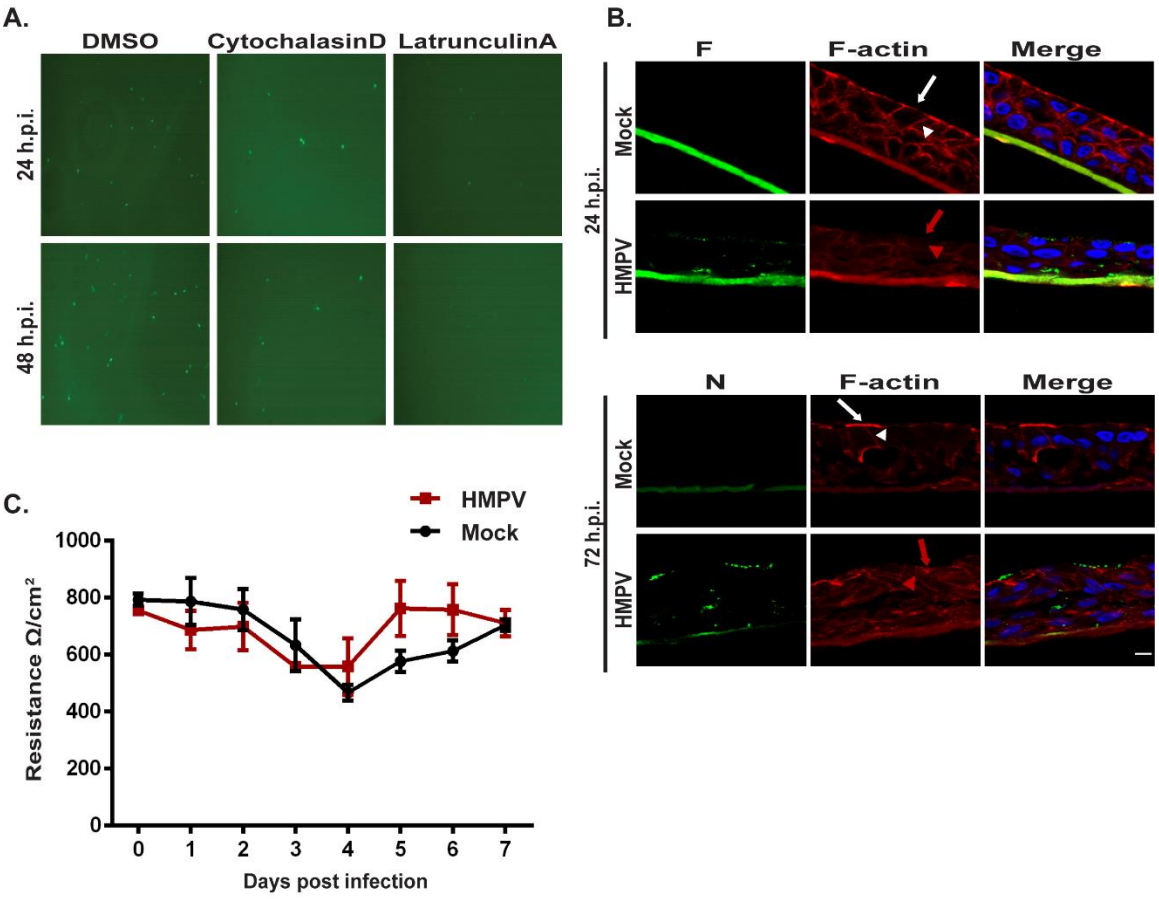

Figure 4.4. Actin cytoskeleton is involved in HMPV infection in HAE.

A) HAE cultures were infected with rgHMPV at an M.O.I. of 3 and 2 hours later media containing DMSO control, cytochalasinD (2µM) or latrunculinA (100nM) was added to the basolateral side. Images were taken 24 and 48 hours post infection on a florescence microscope B) HAE tissues were infected with HMPV and 24 or 72 hours later, tissues were fixed and processed for immunofluorescence. Arrows indicate apical actin belt and arrowheads indicate actin on the lateral membrane. C) TEER was measured before infection and at different times post infection in mock and HMPV infected HAE cultures using an ohm-meter. Error bars represent mean ± standard deviation for three experiments. Scale bar, 10µm.

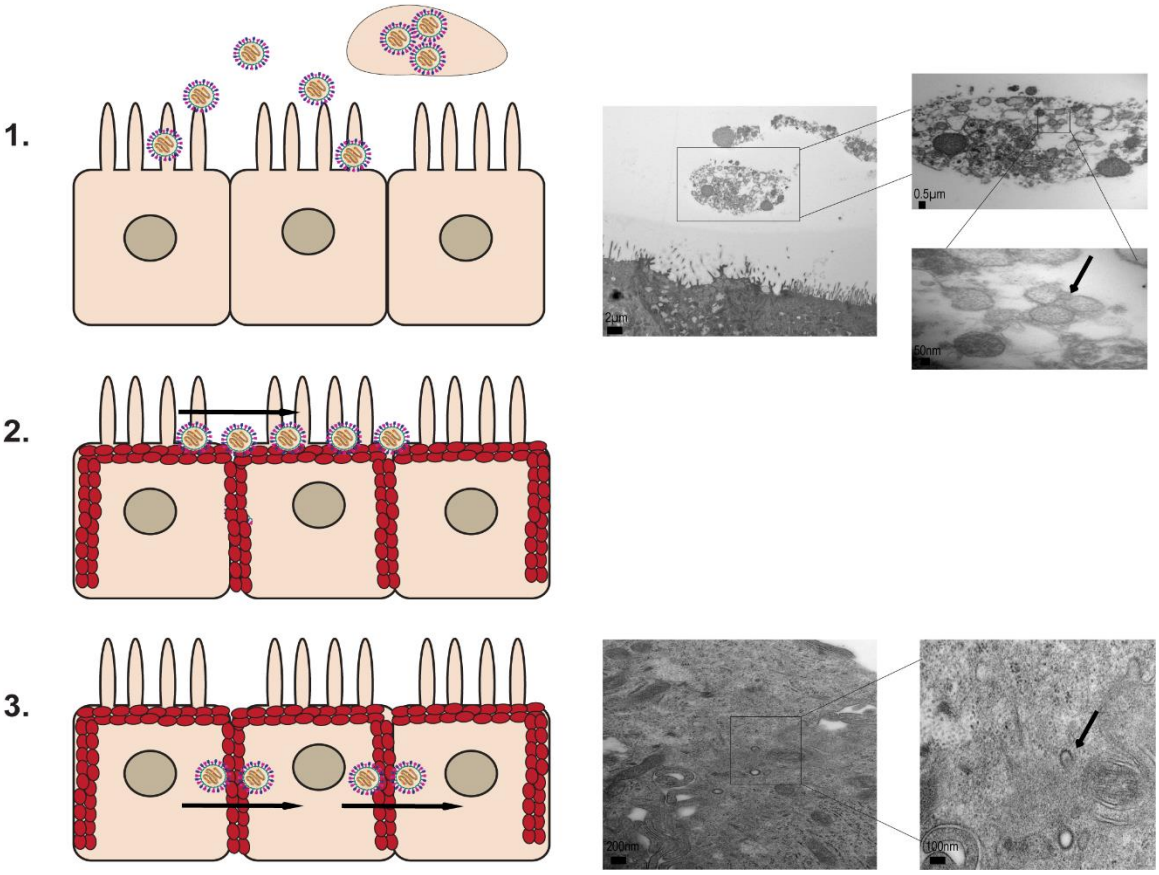

Figure 4.5. Possible models for HMPV spread in HAE.

Electron microscopy images show HMPV infected HAE and arrows indicate virus-like bodies.

CHAPTER 5: ROLE OF HMPV PHOSPHOPROTEIN IN LATE STAGES OF INFECTION

*This work was initiated by Brent Hackett who contributed intellectually to the project, generated the pCAGGS-P and pCAGGS-P-FLAG constructs. The pCAGGS-N construct was generated by Ursula Buchholz and pCAGGS-M by made by Andrea Eastes. The experiments shown in the figures in this chapter were performed by me.

Introduction

Paramyxovirus particles are generally formed by a budding process that follows assembly of virus components at the plasma membrane [82,83,333]. The matrix protein (M) is considered the driver of assembly and budding of paramyxoviruses due to its ability to bind and deform membranes and to bind to envelope proteins and inner ribonucleoprotein complex components (RNP) and several host factors that aid in the assembly and budding process; however, other virus components including surface glycoproteins, nucleocapsid (N) proteins or accessory protein C have been shown to contribute to the assembly and budding processes of different paramyxoviruses [14,54,55,69]. HMPV M protein has been shown to play an essential role in production of virus particles and virus spread [334]. In addition, it has been demonstrated that formation of HMPV virus-like particles (VLPs) occurs following co-expression of the F and M proteins, with the G protein enhancing this process, thus indicating an important role of these protein in the HMPV assembly process [10,233]. We have shown that HMPV assembly and spread in human bronchial epithelial cells involves manipulation of the cell cytoskeleton leading to the formation of branched networks of filaments and induction of intercellular extensions, structures that have not yet been reported for any members of the paramyxovirus family. Thus, we sought to determine what viral proteins contribute to the formation of these structures that are seen during HMPV infection. Interestingly, our results indicate that HMPV phosphoprotein (P) co-localizes with actin and reveal a novel role of P in inducing plasma membrane deformation and cellular extensions similar to those seen at late stages of HMPV infection.

Results

HMPV P protein induces remodeling of the plasma membrane

The ability of enveloped viruses to bud infectious particles at cell membranes requires induction of membrane curvature and envelopment of viral components with a cell-derived membrane. For paramyxoviruses, membrane budding is driven principally by matrix protein, at least partly due to its ability to bind and deform membranes, but efficiency can increase with envelope proteins or N proteins [82,83]. We have shown that the late stages of HMPV infection involve budding of complex structures of branched filaments from the plasma membrane and intercellular extensions. To determine what viral proteins contribute to membrane remodeling during HMPV infection, we performed single transfections of N, P, M and F in BEAS-2B cells. We did not include G and SH in our single transfection studies since branched filaments were seen in BEAS-2B cells infected with HMPV lacking G and SH (ΔG/ΔSH) (Figure 5.1B) indicating that G and SH proteins are not required for the formation of these structures. Expression of F or M proteins induced formation of short membrane extensions (Figure 5.1A insets) whereas N protein was primarily cytosolic, and no alteration of the membrane was observed with N expression. HMPV M protein has been shown to bind lipid membranes and self-assemble into long helical filaments and co-expression of both M and F induces filamentous VLP formation at the surface of Vero cells, thus it is not surprising that both F and M can induce membrane extensions [10,233,287]. Interestingly, expression of the HMPV P protein induced changes to the plasma membrane and formation of membrane extensions that resemble those seen in HMPV infection, in contrast to what has been seen for other paramyxovirus P proteins (Figure 5.1A arrow). In addition, branched filaments were seen in some cells expressing P (Figure 5.1A arrowhead). To determine whether P can induce membrane extensions in another cell line, we transfected P into A549 cells. Expression of P also resulted in deformation of the plasma membrane and induction of membrane ruffling (Fig 5.1C, inset). This indicates that P can induce changes to ~~the~~ plasma membrane morphology in two different human airway cell lines, A549 and BEAS-2B, thus suggesting a novel role of HMPV P in HMPV exit from the cell.

Spatio-temporal dynamics of cellular localization of HMPV P during the course of HMPV infection

Paramyxovirus P proteins are known for their role in regulating viral RNA transcription and replication due to their ability to bind both the viral polymerase L and the RNA encapsidating protein N. However, our results above suggest a role for HMPV P in late stages of the infection cycle. Production of infectious virus particles is a highly complex and coordinated process that requires spatio-temporal coordination of the different viral components. To examine the involvement of P at different stages of HMPV replication cycle and its possible involvement in assembly and budding stages, we investigated the dynamics of the distribution of M and P during HMPV replication cycle. Cells infected with HMPV were fixed at various times post infection, and immunolabeled with antibodies to detect viral proteins. At 6 hours post infection (h.p.i.), P was located in small punctate bodies in the cytoplasm (Figure 5.2A, P inset) and surprisingly P co-localized with M in short filaments within the cell (Figure 5.2A, merge, inset). To more closely examine these structures, high resolution STORM microscopy was performed. P was visualized in branched filaments, whereas M had a more diffuse localization (Figure 5.2B). Paramyxovirus P proteins are characterized by the presence of a central oligomerization domain, and recently a core tetramerization domain has been identified in HMPV P [335]; thus it is possible that oligomerization of P resulted in the formation of branched filaments or that P binds a host factor that promotes filament formation. By 9 hours, P was present in inclusion bodies in the cytosol (Figure 5.2A, inset), which are thought to be sites of viral RNA synthesis and we have shown earlier that they contain viral RNA (Figure 3.). At this time, P was also detected at the cell periphery along with M (Figure 5.2A arrow). Localization in inclusion bodies (inset) and at the cell periphery (arrow) was also seen by 12 h.p.i., but at this time point, both M and P localized in short cellular extensions (Figure 5.2A, arrowheads). By 18 h.p.i., P and M were primarily at the plasma membrane and also in filamentous structures (arrowheads). In addition, M was located in inclusion bodies with P possibly forming M-RNP complexes (inset). As infection progressed, both P and M were detected in intercellular extensions (red arrow) and in branched filaments (red arrowhead) at 24 h.p.i. These results show distinct localization patterns of P during the course of HMPV infection.

While P was detected in cellular inclusions as was previously reported [285] and which would correlate with its role in viral transcription and replication, P co-localized with M at different cellular locations throughout the infection cycle including intracellular branched protein filaments within the cell during early infection, which has not been previously reported for paramyxovirus replication. In addition, P was seen at the cell periphery, along with M, early in the infection cycle (9 h.p.i). A virus egress assay revealed that release of virus particles occurred between 12 and at 18 h.p.i. and not prior to that (Figure 5.2C) suggesting that localization of P at the cell periphery precedes viral budding. The coordinated localization of P and M during the course of infection and the peripheral localization of P early during infection implicate a role of P in HMPV assembly and egress. Taken together, these observations suggest that HMPV P has different roles during the infection cycle.

Addition of FLAG-tag at the C-terminus favors membrane deformation role of P

It has been previously demonstrated that co-expression of HMPV N and P in the absence of infection results in the formation of cytoplasmic bodies that resemble inclusion bodies in infected cells and that the two proteins interacted within the inclusion bodies [285]; however single expression of P protein induces membrane deformation (Figure 5.1A,C). We have shown that P during infection is present in inclusion bodies, in filaments and at the plasma membrane (Figure 5.2A) indicating that in infected cells, HMPV P may be interacting with other viral or cellular factors that alter its cellular distribution. Paramyxovirus phosphoproteins vary greatly in length, ranging from 241 amino acid residues for RSV P to 709 residues in Nipah P; however several reports have demonstrated that P proteins share a common domain organization with central oligomerization domains and regions of high intrinsic disorder, consistent with the ability of P proteins to bind multiple interaction partners during the course of infection [336]. In an attempt to further characterize the role of P in HMPV infection, we generated a FLAG-tagged construct of HMPV P with the FLAG tag at the C-terminus. To examine whether addition of the tag had an effect on the function of P protein, we transfected A549 cells with untagged or tagged P constructs alone or with a plasmid expressing

HMPV N. As was documented before [285], co-expression of P and N resulted in inclusion body formation (Figure 5.3 inset); however, interestingly, addition of the FLAG tag at the C-terminus of P prevented formation of inclusion bodies upon co-expression with N, and N was localized predominantly at the cell periphery (Figure 5.3, arrow). Thus, expression of P-FLAG with N, while preventing inclusion body formation, did not abrogate association of P and N, as seen by the predominant peripheral localization of both P-FLAG and N. In addition, P-FLAG induced more pronounced membrane extensions than the untagged P protein (Figure 5.3, arrowhead). This suggests that presence of the FLAG at the C-terminus of P enhances the role of the protein in inducing membrane deformation and thus mimicked the role of P at late stages of HMPV infection.

HMPV P co-localizes with actin

The ability of HMPV P to induce curvature and deformation of the plasma membrane raises two possibilities, either that P can bind membranes and its oligomerization at the plasma membrane induces membrane curvature or that P can interact with cellular factor (s) that induce changes in the shape of the plasma membrane. We have shown that the ability of HMPV to induce budding of branched filaments and elongation of intercellular elongation depends primarily on the actin cytoskeleton. The actin cytoskeleton plays an important role in regulating the shape and dynamics of the plasma membrane and thus we wanted to test the association between P and actin. Immunostaining showed co-localization of P with F actin in transfected cells in structures that resemble stress fibers (Fig 5.4A, inset) and in cell extensions (Fig 5.4A, arrow). To further demonstrate the association between P and actin, we performed a proximity ligation assay using antibodies against the P protein and beta actin. Figure 5.4B indicates that the percentage of cells with a positive red signal where each signal represents a single positive reaction for two proteins in close proximity. For paramyxoviruses, virus proteins that were shown to bind actin include M proteins of Sendai virus and NDV [231,337]. While our data show the first example of a paramyxovirus phosphoprotein that co-localizes with actin during infection and transfection, further studies are clearly needed to understand the role that HMPV P is playing at late stages of infection. These

results show a close association between P and actin in transfected and infected cells suggesting a possible role of actin in P-induced changes to the cell membrane; however whether P binds actin directly or an actin-binding protein remains to be demonstrated.

Discussion

Paramyxovirus P proteins are major components of the viral replication complex and can interact with both N and the polymerase L to regulate viral RNA transcription and replication [338]. P proteins are also characterized by the presence of intrinsically disordered regions, thus supporting interaction with multiple partners during the course of infection [336]. Recently, it has been shown that paramyxovirus P proteins can have roles beyond regulating viral RNA synthesis. The P protein of HPIV3 was found to bind SNAP29 protein and inhibit autophagosomal degradation to enhance release of virus particles [339]. In this chapter, we report a novel role for a paramyxovirus P protein in deforming the plasma membrane, suggesting the involvement of P in late stages of HMPV infection. The intracellular localization of P changed dramatically at different times post infection and had localization patterns in coordination with M, the master regulator of particle assembly. In addition, expression of P by itself resulted in formation of membrane extensions that resemble those seen at budding and egress steps of HMPV infection. Interestingly, addition of a FLAG epitope tag at the C-terminus of P enhanced the membrane deforming properties of the P protein and prevented the formation of inclusion bodies upon co-expression with N, while still allowing co-localization of P-FLAG and N at the cell periphery. Recent structural analyses of HMPV P revealed a domain organization similar to other paramyxovirus P proteins. N-terminus residues 1-30 form a conserved domain with predicted α-helical propensity, residues 31-157 and 238-294 are predicted to be disordered, residues 158-237 are predicted to form an α-helical region, while the region between residues 171 and 194 is the core tetramerization domain. Sequence alignment of HMPV P with the P protein of respiratory syncytial virus RSV showed that, similar to other paramyxoviruses, putative L and N binding regions are located at the C-terminus region [335]. Several reports support a role of the carboxy terminal region of paramyxovirus P in binding L and N:RNA complexes and the C-terminus end in binding the soluble form of N protein, acting as a chaperone [340-344].

Co-expression of P-FLAG and N was associated with strong co-localization of the two proteins at the cell periphery, in membrane extensions and membrane blebs, but not in inclusion bodies. This suggests that the FLAG peptide might be preventing or displacing binding of P to a host factor(s) at the carboxy terminus that is involved in inclusion body formation while at the same time favoring an interaction with other host factor(s) that might play a role in the ability of HMPV P to deform membranes. The presence of an intrinsically disordered region at the C-terminus (residues 238-294) of P would be consistent partner binding to this region. However, it is also possible that the FLAG peptide affects the overall conformation of the protein, altering its function and its interaction with N. Thus, how addition of the FLAG peptide alters the conformation of P and its ability to bind N or cellular factors requires further investigation. In addition, very little is currently known about inclusion bodies and the cellular factors that contribute to their formation; P-FLAG presents a tool for future studies aiming at the identification of host factors that can play a role in inclusion body formation at early stages of the replication cycle and other factors that promote the ability of P to deform membranes by comparing cellular proteins that can bind P and P-FLAG.

While our attempts to identify possible interaction partners for P-FLAG and P that can play a role in membrane deformation by doing co-immunoprecipitation were not successful (data not shown), we were able to show close association of P with cellular actin. A large number of viruses encode proteins that directly bind actin, actin binding proteins or other effectors of actin mediated signaling [216,345]. For paramyxoviruses, virus proteins that were shown to bind actin include M proteins of Sendai virus and NDV [231,337]. Our data show the first example of a paramyxovirus phosphoprotein that can deform membranes and co-localizes with actin during infection and transfection; further studies are clearly needed to understand the role that HMPV P is playing at late stages of infection, whether HMPV P can bind actin directly or actin-binding proteins, how the association of P with actin is regulated during infection and what role actin is playing in the ability of P to induce membrane remodeling.

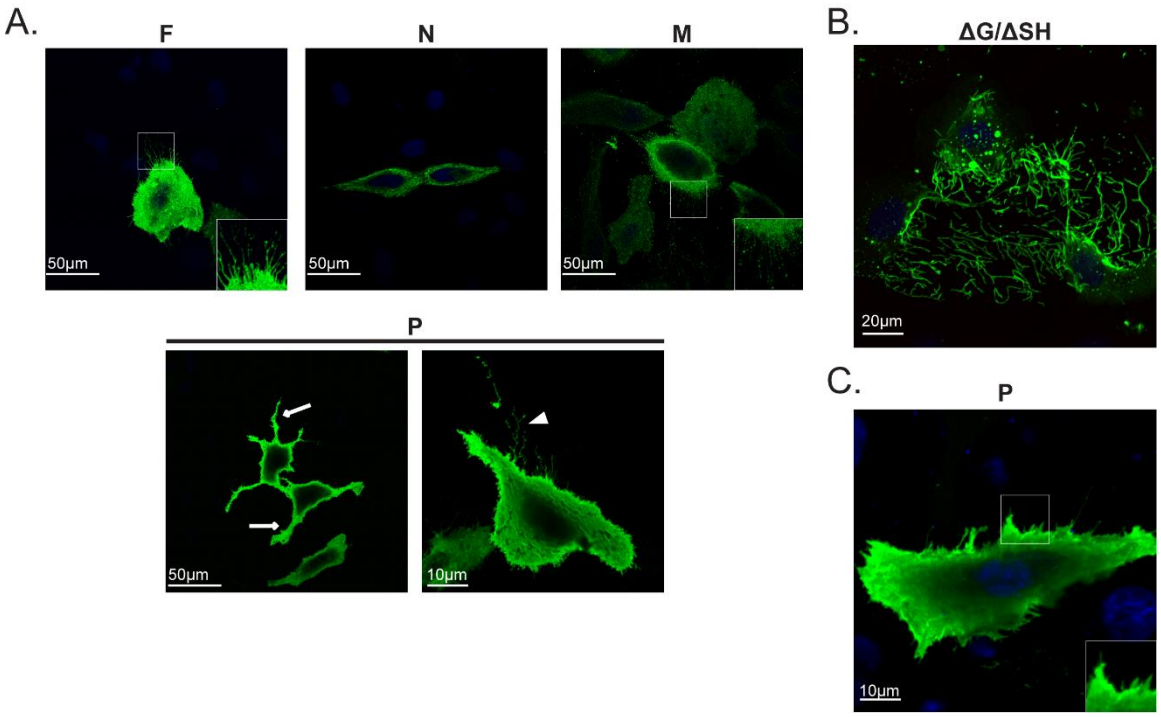

Figure 5.1. HMPV P induces remodeling of the plasma membrane in BEAS-2B and A549 cells.

A) BEAS-2B cells were transfected with pCAGGS plasmid encoding F, N, M or P. 24 hours after transfection, cells were fixed in 4% paraformaldehyde, processed for immunofluorescence and stained for the indicated protein and DAPI (4',6-diamino-2-phenylindole) to stain the nucleus. Images shown are merged images for the viral protein (green) and nucleus (blue). Insets show membrane extensions in cells transfected with F and M, arrow indicates a long membrane extension and arrowhead shows a branched filament. B) BEAS-2B cells were infected with HMPV lacking G and SH proteins (ΔG/ΔSH) and 24 hours post infection (h.p.i.), cells were fixed and stained for P protein (green) and nuclei (blue). C) A549 cells were transfected with pCAGGS plasmid encoding HMPV P and 24 hours later, cells were fixed, processed for immunofluorescence and stained for P. Inset shows membrane deformation induced by P.

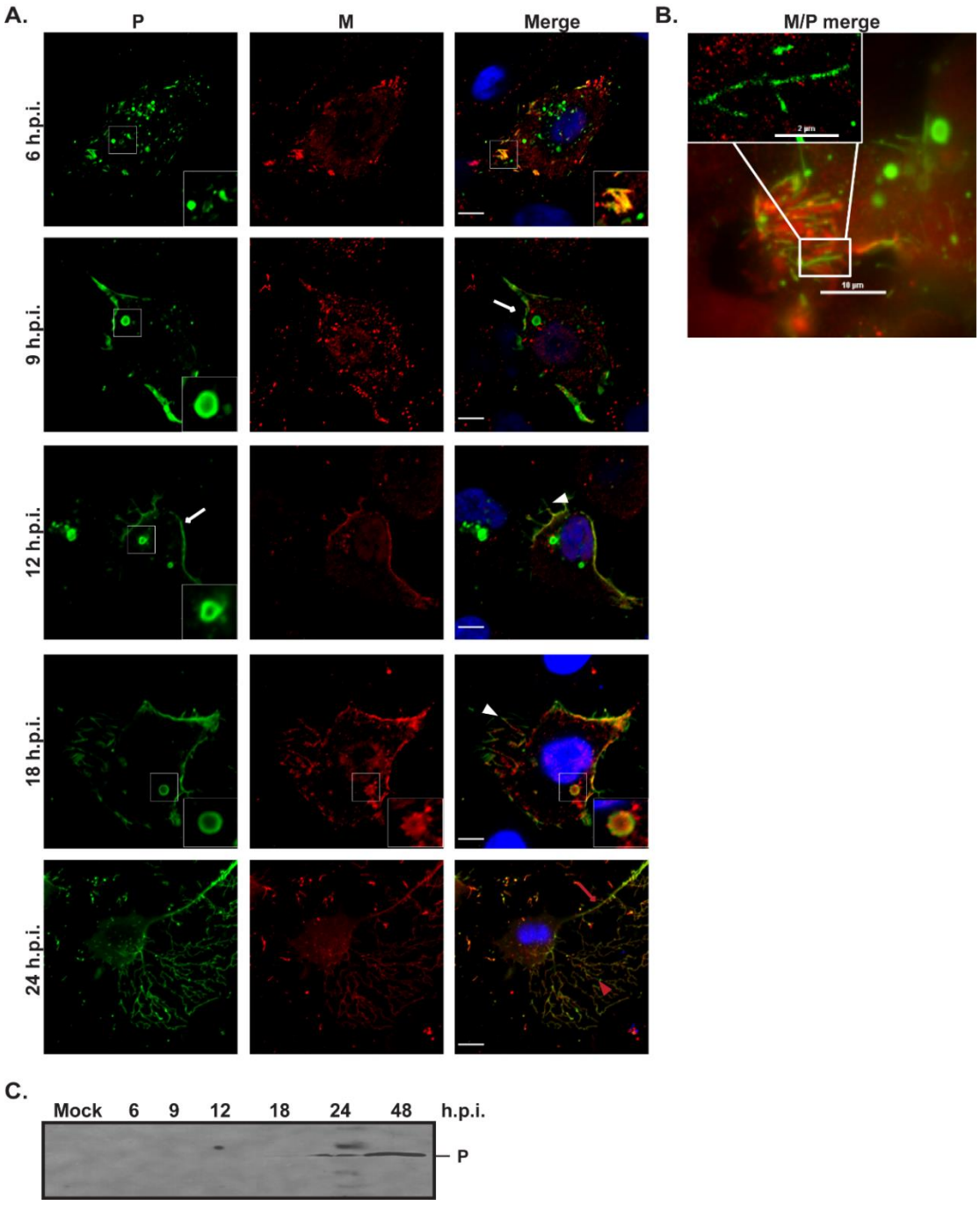

Figure 5.2. Spatio-temporal analysis of cellular localization of P during the course of HMPV infection.

A) BEAS-2B cells were infected with HMPV and at various hours post infection, cells were processed for immunofluorescence and stained with an anti-HMPV P antibody followed by a FITC-conjugated antibody (green) and an antibody that recognizes HMPV

M followed by a TRITC-conjugated secondary antibody (red). Scale bars = 10µm. B) BEAS-2B cells were infected with HMPV and 8 h.p.i., cells were fixed and processed for Stochastic Optical Reconstruction Microscopy. Cells were stained with antibodies for HMPV M (red) and P (green) and images were taken on a Nikon N-STORM super resolution microscope. C) Virus egress assay: BEAS-2B cells were infected with HMPV and at different h.p.i., culture media was collected and released virus was then pelleted by centrifugation on a 20% sucrose cushion. Virus pellets were suspended in 2x SDS (sodium dodecyl sulfate) loading buffer and analyzed by SDS-PAGE followed by western blotting, Band corresponds to HMPV P protein in released virus particles.

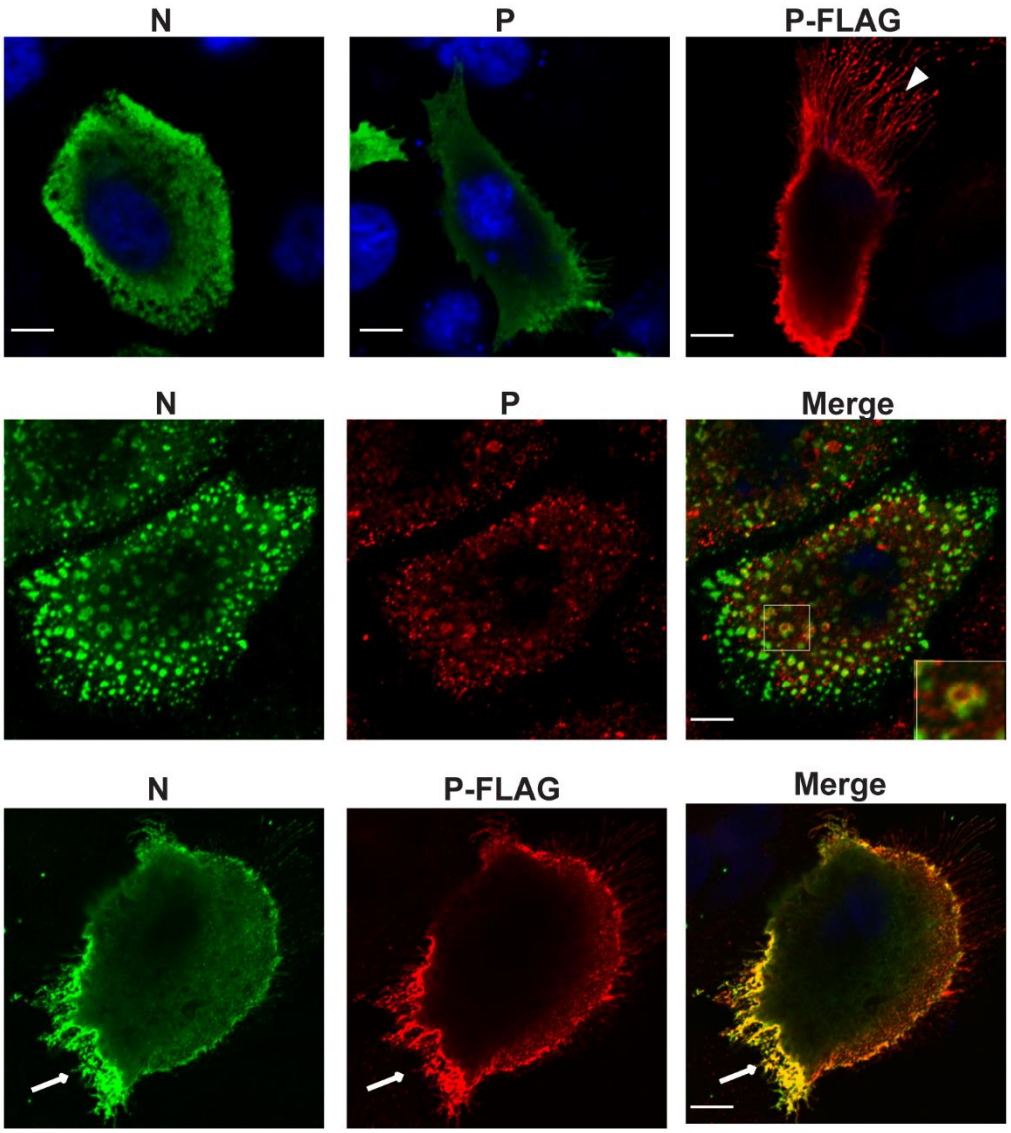

Figure 5.3. Addition of FLAG epitope tag at the C-terminus of P alters function of HMPV P.

A549 cells were transfected with plasmids encoding HMPV N, P and P-FLAG or the indicated plasmids. 24 hours later, cells were fixed and processed for immunofluorescence using antibodies for HMPV P or FLAG (red) and HMPV N (green). Inset shows inclusion –like body in cells coexpressing P and N. Arrowhead indicates membrane extensions induced by P-FLAG and arrow shows colocalization of P-FLAG and N at the cell periphery. Scale bars=10µm.

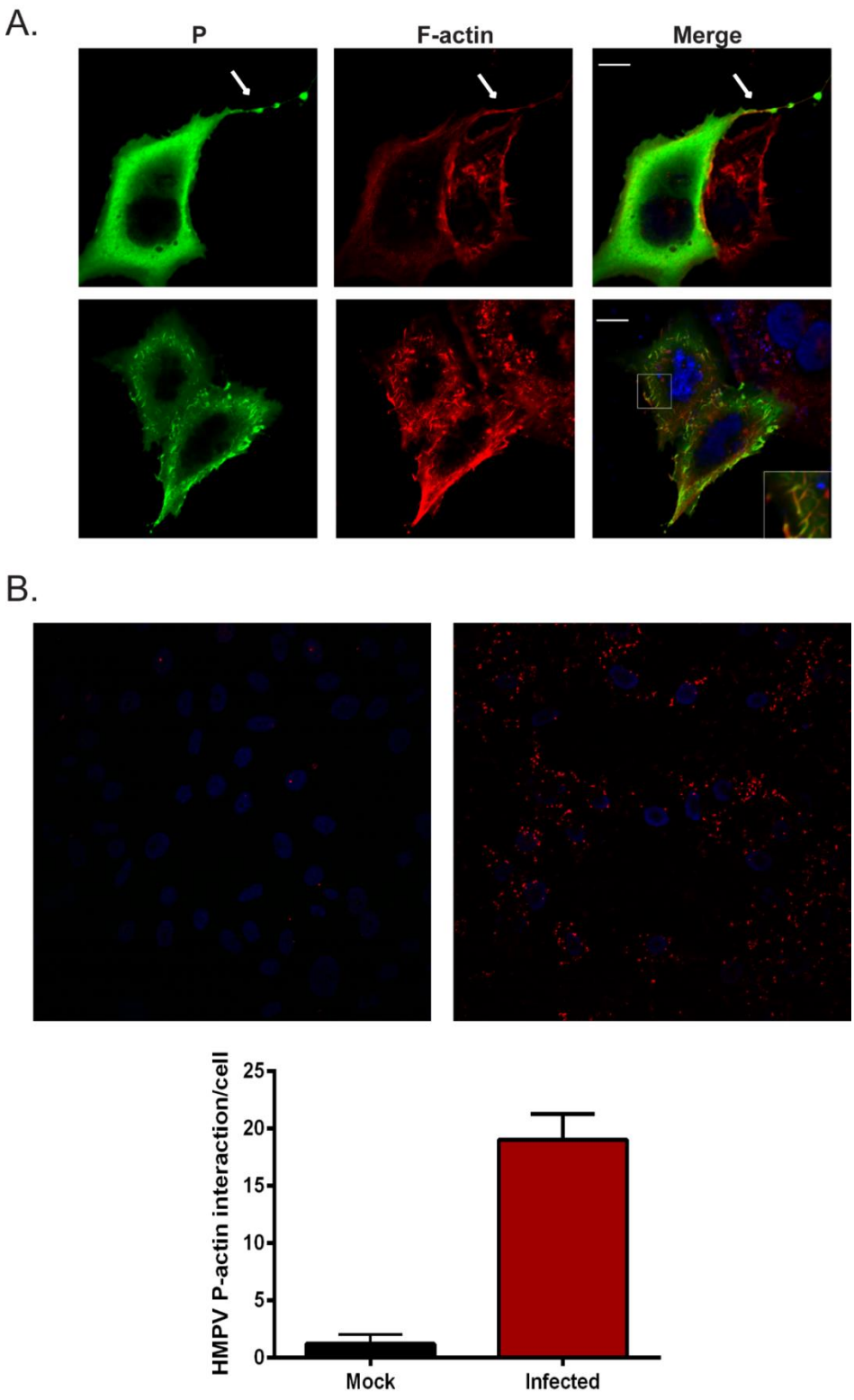

Figure 5. 4. HMPV P colocalizes with actin in transfected and infected cells.

A) BEAS-2B cells were transfected with pCAGGS-HMPV P and 24 hours later, cells were fixed and stained with P (green) and F-actin (red). Inset shows colocalization of P and F-actin in structures that resemble stress fibers and arrow indicates colocaliation of P and F-actin in a cellular extensions. Scale bars=10µm. B) BEAS-2b cells were infected with HMPV and 24 h.p..i, cells were fixed and proximity ligation assay was performed using antibodies for HMPV-P and beta actin. Each red signal signifies a reaction due to proximity of P and actin. Scale=50µm.

CHAPTER 6: HMPV SMALL HYDROPHOBIC PROTEIN HAS CHARACTERISTICS CONSISTENT WITH A PUTATIVE VIROPORIN

*Parts of this chapter are Adapted from the published paper: Copyright © American Society of Microbiology , [Journal of Virology, 88, 2014, 6523-6433, 10.1128/JVI.02848-13]. Masante C, El Najjar F, Chang A, Jones A, Moncman CL, et al. (2014). The human metapneumovirus small hydrophobic protein has properties consistent with those of a viroporin and can modulate viral fusogenic activity. J Virol 88: 6423-6433 [346]. I started this work as a rotation project under the supervision of Cyril Masante [346]. Experiments for testing cell viability and permeability were done partly by me and statistical analysis was performed by Cyril Masante. Cellular localization of SH and cell tracker experiments were performed by me. The gene for HMPV F was provided by Ursula Buchholz. The HA-tagged SH constructs were generated by Angela Jones

Introduction

Human metapneumovirus (HMPV) is an enveloped virus that belongs to the *Pneumovirinae* subfamily of the *Paramyxoviridae* family. Entry of paramyxoviruses into target cells requires the concerted effort of two glycoproteins on the viral membrane: the attachment protein and the fusion protein (F). The attachment protein is generally responsible for primary adsorption of the virus to the cell surface by binding proteinaceous or sialic acid receptor, while the F protein promotes fusion of the viral envelope to a target cell membrane, a process that is driven by very large conformational changes in the F protein [228]. Similar to other paramyxoviruses, HMPV has two surface glycoproteins on its envelope, the putative attachment protein G and the F protein. Studies have shown that HMPV and other pneumoviruses can be infectious in the absence of the attachment protein G and previous work in our laboratory and others indicated that F is sufficient for attachment and entry of HMPV [16,232]. Interestingly, some paramyxoviruses including members of the *Pneumovirinae* subfamily, rubulaviruses, and the unclassified J virus have an additional glycoprotein on the viral

membrane, termed SH for small hydrophobic protein. Studies have shown that SH is dispensable for virus replication *in vitro*; however deletion *in vivo* can attenuate viral replication and pathogenicity [17-19].

SH proteins are all type II integral transmembrane proteins, but the size and proposed function of these proteins differs between viruses. For some paramyxoviruses, SH can inhibit apoptosis by interfering with TNF-α signaling [15,347]. In addition, the SH protein of RSV has been proposed to function as a viroporin, as it can oligomerize into pentamers and/or hexamers, create ion channels in artificial membranes and also change the membrane permeability in bacteria [348-351]. Viroporins in general are small, hydrophobic viral proteins that form homo-oligomers in membranes, creating channels which allow passage of ions and small molecules [352]. HMPV has the largest SH within paramyxoviruses and can exist in three different glycosylated forms: unglycosylated, N-glycosylated and heavily glycosylated [16]. Recombinant HMPV lacking SH was shown to replicate efficiently in hamsters and in nonhuman primates [16,93], indicating that SH is not required for HMPV infectivity in these systems. In addition, a recent study indicated that SH does not affect viral replication or host gene expression [353]. However, every clinical isolate for HMPV to this date has SH [354], indicating that the protein plays a role during HMPV infection. Previous studies revealed that HMPV SH can modulate the host immune response and contribute to viral pathogenicity by inhibiting NF-κB [355], and recently it has been shown that SH inhibits HMPV uptake in dendritic cells [356].

We have shown that HMPV SH transmembrane domains can form higher order oligomers, consistent with the properties of a viroporin [346]. Thus, to test potential viroporin activity of HMPV SH, we determined the cellular localization of HMPV SH and its effect on cell viability and cell permeability. HMPV SH was expressed in intracellular organelles and at the cell periphery. In addition, expression of SH increased cellular permeability of Hygromycin B and altered the intracellular localization of a fluorescent dye without affecting cell viability. Taken together, these results suggest that HMPV SH has viroproin-like activity.

Results

HMPV SH localizes at the cell periphery and in intracellular organelles

To examine the cellular localization of HMPV SH and determine whether infection altered the location of SH, BEAS-2B cells (human bronchial airway epithelial cells) were transfected with plasmids encoding SH with the HA tag inserted at the N terminus (HA-SH) or the C-terminus (SH-HA). Twenty four hours later, cells were either mock infected or infected with HMPV. Cells were then fixed and processed for immunofluorescence analysis using antibodies for the HA tag and HMPV M protein. Both HA-SH and SH-HA were mainly distributed internally and had partial localization at the cell periphery (Figure. 6.1). In addition, infection did not alter the cellular distribution of HMPV SH suggesting that location of SH in the cell is not determined by the presence of other viral proteins.

Expression of HMPV SH increases the cellular permeability to hygromycin B without affecting cell viability

To test the possible activity of HMPV SH as a viroporin, we tested the effect of SH expression on cellular permeability to hygromycin B. Hygromycin B is an antibiotic that does not penetrate cells when present at low concentrations; however, when membrane integrity is compromised, hygromycin B can enter cells and block cellular protein synthesis. COS-7 cells were transiently transfected with plasmids encoding HMPV HA-SH, SH-HA and as a control, F. Twenty-four hours post-transfection, cells were metabolically labeled for 1,2 or 3 hours in the absence or presence of 500 µg/ml of hygromycin B. HA-tagged SH or F were then immunoprecipitated and levels of the newly synthesized proteins were analyzed by SDS-PAGE followed by imaging on the Typhoon (Figure. 6.2A). As seen in Figure 6.2B, a minor reduction in the protein levels of F was seen after 1 hour of hygromycin B treatment (around 15%) compared to the control non-treated sample. However, reduction of protein synthesis was seen to a higher extent in cells expressing either HA-SH or SH-HA with further decreases seen after 2 or 3 hours of hygromycin B treatment (Figure. 6.2B). This indicates that the cell

permeability to hygromycin B increases with the expression of HMPV SH, thus supporting a potential role of SH as a viroporin.

To demonstrate that the effects on protein levels seen with hygromycin B treatment were not a result of a decrease in cell viability induced by SH, we determined whether SH induced cell cytotoxicity. Vero or COS-7 cells were transfected with plasmids encoding HA-SH, SH-HA, F or empty vector as a control and 48 hours later, a CellTiter96 assay was performed. The average slope of the increase in optical density (OD) was calculated and normalized to that of control cells transfected with the empty vector. Expression of SH did not result in any significant differences in the number of viable cells compared to cells expressing F or cells transfected with the empty vector (Figure. 6.3). In addition, no differences in cell viability were seen when similar analysis was done on cells infected with wild type HMV or HMPV lacking G and SH proteins (data not shown). Thus, these data indicate that HMPV SH does not induce cell cytotoxicity.

HMPV SH alters the localization of an intracellular fluorescent dye

To further examine the activity of HMPV SH as a viroporin, we determined the effect of expression of SH on CellTracker green CMFDA, a cell permeable dye that is normally processed into an impermeable fluorescent form once it enters the cells resulting in low diffuse florescence signal in the cytoplasm and in the nucleus. This staining pattern was seen in cells transfected with the empty plasmid (Figure. 6.4A and B, MSC); however, expression of SH resulted in alteration to the fluorescent pattern of the CellTracker green CMFDA. A more intense green signal was seen in cells expressing SH (Figure. 6.4A); in addition, the florescent signal was mainly localized in discrete structures near the plasma membrane in SH-expressing cells (Figure. 6.4B). These structures could correspond to vesicles or endosomes. SH was shown to localize both at the cell surface and in intracellular organelles (Figure. 6.1), thus it is possible that SH is altering permeability of the plasma membrane and membranes of internal organelles.

Discussion

Studies done in vitro and in animal models in vivo indicate that HMPV particles lacking SH protein can replicate efficiently with a minor reduction in viral titers in a nonhuman primate model [93,353]; however SH is present in all primary isolates of HMPV so far indicating a functional importance for this protein [357]. Previously documented functions of SH include modulation of the immune response by altering NF-κB activity [355] and inhibition of virus uptake in dendritic cells [356]. In addition, recent results from our laboratory show a role of SH in reduction in HMPV F-mediated membrane fusion [232]. The results presented here suggest an additional role of HMPV SH associated with a viroporin-like activity.

Viroporins have been described for a number of viruses of unrelated families and the functional role of these viral proteins in affecting pathogenicity can vary. HRSV, the closest human pathogen to HMPV, also encodes an SH protein with activities that are similar to those seen here for HMPV SH. HRSV SH was shown to increase membrane permeability [349], similar to the increase in hygromycin permeability upon HMPV SH expression (Figure. 6.2A). In addition, both HMPV SH and HRSV SH have similar cellular localization in intracellular compartments and at the plasma membrane (Figure. 6.1). Recent work indicated that HRSV can form a cation-selective ion channel and that it plays a role in inflammasome activation [348,350]. The exact role of a viroporin in the infection cycle of HMPV remains to be determined. Interestingly, recent structural analysis of HMPV matrix protein M revealed the presence of a calcium binding site in the N-terminal domain of the protein [287], which have not been reported for other paramyxovirus M proteins with solved structures. Calcium binding was shown to increase the thermal stability of the protein and it was hypothesized that intracellular calcium levels may play a role in regulating interaction of M with other proteins and with lipid membranes. Localization of SH at the plasma membrane and intracellular organelles suggest possible involvement of SH in altering membrane integrity to modulate calcium levels in the cell. Thus, further studies are needed to determine how HMPV SH can affect calcium homeostasis during the course of infection and what the effects of the absence of SH are on matrix protein localization and function.

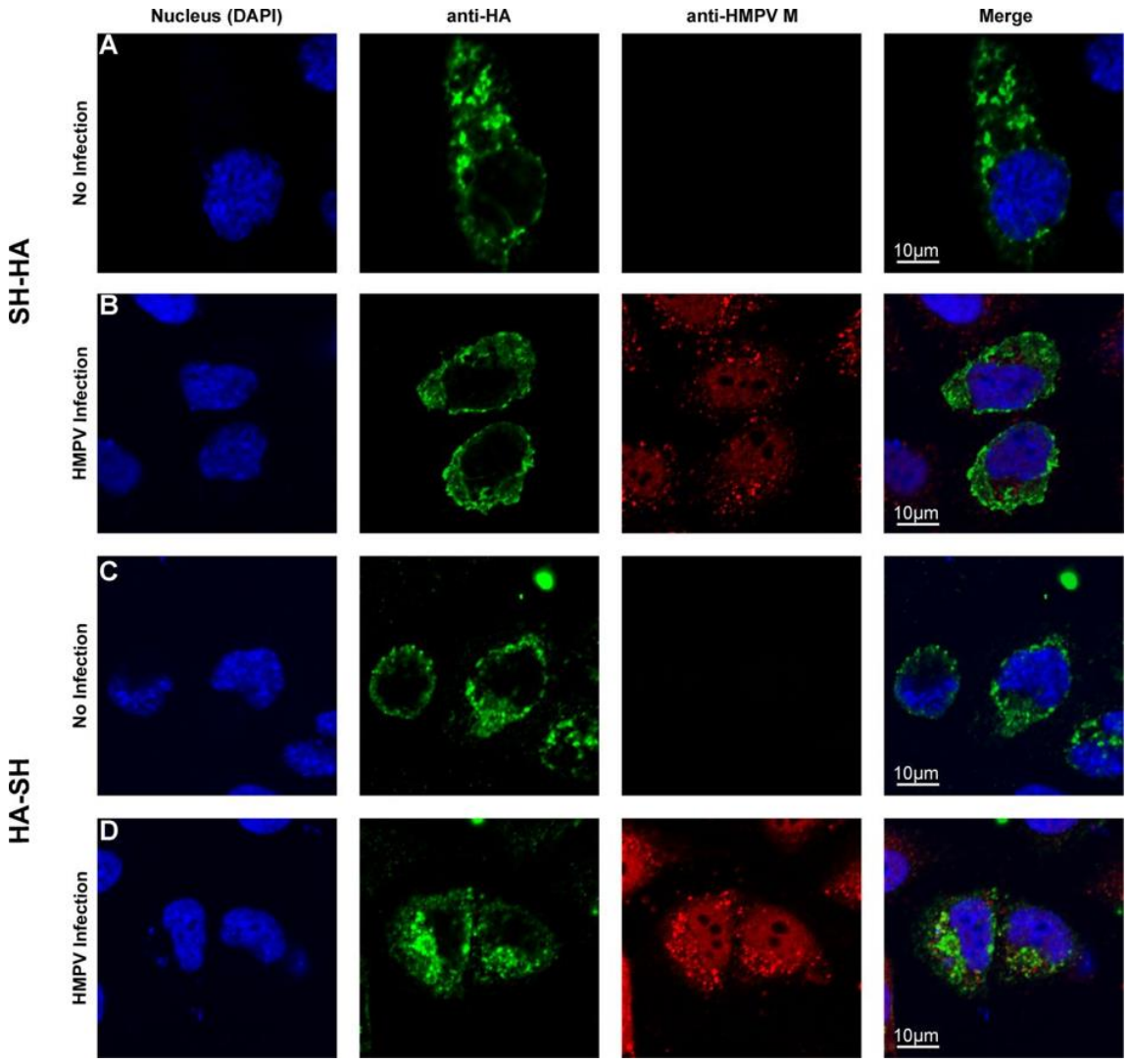

Figure 6.1. Cellular localization of HMPV SH at plasma membrane and internal organelles.

BEAS-2B cells transfected with plasmids encoding HA-tagged HMPV SH were infected with HMPV 24 h post transfection. The following day, cells were fixed and stained with anti-HA antibody followed by a FITC-conjugated secondary antibody (green) and an antibody that recognized HMPV M followed by a TRITC-conjugated secondary antibody (red). DAPI (4',6-diamino-2-phenylindole) stain was sued ti satin the cell nucleus (blue).

Control images of cells expressing HA-tagged HMPV SH in the absence of infection are shown.

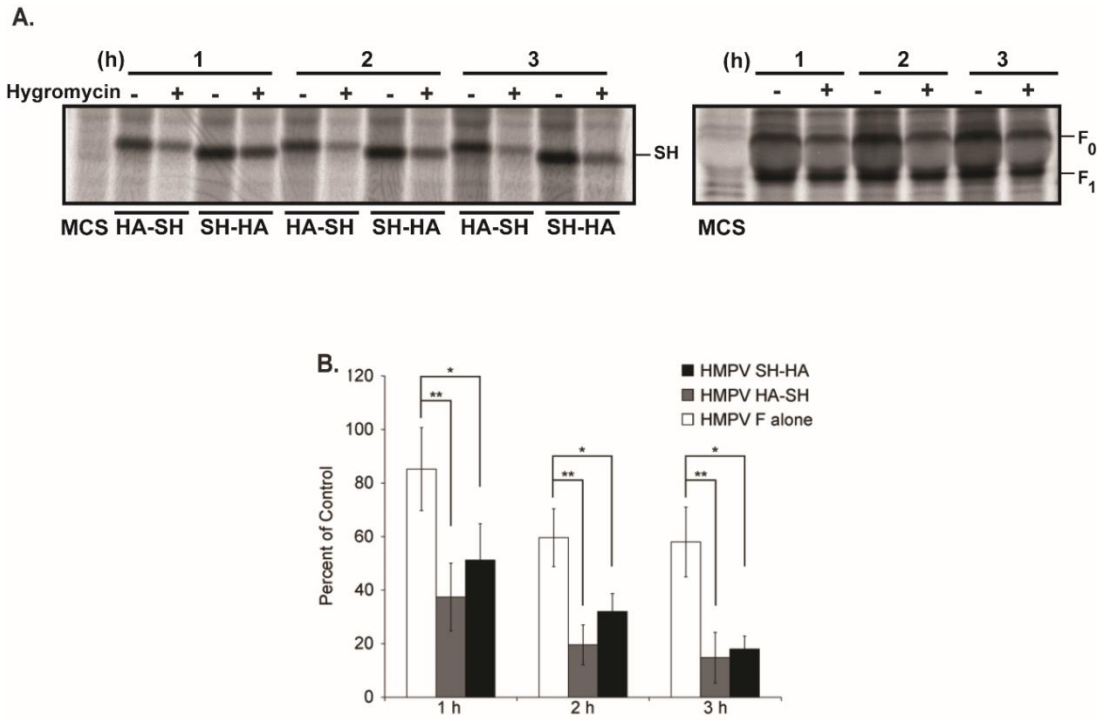

Figure 6.2. HMPV SH increases cellular permeability to hygromycin B.

A) COS-7 cells were transfected with empty vector (MCS) or with plasmids encoding HMPV F or an HA-tagged HMPV SH protein. Twenty hours post transfection, cells were treated with 500 µg/ml of hygromycin B (no treatment as the control) followed by radiolabeling for 1, 2 or 3 hours (h) in the absence or presence of hygromycin B. Proteins were then immunoprecipitated using antibodies for HMPV F or HA and analyzed by DS-PAGE. B) Bands were quantified and the signal intensity of the band for samples treated with hygromycin B was normalized to that of untreated samples at the same time point. White column: F only, grey column: HA-SH, white column: SH-HA. Significance was analyzed by Student's t test and is indicated by asterisks (*, $P<0.09$, **, $P<0.05$). Error bars=standard errors of the means (SEM) for n=3.

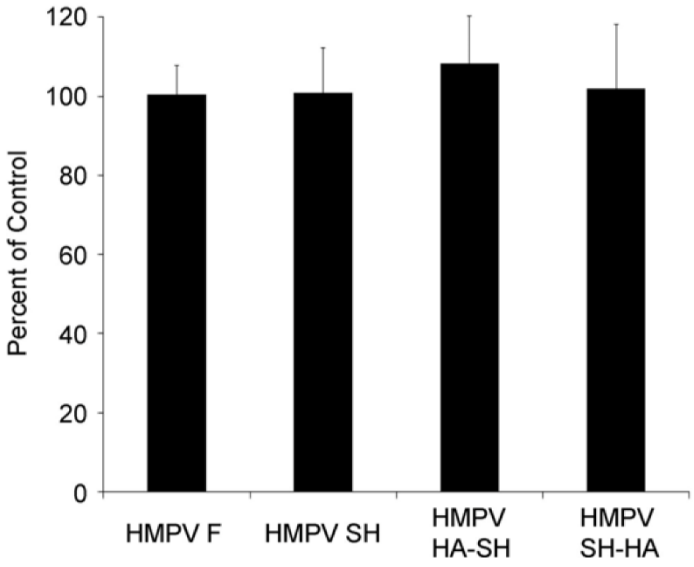

Figure 6.3. HMPV SH does not affect cell viability.

Cell titer viability assay was performed on COS-7 cells transfected with empty plasmid or with plasmids encoding HMPV F, G or a tagged HMPV SH protein. Transfected cells in a 96-well plate were treated with a substrate to detect metabolic activity and formazan product detection was measured at 10-min intervals until the optical density (OD) of control cells transfected with empty vector reached 1. Graph represents the slope increase normalized to cells transfected with HMPV G for four independent experiments. Statistical analysis was performed using analysis of variance (ANOVA).

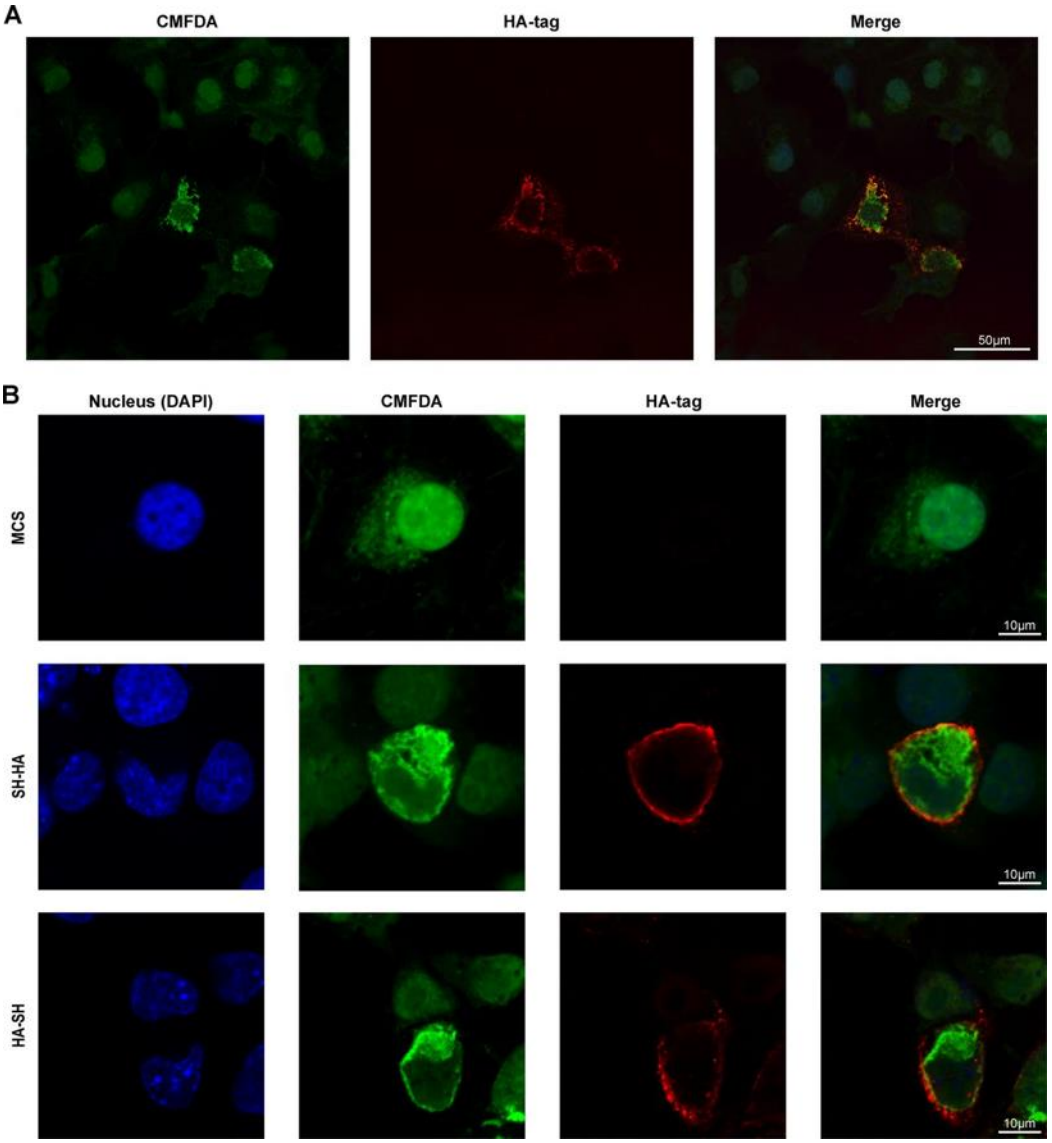

Figure 6.4. HMPV SH alters membrane permeability to a fluorescent dye.

A) COS-7 cells were transfected with a plasmid encoding an HA-tagged HMPV SH protein, and 24 h post-transfection, cells were incubated with 10µM CellTracker CMFDA for 30 min at 37°C. Cells were then incubated for an additional 30 min in culture medium, fixed with 3.7% formaldehyde, and stained with an anti-HA antibody followed by a TRITC-conjugated secondary antibody (red). B) COS-7 cells were transfected with empty plasmid or plasmids encoding HA-tagged HMPV SH protein and processed as described for panel A. DAPI stain was used to stain the cell nucleus (blue).

CHAPTER 7: DISCUSSION AND FUTURE DIRECTIONS

Substantial progress has been made in understanding the mechanisms of paramyxovirus particle production. Paramyxoviruses form by a budding process at selected sites of the plasma membrane of host cells as a result of coordinated interactions between viral components and between viral and cellular factors. Although most paramyxoviruses fit this general model, studies on the molecular mechanisms involved in the assembly and budding of paramyxovirus particles revealed significant differences between members of this family [82,83]. Since its initial discovery in 2001 [2], very few studies have focused on investigating the late stages of HMPV infection. Budding of HMPV depends on the M protein and occurs in an ESCRT-independent manner [160]. In addition, HMPV buds in a filamentous form in LLC-MK2 cells and co-expression of F and M proteins results in production of VLPs that resemble the filamentous morphology of HMPV in infected cells [10,358], indicating an important role of these two proteins in HMPV assembly. Beyond this, very little is known about the mechanisms underlying HMPV assembly and budding and the host factors involved in these late stages of the replication cycle. Work within this dissertation uncovered unique features for the exit pathway of HMPV in human bronchial airway epithelial cells which differ from other paramyxoviruses and elucidated an important role of the actin cytoskeleton in late stages of HMPV infection. We showed that HMPV infection induced distinct structures (branched filamentous networks and intercellular extensions) during late infection and was associated with direct cell-to-cell spread of particles (Chapter 3). We explored mechanistically the formation of these structures and provided evidence for an important role of the cell actin cytoskeleton and the HMPV P protein (Chapters 3 and 5). Furthermore, we studied HMPV infection in a model of human airway epithelium and showed that HMPV releases particles at low levels at the apical side and that the actin cytoskeleton is involved in HMPV spread in this model (Chapter 4). These studies represent a significant step forward in understanding how HMPV particles are formed and transmitted and pave the way for several areas of investigation that can potentially provide targets for development of therapeutic agents.

HMPV assembly and spread: a new paradigm for paramyxoviruses. As with every step during the replication cycle, virus egress from the cell is faced with several barriers including the cortical F-actin meshwork and the plasma membrane. Viruses have evolved fascinating ways to manipulate the actin cytoskeleton to promote their exit pathway. The involvement of the actin cytoskeleton in paramyxovirus budding was initially proposed based on the detection of large amounts of actin in Sendai virus and measles virus particles [359,360]. Later studies revealed that Sendai virus M protein can interact with actin and induce actin remodeling for efficient release of virus particles [239,361]. In addition, electron microscopic images showed a close association between budding measles and RSV with actin [272,362] and disruption of actin polymerization decreased release of both viruses [207,213]. How the actin cytoskeleton is involved in the budding process is not well understood. Budding of RSV, measles virus, Sendai virus and HMPV occur in an ESCRT independent manner [139,158,160,363]. It is likely that the forces generated by the scaffolding and polymerization of actin in combination with the clustering of the glycoproteins creating a pulling force and the matrix protein underneath the plasma membrane allowing a pushing force are sufficient for membrane budding. For HMPV, clustering of the viral proteins induced membrane deformation independent of actin polymerization, but release of virus particles was significantly reduced. A question thus remains regarding the final membrane scission step that allows release of virus particles from the cell. Influenza A virus also buds in an ESCRT independent manner [236,237] and recent studies indicated a role of Rab11 in release of virus particles and of Rab11-FIP3 (family interacting protein 3) in the maturation of viral filaments at the plasma membrane [161,364]. Rab11 was also shown earlier to play a role in release of RSV particles as expression of a dominant negative form of Rab11-FIP2 resulted in retention of long filamentous structures at the plasma membrane [139]. Interestingly, while Rab11-mediated transport of viral RNPs along microtubules was shown for several viruses including influenza virus, Sendai virus and measles virus [137,138,364], RNPs of RSV showed characteristics of actin-based motility [136]. Rab11-FIP2 forms a complex with Rab11a and myosin Vb to regulate plasma membrane recycling [365,366] . Thus, it would be interesting to determine whether HMPV utilizes Rab11-FPI2 or any other components of the Rab11 pathway in RNP transport, budding and release. Rab11 is

involved in directing vesicular transport from the *trans*-golgi network and perinuclear endosomes to apical recycling endosomes (ARE) [302] and thus can sort viral components to the apical side of polarized epithelial tissues favoring localized viral infections. HMPV proteins were localized primarily at the apical surface of HAE (Figure. 4.2A); thus the role of Rab11 in polarized sorting of HMPV proteins also remains to be elucidated.

The studies obtainable in Chapter 3 present a novel role for the actin cytoskeleton in late stages of HMPV infection that has not been reported for paramyxoviruses to date. HMPV induced formation of branched filamentous networks and elongation of intercellular extensions, unique elements of assembly and direct cell-to-cell spread, respectively. The extensive remodeling of the plasma membrane and the cortical actin underneath most likely involves manipulation of several factors that act to control cell shape at the plasma membrane. The actin cytoskeleton and Rho GTPase signaling controlling actin dynamics are involved in maintaining plasma membrane shape and inducing remodeling. Inhibition of actin polymerization and each of the main Rho GTPases (RhoA, Cdc42 and Rac1) involved in actin dynamics resulted in decreased branching of filamentous networks in HMPV infected cells indicating a specific role for each in the formation of the extensive networks of filamentous branches. While it was originally thought that each of the GTPases could have isolated effects, an accumulation of studies indicates that specific and precise interrelationships exist between the different GTPases to exert a coordinated effect on the cell [277]. A number of viruses have been shown to manipulate signaling mediated by the Rho GTPases to induce actin reorganization. One of the most extensively studied viruses is the poxvirus, vaccinia virus. The F11 protein of vaccinia was shown to inhibit RhoA resulting in stress fiber disassembly and increased actin polymerization [367,368]; whereas the A36 protein, initially activated by Src kinase upon binding of cell-associated virus particles, was shown to activate Ccdc42/N-WASP-WIP cascade and Arp2/3 downstream [176]. In addition, it was recently revealed that actin-based motility of vaccinia is driven by Rac1 and its downstream effector formin-type actin nucleator FHOD1 [369]. HIV-1 Nef protein can interact with and activate diaphanous interacting protein (DIP), a regulator of

RhoA and Rac1, activating Rac1 and inhibiting RhoA [370], while other viruses such as baculuvirus can activate Arp2/3 directly by encoding a WASP-like protein [371]. This indicates the complexity of the actin-associated signaling that is manipulated by viruses to reorganize the actin cytoskeleton for exit from the cell. While all three GTPases were involved in filamentous branching, inhibition of Cdc42 and Arp2/3 or N-WASP downstream had the most prominent effect on formation of budding branched filamentous networks indicating an important role of this pathway in HMPV-induced actin remodeling for budding of these structures. It was interesting however that inhibition of actin polymerization did not have the same effect as inhibition of Rac1, RhoA or Cdc42, as in the presence of cytochalasinD or latrunculinA, smaller filamentous structures were seen retained at the cell while these filaments were not seen in cells treated with the GTPase inhibitors, indicating the involvement of factors other than actin itself. In addition, actin polymerization, Cdc42 and Rac1 were needed for HMPV-induced elongation of intercellular extensions. How HMPV is able to coordinate activation of these different pathways requires further investigation. First, activation assays are needed to demonstrate activation of the different Rho GTPase in HMPV infection and the temporal regulation of this activation. In addition, the mechanism by which HMPV activates the different pathways is needed. It is likely that each of the GTPases are manipulated by different viral components at various times during the course of the infection cycle. Previous work in our laboratory revealed that HMPV F protein binds heparan sulfate proteoglycans (HSPGs) at the cell surface [232]. Interactions between specific HSPGs and integrins at the cell surface can activate downstream signaling pathways that activate Rho GTPases and remodel the actin cytoskeleton [372,373]. To test the involvement of HSPGs binding at the cell surface on the different Rho GTPases, the effect of virus binding on activation of Rac1, Cdc42 and RhoA should be tested. In addition, one main observation for HMPV infection in BEAS-2B cells was that, while filaments were seen at the cell surface at 18 h.p.i., the formation of the extensive branched filamentous networks in infected cells was mostly prominent later during infection starting at 24 h.p.i. and developing further at 48 h.p.i.. This suggests that the actin remodeling associated with these cellular changes was mediated by an accumulation of viral products. Single expression of HMPV P resulted in plasma

membrane remodeling and formation of cellular extensions having characteristics similar to those seen in late stages of HMPV infection (Figure. 4.1) and P was found in close proximity to actin. In addition, levels of P protein were shown to increase at later stages of infection (48 h.p.i.) more than the levels of N protein (data not shown). These results indicate a possible role of P in inducing the prominent changes in the actin cytoskeleton at this time of infection. Viruses have the ability to manipulate the actin cytoskeleton by encoding viral proteins that can directly bind actin or actin binding proteins or upstream mediators of actin signaling, the Rho GTPase family. For paramyxoviruses, virus proteins that were shown to bind actin include the M proteins of Sendai virus and NDV [231,337]. Here we provide the first example of a paramyxovirus P protein that can associate with actin and induce changes to the plasma membrane (Figure. 5A). Interestingly, US3 kinase of alphaviruses was shown to induce formation of structures similar to those that were seen cells transfected with HMPV P and it was later revealed that the ability of US3 kinase to cause changes to the actin cytoskeleton is due to activation of PAK1 downstream of Rac1 [220,250]. Whether P is binding actin directly or an ABP or whether it is activating actin-associated signaling requires further studies. Identification of interaction partners of P may help uncover the mechanism behind P-induced plasma membrane remodeling. In addition, it is important to address how the function of P is regulated during the course of infection from viral RNA synthesis at early stages of infection to inducing plasma membrane deformation and possibly contributing to HMPV exit from the cell at the end of the replication cycle. The localization of P changed at different times post infection including localization in inclusion bodies to short cytoplasmic filaments followed by localization at the cell periphery and in cellular extensions and branched filaments, while upon single transfection P was cytosolic and in cellular extensions. This indicates that presence of other viral proteins alters the cellular distribution of P. Our results show that the cellular expression levels of P increase as infection progresses from 24 to 48 h.p.i., to a greater extent than the increase in N levels. It is possible that as the global concentration of P in the cell increases at late times after infection, which would mimic levels seen in transfected cells, the effect of P on membrane deformation becomes more prominent. In addition, mass spectrometric analysis of P from infected and transfected cells showed the presence of a truncated form

of P, with truncation at the N-terminus. Since the C-terminus region of P is thought to be responsible for binding both L and N, it is possible that the truncated form of P can bind L and N, and thus can function mainly in RNA transcription and replication while the intact full length P may be interacting with some cellular or viral factors (M protein) that would promote the function of P at late stages of infection. In addtion, differnt phosphorylation states of P may regulate its function during infection. Furthermore, the role of membrane lipids in HMPV-induced remodeling remains to be addressed. Several studies have reported that assembly of different paramyxoviruses is selectively targeted to raft microdomains in cellular membranes [84,374,375]. Association between actin, rafts and assembly of viral filaments have been shown for influenza and RSV [214,376]. Co-localization between HMPV and glycoproteins and the lipid raft ganglioside GM1 has been recently indicated [264]. Thus, it would interesting to determine how rafts affect assembly of HMPV into the branched filamentous structures.

The actin rearrangements seen upon HMPV infection must require coordinated effects of different viral and cellular effects of different viral and cellular factors at different times during the infection cycle While several aspects of this process remain to be elucidated, we have shown a role for HMPV-induced intercellular extensions in direct cell-to-cell spread of particles, presenting a novel mechanism by which paramyxoviruses can spread infection. Several models have been proposed for direct cell-to-cell spread that could be applicable to our findings with HMPV. One model involves budding of particles at the plasma membrane and their movement across intercellular extensions from an infected cell to a donor cell. This process, known as virus surfing, has been documented for several viruses including HIV-1, and MLV [197,377]. However, binding of virus to a cell surface receptor is required for entry and infection in this model, and our results demonstrate that infection of HMPV by direct cell-to-cell spread occurs independently of heparan sulfate which was shown to be an important binding factor for cell-free HMPV infection [232]. Studies for cell-to-cell spread of viruses revealed differential requirements for receptor binding in cell-free and cell-to-cell infection. For example, cell-to-cell transmission of hepatitis C virus was shown to occur independent of the scavenger receptor class B type I (SR-BI) in contrast to cell-free infection. Thus, it is

possible that movement of particles across the extensions from one cell to another does not require HMPV binding to heparan sulfate. In this case, however, a prerequisite for transmission would entail downregulation of the virus receptor at the surface of the infected cell, high affinity binding of the virus on the receptor of the target cell and transfer of particles by actin-flow. Another model is that intercellular extensions are open-ended and act as tunnels through which HMPV particles travel along actin filaments on the inside of the extension, allowing entry into the target cell. One other possible mechanism by which HMPV can spread infection directly from cell-to-cell is by transfer of the RNP complex from an infected cell to a donor cell. Detection of vRNA by FISH analysis showed the presence of structures similar to replication bodies at the tips of extensions approaching another cell. Spread of genetic material without release of infectious virus particles has been suggested to occur for measles virus, both in neurons and in epithelial tissues [254,257]. We have shown that P can associate with actin and STORM imaging revealed that P is present on the outside of the inclusion body (data not shown); thus transport of an RNP along actin could be mediated by P protein while further inducing elongation of the intercellular extensions as our data revealed a role of P in cell extension formation. The last two models of spread would protect the virus from neutralizing antibodies and bypass the need for receptor binding. Our data show that passive diffusion of GFP from donor to target cells does not occur (Figure. 6G), arguing against an open-ended connection. However, intercellular extensions have shown to selectively transport cellular cargo from one cell to another [284] and thus further studies are needed to demonstrate whether intercellular extensions are open or close ended. The movement of virus particles or RNP complex on actin filaments would require motor proteins. Different myosin motor proteins, myosin 9, 11 and Ib, were identified in HMPV particle and thus their role in possible actin-based motility of HMPV or HMPV RNPs requires further investigation. In addition, if virus particles or components are moving along F-actin, it is not clear how they "break free" to enter a new cell. One possibility would be that myosin-based movement creates enough force to release particles. It is also possible that factors promoting actin depolymerization or disassembly may have a role. We identified cofilin in purified HMPV particles.

Although several respiratory viruses, including influenza virus [267], RSV [268] and PIV3 [9] are known to form filamentous particles, HMPV formed networks of branched viral filaments, with a central core of N surrounded by M protein, in two human bronchial epithelial cells, BEAS-2B and 16HBE cells. We did not detect these structures in A549 or Vero cells and previous studies showed that HMPV forms filamentous structures, but not networks, at the plasma membrane of 293T and LLC-MK2 cells [10,264]. This suggests that these structures are unique for bronchial epithelial cells, the more physiologically relevant model for HMPV infection. Interestingly, electron microscopic images of HMPV shows aggregates of virus particles [34,289] and imaging single HMPV particles in our preparation in Vero cells proved to be challenging (data not shown). In addition, the apical surface of infected HAE showed the presence of aggregates of virus-like bodies in infected tissues. These observations raise the possibility that HMPV is budding as "networks" of particles. Interestingly, a recent report showed the formation of a branched network of extracellular viral assemblies in HTLV-1 infected lymphocytes, "viral biofilms" [291], that were involved in viral spread and stability. Electron microscopic images of BEAS-2B cells infected with HMPV (data not shown) revealed the high similarity between the biofilms seen in HTLV-1 infected cells and the branched filamentous structures seen at the surface of HMPV infected cells. Examination of the content of the branched filamentous networks in HMPV infected cells by laser dissection microscopy could help uncover whether these structures are consistent with viral biofilms. A central paradigm that has recently emerged is defining an infectious unit. It had been thought that all viruses exit the cell as single particles with each particle acting as an independent infectious unit. However, research over the past several years provided evidence that viruses of different families can exit the infected cell as multiple virus particles and that the fate of these particles is related. It was recently shown that clusters of mature enterovirus particles are released from the cell within phosphatidyl-serine rich vesicles and that this mode of transmission enhances efficiency of infection [290]. In addition, poliovirus was found to exit the host in a bacteria-bound form that provided fitness benefits to the virus [378]. These different forms of virus transmission units enhance the stability of virus particles as they transmit infection and provide an opportunity for genetic diversity and viral evolution as multiple particles infect a single

cell. Our results indicate that HMPV buds primarily as a network of cell-associated viral filaments and that titers of cell-associated particles are higher than that of released particles. Infection of HAE showed inefficient release of HMPV at the apical side, but was associated with spread. Thus, this raises the question of how host-to-host transmission occurs if HMPV remains mainly cell-associated. One possibility is that HMPV could be shed from the epithelium in a cell-bound form. Enhanced cell shedding and loss of GFP-positive cells were seen at 3 d.p.i. in HAE indicating loss of infected cells from the tissues, thus it is possible that cell-associated HMPV that is shed from the apical surface is the transmitted form of the virus. Clusters of virus-like bodies were seen at the HAE apical surface that could be in association with cell-remnants. This form of cell-associated clusters of HMPV could help increase stability of the virus particles and it has been postulated that cell-associated viruses can enter the mucosal barrier easier through transmigration [271].

HMPV and the actin cytoskeleton: implications for spread in the airway epithelium.

One important question that arises from the results presented here is how actin remodeling via activation of Rho GTPases is involved in HMPV assembly and spread in a human airway epithelium. While the observed structures in BEAS-2B cells or other respiratory cell lines in culture do not directly translate to what is observed in a human airway model, the ability of HMPV to reorganize the actin cytoskeleton and evidence of cell-to-cell spread was observed in both systems. Cell-to-cell spread of virus particles independent of particle release to the extracellular surface would be favored in the environment of the airway epithelium where cells are in close contact, providing a way for coordinating release and entry in space and time. This mechanism of spread would also provide a way for infection to spread while evading the immune response and the relatively harsh environment of the mucosal surface. However, the tight contacts between epithelial cells, either adherens junction or tight junctions, can create a barrier for direct cell-to-cell spread of particles. The actin cytoskeleton anchors the apical junction complex (AJC) to the plasma membrane; however the AJC is not stable but dynamic and requires complex remodeling mediated, in part, by Rho GTPase induced rearrangements of actin. Rho GTPases, Cdc42, Rac1 and RhoA play an important role in establishing

epithelial cell polarity and in epithelial junction formation. Thus, intercellular spread of viruses in the epithelium would require remodeling of the actin and thus the AJC via activation of Rho GTPases. Several reports indicate that some important human viruses, including HSV-1 and measles virus, use proteins of the AJC as their receptors and both viruses have a direct cell-to-cell mode of transmission [257,379]. Moreover, the bacteria Listeria monocytogenes and Shigella flexneri represent examples of intracellular pathogens that have been known to utilize F-actin for propelling the pathogen from cell-to-cell and recent studies have revealed that both bacteria have distinct mechanisms for manipulating epithelial cell-cell junctions for direct spread [380], further supporting the link between actin cytoskeleton rearrangement, epithelial cell junctions and spread. During infection in HAE, HMPV induced remodeling of actin at apical and lateral membranes and the evidence suggests intercellular spread. Thus, it would be interesting to hypothesize that HMPV-induced activation of Rho GTPases that in cell-culture manifests as production of actin-based branched filaments and intercellular extensions is a way by which the virus manipulates the airway epithelium to mediate its assembly and spread. Influenza virus and PIV5, two respiratory pathogens were recently shown to spread intercellularly [258]; but this mode of spread has not been investigated in an HAE model, so whether other respiratory viruses can induce actin remodeling to mediate intercellular spread in the airway epithelium needs further investigation.

Key unanswered questions for paramyxovirus assembly, budding and spread.

For a long time, it was thought that enveloped viruses spread infection from cell to cell and host to host by budding through a cellular membrane followed by membrane-scission and release of single particles into the extracellular matrix. However, strong evidence over the years indicates that the mechanisms of virus spread is more complicated than what was previously thought. We have provided support for a novel mechanism for paramyxovirus spread from cell-to-cell independent from particle release. The results presented in this dissertation raise additional questions for the late stages of paramyxovirus infection, in addition to some general questions that remains to be addressed for paramyxovirus particle

formation in general. Recently it was revealed that PIV5 can spread in a neutralizing antibody independent manner, however the role of the actin cytoskeleton has not been addressed. In addition, RSV filaments have been proposed to play a role in intercellular virus spread. Thus whether RSV, PIV5 or other paramyxoviruses have a direct cell-to-cell spread mechanism similar to HMPV involving remodeling of the actin cytoskeleton remains to be answered. In addition, while a role of M protein and glycoproteins in virus assembly and budding have been well-elucidated, the role of other viral proteins in late stages of infection should be investigated further as we have revealed a role of HMPV in membrane deformation.

One of the key unanswered questions in paramyxovirus assembly is how are assembly sites initiated? Is the clustering of surface glycoproteins in membrane raft domains sufficient to create an outward bud in the plasma membrane to which other viral components are recruited, or is the interaction of M with the cytoplasmic tail of glycoproteins and its self-oligomerization the main driver for the formation of assembly nucleation sites? The requirements for the formation of budding precursor sites may vary among different paramyxoviruses. For RSV, the fusion protein seems to be the significant contributor for the formation of short viral filaments. On the other hand, the actin cytoskeleton and the interaction between M and the cytoplasmic tail of F appear to drive SeV particle formation at the plasma membrane. Another significant area of study is to determine the cellular pathways that are utilized by the matrix proteins and the RNP core that allows their delivery to assembly sites and subsequent packaging of the RNA genome into virions. Important questions also remain regarding how membrane budding and the final scission process are established for paramyxoviruses, particularly for those viruses that do not utilize the well-characterized ESCRT proteins. What are the cellular factors that play a role in budding of paramyxoviruses, and how are they recruited by viral proteins? Thus, further studies are still required to clarify multiple aspects of paramyxovirus particle production and to uncover the differences that exist in the molecular mechanisms utilized by different paramyxoviruses to form new infectious particles.

Since its initial identification in 2001, studies on different aspects of HMPV provided evidence that the entry pathway of HMPV differs from other paramyxoviruses. Only F protein is required for virus entry, cleavage of F occurs by an exogenous protease and F triggering of some strains requires low pH. In this dissertation, we provide evidence that HMPV also has unique features at late stages of infection that involves manipulation of the cell cytoskeleton to spread infection in a way previously undocumented for paramyxoviruses. A better understanding of the mechanisms involved in HMPV-induced actin remodeling involving viral and cellular factors will significantly advance our knowledge of the life cycle of this important respiratory virus, paving the way for identification of new targets for antiviral therapeutic development.

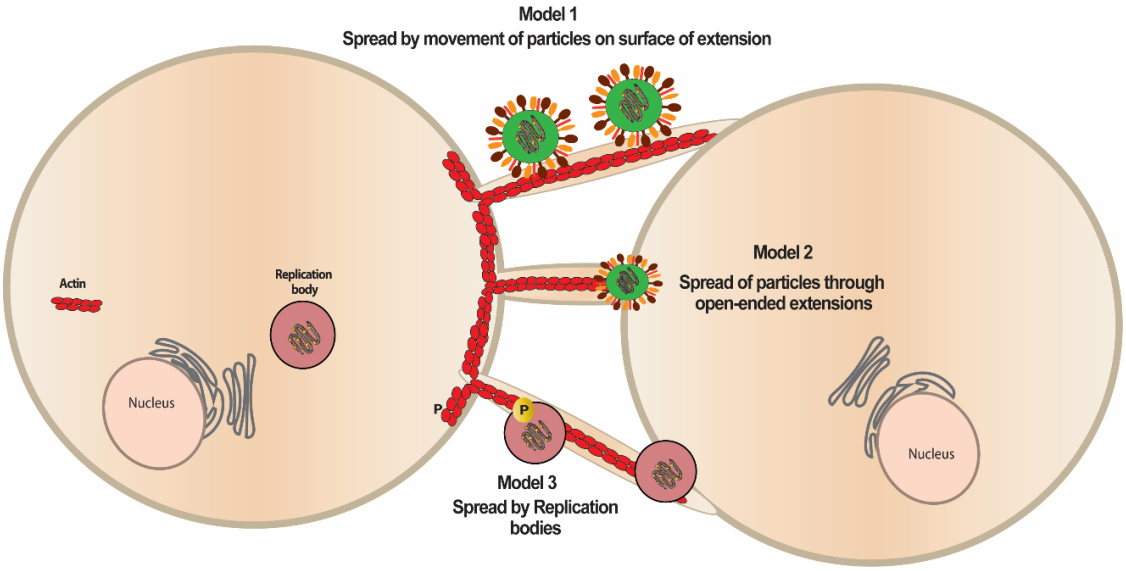

Figure 7. 1. Possible models for HMPV cell-to-cell spread across actin based extensions.

Appendix 1

List of Abbreviations

HMPV	Human metapneumovirus
RSV	Respiratory syncytial virus
HIV-1	Human Immunodeficiency virus-1
HSV	Herpes simplex virus
NDV	Newcastle disease virus
RNP	Ribonucleoprotein
N	Nucleoprotein
P	Phosphoprotein
F	Fusion
L	Large polymerase
M	Matrix
VLPs	Virus like particles
G	Attachment
SH	Small hydrophobic
ESCRT	Endosomal sorting complex required for transport
FIP	Family interacting protein
NLS	Nuclear localization signal
NES	Nuclear export signal
VPS	Vacuolar protein sorting
F-actin	Filamentous actin
G-actin	Globular actin
WASP	Wiskott–Aldrich syndrome protein
NPFs	Nucleation Promoting Factors
GFPs	Guanine nucleotide exchange factors
GDIs	Guanine nucleotide-dissociation inhibitors
GAPs	GTPase activating proteins
FISH	Fluorescent in situ hybridization

Appendix 2

Analysis of Cathepsin and Furin Proteolytic Enzymes Involved in Viral Fusion Protein Activation in Cells of the Bat Reservoir Host

Farah El Najjar, Levi Lampe, Michelle L. Baker, Lin-Fa Wang, Rebecca Ellis Dutch

PLOS Published: February 23, 2015 DOI: 10.1371/journal.pone.0115736

Abstract

Bats of different species play a major role in the emergence and transmission of highly pathogenic viruses including Ebola virus, SARS-like coronavirus and the henipaviruses. These viruses require proteolytic activation of surface envelope glycoproteins needed for entry, and cellular cathepsins have been shown to be involved in proteolysis of glycoproteins from these distinct virus families. Very little is currently known about the available proteases in bats. To determine whether the utilization of cathepsins by bat-borne viruses is related to the nature of proteases in their natural hosts, we examined proteolytic processing of several viral fusion proteins in cells derived from two fruit bat species, Pteropus alecto and Rousettus aegyptiacus. Our work shows that fruit bat cells have homologs of cathepsin and furin proteases capable of cleaving and activating both the cathepsin-dependent Hendra virus F and the furin-dependent parainfluenza virus 5 F proteins. Sequence analysis comparing Pteropus alecto furin and cathepsin L to proteases from other mammalian species showed a high degree of conservation; however significant amino acid variation occurs at the C-terminus of Pteropus alecto furin. Further analysis of furin-like proteases from fruit bats revealed that these proteases are catalytically active and resemble other mammalian furins in their response to a potent furin inhibitor. However, kinetic analysis suggests that differences may exist in the cellular localization of furin between different species. Collectively, these results indicate that the unusual role of cathepsin proteases in the life cycle of bat-borne viruses is not due to the lack of active furin-like proteases in these natural reservoir species; however, differences may exist between furin proteases present in fruit bats compared to furins in

other mammalian species, and these differences may impact protease usage for viral glycoprotein processing.

Introduction

In the past twenty years, bats of different species have been recognized as important hosts of viruses from different families including rhabdoviruses [1–3], coronaviruses [4–9], filoviruses [10–12], flaviviruses [13,14], orthomyxoviruses [15–17], paramyxoviruses [18,19] and others [20,21]. Numerous studies have shown that bats not only harbor a large number of viruses, but are also a major source for the emergence and transmission of viruses that cause highly pathogenic infectious diseases in humans, most importantly Severe Acute Respiratory Syndrome-like coronavirus (SARS-like CoV) [7], Ebola virus [10,22] and the henipaviruses, Hendra virus [23–26] and Nipah virus [27–29], which are members of the paramyxovirus family. Hendra virus first emerged in 1994 in Australia in an outbreak that occurred in horses [30], and more than thirty subsequent outbreaks have occurred, with a total of four human deaths associated with the virus infection [31,32]. Another closely related virus, Nipah virus was identified in Malaysia in 1999 causing an outbreak of viral encephalitis [33]; with additional outbreaks showing high mortality rates that reached 70%. Several species of bats within the genus Pteropus, commonly known as flying foxes, have been confirmed as the natural primary reservoir of henipaviruses [23,25,27,34–36]. Cedar virus, a novel henipavirus that does not seem to cause clinical disease in several animals which are known to be susceptible to Hendra and Nipah viruses, was identified recently and also has Pteropus bats as its natural reservoir [37]. Recent evidence suggests that henipaviruses are also present in non-Pteropus fruit bats in Africa [38,39]. Despite the important role of bats in the emergence of henipaviruses and other highly pathogenic viruses, very little is known about the viral life cycle or virus-host interactions in this natural reservoir.

Entry of henipaviruses into host cells requires fusion of the viral envelope with the cell membrane. The fusion event is mediated by two glycoproteins present on the viral envelope, the attachment protein, G, required for initial binding of the virus, and the fusion protein, F, which drives subsequent fusion of the two membranes by undergoing a

series of conformational changes [40–42]. The fusion protein of paramyxoviruses is synthesized as an inactive precursor F0 that is cleaved by host proteases into the fusogenically active disulfide-linked heterodimer F1+F2. For the majority of paramyxoviruses, including measles virus [43], parainfluenza virus 5 (PIV5) [44] and Newcastle disease virus [45], this cleavage is mediated by the protease furin in the medial- and trans-golgi network (TGN). For some paramyxoviruses, an extracellular protease is responsible for the proteolytic activation (reviewed in [46]). However, henipaviruses are unique in that they utilize the endosomal/lysosomal protease cathepsin L, and in some cases cathepsin B, to cleave and activate the fusion protein [47,48]. This unusual role of cathepsins in the henipavirus life cycle requires a complex trafficking pathway for the activation of F protein in which the protein is synthesized and traffics to the plasma membrane in the uncleaved precursor form, F0. The protein is then endocytosed, cleaved in the endosomal compartments by cathepsin L or B and recycled back to the plasma membrane as the fusogenically active F1+F2 heterodimer [47–54]. The reason for this complex method of proteolytic activation remains unclear, but the cathepsin activation of henipavirus F proteins cannot be functionally replaced by other proteases, as a Nipah F protein mutant containing trypsin- or furin- cleavable sites displays reduced F processing [55]. Cleavage of the Hendra and Nipah F proteins occurs at a monobasic cleavage site GDV-K/R [56,57]; however, mutagenesis studies demonstrated that mutation of the basic residue at the cleavage site or of amino acids upstream of this site did not eliminate F protein processing [57,58], contradictory to other viral fusion proteins [59–62].

Cathepsins have been shown to be involved in the processing of several viral proteins. Cathepsin L proteolysis of the spike protein S of SARS-CoV is necessary for membrane fusion activation [63]; in addition, Ebola virus utilizes cathepsin L and B for processing and priming of the GP glycoprotein [64,65]. Interestingly, bats have been recently confirmed as the primary reservoir for SARS-CoV [8], SARS-like CoV [7] and the filovirus Marburg virus [11], while serological evidence suggests that Rousettus aegyptiacus fruit bats are potential reservoirs for Ebola virus [66]. This raises the question of whether the unique utilization of cathepsins by henipaviruses may be an

evolutionary adaptation to the nature of proteases present in their natural reservoirs, the fruit bats. To address this, we examined the proteolytic processing of the cathepsin-dependant Hendra virus F protein and the furin-dependent PIV5 F in cells of two species of fruit bats, Pteropus alecto and R. aegyptiacus. Our results show that cell lines from fruit bats have both active cathepsin and furin-like proteases capable of cleaving and activating viral fusion proteins. In addition, we demonstrate that the dependence of Hendra virus on cathepsin L and vesicular trafficking for proteolytic processing of its fusion protein also occurs in cells of its natural fruit bat reservoir. Comparison of amino acid sequences of P. alecto cathepsin L and furin proteases to those of different mammalian species revealed that both cathepsin L and furin show a high degree of conservation among mammals but there are bat-specific amino acid changes, primarily in the C-terminus of P. alecto furin. Closer examination of furin-like proteases revealed that fruit bats have active furins that resemble other mammalian furins in terms of activity and response to protease inhibitors, but our results suggest differences in intracellular localization of furin in fruit bats which may influence accessibility of viral proteins to furin proteases in these natural reservoir hosts.

Materials and Methods

Cell lines and reagents

Vero cells, baby hamster kidney (BHK) cells and P. alecto bat cells derived from different organs, Kidney (PaKi), brain (PaBr), lung (PaLu) and fetus (PaFe) [67] were grown in Dulbecco's modified Eagle's medium (DMEM; Gibco Invitrogen) supplemented with 10% fetal bovine serum (FBS) and 1% penicillin and streptomycin. R. aegyptiacus fetus body cells (R06E) or head cells (R05T) [68] were maintained in DMEM-F12 media (Gibco Invitrogen) supplemented with 10% FBS and 500μg of gentamicin. A549 cells were grown in Roswell Park Memorial Institute medium (RPMI; Lonza) supplemented with 10% FBS and 1% penicillin and streptomycin. BEAS-2B cells, a human lung/bronchial epithelial cell line, obtained from ATCC were maintained in BEGM medium containing all the recommended supplements (Lonza). The protease inhibitor E64d was obtained from Sigma, cathepsin L inhibitor I and furin inhibitor, decanoyl-RVKR-chloromethylketone (dec-RVKR-CMK), were purchased from

Calbiochem EMD Millipore. Fluorogenic furin substrate was obtained from Calbiochem EMD Millipore.

Plasmids and antibodies

Hendra virus F and G coding sequences were subcloned into the pCAGGS mammalian expression plasmid as previously described [52]. pCAGGS vectors containing PIV5 F and HN genes were kindly provided by Robert Lamb (Howard Hughes Medical Institute, Northwestern University). Polyclonal antibodies (commercially produced by GenemedCustomPeptide Antibody Service, San Francisco, CA) to amino acid residues 526–539 or 516–529 in the cytoplasmic tails of Hendra virus F or PIV5 F, respectively, were used to immunoprecipitate the F protein [52].

Expression of Hendra virus and PIV5 fusion proteins

Subconfluent monolayers of Vero cells and bat cells: R06E and PaKi were transfected with the expression vectors pCAGGS-Hendra F or pCAGGS-PIV5 F, encoding the Hendra virus F or PIV5 F proteins, using Lipofectamine Plus (Life Technologies) according to manufacturer's protocol. Vero cells in 35-mm dishes were transfected with 2 μg of plasmid DNA, 6 μl of plus reagent and 4 μl of lipofectamine in 0.8 ml of Opti-MEM (Gibco Invitrogen). The transfection efficiency in bat cells in general was much lower than Vero cells, so transfections were performed in 100mm dishes to allow for sufficient protein expression. For expression of fusion proteins in bat cells, 12 μg of DNA, 18 μl of plus reagent, 12 μl of lipofectamine and 1.2 ml of Opti-MEM (Gibco Invitrogen) were combined and added to cells grown in 100-mm dishes. At 3–4 hours post-transfection, cells were washed with phosphate buffered saline (PBS) and incubated overnight at 37°C in DMEM or DMEM-F12 media supplemented with 10% FBS and antibiotics.

Metabolic labeling and immunoprecipitation

Twenty-four hours post-transfection, cells were starved in cysteine- and methionine-deficient DMEM media for 45 minutes followed by labeling in Tran35S-label (100 μCi/ml; Perkin Elmer, Waltham, Massachusetts). To determine total expression of fusion

proteins, cells were labeled for 3 hours at 37°C and lysed immediately. For pulse chase experiments, cells were labeled for 30 minutes, washed twice with PBS, normal DMEM or DMEM-F12 media was then added, and cells were chased for varying times. At the end of the chase periods, cells were washed and lysed in radioimmunoprecipitation assay (RIPA) lysis buffer (100 mM Tris-HCl [pH 7.4], 150 mM NaCl, 0.1% SDS, 1% Triton X-100, 1% deoxycholic acid) containing 0.15 M NaCl and supplemented with protease inhibitors. Lysates were then clarified by centrifugation at 136,000xg for 15 minutes at 4°C and supernatants were immunoprecipitated with anti-peptide sera to the F proteins and protein-A conjugated sepharose beads [69]. Immunoprecipitated proteins were analyzed on 10% sodium dodecyl sulfate-polyacrylamide gel electrophoresis (SDS-PAGE) and visualized using the Typhoon imaging system (Amersham Biosciences/GE Healthcare Life Sciences, New Jersey). ImageQuant TL (GE Healthcare, Piscataway, NJ) was used to determine band densitometry and results were expressed as percent cleavage defined as F1/(F1+F0).

Syncytia assay

Vero cells or PaKi cells in 35-mm dishes were transiently transfected with Hendra virus F or PIV5 F alone or in combination with the homotypic attachment protein (G or HN). The F:G/HN ratio used was 1:3 for Hendra virus and 1:1 for PIV5. Twenty-four to 48 hours post transfection, syncytia formation was examined and photographs were taken using a Nikon digital camera mounted atop a Nikon TS100 microscope with 10x objective.

Furin-like enzyme activity

A furin-like enzyme activity assay on whole cell lysates was performed as described [70] with minor modifications. 2×106 cells were collected, washed with PBS and lysed for 10 minutes on ice in 200 μl of 5× lysis/reaction buffer (500 mM HEPES, pH 7.0, 2.5% Triton X-100, 5 mM calcium chloride, 5 mM β-mercaptoethanol). Cells were then sheared with a 23-gauge needle followed by centrifugation at 13,000xg for 10 minutes at 4°C, and supernatants were stored at -80°C. For determination of furin-like enzyme activity, cell lysates were diluted 2 fold in 5x lysis buffer. In a black opaque 96-well plate, 20 μl of cell lysates were added to 70 μl of ultrapure water and the plate was

incubated for 15 minutes at 37°C. After incubation, 10 µl of 1 mM furin fluorogenic substrate, previously pre-warmed at 37°C for 30 minutes, was added and fluorescent intensity was immediately measured on a SpectraMax Gemini XPS plate reader (Molecular Devices) every 3 minutes for 240 minutes with excitation at 355 nm and emission at 460 nm. For determination of the effect of a furin inhibitor on furin-like activity, cell lysates were incubated with increasing concentrations of the inhibitor for 3 hours at 37°C and cells were then processed for the enzyme activity assay as mentioned above.

Multiple sequence alignment of mammalian furin and cathepsin L

Sequences of P. alecto furin and cathepsin L were identified using BLAST searches of the P. alecto genome and transcriptome databases generated previously [71,72]. Sequences of other mammalian proteases were obtained from GenBank. Multiple sequence alignment of mammalian proteases was generated using ClustalW [73]. P. alecto bat furin or P. alecto cathepsin L was used as a standard reference for amino acid numbering.

Results

The Hendra virus and PIV5 fusion proteins are efficiently cleaved in fruit bat cells

Several cell lines derived from different bat species have been established, providing a valuable tool for in vitro studies of virus life cycles in their natural reservoir. In this study, we utilized cells previously established from two pteropid fruit bats, P. alecto [67] and R. aegyptiacus [68]. P. alecto cells derived from different tissues were shown to be permissive to henipavirus replication and cells derived R. aegyptiacus permitted filovirus infection, indicating that these cells contain the necessary host factors required for virus replication [67,74]. However, very little is currently known about the nature of proteases present in these bat species. To assess the ability of pteropus host cell proteases to proteolytically process viral fusion proteins, we examined the proteolytic processing of the cathepsin-dependent Hendra virus F protein and the furin-dependent PIV5 F protein in P. alecto kidney cells (PaKi) and R. aegyptiacus cells obtained from body tissues (R06E). Bat cells and Vero cells, used as a control, were transiently

transfected to express the Hendra virus F or PIV5 F protein and metabolically labeled. The fusion proteins were subsequently immunoprecipitated and analyzed on 10% SDS-PAGE. As seen in Figure 1A, both fusion proteins were proteolytically processed into the F1 and F2 heterodimer in R06E and PaKi cells. This indicates that cells from both P. alecto and R. aegyptiacus have active cathepsin-like and furin-like proteases capable of cleaving the Hendra viurs and PIV5 F proteins. To assess whether the processed proteins were fusogenically active, syncytia assays were performed. Syncytia formation was not observed in the presence of the attachment (Hendra G or PIV5 HN) protein alone, consistent with the role of the F protein in promoting fusion. However, syncytia were observed in all three cell types upon expression of the fusion and attachment proteins of either Hendra virus or PIV5 (Figure 1B, arrows). Syncytia formed in R06E and PaKi were smaller in size compared to syncytia seen in Vero cells and the total number of syncytia observed in the two fruit bat cell lines was less than in Vero cells, likely as a result of lower transfection efficiency in bat cells versus Vero cells. These results indicate that P. alecto and R. aegyptiacus fruit bat cells can cleave and activate cathepsin-dependent and furin-dependent viral fusion proteins.

Kinetics of PIV5 F processing differs between Vero cells and fruit bat cells

The Hendra virus fusion protein undergoes a complex trafficking pathway for cleavage and activation [47,51,52], while PIV5 F is cleaved by furin as it passes through the TGN [44]. It has been previously shown that the majority of Hendra virus F cleavage occurs within 4 hours of protein synthesis [52]. To compare the kinetics of processing of Hendra virus and PIV5 F proteins in bat cells versus Vero cells, cleavage was monitored by pulse chase analysis. Vero cells or fruit bat cells were labeled for 30 minutes, washed and incubated for 0 to 4 hours in chase media. Directly following labeling (0 hours), almost only the uncleaved F0 form of Hendra virus F was detected in all cell types, while a small percentage of PIV5 F0 was cleaved to F1 in bat PaKi and R06E cells (Figure 2A). Cleavage of F0 to F1 increased during the 4 hour chase period in all cell types for both Hendra virus F and PIV5 F. For Hendra virus F, R06E and PaKi cells showed similar processing kinetics to Vero cells, with no significant difference in percentage of cleavage observed at any point following synthesis. In contrast, PIV5 F was cleaved more rapidly

in both bat cell types compared to Vero cells. After one hour of synthesis, more than 40% of PIV5 F0 had been proteolytically processed in both PaKi and R06E fruit bat cell lines, a significantly higher level than the 17% cleavage observed in Vero cells (Figure 2B). As similar processing kinetics were observed for Hendra virus F protein, it is unlikely that the differences observed for PIV5 F are due to changes in the rate intracellular of trafficking in fruit bat cells. Cleavage of PIV5 F by furin generally occurs in secretory vesicles budding from the TGN. Thus, these data suggest a potential difference either in the intracellular localization or expression of furin present in PaKi and R06E cells compared to Vero cells.

Hendra virus F cleavage in fruit bat cells depends on vesicular trafficking and cathepsin L

The requirements for the activation of henipavirus fusion proteins differ remarkably from other paramyxovirus F proteins. Cleavage of Hendra and Nipah F proteins occurs by the action of cathepsin L at a monobasic cleavage site GDV-K/R [56,57]. While the kinetics of processing in bat cells were consistent with cleavage following trafficking to the endosome (Figure 2), the dependence of henipaviruses on the endosomal cysteine protease cathepsin L in their natural reservoir was verified using non-specific and specific cathepsin inhibitors. Treatment of PaKi and R06E bat cells with the general cysteine protease inhibitor E-64d, which inhibits calpain and cathepsins B, H and L [75] prevented cleavage of Hendra virus F in all cell types (Figure 3A). To verify that cathepsin L is specifically involved in Hendra F proteolytic processing in bat cells, an inhibitor that targets cathepsin L was used. Similar to Vero cells, inhibition of cathepsin L also ablated cleavage of F0 into the F1 and F2 heterodimer, indicating that processing of Hendra virus F protein is under the control of cathepsin L in its natural reservoir host (Figure 3A). Interestingly, in PaKi cells, an extra band of higher molecular weight, which is not detected in other cell lines, was seen above F0 upon inhibition of Hendra F processing. A similar band was seen when a cell line derived from P. alecto brain (PaBr) was treated with E64-d and cathepsin L inhibitor (data not shown). This suggests that additional post translational modifications may occur in the uncleaved Hendra F protein in its natural reservoir P. alecto.

Proteolytic activation of Henipavirus F protein requires endocytosis [49–52], cleavage by cathepsin L and recycling of the cleaved F1-F2 heterodimer to the cell surface [47,48]. Temperature block experiments have been used to influence both exocytic and endocytic transport [76,77]. We therefore determined the effect of reduced temperature on the cleavage of Hendra virus F and PIV5 F. Cells expressing Hendra virus F or PIV5 F were metabolically labeled and chased for 3 hours either at 20°C or 37°C. The cleaved F1 product of Hendra F and PIV5 F was observed following incubation at 37°C. While a background band of slightly lower molecular weight than Hendra F1 was seen, incubation of R06E and PaKi at 20°C abolished proteolytic processing of Hendra F in bat cells (Figure 3B), as was previously shown in Vero cells [52], consistent with the cleavage of Hendra F depending on temperature-sensitive vesicular trafficking in bat cells. Interestingly, while incubation of Vero cells at 20°C abolished PIV5 F processing, the F1 cleavage product could still be observed in PaKi and to an even greater extent in R06E cells (Figure 3C). To determine whether this was specific for bat cells, we utilized an additional mammalian cell line from baby hamster kidney cells, BHK. Similar to fruit bat cells, incubation of BHK cells at 20°C did not completely inhibit PIV5 F proteolytic processing. In addition, while the majority of PIV5 F0 was cleaved to F1 in BHK, PaKi and R06E cells upon incubation for 3 hours at 37°C, F0 was clearly visible in Vero cells at this time point. Furin is primarily located in the Golgi and TGN, and it can also circulate between the cell surface and the TGN [78–80]. Inhibition of Hendra virus F cleavage by lowering the temperature to 20°C (Figure 3B) indicate that endosomal trafficking is blocked in R06E and PaKi cells under this condition; however the varying effects of lower temperature on PIV5 F processing in different cell types suggest that the temperature dependence of trafficking through the TGN may differ between different cell types. These results, combined with our previous findings on the more rapid furin processing of PIV5 F in bat cells, suggest that subtle differences in cellular distribution and localization of furin or trafficking through TGN may exist between different mammalian species.

Effect of dec- RVKR-cmk on furin-like proteases in fruit bat cells

Results in Figure 1A demonstrated that bat cells can cleave the fusion protein of PIV5, which is proteolytically processed by furin in other cell types [44], suggesting that bat cells have active furin or furin-like proteases. To verify the involvement of a furin protease in the cleavage of the PIV5 fusion protein, we utilized a small molecule inhibitor of furin, decanoyl-Arg-Val-Lys-Arg-chloromethyl ketone (dec-RVKR-cmk), which binds the catalytic sites of all seven mammalian proprotein convertases and inhibits their activity [81,82]. This inhibitor has also been shown to be effective in inhibiting Kex-2, the yeast endoproteinase homologue of furin as well [83]. Vero cells and fruit bat cells were treated with inhibitors of furin and cathepsin L, and cleavage of PIV5 fusion protein was assessed. Addition of cathepsin L inhibitor to Vero, PaKi or R06E cells had no effect on proteolytic processing of PIV5 F protein (Figure 4A). In Vero cells, addition of the potent furin inhibitor dec-RVKR-cmk resulted in a marked decrease in cleavage of PIV5 F0 to F1. In contrast, the effect of the inhibitor on processing of PIV5 F in PaKi and R06E cells was minimal (Figure 4A). Dec-RVKR-cmk has been widely used to prevent the proteolytic activation of a variety of viral glycoproteins [84–87], and inhibition of cleavage usually requires a concentration range from 25 μM to over 40 μM. In the presence of 50 μM dec-RVKR-cmk, the percentage of inhibition of PIV5 F cleavage in Vero cells was approximately 70% compared to the control without inhibitor, while only 20% inhibition in PaKi and RO6E cells was observed compared to the control. We next determined the effect of the inhibitor on furin-like enzyme activity in cell lysates from different fruit bat cells and other mammalian cells, Vero cells, A549, and BEAS-2B. Cell lysates prepared from equal number of cells for each cell type were incubated with increasing concentrations of dec-RVKR-cmk (50 μM, 80 μM, 100 μM,150 μM) for 3 hours at 37°C prior to the addition of the flourogenic furin substrate, Pyr-Arg-Thr-Lys-Arg-AMC, and release of the fluorescent AMC product was subsequently determined. All cell types showed a dose-dependent response to the drug, and as shown in Figure 4B, there were no significant statistical differences in the effect of the inhibitor between the different cell types at all the tested concentrations, indicating that binding of the competitive inhibitor dec-RVKR-cmk to the catalytic site of furin-like proteases is comparable in the different cell types. The observed differences in the response to the potent furin inhibitor in fruit bat cells seen in Figure 3A may therefore reflect differences

in the accessibility of the inhibitor to the enzyme, i.e. the level of uptake and metabolism between the different cell types, or differences in the expression or localization of furin-like proteases.

Bat lung cells display slower kinetics of furin-like enzyme activity than human lung cells

Fruit bat cells have functional furin-like proteases, and processing of PIV5 F occurs more rapidly in these cells than in Vero cells (Figure 2A). To compare the enzymatic activity of furin homologs present in bat cells to that present in other mammalian cell types, we performed a furin-like enzyme activity assay. This assay, which is not specific for furin but determines the activity of all proprotein convertases, allows determination of endogenous enzymatic activity of furin-like enzymes in whole cell lysates [70], and was used to compare the kinetics of the protease activities per cell in different cell lines. Cell lysates from 2×106 cells of each cell type were added to the flourogenic substrate, Pyr-Arg-Thr-Lys-Arg-AMC, and fluorescence was monitored for 4 hours. The progress curves obtained for each cell type allowed determination of differences in total furin-like enzyme activity (Figure 5). P. alecto fetus cells (PaFe) generated the lowest total amount of fluorescent product at each time point, indicating that both the rate and extent of furin processing per cell is lowest in these cells. R. aegyptiacus cells R06E and R05T displayed the next lowest furin-like activity. Statistical analysis showed that there was no significant difference in furin-like activity between Vero and PaKi cells suggesting that the total cellular furin-like activity is comparable in these two kidney cell lines. However, comparison of AMC release in R06E to Vero or PaKi cells showed significant difference starting 18 minutes after addition of the substrate (p value <0.05) and during the 4 hour incubation period, with a p value <0.0001 between 30 and 90 minutes. Furin-like activity in cells obtained from P. alecto brain (PaBr) was significantly higher than the other fruit bat cells P. alecto lung (PaLu) and PaFe, R06E and R05T one hour post incubation with the substrate. Interestingly, the progress curves for the total furin-like activity in the two lung human cell lines, A549 and BEAS-2B, were different from other tested cell lines. Release of AMC was faster and fluorescence reached maximum levels by 30 minutes or 60 minutes in A549 and BEAS-

2B, respectively. In contrast, this rapid proteolysis of the Pyr-Arg-Thr-Lys-Arg-AMC substrate was not observed in PaLu cells and the total furin-like activity in the P. alecto lung cells was significantly lower than that of A549 and BEAS-2B cells at all timepoints, with a p value <0.0001 during the first three hours. These data reveal that bat cells have functional and active furin-like enzymes that can recognize and cleave a furin substrate, with variation seen in the total furin-like enzyme activity between cells derived from different tissues. Furin-like pro-protein convertases are expressed differently in various body tissues and the variation seen in the total furin-like activity between the different cells types is expected. However, the significant difference between the processing of the furin substrate between P. alecto lung cells and the two human lung cells suggest differences either in the activity or in the expression levels of the furin-like proteases in the lungs of the two species.

Bat furin and cathepsin L proteases have specific amino acid sequence variations not detected in other mammalian counterparts

To compare amino acid sequences of bat cathepsin L and furin to other mammalian proteases, we performed multiple sequence alignment analysis. Whole genome sequencing of different bat species has been performed [72,88]; however the furin sequences from both P. vampyrus and Myotis davidii were not complete. Sequences of furin and cathepsin L from the P. alecto transcriptome were previously generated [71]. Multiple sequence alignments of furin and cathepsin L1 amino acid sequences from P. alecto and a variety of other mammals were performed using ClustalW [89]. Both furin and cathepsin L1 showed a high level of conservation among different mammalian species however, furin showed a higher degree of conservation. The sequence alignment for mammalian cathepsin L1 proteases (Figure 6) shows amino acid changes between the different species spread across the whole protein sequence, with some amino acid changes that are specific to P. alecto cathepsin L (marked in yellow). Compared to cathepsin L1, furin from various mammalian species had fewer amino acid changes across the entire sequence (Figure 7). Furin is a type I membrane protein composed of an N-terminal pro-peptide followed by a catalytic site, a P/homo B domain which is essential for activity of the catalytic domain, and a C-terminal region containing a

transmembrane domain [90]. The N-terminal region of P. alecto furin contained one amino acid change not observed in any other mammalian furin, as the leucine at position 57 in other mammalian furins is substituted by glutamine in P. alecto. The catalytic site (shown in gray), encompassing amino acid residues G146 to L382 [45,90] was extremely conserved, with a single glutamate to aspartate change in the catalytic site of Pteropus furin at position 299. The highest degree of variation observed for P. alecto furin occurred at the C-terminus, including the following unique amino acid changes: A at position 619 in P. Alecto furin in contrast to P at this position in all other mammalian furins (P619>A), D623>A, S627>N, P642>R, Q651>R, T673>K, G781>R, K788>R, A792>V, deletion of N at position 496 and deletion of E at position 768 (highlighted in green). The cytoplasmic tail controls the trafficking and cellular localization of furin. The sequences at the cytoplasmic tail of furin that are known to be critical for intracellular trafficking of furin include the acidic cluster (EECPpSDpSEEDE) and the two membrane proximal motifs YKGL and LI [78,79,91–93]. The YKGL and LI motifs are conserved in P. alecto; however, the first aspartate (position 768) in the acidic cluster sequence, which is required for phosphorylation by casein kinase II, is absent in P. alecto furin. It is possible that the deletion of the acidic aspartate affects the phosphorylation of serine 772 and thus alters the intracellular localization or distribution of furin in P. alecto.

Discussion

Bats have recently been shown to carry a number of novel viruses [94]; however, our knowledge of the natural history of viruses in their bat reservoir host and the special features of bats that allow them to co-exist with this wide range of viruses is limited. Bats and bat-derived cells are susceptible to infection by many viruses including filoviruses, paramyxoviruses, coronaviruses and influenza virus [74,95] indicating that bats have the necessary cellular factors to mediate many viral infections. Cellular proteases play an essential role in proteolytic activation of the majority of viral glycoproteins and in the spread of infection, but very little is currently known about the protease profile of the bat hosts. Interestingly, a number of bat-borne viruses utilize the endosomal cathepsin proteases during their life cycle [47,48,63–65], in contrast to the more common use of furin proteases for intracellular viral glycoprotein processing. To address the ability of

bat cells to proteolytically process viral fusion proteins, we examined the proteolytic processing of the PIV5 F protein, normally cleaved by furin, and the Hendra virus F protein, normally cleaved by cathepsin L, in cells derived from two species of bats of the Pteropodidae family. We showed that P. alecto and R. aegyptiacus have homologues of cathepsin and furin proteases capable of cleaving and activating cathepsin-dependent (Hendra virus F) and furin-dependent (PIV5 F) viral fusion proteins. This finding is consistent with previous studies showing that cells from different bat species can cleave glycoproteins of some viruses such as Ebola virus [96], and an African henipavirus [97,98]. Our data also indicate that the requirements for proteolytic processing of Hendra virus F in bat cells are analogous to those previously determined in Vero cells [47,52]. Temperature reduction experiments or inhibition of cathepsin L prevented both cleavage of Hendra virus F and syncytia formation (data not shown), indicating that vesicular trafficking and a bat homolog of cathepsin L are involved in activation of Hendra virus F in bat cells. In addition, we did not detect a significant difference in the kinetics of Hendra F cleavage in PaKi or R06E compared to Vero cells and levels of cleaved F1 on the cell surface of Vero cells and bat cells were similar (data not shown). These results indicate that Hendra virus F trafficking in bat cells is analogous to that in Vero cells, suggesting that Hendra virus evolved its dependence on cathepsin L to mediate infection through adaptation in its bat natural host.

Cleavage of PIV5 F protein and the furin-like enzyme activity assay indicate that bat cells from P. alecto and R. aegyptiacus have active furin-like proteases capable of recognizing and cleaving the furin consensus site R-X-K/R-R in PIV5 F protein and in the fluorogenic furin substrate. These results support recent evidence that R06E cells and other cells derived from different Pteropodidae bat species are sensitive to infection of viruses that utilize furin for mediating infection including filoviruses and paramyxoviruses [74,95,96]. However, kinetics of PIV5 F cleavage indicated that proteolytic processing of the furin-dependent PIV5 F is more rapid in bat cells than in Vero cells with the most rapid cleavage seen in R06E cells; however, the total furin-like enzyme activity assay showed lower total cellular furin-like activity in R06E cells compared to Vero cells. A more rapid cleavage of PIV5 F even with less furin activity

per cell could result from differences in the cellular localization of the furin homologues in the bat cell types. Consistent with this, we found that reduction of temperature to 20°C did not completely inhibit cleavage of PIV5 F in R06E cells and PaKi cells, but significantly reduced proteolysis of PIV5 F in Vero cells as was previously shown [52]. Furin is a membrane-bound protease that circulates between the cell surface and the TGN through endosomes [79]; however, the cellular localization and distribution of furins may vary between the different cell types. Specific motifs in the cytoplasmic tail at the C-terminus of furin control its intracellular trafficking [78,91]. Amino acid sequence alignment of P. alecto furin and multiple other mammalian furins shows that the two membrane proximal motifs YKGL and LI required for trafficking of furin from the TGN to endosomes and the CPpSDpSEEDE motif that is important for retention of furin in the TGN are conserved in P. alecto furin [91,99]. The phosphorylated acidic cluster (EECPpSDpSEEDE) which directs trafficking from endosomes to the TGN [92] lacks the first glutamate in furin from P. alecto. In addition, several differences in specific amino acid residues occur at the C-terminus of P. alecto furin compared to other mammalian furins that may influence the localization of furin in P. alecto cells and possibly other members within the pteropodidae family.

Our data also show differences between the total cellular activity of furin-like enzymes in various cell types. Furin is ubiquitously expressed at different levels in all tissues [100,101]. The mRNA levels of furin determined in different tissues of an African monkey showed highest levels in kidney and liver, lower levels in brain, spleen and thymus and lowest levels were detected in tissues from lung, heart and testis [101]. Our results show that P. alecto kidney cells had higher activity than other Pteropus cell types, followed by brain cells (PaBr), lung cells (PaLu) and fetus cells, which showed the lowest furin-like activity. Interestingly, furin-like activity in PaLu cells was significantly lower and showed slower kinetics relative to the two human lung cell lines, A549 and BEAS-2B. This finding could indicate either that human lung cells have a greater number of active furin-like enzymes than P. alecto lung cells, or that the individual furin proteases in human lung cells have increased proteolytic activity. BEAS-2B cells are isolated from human bronchial epithelium, A549 are type II alveolar basal epithelial cells

while the PaLu cells are mainly cuboidal epithelial cells derived from lung tissues [67]. Differences in cell type between these three cell lines may also contribute to the differences seen in the total furin-like activity.

In conclusion, our results show that bats have cathepsin-like and furin-like proteases analogous to their counterparts in other mammalian species, suggesting that the utilization of cathepsins for viral glycoprotein processing in a number of bat-resident viruses is not due to a lack of furin-like enzymes in the bat reservoir host. However, potential alterations in furin localization or activity in the bat host may affect virus replication. Newly emerging viruses can be major threats to public health, so further investigation of virus biology in bat reservoirs is needed to provide a global perspective on the changes that occur in viruses within their natural hosts that contribute to the emergence of the virus and transmission to other species.

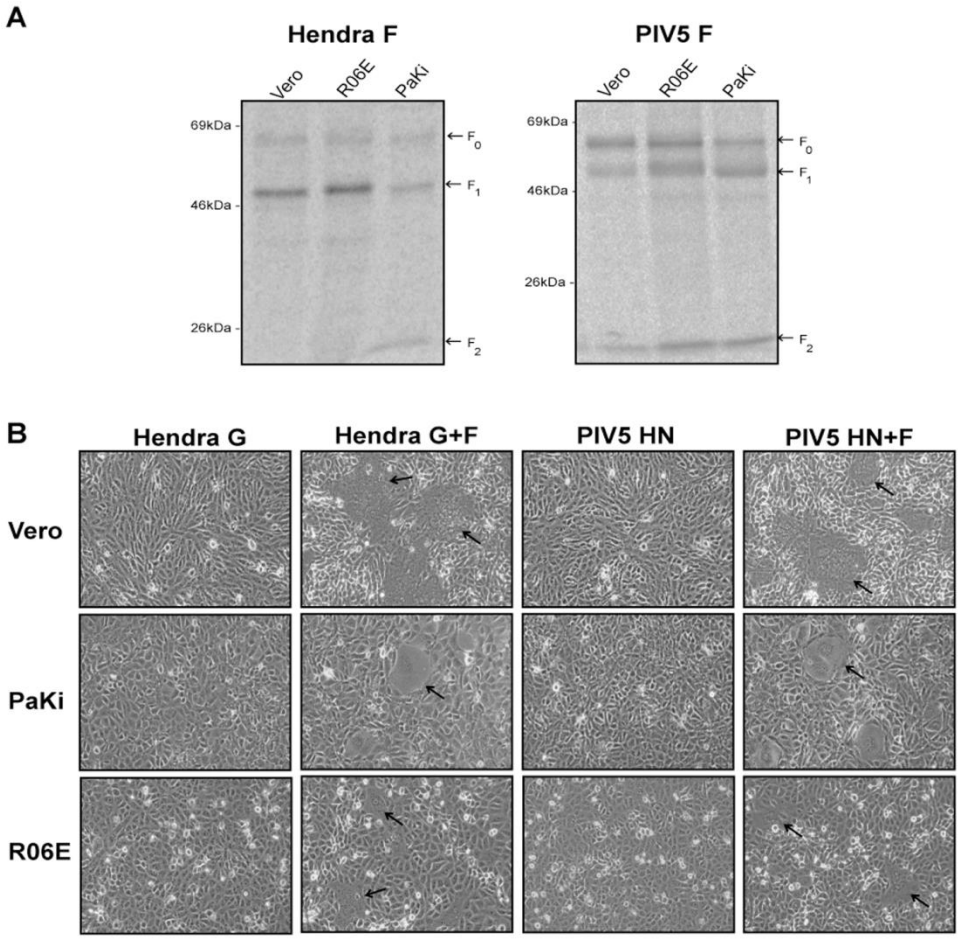

Figure 1. Bat cells cleave cathepsin-dependant Hendra virus F and furin-dependant PIV5 F.

(A) Cells were transfected with pCAGGS-Hendra virus F or pCAGGS-PIV5 F and 18–24 hours post transfection, metabolically labeled with Tran ^{35}S for 3 hours at 37°C. Following labeling, cells were lysed and immunoprecipitated. Proteins were analyzed by 10%SDS-PAGE and visualized by autoradiography. (B) Cells were transfected with Hendra virus F or PIV5 F alone or in combination with Hendra virus G or PIV5 HN. 24 to 48 hours post transfection, cells were washed and images were taken using a Nikon digital camera mounted atop a Nikon TS100 microscope with 10x objective. Arrows indicate syncytia.

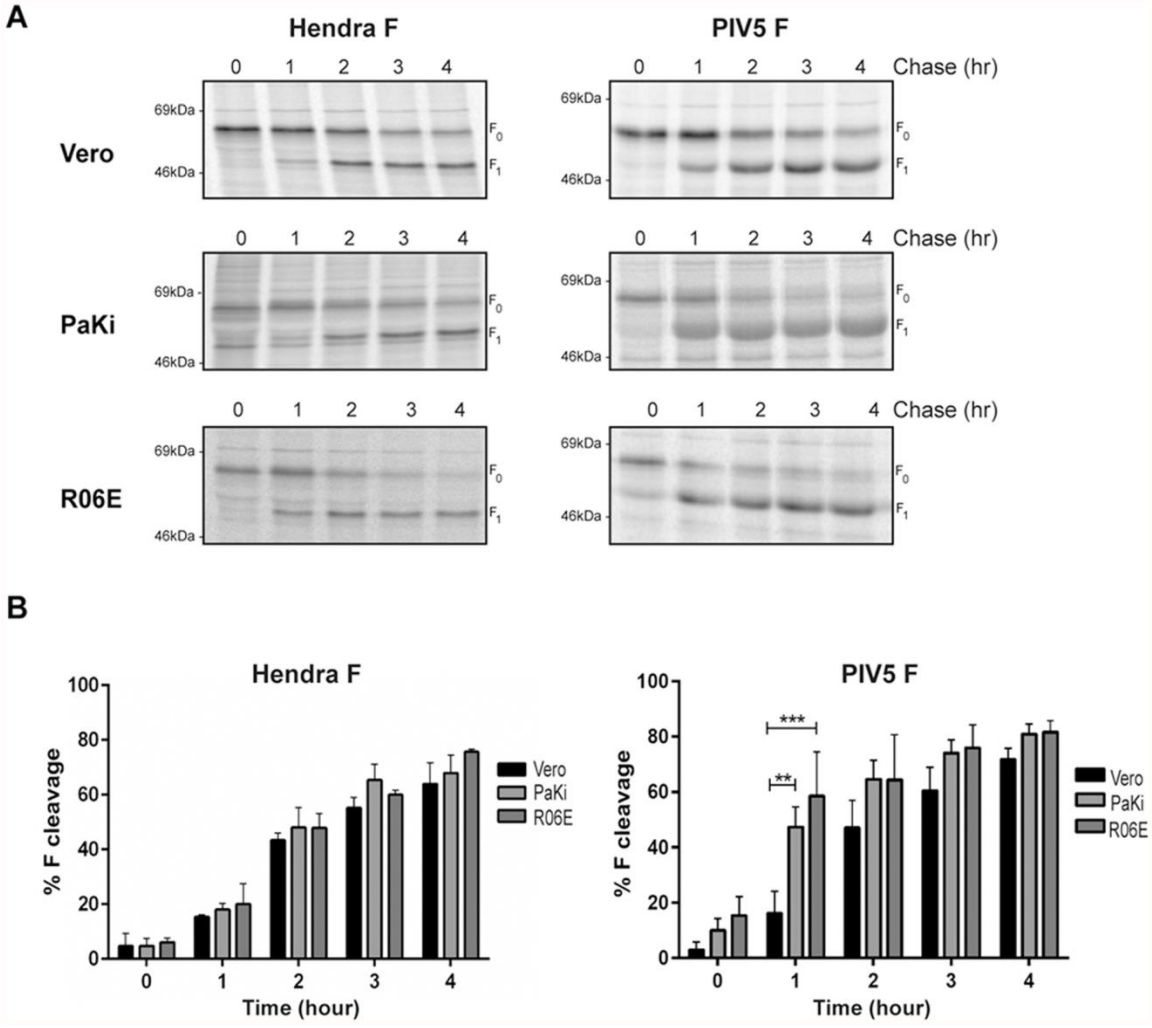

Figure 2. Kinetics of PIV5 Fusion protein cleavage is faster in bat cells compared to Vero cells.

(A) Cells transiently transfected with pCAGGS-Hendra virus F or pCAGGS-PIV5 F were metabolically labeled with Tran ^{35}S for 30 minutes and chased for the indicated times. Cells were immediately lysed and cell lysates were immunoprecipitated. Proteins were migrated on 10% SDS-PAGE and analyzed by autoradiography. (B) Quantification of F1 densitometry was done using ImageQuant, TL software (GE Healthcare, Piscataway, NJ) and results are represented as percent cleavage defined as $F_1/(F_1+F_0)$. Error bars represent the mean ± standard deviation for three independent experiments. Two-way ANOVA, **p<0.01, ***p<0.001.

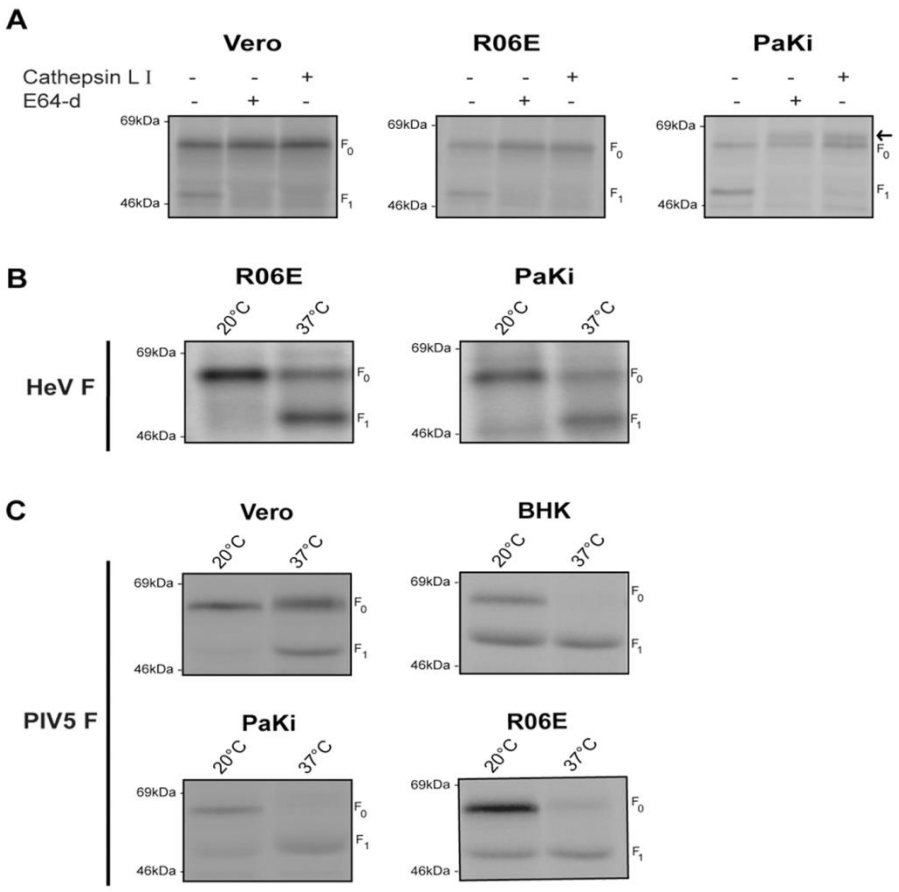

Figure 3. Inhibition of cathepsin L and vesicular trafficking prevent cleavage of Hendra virus F.

(A) Vero cells or bat cells were transfected with pCAGGS-Hendra virus F and 24 hours post transfection, cells were metabolically labeled with Tran ^{35}S in the absence or presence of the indicated inhibitor. E64-d and cathepsin L inhibitor I were added at 20μM. Cells were lysed, immunoprecipitated and anaylzed on 10% SDS-PAGE. Arrow indicates the position of a novel band. (B, C) Cells transiently transfected with Hendra virus F (B) or PIV5 F (C) were labeled with Tran ^{35}S for 45 minutes and then chased for 3 hours at either 20°C or 37°C. Following lysis and immunoprecipitation, proteins were run on 10% SDS-PAGE and visualized by autoradiography.

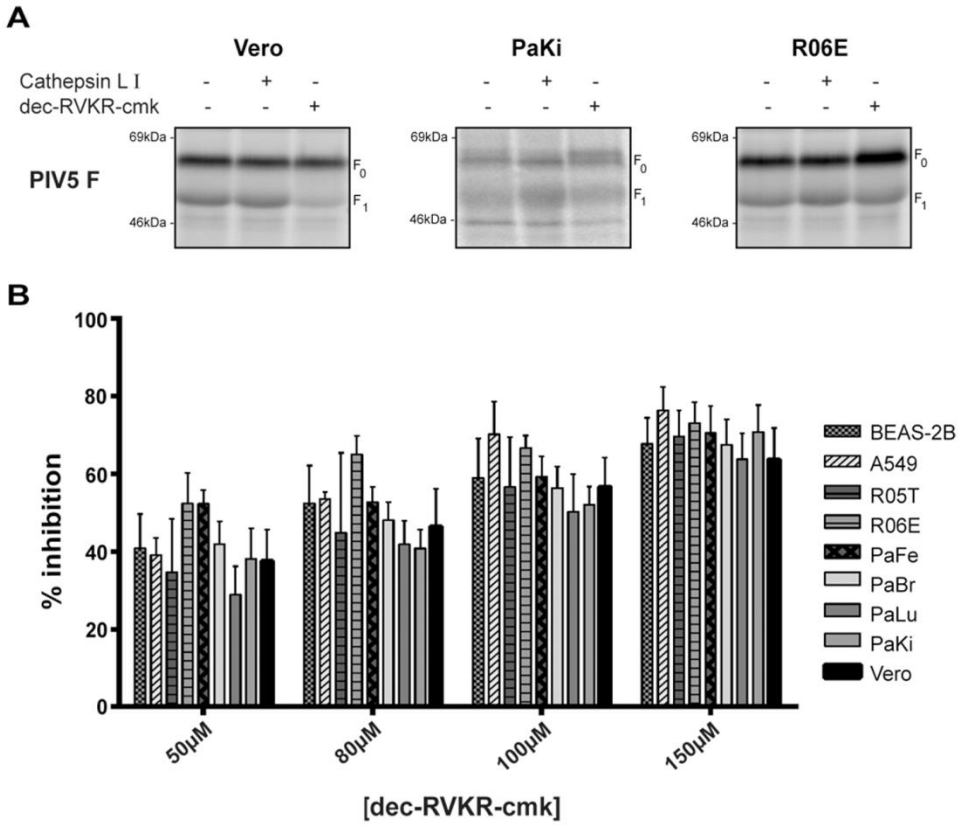

Figure 4. Effect of dec-RVKR-cmk on PIV5 F cleavage and furin enzyme activity in fruit bat cells.

(A) Cells transfected with pCAGGS-PIV5 F were labeled with Tran ^{35}S for 3 hours in the absence or presence of cathepsinL I (20μM) or dec-RVKR-cmk (50 μM). Prior to SDS-PAGE analysis, cells were lysed and subject to immunoprecipitation. Images were visualized by autoradiography. (B) 2×10^6 cells of each cell type were lysed for 10 minutes on ice followed by shearing with a 10-gauge needle. Cell lysates were incubated with increasing concentrations of dec-RVKR-cmk for 3 hours at 37°C prior to addition of Pyr-Arg-Thr-Lys-Arg-AMC furin substrate. End-point fluorescence was measured after 4 hours using an XPS plate reader. Error bars represent the mean ± standard deviation for three independent experiments.

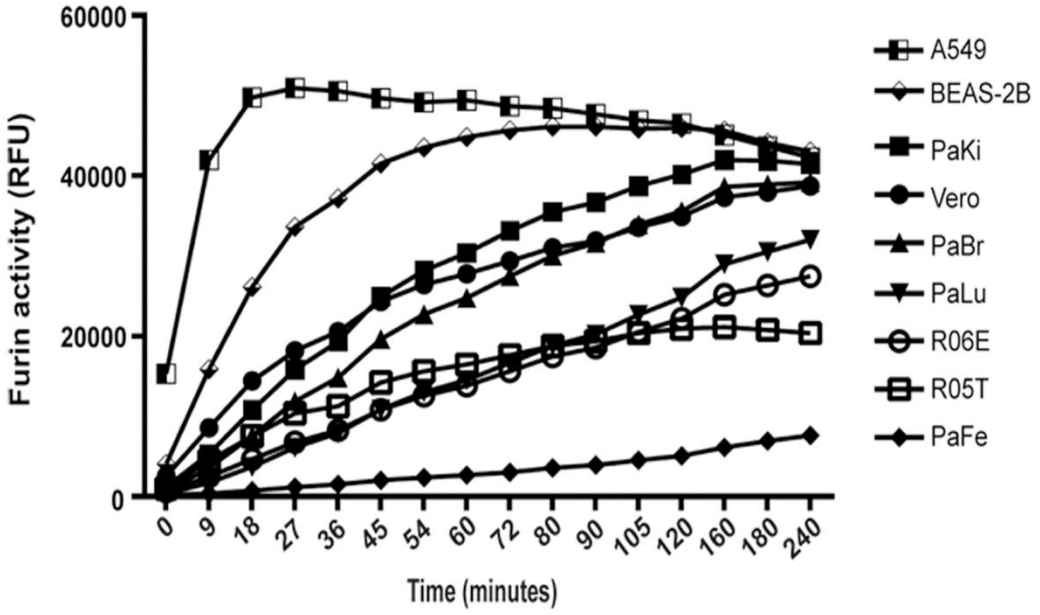

Figure 5. Different mammalian cell types show differences in furin-like enzyme activity.

2×10^6 cells of each cell type were lysed for 10 minutes on ice followed by shearing with a 10-gauge needle. Clarified lysates were then incubated with 10 μM of Pyr-Arg-Thr-Lys-Arg-AMC furin substrate for 4 hours at 37°C with fluorescence measured every 3 minutes. Each cell type was assayed in duplicate and the progress curves are representative of 3 separate experiments.

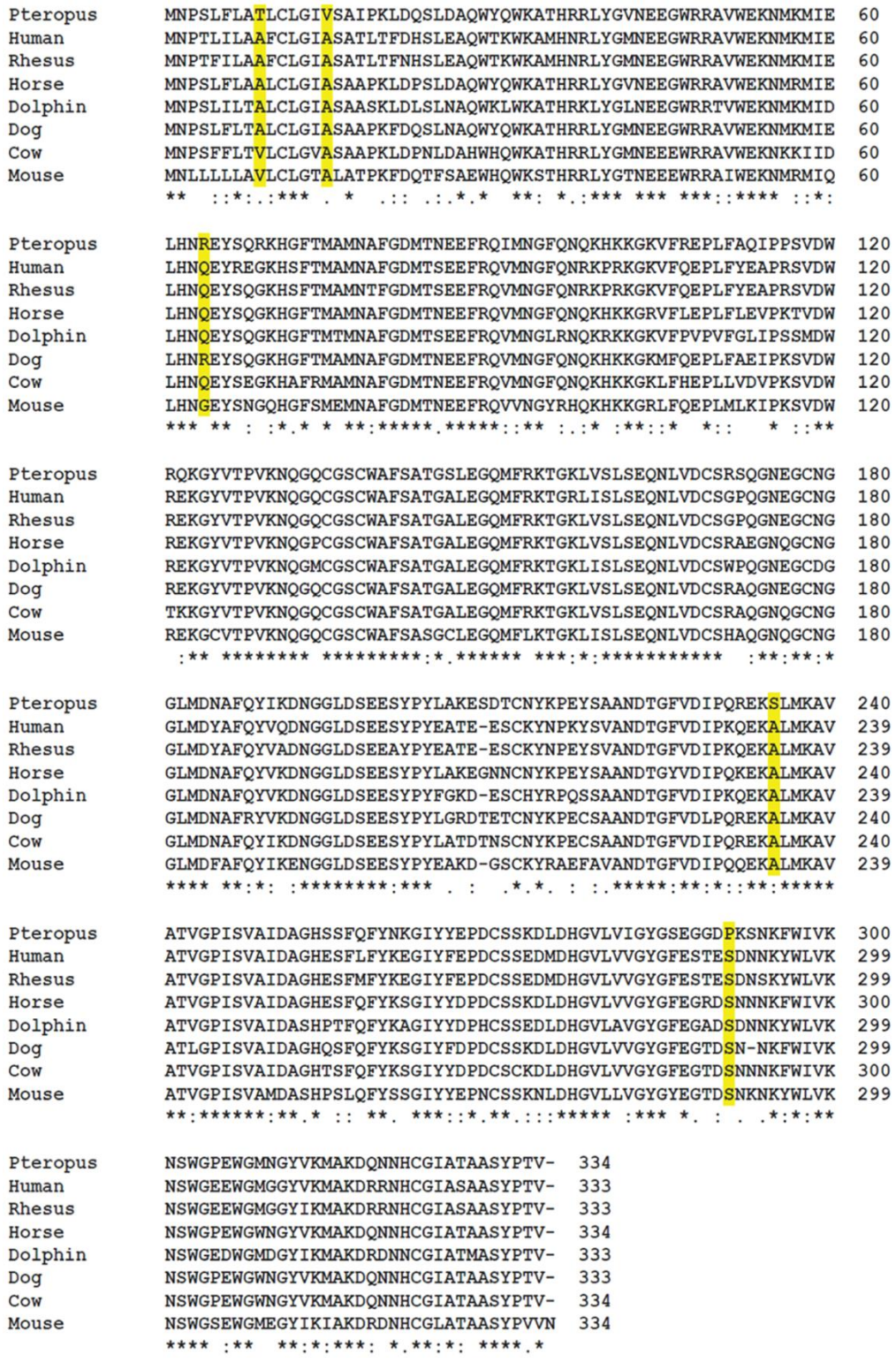

Figure 6. Sequence alignment of *Pteropus alecto* cathepsin L1 and cathepsin L1 of other mammalian species show Pteropus-specific amino acid changes.
Sequence alignment was generated using ClustalW. (GenBank accession numbers are given in parentheses): human (P07711.2), rhesus macaque (EHH24212.1), horse

(XP_001494409.1), dolphin (XP_004320974.1), dog (Q9GL24.1), cow (P25975.3), mouse (NP_034114.1). Yellow indicates amino acid changes that are specific to *P. alecto* cathepsin L. The asterisk "*" indicates identical residues, ":" indicates conserved substitutions and "." semi-conserved substitutions.

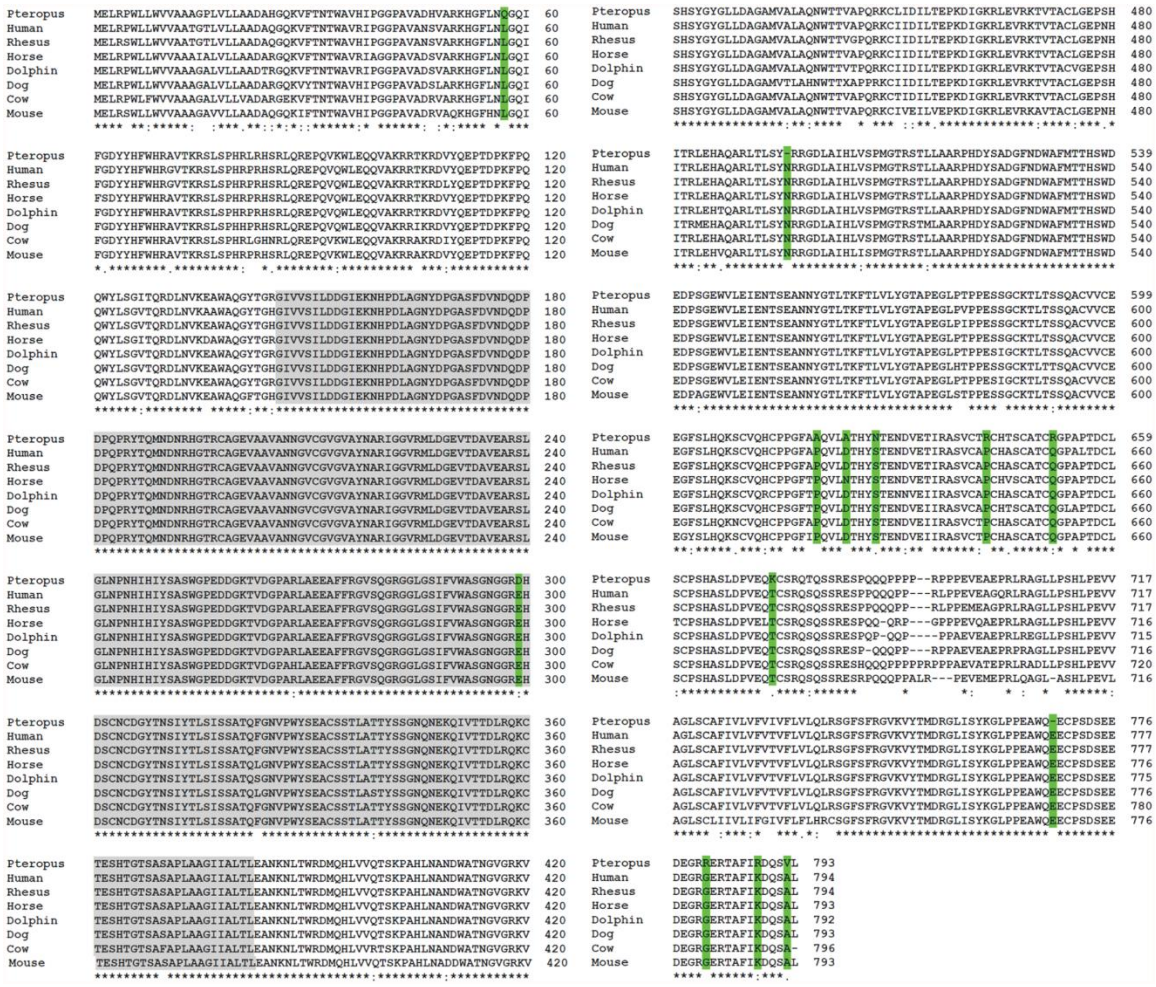

Figure 7. The C-terminus region of *P. alecto* furin has the highest degree of amino acid variation compared to furin proteases from other mammalian species.
Sequence alignment was generated using ClustalW. (GenBank accession numbers are given in parentheses): human (NP_002560.1), rhesus macaque (EHH27600.1), horse (XP_005602832.1), dolphin (XP_004322334.1), dog (XP_850069.2), cow (NP_776561.1), mouse (NP_001074923.1). Highlighted in gray is the catalytic site of furin and in green the changes in amino acid residues in *P. alecto* compared to other mammalian furins. The asterisk "*" indicates identical residues, ":" indicates conserved substitutions and "." semi-conserved substitutions.

Appendix 2 References

1. Iwasaki T, Inoue S, Tanaka K, Sato Y, Morikawa S, et al. (2004) Characterization of Oita virus 296/1972 of Rhabdoviridae isolated from a horseshoe bat bearing characteristics of both lyssavirus and vesiculovirus. Arch Virol 149: 1139–1154. pmid:15168201 doi: 10.1007/s00705-003-0271-x

2. Fraser GC, Hooper PT, Lunt RA, Gould AR, Gleeson LJ, et al. (1996) Encephalitis caused by a Lyssavirus in fruit bats in Australia. Emerg Infect Dis 2: 327–331. pmid:8969249 doi: 10.3201/eid0204.960408

3. Harris SL, Mansfield K, Marston DA, Johnson N, Pajamo K, et al. (2007) Isolation of European bat lyssavirus type 2 from a Daubenton's bat (Myotis daubentonii) in Shropshire. Vet Rec 161: 384–386. pmid:17873269 doi: 10.1136/vr.161.11.384

4. Pfefferle S, Oppong S, Drexler JF, Gloza-Rausch F, Ipsen A, et al. (2009) Distant relatives of severe acute respiratory syndrome coronavirus and close relatives of human coronavirus 229E in bats, Ghana. Emerg Infect Dis 15: 1377–1384. doi: 10.3201/eid1509.090224. pmid:19788804

5. Poon LL, Chu DK, Chan KH, Wong OK, Ellis TM, et al. (2005) Identification of a novel coronavirus in bats. J Virol 79: 2001–2009. pmid:15681402 doi: 10.1128/jvi.79.4.2001-2009.2005

6. Tang XC, Zhang JX, Zhang SY, Wang P, Fan XH, et al. (2006) Prevalence and genetic diversity of coronaviruses in bats from China. J Virol 80: 7481–7490. pmid:16840328 doi: 10.1128/jvi.00697-06

7. Li W, Shi Z, Yu M, Ren W, Smith C, et al. (2005) Bats are natural reservoirs of SARS-like coronaviruses. Science 310: 676–679. pmid:16195424 doi: 10.1126/science.1118391

8. Ge XY, Li JL, Yang XL, Chmura AA, Zhu G, et al. (2013) Isolation and characterization of a bat SARS-like coronavirus that uses the ACE2 receptor. Nature 503: 535–538. doi: 10.1038/nature12711. pmid:24172901

9. Du L, Zhao G, Kou Z, Ma C, Sun S, et al. (2013) Identification of a receptor-binding domain in the S protein of the novel human coronavirus Middle East respiratory syndrome coronavirus as an essential target for vaccine development. J Virol 87: 9939–9942. doi: 10.1128/JVI.01048-13. pmid:23824801

10. Leroy EM, Kumulungui B, Pourrut X, Rouquet P, Hassanin A, et al. (2005) Fruit bats as reservoirs of Ebola virus. Nature 438: 575–576. pmid:16319873 doi: 10.1038/438575a

11. Towner JS, Amman BR, Sealy TK, Carroll SA, Comer JA, et al. (2009) Isolation of genetically diverse Marburg viruses from Egyptian fruit bats. PLoS Pathog 5: e1000536. doi: 10.1371/journal.ppat.1000536. pmid:19649327

12. Towner JS, Pourrut X, Albarino CG, Nkogue CN, Bird BH, et al. (2007) Marburg virus infection detected in a common African bat. PLoS One 2: e764. pmid:17712412 doi: 10.1371/journal.pone.0000764

13. Sotomayor-Bonilla J, Chaves A, Rico-Chavez O, Rostal MK, Ojeda-Flores R, et al. (2014) Dengue virus in bats from southeastern Mexico. Am J Trop Med Hyg 91: 129–131. doi: 10.4269/ajtmh.13-0524. pmid:24752688

14. Thompson NN, Auguste AJ, Travassos da Rosa AP, Carrington CV, Blitvich BJ, et al. (2014) Seroepidemiology of Selected Alphaviruses and Flaviviruses in Bats in Trinidad. Zoonoses Public Health. doi: 10.1111/zph.12175. pmid:25557350

15. Tong S, Li Y, Rivailler P, Conrardy C, Castillo DA, et al. (2012) A distinct lineage of influenza A virus from bats. Proc Natl Acad Sci U S A 109: 4269–4274. doi: 10.1073/pnas.1116200109. pmid:22371588

16. Sun X, Shi Y, Lu X, He J, Gao F, et al. (2013) Bat-derived influenza hemagglutinin H17 does not bind canonical avian or human receptors and most likely uses a unique entry mechanism. Cell Rep 3: 769–778. doi: 10.1016/j.celrep.2013.01.025. pmid:23434510

17. Tong S, Zhu X, Li Y, Shi M, Zhang J, et al. (2013) New world bats harbor diverse influenza A viruses. PLoS Pathog 9: e1003657. doi: 10.1371/journal.ppat.1003657. pmid:24130481

18. Drexler JF, Corman VM, Muller MA, Maganga GD, Vallo P, et al. (2012) Bats host major mammalian paramyxoviruses. Nat Commun 3: 796. doi: 10.1038/ncomms1796. pmid:22531181

19. Kurth A, Kohl C, Brinkmann A, Ebinger A, Harper JA, et al. (2012) Novel paramyxoviruses in free-ranging European bats. PLoS One 7: e38688. doi: 10.1371/journal.pone.0038688. pmid:22737217

20. Calisher CH, Childs JE, Field HE, Holmes KV, Schountz T (2006) Bats: important reservoir hosts of emerging viruses. Clin Microbiol Rev 19: 531–545. pmid:16847084 doi: 10.1128/cmr.00017-06

21. Smith I, Wang LF (2013) Bats and their virome: an important source of emerging viruses capable of infecting humans. Curr Opin Virol 3: 84–91. doi: 10.1016/j.coviro.2012.11.006. pmid:23265969

22. Taniguchi S, Watanabe S, Masangkay JS, Omatsu T, Ikegami T, et al. (2011) Reston Ebolavirus antibodies in bats, the Philippines. Emerg Infect Dis 17: 1559–1560. doi: 10.3201/eid1708.101693. pmid:21801651

23. Halpin K, Hyatt AD, Fogarty R, Middleton D, Bingham J, et al. (2011) Pteropid bats are confirmed as the reservoir hosts of henipaviruses: a comprehensive experimental study of virus transmission. Am J Trop Med Hyg 85: 946–951. doi: 10.4269/ajtmh.2011.10-0567. pmid:22049055

24. Young PL, Halpin K, Selleck PW, Field H, Gravel JL, et al. (1996) Serologic evidence for the presence in Pteropus bats of a paramyxovirus related to equine morbillivirus. Emerg Infect Dis 2: 239–240. pmid:8903239 doi: 10.3201/eid0203.960315

25. Field H, de Jong C, Melville D, Smith C, Smith I, et al. (2011) Hendra virus infection dynamics in Australian fruit bats. PLoS One 6: e28678. doi: 10.1371/journal.pone.0028678. pmid:22174865

26. Smith I, Broos A, de Jong C, Zeddeman A, Smith C, et al. (2011) Identifying Hendra virus diversity in pteropid bats. PLoS One 6: e25275. doi: 10.1371/journal.pone.0025275. pmid:21980413

27. Chua KB, Koh CL, Hooi PS, Wee KF, Khong JH, et al. (2002) Isolation of Nipah virus from Malaysian Island flying-foxes. Microbes Infect 4: 145–151. pmid:11880045 doi: 10.1016/s1286-4579(01)01522-2

28. Epstein JH, Prakash V, Smith CS, Daszak P, McLaughlin AB, et al. (2008) Henipavirus infection in fruit bats (Pteropus giganteus), India. Emerg Infect Dis 14: 1309–1311. doi: 10.3201/eid1408.071492. pmid:18680665

29. Yadav PD, Raut CG, Shete AM, Mishra AC, Towner JS, et al. (2012) Detection of Nipah virus RNA in fruit bat (Pteropus giganteus) from India. Am J Trop Med Hyg 87: 576–578. doi: 10.4269/ajtmh.2012.11-0416. pmid:22802440

30. Selvey LA, Wells RM, McCormack JG, Ansford AJ, Murray K, et al. (1995) Infection of humans and horses by a newly described morbillivirus. Med J Aust 162: 642–645. pmid:7603375

31. Field H, Crameri G, Kung NY, Wang LF (2012) Ecological aspects of hendra virus. Curr Top Microbiol Immunol 359: 11–23. doi: 10.1007/82_2012_214. pmid:22476530

32. Clayton BA, Wang LF, Marsh GA (2013) Henipaviruses: an updated review focusing on the pteropid reservoir and features of transmission. Zoonoses Public Health 60: 69–83. doi: 10.1111/j.1863-2378.2012.01501.x. pmid:22709528

33. Harcourt BH, Tamin A, Ksiazek TG, Rollin PE, Anderson LJ, et al. (2000) Molecular characterization of Nipah virus, a newly emergent paramyxovirus. Virology 271: 334–349. pmid:10860887 doi: 10.1006/viro.2000.0340

34. Breed AC, Breed MF, Meers J, Field HE (2011) Evidence of endemic Hendra virus infection in flying-foxes (Pteropus conspicillatus)—implications for disease risk management. PLoS One 6: e28816. doi: 10.1371/journal.pone.0028816. pmid:22194920

35. Mahalingam S, Herrero LJ, Playford EG, Spann K, Herring B, et al. (2012) Hendra virus: an emerging paramyxovirus in Australia. Lancet Infect Dis 12: 799–807. doi: 10.1016/S1473-3099(12)70158-5. pmid:22921953

36. Yob JM, Field H, Rashdi AM, Morrissy C, van der Heide B, et al. (2001) Nipah virus infection in bats (order Chiroptera) in peninsular Malaysia. Emerg Infect Dis 7: 439–441. pmid:11384522 doi: 10.3201/eid0703.010312

37. Marsh GA, de Jong C, Barr JA, Tachedjian M, Smith C, et al. (2012) Cedar virus: a novel Henipavirus isolated from Australian bats. PLoS Pathog 8: e1002836. doi: 10.1371/journal.ppat.1002836. pmid:22879820

38. Drexler JF, Corman VM, Gloza-Rausch F, Seebens A, Annan A, et al. (2009) Henipavirus RNA in African bats. PLoS One 4: e6367. doi: 10.1371/journal.pone.0006367. pmid:19636378

39. Peel AJ, Baker KS, Crameri G, Barr JA, Hayman DT, et al. (2012) Henipavirus neutralising antibodies in an isolated island population of African fruit bats. PLoS One 7: e30346. doi: 10.1371/journal.pone.0030346. pmid:22253928

40. Bossart KN, Wang LF, Flora MN, Chua KB, Lam SK, et al. (2002) Membrane fusion tropism and heterotypic functional activities of the Nipah virus and Hendra virus envelope glycoproteins. J Virol 76: 11186–11198. pmid:12388678 doi: 10.1128/jvi.76.22.11186-11198.2002

41. Bossart KN, Wang LF, Eaton BT, Broder CC (2001) Functional expression and membrane fusion tropism of the envelope glycoproteins of Hendra virus. Virology 290: 121–135. pmid:11882997 doi: 10.1006/viro.2001.1158

42. Wang L, Harcourt BH, Yu M, Tamin A, Rota PA, et al. (2001) Molecular biology of Hendra and Nipah viruses. Microbes Infect 3: 279–287. pmid:11334745 doi: 10.1016/s1286-4579(01)01381-8

43. Bolt G, Pedersen IR (1998) The role of subtilisin-like proprotein convertases for cleavage of the measles virus fusion glycoprotein in different cell types. Virology 252: 387–398. pmid:9878618 doi: 10.1006/viro.1998.9464

44. Garten W, Hallenberger S, Ortmann D, Schafer W, Vey M, et al. (1994) Processing of viral glycoproteins by the subtilisin-like endoprotease furin and its inhibition by specific peptidylchloroalkylketones. Biochimie 76: 217–225. pmid:7819326 doi: 10.1016/0300-9084(94)90149-x

45. Gotoh B, Ohnishi Y, Inocencio NM, Esaki E, Nakayama K, et al. (1992) Mammalian subtilisin-related proteinases in cleavage activation of the paramyxovirus fusion glycoprotein: superiority of furin/PACE to PC2 or PC1/PC3. J Virol 66: 6391–6397. pmid:1404596

46. Smith EC, Popa A, Chang A, Masante C, Dutch RE (2009) Viral entry mechanisms: the increasing diversity of paramyxovirus entry. FEBS J 276: 7217–7227. doi: 10.1111/j.1742-4658.2009.07401.x. pmid:19878307

47. Pager CT, Dutch RE (2005) Cathepsin L is involved in proteolytic processing of the Hendra virus fusion protein. J Virol 79: 12714–12720. pmid:16188974 doi: 10.1128/jvi.79.20.12714-12720.2005

48. Pager CT, Craft WW Jr., Patch J, Dutch RE (2006) A mature and fusogenic form of the Nipah virus fusion protein requires proteolytic processing by cathepsin L. Virology 346: 251–257. pmid:16460775 doi: 10.1016/j.virol.2006.01.007

49. Diederich S, Moll M, Klenk HD, Maisner A (2005) The nipah virus fusion protein is cleaved within the endosomal compartment. J Biol Chem 280: 29899–29903. pmid:15961384 doi: 10.1074/jbc.m504598200

50. Vogt C, Eickmann M, Diederich S, Moll M, Maisner A (2005) Endocytosis of the Nipah virus glycoproteins. J Virol 79: 3865–3872. pmid:15731282 doi: 10.1128/jvi.79.6.3865-3872.2005

51. Meulendyke KA, Wurth MA, McCann RO, Dutch RE (2005) Endocytosis plays a critical role in proteolytic processing of the Hendra virus fusion protein. J Virol 79: 12643–12649. pmid:16188966 doi: 10.1128/jvi.79.20.12643-12649.2005

52. Pager CT, Wurth MA, Dutch RE (2004) Subcellular localization and calcium and pH requirements for proteolytic processing of the Hendra virus fusion protein. J Virol 78: 9154–9163. pmid:15308711 doi: 10.1128/jvi.78.17.9154-9163.2004

53. Popa A, Carter JR, Smith SE, Hellman L, Fried MG, et al. (2012) Residues in the hendra virus fusion protein transmembrane domain are critical for endocytic recycling. J Virol 86: 3014–3026. doi: 10.1128/JVI.05826-11. pmid:22238299

54. Diederich S, Sauerhering L, Weis M, Altmeppen H, Schaschke N, et al. (2012) Activation of the Nipah virus fusion protein in MDCK cells is mediated by cathepsin B within the endosome-recycling compartment. J Virol 86: 3736–3745. doi: 10.1128/JVI.06628-11. pmid:22278224

55. Diederich S, Dietzel E, Maisner A (2009) Nipah virus fusion protein: influence of cleavage site mutations on the cleavability by cathepsin L, trypsin and furin. Virus Res 145: 300–306. doi: 10.1016/j.virusres.2009.07.020. pmid:19665506

56. Michalski WP, Crameri G, Wang L, Shiell BJ, Eaton B (2000) The cleavage activation and sites of glycosylation in the fusion protein of Hendra virus. Virus Res 69: 83–93. pmid:11018278 doi: 10.1016/s0168-1702(00)00169-6

57. Moll M, Diederich S, Klenk HD, Czub M, Maisner A (2004) Ubiquitous activation of the Nipah virus fusion protein does not require a basic amino acid at the cleavage site. J Virol 78: 9705–9712. pmid:15331703 doi: 10.1128/jvi.78.18.9705-9712.2004

58. Craft WW RE Jr. (2005) Sequence motif upstream of the Hendra virus fusion protein cleavage site is not sufficient to promote efficient proteolytic processing. Virology 341: 130–140. pmid:16083935 doi: 10.1016/j.virol.2005.07.004

59. Li Z, Sergel T, Razvi E, Morrison T (1998) Effect of cleavage mutants on syncytium formation directed by the wild-type fusion protein of Newcastle disease virus. J Virol 72: 3789–3795. pmid:9557661

60. Paterson RG, Shaughnessy MA, Lamb RA (1989) Analysis of the relationship between cleavability of a paramyxovirus fusion protein and length of the connecting peptide. J Virol 63: 1293–1301. pmid:2644448

61. Dubay JW, Dubay SR, Shin HJ, Hunter E (1995) Analysis of the cleavage site of the human immunodeficiency virus type 1 glycoprotein: requirement of precursor cleavage for glycoprotein incorporation. J Virol 69: 4675–4682. pmid:7609032

62. Senne DA, Panigrahy B, Kawaoka Y, Pearson JE, Suss J, et al. (1996) Survey of the hemagglutinin (HA) cleavage site sequence of H5 and H7 avian influenza viruses: amino acid sequence at the HA cleavage site as a marker of pathogenicity potential. Avian Dis 40: 425–437. pmid:8790895 doi: 10.2307/1592241

63. Simmons G, Gosalia DN, Rennekamp AJ, Reeves JD, Diamond SL, et al. (2005) Inhibitors of cathepsin L prevent severe acute respiratory syndrome coronavirus entry. Proc Natl Acad Sci U S A 102: 11876–11881. pmid:16081529 doi: 10.1073/pnas.0505577102

64. Schornberg K, Matsuyama S, Kabsch K, Delos S, Bouton A, et al. (2006) Role of endosomal cathepsins in entry mediated by the Ebola virus glycoprotein. J Virol 80: 4174–4178. pmid:16571833 doi: 10.1128/jvi.80.8.4174-4178.2006

65. Chandran K, Sullivan NJ, Felbor U, Whelan SP, Cunningham JM (2005) Endosomal proteolysis of the Ebola virus glycoprotein is necessary for infection. Science 308: 1643–1645. pmid:15831716 doi: 10.1126/science.1110656

66. Pourrut X, Souris M, Towner JS, Rollin PE, Nichol ST, et al. (2009) Large serological survey showing cocirculation of Ebola and Marburg viruses in Gabonese bat populations, and a high seroprevalence of both viruses in Rousettus aegyptiacus. BMC Infect Dis 9: 159. doi: 10.1186/1471-2334-9-159. pmid:19785757

67. Crameri G, Todd S, Grimley S, McEachern JA, Marsh GA, et al. (2009) Establishment, immortalisation and characterisation of pteropid bat cell lines. PLoS One 4: e8266. doi: 10.1371/journal.pone.0008266. pmid:20011515

68. Jordan I, Horn D, Oehmke S, Leendertz FH, Sandig V (2009) Cell lines from the Egyptian fruit bat are permissive for modified vaccinia Ankara. Virus Res 145: 54–62. doi: 10.1016/j.virusres.2009.06.007. pmid:19540275

69. Smith EC, Culler MR, Hellman LM, Fried MG, Creamer TP, et al. (2012) Beyond anchoring: the expanding role of the hendra virus fusion protein transmembrane domain in protein folding, stability, and function. J Virol 86: 3003–3013. doi: 10.1128/JVI.05762-11. pmid:22238302

70. Bourne GL, Grainger DJ (2011) Development and characterisation of an assay for furin activity. J Immunol Methods 364: 101–108. doi: 10.1016/j.jim.2010.11.008. pmid:21112328

71. Papenfuss AT, Baker ML, Feng ZP, Tachedjian M, Crameri G, et al. (2012) The immune gene repertoire of an important viral reservoir, the Australian black flying fox. BMC Genomics 13: 261. doi: 10.1186/1471-2164-13-261. pmid:22716473

72. Zhang G, Cowled C, Shi Z, Huang Z, Bishop-Lilly KA, et al. (2013) Comparative analysis of bat genomes provides insight into the evolution of flight and immunity. Science 339: 456–460. doi: 10.1126/science.1230835. pmid:23258410

73. Thompson JD, Higgins DG, Gibson TJ (1994) CLUSTAL W: improving the sensitivity of progressive multiple sequence alignment through sequence weighting, position-specific gap penalties and weight matrix choice. Nucleic Acids Res 22: 4673–4680. pmid:7984417 doi: 10.1093/nar/22.22.4673

74. Krahling V, Dolnik O, Kolesnikova L, Schmidt-Chanasit J, Jordan I, et al. (2010) Establishment of fruit bat cells (Rousettus aegyptiacus) as a model system for the investigation of filoviral infection. PLoS Negl Trop Dis 4: e802. doi: 10.1371/journal.pntd.0000802. pmid:20808767

75. Wilcox D, Mason RW (1992) Inhibition of cysteine proteinases in lysosomes and whole cells. Biochem J 285 (Pt 2): 495–502.

76. Matlin KS, Simons K (1983) Reduced temperature prevents transfer of a membrane glycoprotein to the cell surface but does not prevent terminal glycosylation. Cell 34: 233–243. pmid:6883510 doi: 10.1016/0092-8674(83)90154-x

77. Griffiths G, Pfeiffer S, Simons K, Matlin K (1985) Exit of newly synthesized membrane proteins from the trans cisterna of the Golgi complex to the plasma membrane. J Cell Biol 101: 949–964. pmid:2863275 doi: 10.1083/jcb.101.3.949

78. Schafer W, Stroh A, Berghofer S, Seiler J, Vey M, et al. (1995) Two independent targeting signals in the cytoplasmic domain determine trans-Golgi network localization and endosomal trafficking of the proprotein convertase furin. EMBO J 14: 2424–2435. pmid:7781597

79. Thomas G (2002) Furin at the cutting edge: from protein traffic to embryogenesis and disease. Nat Rev Mol Cell Biol 3: 753–766. pmid:12360192 doi: 10.1038/nrm934

80. Plaimauer B, Mohr G, Wernhart W, Himmelspach M, Dorner F, et al. (2001) 'Shed' furin: mapping of the cleavage determinants and identification of its C-terminus. Biochem J 354: 689–695. pmid:11237874 doi: 10.1042/0264-6021:3540689

81. Stieneke-Grober A, Vey M, Angliker H, Shaw E, Thomas G, et al. (1992) Influenza virus hemagglutinin with multibasic cleavage site is activated by furin, a subtilisin-like endoprotease. EMBO J 11: 2407–2414. pmid:1628614

82. Tian S, Jianhua W (2010) Comparative study of the binding pockets of mammalian proprotein convertases and its implications for the design of specific small molecule inhibitors. Int J Biol Sci 6: 89–95. pmid:20151049 doi: 10.7150/ijbs.6.89

83. Angliker H, Wikstrom P, Shaw E, Brenner C, Fuller RS (1993) The synthesis of inhibitors for processing proteinases and their action on the Kex2 proteinase of yeast. Biochem J 293 (Pt 1): 75–81.

84. Stadler K, Allison SL, Schalich J, Heinz FX (1997) Proteolytic activation of tick-borne encephalitis virus by furin. J Virol 71: 8475–8481. pmid:9343204

85. Volchkov VE, Feldmann H, Volchkova VA, Klenk HD (1998) Processing of the Ebola virus glycoprotein by the proprotein convertase furin. Proc Natl Acad Sci U S A 95: 5762–5767. pmid:9576958 doi: 10.1073/pnas.95.10.5762

86. Ortmann D, Ohuchi M, Angliker H, Shaw E, Garten W, et al. (1994) Proteolytic cleavage of wild type and mutants of the F protein of human parainfluenza virus type 3 by two subtilisin-like endoproteases, furin and Kex2. J Virol 68: 2772–2776. pmid:8139055

87. Sugrue RJ, Brown C, Brown G, Aitken J, Mc LRHW (2001) Furin cleavage of the respiratory syncytial virus fusion protein is not a requirement for its transport to the surface of virus-infected cells. J Gen Virol 82: 1375–1386. pmid:11369882

88. Lindblad-Toh K, Garber M, Zuk O, Lin MF, Parker BJ, et al. (2011) A high-resolution map of human evolutionary constraint using 29 mammals. Nature 478: 476–482. doi: 10.1038/nature10530. pmid:21993624

89. Thompson JD, Gibson TJ, Plewniak F, Jeanmougin F, Higgins DG (1997) The CLUSTAL_X windows interface: flexible strategies for multiple sequence alignment

aided by quality analysis tools. Nucleic Acids Res 25: 4876–4882. pmid:9396791 doi: 10.1093/nar/25.24.4876

90. Henrich S, Cameron A, Bourenkov GP, Kiefersauer R, Huber R, et al. (2003) The crystal structure of the proprotein processing proteinase furin explains its stringent specificity. Nat Struct Biol 10: 520–526. pmid:12794637 doi: 10.1038/nsb941

91. Bosshart H, Humphrey J, Deignan E, Davidson J, Drazba J, et al. (1994) The cytoplasmic domain mediates localization of furin to the trans-Golgi network en route to the endosomal/lysosomal system. J Cell Biol 126: 1157–1172. pmid:7914893 doi: 10.1083/jcb.126.5.1157

92. Jones BG, Thomas L, Molloy SS, Thulin CD, Fry MD, et al. (1995) Intracellular trafficking of furin Is modulated by the phosphorylation state of a casein kinase-Ii site in Its cytoplasmic tail. EMBO Journal 14: 5869–5883. pmid:8846780

93. Takahashi S, Nakagawa T, Banno T, Watanabe T, Murakami K, et al. (1995) Localization of furin to the trans-Golgi network and recycling from the cell surface involves Ser and Tyr residues within the cytoplasmic domain. J Biol Chem 270: 28397–28401. pmid:7499343 doi: 10.1074/jbc.270.47.28397

94. Wong S, Lau S, Woo P, Yuen KY (2007) Bats as a continuing source of emerging infections in humans. Rev Med Virol 17: 67–91. pmid:17042030 doi: 10.1002/rmv.520

95. Hoffmann M, Muller MA, Drexler JF, Glende J, Erdt M, et al. (2013) Differential sensitivity of bat cells to infection by enveloped RNA viruses: coronaviruses, paramyxoviruses, filoviruses, and influenza viruses. PLoS One 8: e72942. doi: 10.1371/journal.pone.0072942. pmid:24023659

96. Kuhl A, Hoffmann M, Muller MA, Munster VJ, Gnirss K, et al. (2011) Comparative analysis of Ebola virus glycoprotein interactions with human and bat cells. J Infect Dis 204 Suppl 3: S840–849. doi: 10.1093/infdis/jir306. pmid:21987760

97. Kruger N, Hoffmann M, Weis M, Drexler JF, Muller MA, et al. (2013) Surface glycoproteins of an African henipavirus induce syncytium formation in a cell line derived from an African fruit bat, Hypsignathus monstrosus. J Virol 87: 13889–13891. doi: 10.1128/JVI.02458-13. pmid:24067951

98. Weis M, Behner L, Hoffmann M, Kruger N, Herrler G, et al. (2014) Characterization of African bat henipavirus GH-M74a glycoproteins. J Gen Virol 95: 539–548. doi: 10.1099/vir.0.060632-0. pmid:24296468

99. Han J, Wang Y, Wang S, Chi C (2008) Interaction of Mint3 with Furin regulates the localization of Furin in the trans-Golgi network. J Cell Sci 121: 2217–2223. doi: 10.1242/jcs.019745. pmid:18544638

100. Hatsuzawa K, Hosaka M, Nakagawa T, Nagase M, Shoda A, et al. (1990) Structure and expression of mouse furin, a yeast Kex2-related protease. Lack of processing of coexpressed prorenin in GH4C1 cells. J Biol Chem 265: 22075–22078. pmid:2266110

101. Schalken JA, Roebroek AJ, Oomen PP, Wagenaar SS, Debruyne FM, et al. (1987) fur gene expression as a discriminating marker for small cell and nonsmall cell lung carcinomas. J Clin Invest 80: 1545–1549. pmid:2824565 doi: 10.1172/jci113240

References

1. Lamb RA, Parks, G.D. (2007) Paramyxoviridae: The viruses and their replication.; Knipe DM, Howley, P.M., editor. Philadelphia, PA,: Lippincott Williams & Wilkins. 1449–1646 p.
2. van den Hoogen BG, de Jong JC, Groen J, Kuiken T, de Groot R, et al. (2001) A newly discovered human pneumovirus isolated from young children with respiratory tract disease. Nat Med 7: 719-724.
3. Chua KB, Bellini WJ, Rota PA, Harcourt BH, Tamin A, et al. (2000) Nipah virus: a recently emergent deadly paramyxovirus. Science 288: 1432-1435.
4. Murray K, Selleck P, Hooper P, Hyatt A, Gould A, et al. (1995) A morbillivirus that caused fatal disease in horses and humans. Science 268: 94-97.
5. Alexander DJ SD (2008) Newcastle Disease, Other Avian Paramyxoviruses, and Pneumovirus Infections; Saif YM FA, Glisson JR, McDougald LR, Nolan LK, Swayne DE, editor. Ames, Iowa, USA: Blackwell Publishing.
6. Govindarajan D, Buchholz UJ, Samal SK (2006) Recovery of avian metapneumovirus subgroup C from cDNA: cross-recognition of avian and human metapneumovirus support proteins. J Virol 80: 5790-5797.
7. Goldsmith CS, Whistler T, Rollin PE, Ksiazek TG, Rota PA, et al. (2003) Elucidation of Nipah virus morphogenesis and replication using ultrastructural and molecular approaches. Virus Res 92: 89-98.
8. Kalica AR, Wright PF, Hetrick FM, Chanock RM (1973) Electron microscopic studies of respiratory syncytial temperature-sensitive mutants. Arch Gesamte Virusforsch 41: 248-258.
9. Yao Q, Compans RW (2000) Filamentous particle formation by human parainfluenza virus type 2. J Gen Virol 81: 1305-1312.
10. Loo LH, Jumat MR, Fu Y, Ayi TC, Wong PS, et al. (2013) Evidence for the interaction of the human metapneumovirus G and F proteins during virus-like particle formation. Virol J 10: 294.
11. Compans RW, Holmes KV, Dales S, Choppin PW (1966) An electron microscopic study of moderate and virulent virus-cell interactions of the parainfluenza virus SV5. Virology 30: 411-426.
12. Peret TC, Boivin G, Li Y, Couillard M, Humphrey C, et al. (2002) Characterization of human metapneumoviruses isolated from patients in North America. J Infect Dis 185: 1660-1663.
13. Ludwig K, Schade B, Bottcher C, Korte T, Ohlwein N, et al. (2008) Electron cryomicroscopy reveals different F1+F2 protein States in intact parainfluenza virions. J Virol 82: 3775-3781.
14. Li M, Schmitt PT, Li Z, McCrory TS, He B, et al. (2009) Mumps virus matrix, fusion, and nucleocapsid proteins cooperate for efficient production of virus-like particles. J Virol 83: 7261-7272.
15. Li Z, Xu J, Patel J, Fuentes S, Lin Y, et al. (2011) Function of the small hydrophobic protein of J paramyxovirus. J Virol 85: 32-42.
16. Biacchesi S, Pham QN, Skiadopoulos MH, Murphy BR, Collins PL, et al. (2005) Infection of nonhuman primates with recombinant human metapneumovirus

lacking the SH, G, or M2-2 protein categorizes each as a nonessential accessory protein and identifies vaccine candidates. J Virol 79: 12608-12613.
17. Takeuchi K, Tanabayashi K, Hishiyama M, Yamada A (1996) The mumps virus SH protein is a membrane protein and not essential for virus growth. Virology 225: 156-162.
18. He B, Leser GP, Paterson RG, Lamb RA (1998) The paramyxovirus SV5 small hydrophobic (SH) protein is not essential for virus growth in tissue culture cells. Virology 250: 30-40.
19. Karron RA, Buonagurio DA, Georgiu AF, Whitehead SS, Adamus JE, et al. (1997) Respiratory syncytial virus (RSV) SH and G proteins are not essential for viral replication in vitro: clinical evaluation and molecular characterization of a cold-passaged, attenuated RSV subgroup B mutant. Proc Natl Acad Sci U S A 94: 13961-13966.
20. Beltran S, Lescure FX, Desailloud R, Douadi Y, Smail A, et al. (2003) Increased prevalence of hypothyroidism among human immunodeficiency virus-infected patients: a need for screening. Clin Infect Dis 37: 579-583.
21. Ebihara T, Endo R, Kikuta H, Ishiguro N, Yoshioka M, et al. (2003) Seroprevalence of human metapneumovirus in Japan. J Med Virol 70: 281-283.
22. Maggi F, Pifferi M, Vatteroni M, Fornai C, Tempestini E, et al. (2003) Human metapneumovirus associated with respiratory tract infections in a 3-year study of nasal swabs from infants in Italy. J Clin Microbiol 41: 2987-2991.
23. Nissen MD, Siebert DJ, Mackay IM, Sloots TP, Withers SJ (2002) Evidence of human metapneumovirus in Australian children. Med J Aust 176: 188.
24. Peiris JS, Tang WH, Chan KH, Khong PL, Guan Y, et al. (2003) Children with respiratory disease associated with metapneumovirus in Hong Kong. Emerg Infect Dis 9: 628-633.
25. Groome MJ, Moyes J, Cohen C, Walaza S, Tempia S, et al. (2015) Human metapneumovirus-associated severe acute respiratory illness hospitalisation in HIV-infected and HIV-uninfected South African children and adults. J Clin Virol 69: 125-132.
26. de Graaf M, Osterhaus AD, Fouchier RA, Holmes EC (2008) Evolutionary dynamics of human and avian metapneumoviruses. J Gen Virol 89: 2933-2942.
27. Yang CF, Wang CK, Tollefson SJ, Piyaratna R, Lintao LD, et al. (2009) Genetic diversity and evolution of human metapneumovirus fusion protein over twenty years. Virol J 6: 138.
28. Larcher C, Pagani E, Rossi P, Amato B, Pescollderungg L, et al. (2008) Comparison of human metapneumovirus genotypes from the province of Bolzano in northern Italy with strains from surrounding regions in Italy and Austria. Jpn J Infect Dis 61: 154-156.
29. Agapov E, Sumino KC, Gaudreault-Keener M, Storch GA, Holtzman MJ (2006) Genetic variability of human metapneumovirus infection: evidence of a shift in viral genotype without a change in illness. J Infect Dis 193: 396-403.
30. Papenburg J, Boivin G (2010) The distinguishing features of human metapneumovirus and respiratory syncytial virus. Rev Med Virol 20: 245-260.
31. Walsh EE, Peterson DR, Falsey AR (2008) Human metapneumovirus infections in adults: another piece of the puzzle. Arch Intern Med 168: 2489-2496.

32. Williams JV, Harris PA, Tollefson SJ, Halburnt-Rush LL, Pingsterhaus JM, et al. (2004) Human metapneumovirus and lower respiratory tract disease in otherwise healthy infants and children. N Engl J Med 350: 443-450.
33. Edwards KM, Zhu Y, Griffin MR, Weinberg GA, Hall CB, et al. (2013) Burden of human metapneumovirus infection in young children. N Engl J Med 368: 633-643.
34. Hamelin ME, Abed Y, Boivin G (2004) Human metapneumovirus: a new player among respiratory viruses. Clin Infect Dis 38: 983-990.
35. Widmer K, Zhu Y, Williams JV, Griffin MR, Edwards KM, et al. (2012) Rates of hospitalizations for respiratory syncytial virus, human metapneumovirus, and influenza virus in older adults. J Infect Dis 206: 56-62.
36. Dollner H, Risnes K, Radtke A, Nordbo SA (2004) Outbreak of human metapneumovirus infection in norwegian children. Pediatr Infect Dis J 23: 436-440.
37. Konig B, Konig W, Arnold R, Werchau H, Ihorst G, et al. (2004) Prospective study of human metapneumovirus infection in children less than 3 years of age. J Clin Microbiol 42: 4632-4635.
38. Kroll JL, Weinberg A (2011) Human metapneumovirus. Semin Respir Crit Care Med 32: 447-453.
39. Greensill J, McNamara PS, Dove W, Flanagan B, Smyth RL, et al. (2003) Human metapneumovirus in severe respiratory syncytial virus bronchiolitis. Emerg Infect Dis 9: 372-375.
40. Semple MG, Cowell A, Dove W, Greensill J, McNamara PS, et al. (2005) Dual infection of infants by human metapneumovirus and human respiratory syncytial virus is strongly associated with severe bronchiolitis. J Infect Dis 191: 382-386.
41. Kahn JS (2006) Epidemiology of human metapneumovirus. Clin Microbiol Rev 19: 546-557.
42. Lai SH, Liao SL, Wong KS, Lin TY (2014) Preceding human metapneumovirus infection increases adherence of Streptococcus pneumoniae and severity of murine pneumococcal pneumonia. J Microbiol Immunol Infect.
43. Seki M, Yoshida H, Gotoh K, Hamada N, Motooka D, et al. (2014) Severe respiratory failure due to co-infection with human metapneumovirus and Streptococcus pneumoniae. Respir Med Case Rep 12: 13-15.
44. Falsey AR, Erdman D, Anderson LJ, Walsh EE (2003) Human metapneumovirus infections in young and elderly adults. J Infect Dis 187: 785-790.
45. Schildgen O, Glatzel T, Geikowski T, Scheibner B, Matz B, et al. (2005) Human metapneumovirus RNA in encephalitis patient. Emerg Infect Dis 11: 467-470.
46. Arnold JC, Singh KK, Milder E, Spector SA, Sawyer MH, et al. (2009) Human metapneumovirus associated with central nervous system infection in children. Pediatr Infect Dis J 28: 1057-1060.
47. Sanchez Fernandez I, Rebollo Polo M, Munoz-Almagro C, Monfort Carretero L, Fernandez Urena S, et al. (2012) Human Metapneumovirus in the Cerebrospinal Fluid of a Patient With Acute Encephalitis. Arch Neurol 69: 649-652.
48. Yoshida T, Nagai Y, Maeno K, Iinuma M, Hamaguchi M, et al. (1979) Studies on the role of M protein in virus assembly using a ts mutant of HVJ (Sendai virus). Virology 92: 139-154.

49. Kondo T, Yoshida T, Miura N, Nakanishi M (1993) Temperature-sensitive phenotype of a mutant Sendai virus strain is caused by its insufficient accumulation of the M protein. J Biol Chem 268: 21924-21930.
50. Baczko K, Liebert UG, Billeter M, Cattaneo R, Budka H, et al. (1986) Expression of defective measles virus genes in brain tissues of patients with subacute sclerosing panencephalitis. J Virol 59: 472-478.
51. Hirano A, Ayata M, Wang AH, Wong TC (1993) Functional analysis of matrix proteins expressed from cloned genes of measles virus variants that cause subacute sclerosing panencephalitis reveals a common defect in nucleocapsid binding. J Virol 67: 1848-1853.
52. Cathomen T, Mrkic B, Spehner D, Drillien R, Naef R, et al. (1998) A matrix-less measles virus is infectious and elicits extensive cell fusion: consequences for propagation in the brain. EMBO J 17: 3899-3908.
53. Mitra R, Baviskar P, Duncan-Decocq RR, Patel D, Oomens AG (2012) The human respiratory syncytial virus matrix protein is required for maturation of viral filaments. J Virol 86: 4432-4443.
54. Takimoto T, Murti KG, Bousse T, Scroggs RA, Portner A (2001) Role of matrix and fusion proteins in budding of Sendai virus. J Virol 75: 11384-11391.
55. Sugahara F, Uchiyama T, Watanabe H, Shimazu Y, Kuwayama M, et al. (2004) Paramyxovirus Sendai virus-like particle formation by expression of multiple viral proteins and acceleration of its release by C protein. Virology 325: 1-10.
56. Pohl C, Duprex WP, Krohne G, Rima BK, Schneider-Schaulies S (2007) Measles virus M and F proteins associate with detergent-resistant membrane fractions and promote formation of virus-like particles. J Gen Virol 88: 1243-1250.
57. Runkler N, Pohl C, Schneider-Schaulies S, Klenk HD, Maisner A (2007) Measles virus nucleocapsid transport to the plasma membrane requires stable expression and surface accumulation of the viral matrix protein. Cell Microbiol 9: 1203-1214.
58. Ciancanelli MJ, Basler CF (2006) Mutation of YMYL in the Nipah virus matrix protein abrogates budding and alters subcellular localization. J Virol 80: 12070-12078.
59. Patch JR, Crameri G, Wang LF, Eaton BT, Broder CC (2007) Quantitative analysis of Nipah virus proteins released as virus-like particles reveals central role for the matrix protein. Virol J 4: 1.
60. Coronel EC, Murti KG, Takimoto T, Portner A (1999) Human parainfluenza virus type 1 matrix and nucleoprotein genes transiently expressed in mammalian cells induce the release of virus-like particles containing nucleocapsid-like structures. J Virol 73: 7035-7038.
61. Pantua HD, McGinnes LW, Peeples ME, Morrison TG (2006) Requirements for the assembly and release of Newcastle disease virus-like particles. J Virol 80: 11062-11073.
62. Liljeroos L, Krzyzaniak MA, Helenius A, Butcher SJ (2013) Architecture of respiratory syncytial virus revealed by electron cryotomography. Proc Natl Acad Sci U S A 110: 11133-11138.

63. Battisti AJ, Meng G, Winkler DC, McGinnes LW, Plevka P, et al. (2012) Structure and assembly of a paramyxovirus matrix protein. Proc Natl Acad Sci U S A 109: 13996-14000.
64. Loney C, Mottet-Osman G, Roux L, Bhella D (2009) Paramyxovirus ultrastructure and genome packaging: cryo-electron tomography of sendai virus. J Virol 83: 8191-8197.
65. Kiss G, Holl JM, Williams GM, Alonas E, Vanover D, et al. (2014) Structural Analysis of Respiratory Syncytial Virus Reveals the Position of M2-1 between the Matrix Protein and the Ribonucleoprotein Complex. J Virol 88: 7602-7617.
66. Liljeroos L, Huiskonen JT, Ora A, Susi P, Butcher SJ (2011) Electron cryotomography of measles virus reveals how matrix protein coats the ribonucleocapsid within intact virions. Proc Natl Acad Sci U S A 108: 18085-18090.
67. Tawar RG, Duquerroy S, Vonrhein C, Varela PF, Damier-Piolle L, et al. (2009) Crystal structure of a nucleocapsid-like nucleoprotein-RNA complex of respiratory syncytial virus. Science 326: 1279-1283.
68. Errington W, Emmerson PT (1997) Assembly of recombinant Newcastle disease virus nucleocapsid protein into nucleocapsid-like structures is inhibited by the phosphoprotein. J Gen Virol 78 (Pt 9): 2335-2339.
69. Schmitt AP, Leser GP, Waning DL, Lamb RA (2002) Requirements for budding of paramyxovirus simian virus 5 virus-like particles. J Virol 76: 3952-3964.
70. Spehner D, Kirn A, Drillien R (1991) Assembly of nucleocapsidlike structures in animal cells infected with a vaccinia virus recombinant encoding the measles virus nucleoprotein. J Virol 65: 6296-6300.
71. Rager M, Vongpunsawad S, Duprex WP, Cattaneo R (2002) Polyploid measles virus with hexameric genome length. EMBO J 21: 2364-2372.
72. Goff PH, Gao Q, Palese P (2012) A majority of infectious Newcastle disease virus particles contain a single genome, while a minority contain multiple genomes. J Virol 86: 10852-10856.
73. Coronel EC, Takimoto T, Murti KG, Varich N, Portner A (2001) Nucleocapsid incorporation into parainfluenza virus is regulated by specific interaction with matrix protein. J Virol 75: 1117-1123.
74. Mottet G, Roux L (1989) Budding efficiency of Sendai virus nucleocapsids: influence of size and ends of the RNA. Virus Res 14: 175-187.
75. Kolakofsky D, Bruschi A (1975) Antigenomes in Sendai virions and Sendai virus-infected cells. Virology 66: 185-191.
76. Iwasaki M, Takeda M, Shirogane Y, Nakatsu Y, Nakamura T, et al. (2009) The matrix protein of measles virus regulates viral RNA synthesis and assembly by interacting with the nucleocapsid protein. J Virol 83: 10374-10383.
77. Schmitt PT, Ray G, Schmitt AP (2010) The C-terminal end of parainfluenza virus 5 NP protein is important for virus-like particle production and M-NP protein interaction. J Virol 84: 12810-12823.
78. Li D, Jans DA, Bardin PG, Meanger J, Mills J, et al. (2008) Association of respiratory syncytial virus M protein with viral nucleocapsids is mediated by the M2-1 protein. J Virol 82: 8863-8870.

79. Hamaguchi M, Yoshida T, Nishikawa K, Naruse H, Nagai Y (1983) Transcriptive complex of Newcastle disease virus. I. Both L and P proteins are required to constitute an active complex. Virology 128: 105-117.
80. Rodriguez L, Cuesta I, Asenjo A, Villanueva N (2004) Human respiratory syncytial virus matrix protein is an RNA-binding protein: binding properties, location and identity of the RNA contact residues. J Gen Virol 85: 709-719.
81. Essaidi-Laziosi M, Shevtsova A, Gerlier D, Roux L (2013) Mutation of the TYTLE motif in the cytoplasmic tail of the sendai virus fusion protein deeply affects viral assembly and particle production. PLoS One 8: e78074.
82. Harrison MS, Sakaguchi T, Schmitt AP (2010) Paramyxovirus assembly and budding: building particles that transmit infections. Int J Biochem Cell Biol 42: 1416-1429.
83. Takimoto T, Portner A (2004) Molecular mechanism of paramyxovirus budding. Virus Res 106: 133-145.
84. Ali A, Nayak DP (2000) Assembly of Sendai virus: M protein interacts with F and HN proteins and with the cytoplasmic tail and transmembrane domain of F protein. Virology 276: 289-303.
85. Sanderson CM, Wu HH, Nayak DP (1994) Sendai virus M protein binds independently to either the F or the HN glycoprotein in vivo. J Virol 68: 69-76.
86. Fouillot-Coriou N, Roux L (2000) Structure-function analysis of the Sendai virus F and HN cytoplasmic domain: different role for the two proteins in the production of virus particle. Virology 270: 464-475.
87. Mottet-Osman G, Iseni F, Pelet T, Wiznerowicz M, Garcin D, et al. (2007) Suppression of the Sendai virus M protein through a novel short interfering RNA approach inhibits viral particle production but does not affect viral RNA synthesis. J Virol 81: 2861-2868.
88. Gosselin-Grenet AS, Mottet-Osman G, Roux L (2010) Sendai virus particle production: basic requirements and role of the SYWST motif present in HN cytoplasmic tail. Virology 405: 439-447.
89. Batonick M, Wertz GW (2011) Requirements for Human Respiratory Syncytial Virus Glycoproteins in Assembly and Egress from Infected Cells. Adv Virol 2011.
90. Ghildyal R, Li D, Peroulis I, Shields B, Bardin PG, et al. (2005) Interaction between the respiratory syncytial virus G glycoprotein cytoplasmic domain and the matrix protein. J Gen Virol 86: 1879-1884.
91. Tahara M, Takeda M, Yanagi Y (2007) Altered interaction of the matrix protein with the cytoplasmic tail of hemagglutinin modulates measles virus growth by affecting virus assembly and cell-cell fusion. J Virol 81: 6827-6836.
92. Teng MN, Whitehead SS, Collins PL (2001) Contribution of the respiratory syncytial virus G glycoprotein and its secreted and membrane-bound forms to virus replication in vitro and in vivo. Virology 289: 283-296.
93. Biacchesi S, Skiadopoulos MH, Yang L, Lamirande EW, Tran KC, et al. (2004) Recombinant human Metapneumovirus lacking the small hydrophobic SH and/or attachment G glycoprotein: deletion of G yields a promising vaccine candidate. J Virol 78: 12877-12887.
94. Stone R, Takimoto T (2013) Critical role of the fusion protein cytoplasmic tail sequence in parainfluenza virus assembly. PLoS One 8: e61281.

95. Shaikh FY, Cox RG, Lifland AW, Hotard AL, Williams JV, et al. (2012) A critical phenylalanine residue in the respiratory syncytial virus fusion protein cytoplasmic tail mediates assembly of internal viral proteins into viral filaments and particles. MBio 3.
96. Moll M, Klenk HD, Maisner A (2002) Importance of the cytoplasmic tails of the measles virus glycoproteins for fusogenic activity and the generation of recombinant measles viruses. J Virol 76: 7174-7186.
97. Cathomen T, Naim HY, Cattaneo R (1998) Measles viruses with altered envelope protein cytoplasmic tails gain cell fusion competence. J Virol 72: 1224-1234.
98. Baviskar PS, Hotard AL, Moore ML, Oomens AG (2013) The respiratory syncytial virus fusion protein targets to the perimeter of inclusion bodies and facilitates filament formation by a cytoplasmic tail-dependent mechanism. J Virol 87: 10730-10741.
99. Jin H, Leser GP, Zhang J, Lamb RA (1997) Influenza virus hemagglutinin and neuraminidase cytoplasmic tails control particle shape. EMBO J 16: 1236-1247.
100. Mebatsion T, Konig M, Conzelmann KK (1996) Budding of rabies virus particles in the absence of the spike glycoprotein. Cell 84: 941-951.
101. Stone-Hulslander J, Morrison TG (1997) Detection of an interaction between the HN and F proteins in Newcastle disease virus-infected cells. J Virol 71: 6287-6295.
102. Plemper RK, Hammond AL, Cattaneo R (2001) Measles virus envelope glycoproteins hetero-oligomerize in the endoplasmic reticulum. J Biol Chem 276: 44239-44246.
103. Tong S, Compans RW (1999) Alternative mechanisms of interaction between homotypic and heterotypic parainfluenza virus HN and F proteins. J Gen Virol 80 (Pt 1): 107-115.
104. Paterson RG, Johnson ML, Lamb RA (1997) Paramyxovirus fusion (F) protein and hemagglutinin-neuraminidase (HN) protein interactions: intracellular retention of F and HN does not affect transport of the homotypic HN or F protein. Virology 237: 1-9.
105. Whitman SD, Smith EC, Dutch RE (2009) Differential rates of protein folding and cellular trafficking for the Hendra virus F and G proteins: implications for F-G complex formation. J Virol 83: 8998-9001.
106. Jardetzky TS, Lamb RA (2014) Activation of paramyxovirus membrane fusion and virus entry. Curr Opin Virol 5C: 24-33.
107. West DS, Sheehan MS, Segeleon PK, Dutch RE (2005) Role of the simian virus 5 fusion protein N-terminal coiled-coil domain in folding and promotion of membrane fusion. J Virol 79: 1543-1551.
108. Sergel-Germano T, McQuain C, Morrison T (1994) Mutations in the fusion peptide and heptad repeat regions of the Newcastle disease virus fusion protein block fusion. J Virol 68: 7654-7658.
109. Sergel TA, McGinnes LW, Morrison TG (2001) Mutations in the fusion peptide and adjacent heptad repeat inhibit folding or activity of the Newcastle disease virus fusion protein. J Virol 75: 7934-7943.

110. Parks GD, Lamb RA (1990) Defective assembly and intracellular transport of mutant paramyxovirus hemagglutinin-neuraminidase proteins containing altered cytoplasmic domains. J Virol 64: 3605-3616.
111. Smith EC, Smith SE, Carter JR, Webb SR, Gibson KM, et al. (2013) Trimeric transmembrane domain interactions in paramyxovirus fusion proteins: roles in protein folding, stability, and function. J Biol Chem 288: 35726-35735.
112. McGinnes L, Sergel T, Morrison T (1993) Mutations in the transmembrane domain of the HN protein of Newcastle disease virus affect the structure and activity of the protein. Virology 196: 101-110.
113. Yao Q, Compans RW (1995) Differences in the role of the cytoplasmic domain of human parainfluenza virus fusion proteins. J Virol 69: 7045-7053.
114. Bagai S, Lamb RA (1995) Individual roles of N-linked oligosaccharide chains in intracellular transport of the paramyxovirus SV5 fusion protein. Virology 209: 250-256.
115. McGinnes L, Sergel T, Reitter J, Morrison T (2001) Carbohydrate modifications of the NDV fusion protein heptad repeat domains influence maturation and fusion activity. Virology 283: 332-342.
116. Segawa H, Yamashita T, Kawakita M, Taira H (2000) Functional analysis of the individual oligosaccharide chains of sendai virus fusion protein. J Biochem 128: 65-72.
117. Carter JR, Pager CT, Fowler SD, Dutch RE (2005) Role of N-linked glycosylation of the Hendra virus fusion protein. J Virol 79: 7922-7925.
118. Moll M, Kaufmann A, Maisner A (2004) Influence of N-glycans on processing and biological activity of the nipah virus fusion protein. J Virol 78: 7274-7278.
119. Sawatsky B, von Messling V (2010) Canine distemper viruses expressing a hemagglutinin without N-glycans lose virulence but retain immunosuppression. J Virol 84: 2753-2761.
120. Biering SB, Huang A, Vu AT, Robinson LR, Bradel-Tretheway B, et al. (2012) N-Glycans on the Nipah virus attachment glycoprotein modulate fusion and viral entry as they protect against antibody neutralization. J Virol 86: 11991-12002.
121. Collins PL, Mottet G (1991) Post-translational processing and oligomerization of the fusion glycoprotein of human respiratory syncytial virus. J Gen Virol 72 (Pt 12): 3095-3101.
122. Zimmer G, Trotz I, Herrler G (2001) N-glycans of F protein differentially affect fusion activity of human respiratory syncytial virus. J Virol 75: 4744-4751.
123. Moll M, Klenk HD, Herrler G, Maisner A (2001) A single amino acid change in the cytoplasmic domains of measles virus glycoproteins H and F alters targeting, endocytosis, and cell fusion in polarized Madin-Darby canine kidney cells. J Biol Chem 276: 17887-17894.
124. Leser GP, Ector KJ, Ng DT, Shaughnessy MA, Lamb RA (1999) The signal for clathrin-mediated endocytosis of the paramyxovirus SV5 HN protein resides at the transmembrane domain-ectodomain boundary region. Virology 262: 79-92.
125. Whitman SD, Dutch RE (2007) Surface density of the Hendra G protein modulates Hendra F protein-promoted membrane fusion: role for Hendra G protein trafficking and degradation. Virology 363: 419-429.

126. Meulendyke KA, Wurth MA, McCann RO, Dutch RE (2005) Endocytosis plays a critical role in proteolytic processing of the Hendra virus fusion protein. J Virol 79: 12643-12649.
127. Vogt C, Eickmann M, Diederich S, Moll M, Maisner A (2005) Endocytosis of the Nipah virus glycoproteins. J Virol 79: 3865-3872.
128. Leser GP, Ector KJ, Lamb RA (1996) The paramyxovirus simian virus 5 hemagglutinin-neuraminidase glycoprotein, but not the fusion glycoprotein, is internalized via coated pits and enters the endocytic pathway. Mol Biol Cell 7: 155-172.
129. Pager CT, Craft WW, Jr., Patch J, Dutch RE (2006) A mature and fusogenic form of the Nipah virus fusion protein requires proteolytic processing by cathepsin L. Virology 346: 251-257.
130. Diederich S, Moll M, Klenk HD, Maisner A (2005) The nipah virus fusion protein is cleaved within the endosomal compartment. J Biol Chem 280: 29899-29903.
131. Diederich S, Thiel L, Maisner A (2008) Role of endocytosis and cathepsin-mediated activation in Nipah virus entry. Virology 375: 391-400.
132. Robach JG, Lamb RA (2010) Analysis of parainfluenza virus-5 hemagglutinin-neuraminidase protein mutants that are blocked in internalization and degradation. Virology 406: 189-201.
133. Spielhofer P, Bachi T, Fehr T, Christiansen G, Cattaneo R, et al. (1998) Chimeric measles viruses with a foreign envelope. J Virol 72: 2150-2159.
134. Roux L, Beffy P, Portner A (1985) Three variations in the cell surface expression of the haemagglutinin-neuraminidase glycoprotein of Sendai virus. J Gen Virol 66 (Pt 5): 987-1000.
135. Stricker R, Mottet G, Roux L (1994) The Sendai virus matrix protein appears to be recruited in the cytoplasm by the viral nucleocapsid to function in viral assembly and budding. J Gen Virol 75 (Pt 5): 1031-1042.
136. Santangelo PJ, Bao G (2007) Dynamics of filamentous viral RNPs prior to egress. Nucleic Acids Res 35: 3602-3611.
137. Nakatsu Y, Ma X, Seki F, Suzuki T, Iwasaki M, et al. (2013) Intracellular transport of the measles virus ribonucleoprotein complex is mediated by Rab11A-positive recycling endosomes and drives virus release from the apical membrane of polarized epithelial cells. J Virol 87: 4683-4693.
138. Chambers R, Takimoto T (2010) Trafficking of Sendai virus nucleocapsids is mediated by intracellular vesicles. PLoS One 5: e10994.
139. Utley TJ, Ducharme NA, Varthakavi V, Shepherd BE, Santangelo PJ, et al. (2008) Respiratory syncytial virus uses a Vps4-independent budding mechanism controlled by Rab11-FIP2. Proc Natl Acad Sci U S A 105: 10209-10214.
140. Ghildyal R, Mills J, Murray M, Vardaxis N, Meanger J (2002) Respiratory syncytial virus matrix protein associates with nucleocapsids in infected cells. J Gen Virol 83: 753-757.
141. Qi M, Williams JA, Chu H, Chen X, Wang JJ, et al. (2013) Rab11-FIP1C and Rab14 direct plasma membrane sorting and particle incorporation of the HIV-1 envelope glycoprotein complex. PLoS Pathog 9: e1003278.

142. Ghildyal R, Ho A, Dias M, Soegiyono L, Bardin PG, et al. (2009) The respiratory syncytial virus matrix protein possesses a Crm1-mediated nuclear export mechanism. J Virol 83: 5353-5362.
143. Wang YE, Park A, Lake M, Pentecost M, Torres B, et al. (2010) Ubiquitin-regulated nuclear-cytoplasmic trafficking of the Nipah virus matrix protein is important for viral budding. PLoS Pathog 6: e1001186.
144. Peeples ME (1988) Differential detergent treatment allows immunofluorescent localization of the Newcastle disease virus matrix protein within the nucleus of infected cells. Virology 162: 255-259.
145. Peeples ME, Wang C, Gupta KC, Coleman N (1992) Nuclear entry and nucleolar localization of the Newcastle disease virus (NDV) matrix protein occur early in infection and do not require other NDV proteins. J Virol 66: 3263-3269.
146. Duan Z, Li Q, He L, Zhao G, Chen J, et al. (2013) Application of green fluorescent protein-labeled assay for the study of subcellular localization of Newcastle disease virus matrix protein. J Virol Methods 194: 118-122.
147. Duan Z, Song Q, Wang Y, He L, Chen J, et al. (2013) Characterization of signal sequences determining the nuclear export of Newcastle disease virus matrix protein. Arch Virol 158: 2589-2595.
148. Duan Z, Chen J, Xu H, Zhu J, Li Q, et al. (2014) The nucleolar phosphoprotein B23 targets Newcastle disease virus matrix protein to the nucleoli and facilitates viral replication. Virology 452-453: 212-222.
149. Duan Z, Hu Z, Zhu J, Xu H, Chen J, et al. (2014) Mutations in the FPIV motif of Newcastle disease virus matrix protein attenuate virus replication and reduce virus budding. Arch Virol.
150. Yuan H, Puckett S, Lyles DS (2001) Inhibition of host transcription by vesicular stomatitis virus involves a novel mechanism that is independent of phosphorylation of TATA-binding protein (TBP) or association of TBP with TBP-associated factor subunits. J Virol 75: 4453-4458.
151. Rajani KR, Pettit Kneller EL, McKenzie MO, Horita DA, Chou JW, et al. (2012) Complexes of vesicular stomatitis virus matrix protein with host Rae1 and Nup98 involved in inhibition of host transcription. PLoS Pathog 8: e1002929.
152. Bian T, Gibbs JD, Orvell C, Imani F (2012) Respiratory syncytial virus matrix protein induces lung epithelial cell cycle arrest through a p53 dependent pathway. PLoS One 7: e38052.
153. Rossman JS, Lamb RA (2013) Viral membrane scission. Annu Rev Cell Dev Biol 29: 551-569.
154. McDonald B, Martin-Serrano J (2009) No strings attached: the ESCRT machinery in viral budding and cytokinesis. J Cell Sci 122: 2167-2177.
155. Schmitt AP, Leser GP, Morita E, Sundquist WI, Lamb RA (2005) Evidence for a new viral late-domain core sequence, FPIV, necessary for budding of a paramyxovirus. J Virol 79: 2988-2997.
156. Chen BJ, Lamb RA (2008) Mechanisms for enveloped virus budding: can some viruses do without an ESCRT? Virology 372: 221-232.
157. Patch JR, Han Z, McCarthy SE, Yan L, Wang LF, et al. (2008) The YPLGVG sequence of the Nipah virus matrix protein is required for budding. Virol J 5: 137.

158. Salditt A, Koethe S, Pohl C, Harms H, Kolesnikova L, et al. (2010) Measles virus M protein-driven particle production does not involve the endosomal sorting complex required for transport (ESCRT) system. J Gen Virol 91: 1464-1472.
159. Weng Y, Lu W, Harmon A, Xiang X, Deng Q, et al. (2011) The cellular endosomal sorting complex required for transport pathway is not involved in avian metapneumovirus budding in a virus-like-particle expression system. J Gen Virol 92: 1205-1213.
160. Sabo Y, Ehrlich M, Bacharach E (2011) The conserved YAGL motif in human metapneumovirus is required for higher-order cellular assemblies of the matrix protein and for virion production. J Virol 85: 6594-6609.
161. Bruce EA, Digard P, Stuart AD (2010) The Rab11 pathway is required for influenza A virus budding and filament formation. J Virol 84: 5848-5859.
162. Acosta D, Adelman J, Affolder T, Akimoto T, Albrow MG, et al. (2005) Evidence for B0 s-->phiphi decay and measurements of branching ratio and A(CP) for B+ -->phiK+. Phys Rev Lett 95: 031801.
163. Halliburton WD (1887) On Muscle-Plasma. J Physiol 8: 133-202.
164. Graceffa P, Dominguez R (2003) Crystal structure of monomeric actin in the ATP state. Structural basis of nucleotide-dependent actin dynamics. J Biol Chem 278: 34172-34180.
165. Holmes KC, Popp D, Gebhard W, Kabsch W (1990) Atomic model of the actin filament. Nature 347: 44-49.
166. Otterbein LR, Graceffa P, Dominguez R (2001) The crystal structure of uncomplexed actin in the ADP state. Science 293: 708-711.
167. Herman IM (1993) Actin isoforms. Current Opinion in Cell Biology 5: 48-55.
168. Pollard TD, Blanchoin L, Mullins RD (2000) Molecular mechanisms controlling actin filament dynamics in nonmuscle cells. Annu Rev Biophys Biomol Struct 29: 545-576.
169. Hall A (1994) Small GTP-binding proteins and the regulation of the actin cytoskeleton. Annu Rev Cell Biol 10: 31-54.
170. Foster R, Hu KQ, Lu Y, Nolan KM, Thissen J, et al. (1996) Identification of a novel human Rho protein with unusual properties: GTPase deficiency and in vivo farnesylation. Mol Cell Biol 16: 2689-2699.
171. Rafelski SM, Theriot JA (2004) Crawling toward a unified model of cell mobility: spatial and temporal regulation of actin dynamics. Annu Rev Biochem 73: 209-239.
172. Zigmond SH (2004) Beginning and ending an actin filament: control at the barbed end. Curr Top Dev Biol 63: 145-188.
173. Mullins RD, Heuser JA, Pollard TD (1998) The interaction of Arp2/3 complex with actin: nucleation, high affinity pointed end capping, and formation of branching networks of filaments. Proc Natl Acad Sci U S A 95: 6181-6186.
174. Machesky LM, Gould KL (1999) The Arp2/3 complex: a multifunctional actin organizer. Curr Opin Cell Biol 11: 117-121.
175. Machesky LM, Mullins RD, Higgs HN, Kaiser DA, Blanchoin L, et al. (1999) Scar, a WASp-related protein, activates nucleation of actin filaments by the Arp2/3 complex. Proc Natl Acad Sci U S A 96: 3739-3744.

176. Moreau V, Frischknecht F, Reckmann I, Vincentelli R, Rabut G, et al. (2000) A complex of N-WASP and WIP integrates signalling cascades that lead to actin polymerization. Nat Cell Biol 2: 441-448.
177. Husson C, Cantrelle FX, Roblin P, Didry D, Le KH, et al. (2010) Multifunctionality of the beta-thymosin/WH2 module: G-actin sequestration, actin filament growth, nucleation, and severing. Ann N Y Acad Sci 1194: 44-52.
178. Rotty JD, Wu C, Bear JE (2013) New insights into the regulation and cellular functions of the ARP2/3 complex. Nat Rev Mol Cell Biol 14: 7-12.
179. Firat-Karalar EN, Welch MD (2011) New mechanisms and functions of actin nucleation. Curr Opin Cell Biol 23: 4-13.
180. Yamashiro S, Yamakita Y, Ono S, Matsumura F (1998) Fascin, an actin-bundling protein, induces membrane protrusions and increases cell motility of epithelial cells. Mol Biol Cell 9: 993-1006.
181. Matsumura F, Yamashiro-Matsumura S, Lin JJ (1983) Isolation and characterization of tropomyosin-containing microfilaments from cultured cells. J Biol Chem 258: 6636-6644.
182. Kohler S, Schaller V, Bausch AR (2011) Collective dynamics of active cytoskeletal networks. PLoS One 6: e23798.
183. Revenu C, Athman R, Robine S, Louvard D (2004) The co-workers of actin filaments: from cell structures to signals. Nat Rev Mol Cell Biol 5: 635-646.
184. Blanchoin L, Boujemaa-Paterski R, Sykes C, Plastino J (2014) Actin dynamics, architecture, and mechanics in cell motility. Physiol Rev 94: 235-263.
185. Carlier MF, Laurent V, Santolini J, Melki R, Didry D, et al. (1997) Actin depolymerizing factor (ADF/cofilin) enhances the rate of filament turnover: implication in actin-based motility. J Cell Biol 136: 1307-1322.
186. DesMarais V, Macaluso F, Condeelis J, Bailly M (2004) Synergistic interaction between the Arp2/3 complex and cofilin drives stimulated lamellipod extension. J Cell Sci 117: 3499-3510.
187. Schmitz AA, Govek EE, Bottner B, Van Aelst L (2000) Rho GTPases: signaling, migration, and invasion. Exp Cell Res 261: 1-12.
188. Govek EE, Newey SE, Van Aelst L (2005) The role of the Rho GTPases in neuronal development. Genes Dev 19: 1-49.
189. Kozma R, Ahmed S, Best A, Lim L (1995) The Ras-related protein Cdc42Hs and bradykinin promote formation of peripheral actin microspikes and filopodia in Swiss 3T3 fibroblasts. Mol Cell Biol 15: 1942-1952.
190. Goldstein B, Macara IG (2007) The PAR proteins: fundamental players in animal cell polarization. Dev Cell 13: 609-622.
191. Ridley AJ, Paterson HF, Johnston CL, Diekmann D, Hall A (1992) The small GTP-binding protein rac regulates growth factor-induced membrane ruffling. Cell 70: 401-410.
192. Koh CG (2006) Rho GTPases and their regulators in neuronal functions and development. Neurosignals 15: 228-237.
193. Garcia-Bernal D, Wright N, Sotillo-Mallo E, Nombela-Arrieta C, Stein JV, et al. (2005) Vav1 and Rac control chemokine-promoted T lymphocyte adhesion mediated by the integrin alpha4beta1. Mol Biol Cell 16: 3223-3235.

194. Fleissner E, Tress E (1973) Chromatographic and electrophoretic analysis of viral proteins from hamster and chicken cells transformed by Rous sarcoma virus. J Virol 11: 250-262.
195. McNutt NS, Culp LA, Black PH (1973) Contact-inhibited revertant cell lines isolated from SV 40-transformed cells. IV. Microfilament distribution and cell shape in untransformed, transformed, and revertant Balb-c 3T3 cells. J Cell Biol 56: 412-428.
196. Goldman RD, Chang C, Williams JF (1975) Properties and behavior of hamster embryo cells transformed by human adenovirus type 5. Cold Spring Harb Symp Quant Biol 39 Pt 1: 601-614.
197. Lehmann MJ, Sherer NM, Marks CB, Pypaert M, Mothes W (2005) Actin- and myosin-driven movement of viruses along filopodia precedes their entry into cells. J Cell Biol 170: 317-325.
198. Schelhaas M, Ewers H, Rajamaki ML, Day PM, Schiller JT, et al. (2008) Human papillomavirus type 16 entry: retrograde cell surface transport along actin-rich protrusions. PLoS Pathog 4: e1000148.
199. Zamudio-Meza H, Castillo-Alvarez A, Gonzalez-Bonilla C, Meza I (2009) Cross-talk between Rac1 and Cdc42 GTPases regulates formation of filopodia required for dengue virus type-2 entry into HMEC-1 cells. J Gen Virol 90: 2902-2911.
200. Oh MJ, Akhtar J, Desai P, Shukla D (2010) A role for heparan sulfate in viral surfing. Biochem Biophys Res Commun 391: 176-181.
201. Schelhaas M, Shah B, Holzer M, Blattmann P, Kuhling L, et al. (2012) Entry of human papillomavirus type 16 by actin-dependent, clathrin- and lipid raft-independent endocytosis. PLoS Pathog 8: e1002657.
202. Pelkmans L, Puntener D, Helenius A (2002) Local actin polymerization and dynamin recruitment in SV40-induced internalization of caveolae. Science 296: 535-539.
203. Veettil MV, Sharma-Walia N, Sadagopan S, Raghu H, Sivakumar R, et al. (2006) RhoA-GTPase facilitates entry of Kaposi's sarcoma-associated herpesvirus into adherent target cells in a Src-dependent manner. J Virol 80: 11432-11446.
204. Sandgren KJ, Wilkinson J, Miranda-Saksena M, McInerney GM, Byth-Wilson K, et al. (2010) A differential role for macropinocytosis in mediating entry of the two forms of vaccinia virus into dendritic cells. PLoS Pathog 6: e1000866.
205. Huang WR, Wang YC, Chi PI, Wang L, Wang CY, et al. (2011) Cell entry of avian reovirus follows a caveolin-1-mediated and dynamin-2-dependent endocytic pathway that requires activation of p38 mitogen-activated protein kinase (MAPK) and Src signaling pathways as well as microtubules and small GTPase Rab5 protein. J Biol Chem 286: 30780-30794.
206. Nogalski MT, Chan GC, Stevenson EV, Collins-McMillen DK, Yurochko AD (2013) The HCMV gH/gL/UL128-131 complex triggers the specific cellular activation required for efficient viral internalization into target monocytes. PLoS Pathog 9: e1003463.
207. Kallewaard NL, Bowen AL, Crowe JE, Jr. (2005) Cooperativity of actin and microtubule elements during replication of respiratory syncytial virus. Virology 331: 73-81.

208. Schowalter RM, Wurth MA, Aguilar HC, Lee B, Moncman CL, et al. (2006) Rho GTPase activity modulates paramyxovirus fusion protein-mediated cell-cell fusion. Virology 350: 323-334.
209. Wurth MA, Schowalter RM, Smith EC, Moncman CL, Dutch RE, et al. (2010) The actin cytoskeleton inhibits pore expansion during PIV5 fusion protein-promoted cell-cell fusion. Virology 404: 117-126.
210. Burke E, Mahoney NM, Almo SC, Barik S (2000) Profilin is required for optimal actin-dependent transcription of respiratory syncytial virus genome RNA. J Virol 74: 669-675.
211. Klauschies F, Gutzkow T, Hinkelmann S, von Messling V, Vaske B, et al. (2010) Viral infectivity and intracellular distribution of matrix (M) protein of canine distemper virus are affected by actin filaments. Arch Virol 155: 1503-1508.
212. De Keuster T, Lamoureux J, Kahn A (2006) Epidemiology of dog bites: a Belgian experience of canine behaviour and public health concerns. Vet J 172: 482-487.
213. Dietzel E, Kolesnikova L, Maisner A (2013) Actin filaments disruption and stabilization affect measles virus maturation by different mechanisms. Virol J 10: 249.
214. Simpson-Holley M, Ellis D, Fisher D, Elton D, McCauley J, et al. (2002) A functional link between the actin cytoskeleton and lipid rafts during budding of filamentous influenza virions. Virology 301: 212-225.
215. Gladnikoff M, Shimoni E, Gov NS, Rousso I (2009) Retroviral assembly and budding occur through an actin-driven mechanism. Biophys J 97: 2419-2428.
216. Sherer NM, Lehmann MJ, Jimenez-Soto LF, Horensavitz C, Pypaert M, et al. (2007) Retroviruses can establish filopodial bridges for efficient cell-to-cell transmission. Nat Cell Biol 9: 310-315.
217. Favoreel HW, Van den Broeke C, Desplanques A, Deruelle M, Van Minnebruggen G, et al. (2010) Alphaherpesvirus use and misuse of cellular actin and cholesterol. Vet Microbiol 143: 2-7.
218. Berkova Z, Crawford SE, Blutt SE, Morris AP, Estes MK (2007) Expression of rotavirus NSP4 alters the actin network organization through the actin remodeling protein cofilin. J Virol 81: 3545-3553.
219. Stolp B, Abraham L, Rudolph JM, Fackler OT (2010) Lentiviral Nef proteins utilize PAK2-mediated deregulation of cofilin as a general strategy to interfere with actin remodeling. J Virol 84: 3935-3948.
220. Van den Broeke C, Radu M, Deruelle M, Nauwynck H, Hofmann C, et al. (2009) Alphaherpesvirus US3-mediated reorganization of the actin cytoskeleton is mediated by group A p21-activated kinases. Proc Natl Acad Sci U S A 106: 8707-8712.
221. Gardet A, Breton M, Fontanges P, Trugnan G, Chwetzoff S (2006) Rotavirus spike protein VP4 binds to and remodels actin bundles of the epithelial brush border into actin bodies. J Virol 80: 3947-3956.
222. David R (2013) Viral infection: Propelling vaccinia virus to the neighbours. Nat Rev Microbiol 11: 595.
223. Cozens AL, Yezzi MJ, Kunzelmann K, Ohrui T, Chin L, et al. (1994) CFTR expression and chloride secretion in polarized immortal human bronchial epithelial cells. Am J Respir Cell Mol Biol 10: 38-47.

224. Niwa H, Yamamura K, Miyazaki J (1991) Efficient selection for high-expression transfectants with a novel eukaryotic vector. Gene 108: 193-199.
225. Liu X, Chen R, Yang Z, Wang J, Lin J, et al. (2014) Characterization of a putative stereoselective oxidoreductase from Gluconobacter oxydans and its application in producing ethyl (R)-4-chloro-3-hydroxybutanoate ester. Mol Biotechnol 56: 285-295.
226. Hamelin ME, Couture C, Sackett M, Kiener P, Suzich J, et al. (2008) The prophylactic administration of a monoclonal antibody against human metapneumovirus attenuates viral disease and airways hyperresponsiveness in mice. Antivir Ther 13: 39-46.
227. Wyde PR, Chetty SN, Jewell AM, Boivin G, Piedra PA (2003) Comparison of the inhibition of human metapneumovirus and respiratory syncytial virus by ribavirin and immune serum globulin in vitro. Antiviral Res 60: 51-59.
228. Smith EC, Popa A, Chang A, Masante C, Dutch RE (2009) Viral entry mechanisms: the increasing diversity of paramyxovirus entry. FEBS J 276: 7217-7227.
229. Chang A, Dutch RE (2012) Paramyxovirus fusion and entry: multiple paths to a common end. Viruses 4: 613-636.
230. El Najjar F, Schmitt AP, Dutch RE (2014) Paramyxovirus glycoprotein incorporation, assembly and budding: a three way dance for infectious particle production. Viruses 6: 3019-3054.
231. Takimoto T, Portner A (2004) Molecular mechanism of paramyxovirus budding. Virus Research 106: 133-145.
232. Chang A, Masante C, Buchholz UJ, Dutch RE (2012) Human metapneumovirus (HMPV) binding and infection are mediated by interactions between the HMPV fusion protein and heparan sulfate. J Virol 86: 3230-3243.
233. Cox RG, Livesay SB, Johnson M, Ohi MD, Williams JV (2012) The human metapneumovirus fusion protein mediates entry via an interaction with RGD-binding integrins. J Virol 86: 12148-12160.
234. Schowalter RM, Smith SE, Dutch RE (2006) Characterization of human metapneumovirus F protein-promoted membrane fusion: critical roles for proteolytic processing and low pH. J Virol 80: 10931-10941.
235. Duan Z, Hu Z, Zhu J, Xu H, Chen J, et al. (2014) Mutations in the FPIV motif of Newcastle disease virus matrix protein attenuate virus replication and reduce virus budding. Arch Virol 159: 1813-1819.
236. Bruce EA, Medcalf L, Crump CM, Noton SL, Stuart AD, et al. (2009) Budding of filamentous and non-filamentous influenza A virus occurs via a VPS4 and VPS28-independent pathway. Virology 390: 268-278.
237. Watanabe R, Lamb RA (2010) Influenza virus budding does not require a functional AAA+ ATPase, VPS4. Virus Res 153: 58-63.
238. Bose S, Malur A, Banerjee AK (2001) Polarity of human parainfluenza virus type 3 infection in polarized human lung epithelial A549 cells: role of microfilament and microtubule. J Virol 75: 1984-1989.
239. Miazza V, Mottet-Osman G, Startchick S, Chaponnier C, Roux L (2011) Sendai virus induced cytoplasmic actin remodeling correlates with efficient virus particle production. Virology 410: 7-16.

240. Timpe JM, Stamataki Z, Jennings A, Hu K, Farquhar MJ, et al. (2008) Hepatitis C virus cell-cell transmission in hepatoma cells in the presence of neutralizing antibodies. Hepatology 47: 17-24.
241. Enquist LW, Tomishima MJ, Gross S, Smith GA (2002) Directional spread of an alpha-herpesvirus in the nervous system. Vet Microbiol 86: 5-16.
242. Tomishima MJ, Enquist LW (2002) In vivo egress of an alphaherpesvirus from axons. J Virol 76: 8310-8317.
243. Tomishima MJ, Smith GA, Enquist LW (2001) Sorting and transport of alpha herpesviruses in axons. Traffic 2: 429-436.
244. Snyder A, Bruun B, Browne HM, Johnson DC (2007) A herpes simplex virus gD-YFP fusion glycoprotein is transported separately from viral capsids in neuronal axons. J Virol 81: 8337-8340.
245. Igakura T, Stinchcombe JC, Goon PK, Taylor GP, Weber JN, et al. (2003) Spread of HTLV-I between lymphocytes by virus-induced polarization of the cytoskeleton. Science 299: 1713-1716.
246. McDonald D, Wu L, Bohks SM, KewalRamani VN, Unutmaz D, et al. (2003) Recruitment of HIV and its receptors to dendritic cell-T cell junctions. Science 300: 1295-1297.
247. Groot F, Welsch S, Sattentau QJ (2008) Efficient HIV-1 transmission from macrophages to T cells across transient virological synapses. Blood 111: 4660-4663.
248. Sanderson CM, Way M, Smith GL (1998) Virus-induced cell motility. J Virol 72: 1235-1243.
249. Iwasaki Y, Clark HF (1975) Cell to cell transmission of virus in the central nervous system. II. Experimental rabies in mouse. Lab Invest 33: 391-399.
250. Favoreel HW, Van Minnebruggen G, Adriaensen D, Nauwynck HJ (2005) Cytoskeletal rearrangements and cell extensions induced by the US3 kinase of an alphaherpesvirus are associated with enhanced spread. Proc Natl Acad Sci U S A 102: 8990-8995.
251. Cudmore S, Cossart P, Griffiths G, Way M (1995) Actin-based motility of vaccinia virus. Nature 378: 636-638.
252. Gill MB, Edgar R, May JS, Stevenson PG (2008) A gamma-herpesvirus glycoprotein complex manipulates actin to promote viral spread. PLoS One 3: e1808.
253. Makhortova NR, Askovich P, Patterson CE, Gechman LA, Gerard NP, et al. (2007) Neurokinin-1 enables measles virus trans-synaptic spread in neurons. Virology 362: 235-244.
254. Lawrence DM, Patterson CE, Gales TL, D'Orazio JL, Vaughn MM, et al. (2000) Measles virus spread between neurons requires cell contact but not CD46 expression, syncytium formation, or extracellular virus production. J Virol 74: 1908-1918.
255. McQuaid S, Campbell S, Wallace IJ, Kirk J, Cosby SL (1998) Measles virus infection and replication in undifferentiated and differentiated human neuronal cells in culture. J Virol 72: 5245-5250.
256. Shigeta S, Hinuma Y, Suto T, Ishida N (1968) The cell to cell infection of respiratory syncytial virus in HEp-2 monolayer cultures. J Gen Virol 3: 129-131.

257. Singh BK, Hornick AL, Krishnamurthy S, Locke AC, Mendoza CA, et al. (2015) The Nectin-4/Afadin Protein Complex and Intercellular Membrane Pores Contribute to Rapid Spread of Measles Virus in Primary Human Airway Epithelia. J Virol 89: 7089-7096.
258. Roberts KL, Manicassamy B, Lamb RA (2015) Influenza A virus uses intercellular connections to spread to neighboring cells. J Virol 89: 1537-1549.
259. Carlos TS, Young DF, Schneider M, Simas JP, Randall RE (2009) Parainfluenza virus 5 genomes are located in viral cytoplasmic bodies whilst the virus dismantles the interferon-induced antiviral state of cells. J Gen Virol 90: 2147-2156.
260. Santangelo P, Nitin N, LaConte L, Woolums A, Bao G (2006) Live-cell characterization and analysis of a clinical isolate of bovine respiratory syncytial virus, using molecular beacons. J Virol 80: 682-688.
261. Lindquist ME, Lifland AW, Utley TJ, Santangelo PJ, Crowe JE, Jr. (2010) Respiratory syncytial virus induces host RNA stress granules to facilitate viral replication. J Virol 84: 12274-12284.
262. Ada GL, Perry BT, Edney M (1957) Infectivity of influenza virus filaments. Nature 180: 1134.
263. Gower TL, Pastey MK, Peeples ME, Collins PL, McCurdy LH, et al. (2005) RhoA signaling is required for respiratory syncytial virus-induced syncytium formation and filamentous virion morphology. J Virol 79: 5326-5336.
264. Jumat MR, Nguyen Huong T, Wong P, Loo LH, Tan BH, et al. (2014) Imaging analysis of human metapneumovirus-infected cells provides evidence for the involvement of F-actin and the raft-lipid microdomains in virus morphogenesis. Virol J 11: 198.
265. Tollefson SJ, Cox RG, Williams JV (2010) Studies of culture conditions and environmental stability of human metapneumovirus. Virus Res 151: 54-59.
266. Chu CM, Dawson IM, Elford WJ (1949) Filamentous forms associated with newly isolated influenza virus. Lancet 1: 602.
267. Mosley VM, Wyckoff RW (1946) Election micrography of the virus of influenza. Nature 157: 263.
268. Roberts SR, Compans RW, Wertz GW (1995) Respiratory syncytial virus matures at the apical surfaces of polarized epithelial cells. J Virol 69: 2667-2673.
269. Akhshi TK, Wernike D, Piekny A (2014) Microtubules and actin crosstalk in cell migration and division. Cytoskeleton (Hoboken) 71: 1-23.
270. Taylor MP, Koyuncu OO, Enquist LW (2011) Subversion of the actin cytoskeleton during viral infection. Nat Rev Microbiol 9: 427-439.
271. Sattentau Q (2008) Avoiding the void: cell-to-cell spread of human viruses. Nat Rev Microbiol 6: 815-826.
272. Jeffree CE, Brown G, Aitken J, Su-Yin DY, Tan BH, et al. (2007) Ultrastructural analysis of the interaction between F-actin and respiratory syncytial virus during virus assembly. Virology 369: 309-323.
273. Sholl DA (1953) Dendritic organization in the neurons of the visual and motor cortices of the cat. J Anat 87: 387-406.
274. Gurke S, Barroso JF, Gerdes HH (2008) The art of cellular communication: tunneling nanotubes bridge the divide. Histochem Cell Biol 129: 539-550.

275. Gerdes HH, Rustom A, Wang X (2013) Tunneling nanotubes, an emerging intercellular communication route in development. Mech Dev 130: 381-387.
276. Zani BG, Indolfi L, Edelman ER (2010) Tubular bridges for bronchial epithelial cell migration and communication. PLoS One 5: e8930.
277. Spiering D, Hodgson L (2011) Dynamics of the Rho-family small GTPases in actin regulation and motility. Cell Adh Migr 5: 170-180.
278. Murali A, Rajalingam K (2014) Small Rho GTPases in the control of cell shape and mobility. Cell Mol Life Sci 71: 1703-1721.
279. Sowinski S, Jolly C, Berninghausen O, Purbhoo MA, Chauveau A, et al. (2008) Membrane nanotubes physically connect T cells over long distances presenting a novel route for HIV-1 transmission. Nat Cell Biol 10: 211-219.
280. Schuster JE, Cox RG, Hastings AK, Boyd KL, Wadia J, et al. (2015) A broadly neutralizing human monoclonal antibody exhibits in vivo efficacy against both human metapneumovirus and respiratory syncytial virus. J Infect Dis 211: 216-225.
281. Williams JV, Chen Z, Cseke G, Wright DW, Keefer CJ, et al. (2007) A recombinant human monoclonal antibody to human metapneumovirus fusion protein that neutralizes virus in vitro and is effective therapeutically in vivo. J Virol 81: 8315-8324.
282. Lidholt K, Weinke JL, Kiser CS, Lugemwa FN, Bame KJ, et al. (1992) A single mutation affects both N-acetylglucosaminyltransferase and glucuronosyltransferase activities in a Chinese hamster ovary cell mutant defective in heparan sulfate biosynthesis. Proc Natl Acad Sci U S A 89: 2267-2271.
283. Kingsley DM, Kozarsky KF, Hobbie L, Krieger M (1986) Reversible defects in O-linked glycosylation and LDL receptor expression in a UDP-Gal/UDP-GalNAc 4-epimerase deficient mutant. Cell 44: 749-759.
284. Abounit S, Zurzolo C (2012) Wiring through tunneling nanotubes--from electrical signals to organelle transfer. J Cell Sci 125: 1089-1098.
285. Derdowski A, Peters TR, Glover N, Qian R, Utley TJ, et al. (2008) Human metapneumovirus nucleoprotein and phosphoprotein interact and provide the minimal requirements for inclusion body formation. J Gen Virol 89: 2698-2708.
286. Shaikh M, Mohanty J, Sundararajan M, Bhasikuttan AC, Pal H (2012) Supramolecular host-guest interactions of oxazine-1 dye with beta- and gamma-cyclodextrins: a photophysical and quantum chemical study. J Phys Chem B 116: 12450-12459.
287. Leyrat C, Renner M, Harlos K, Huiskonen JT, Grimes JM (2014) Structure and self-assembly of the calcium binding matrix protein of human metapneumovirus. Structure 22: 136-148.
288. Leyrat C, Renner M, Harlos K, Huiskonen JT, Grimes JM (2013) Structure and Self-Assembly of the Calcium Binding Matrix Protein of Human Metapneumovirus. Structure.
289. Schildgen V, van den Hoogen B, Fouchier R, Tripp RA, Alvarez R, et al. (2011) Human Metapneumovirus: lessons learned over the first decade. Clin Microbiol Rev 24: 734-754.

290. Chen YH, Du W, Hagemeijer MC, Takvorian PM, Pau C, et al. (2015) Phosphatidylserine vesicles enable efficient en bloc transmission of enteroviruses. Cell 160: 619-630.
291. Pais-Correia AM, Sachse M, Guadagnini S, Robbiati V, Lasserre R, et al. (2010) Biofilm-like extracellular viral assemblies mediate HTLV-1 cell-to-cell transmission at virological synapses. Nat Med 16: 83-89.
292. Taylor MP, Kratchmarov R, Enquist LW (2013) Live cell imaging of alphaherpes virus anterograde transport and spread. J Vis Exp.
293. Martinez MG, Snapp EL, Perumal GS, Macaluso FP, Kielian M (2014) Imaging the alphavirus exit pathway. J Virol 88: 6922-6933.
294. Fackler OT, Grosse R (2008) Cell motility through plasma membrane blebbing. J Cell Biol 181: 879-884.
295. Zaoui K, Honore S, Isnardon D, Braguer D, Badache A (2008) Memo-RhoA-mDia1 signaling controls microtubules, the actin network, and adhesion site formation in migrating cells. J Cell Biol 183: 401-408.
296. Esper F, Boucher D, Weibel C, Martinello RA, Kahn JS (2003) Human metapneumovirus infection in the United States: clinical manifestations associated with a newly emerging respiratory infection in children. Pediatrics 111: 1407-1410.
297. Williams JV, Tollefson SJ, Johnson JE, Crowe JE, Jr. (2005) The cotton rat (Sigmodon hispidus) is a permissive small animal model of human metapneumovirus infection, pathogenesis, and protective immunity. J Virol 79: 10944-10951.
298. Kuiken T, van den Hoogen BG, van Riel DA, Laman JD, van Amerongen G, et al. (2004) Experimental human metapneumovirus infection of cynomolgus macaques (Macaca fascicularis) results in virus replication in ciliated epithelial cells and pneumocytes with associated lesions throughout the respiratory tract. Am J Pathol 164: 1893-1900.
299. Hamelin ME, Yim K, Kuhn KH, Cragin RP, Boukhvalova M, et al. (2005) Pathogenesis of human metapneumovirus lung infection in BALB/c mice and cotton rats. J Virol 79: 8894-8903.
300. Alvarez R, Tripp RA (2005) The immune response to human metapneumovirus is associated with aberrant immunity and impaired virus clearance in BALB/c mice. J Virol 79: 5971-5978.
301. Wyde PR, Chetty SN, Jewell AM, Schoonover SL, Piedra PA (2005) Development of a cotton rat-human metapneumovirus (hMPV) model for identifying and evaluating potential hMPV antivirals and vaccines. Antiviral Res 66: 57-66.
302. Mellman I, Nelson WJ (2008) Coordinated protein sorting, targeting and distribution in polarized cells. Nat Rev Mol Cell Biol 9: 833-845.
303. Roche WR, Montefort S, Baker J, Holgate ST (1993) Cell adhesion molecules and the bronchial epithelium. Am Rev Respir Dis 148: S79-82.
304. Maisner A, Klenk H, Herrler G (1998) Polarized budding of measles virus is not determined by viral surface glycoproteins. J Virol 72: 5276-5278.
305. Lamp B, Dietzel E, Kolesnikova L, Sauerhering L, Erbar S, et al. (2013) Nipah virus entry and egress from polarized epithelial cells. J Virol 87: 3143-3154.

306. Tahara M, Takeda M, Shirogane Y, Hashiguchi T, Ohno S, et al. (2008) Measles virus infects both polarized epithelial and immune cells by using distinctive receptor-binding sites on its hemagglutinin. J Virol 82: 4630-4637.
307. Liesman RM, Buchholz UJ, Luongo CL, Yang L, Proia AD, et al. (2014) RSV-encoded NS2 promotes epithelial cell shedding and distal airway obstruction. J Clin Invest 124: 2219-2233.
308. Weise C, Erbar S, Lamp B, Vogt C, Diederich S, et al. (2010) Tyrosine residues in the cytoplasmic domains affect sorting and fusion activity of the Nipah virus glycoproteins in polarized epithelial cells. J Virol 84: 7634-7641.
309. Brock SC, Goldenring JR, Crowe JE, Jr. (2003) Apical recycling systems regulate directional budding of respiratory syncytial virus from polarized epithelial cells. Proc Natl Acad Sci U S A 100: 15143-15148.
310. Naim HY, Ehler E, Billeter MA (2000) Measles virus matrix protein specifies apical virus release and glycoprotein sorting in epithelial cells. EMBO J 19: 3576-3585.
311. Tashiro M, McQueen NL, Seto JT, Klenk HD, Rott R (1996) Involvement of the mutated M protein in altered budding polarity of a pantropic mutant, F1-R, of Sendai virus. J Virol 70: 5990-5997.
312. Samal S, Khattar SK, Paldurai A, Palaniyandi S, Zhu X, et al. (2013) Mutations in the cytoplasmic domain of the Newcastle disease virus fusion protein confer hyperfusogenic phenotypes modulating viral replication and pathogenicity. J Virol 87: 10083-10093.
313. Zhang L, Peeples ME, Boucher RC, Collins PL, Pickles RJ (2002) Respiratory syncytial virus infection of human airway epithelial cells is polarized, specific to ciliated cells, and without obvious cytopathology. J Virol 76: 5654-5666.
314. Zhang L, Collins PL, Lamb RA, Pickles RJ (2011) Comparison of differing cytopathic effects in human airway epithelium of parainfluenza virus 5 (W3A), parainfluenza virus type 3, and respiratory syncytial virus. Virology 421: 67-77.
315. Villenave R, Touzelet O, Thavagnanam S, Sarlang S, Parker J, et al. (2010) Cytopathogenesis of Sendai virus in well-differentiated primary pediatric bronchial epithelial cells. J Virol 84: 11718-11728.
316. Rodriguez-Boulan E, Macara IG (2014) Organization and execution of the epithelial polarity programme. Nat Rev Mol Cell Biol 15: 225-242.
317. Wedlich-Soldner R, Li R (2004) Closing the loops: new insights into the role and regulation of actin during cell polarization. Exp Cell Res 301: 8-15.
318. Chifflet S, Hernandez JA (2012) The plasma membrane potential and the organization of the actin cytoskeleton of epithelial cells. Int J Cell Biol 2012: 121424.
319. Delorme-Axford E, Coyne CB (2011) The actin cytoskeleton as a barrier to virus infection of polarized epithelial cells. Viruses 3: 2462-2477.
320. Rezaee F, DeSando SA, Ivanov AI, Chapman TJ, Knowlden SA, et al. (2013) Sustained protein kinase D activation mediates respiratory syncytial virus-induced airway barrier disruption. J Virol 87: 11088-11095.
321. MacPhail M, Schickli JH, Tang RS, Kaur J, Robinson C, et al. (2004) Identification of small-animal and primate models for evaluation of vaccine candidates for human metapneumovirus (hMPV) and implications for hMPV vaccine design. J Gen Virol 85: 1655-1663.

322. Hamelin ME, Prince GA, Gomez AM, Kinkead R, Boivin G (2006) Human metapneumovirus infection induces long-term pulmonary inflammation associated with airway obstruction and hyperresponsiveness in mice. J Infect Dis 193: 1634-1642.
323. Zhang L, Bukreyev A, Thompson CI, Watson B, Peeples ME, et al. (2005) Infection of ciliated cells by human parainfluenza virus type 3 in an in vitro model of human airway epithelium. J Virol 79: 1113-1124.
324. Thompson CI, Barclay WS, Zambon MC, Pickles RJ (2006) Infection of human airway epithelium by human and avian strains of influenza a virus. J Virol 80: 8060-8068.
325. Shen L, Turner JR (2005) Actin depolymerization disrupts tight junctions via caveolae-mediated endocytosis. Mol Biol Cell 16: 3919-3936.
326. Van Itallie CM, Fanning AS, Bridges A, Anderson JM (2009) ZO-1 stabilizes the tight junction solute barrier through coupling to the perijunctional cytoskeleton. Mol Biol Cell 20: 3930-3940.
327. Talaat KR, Karron RA, Thumar B, McMahon BA, Schmidt AC, et al. (2013) Experimental infection of adults with recombinant wild-type human metapneumovirus. J Infect Dis 208: 1669-1678.
328. Clements ML, Belshe RB, King J, Newman F, Westblom TU, et al. (1991) Evaluation of bovine, cold-adapted human, and wild-type human parainfluenza type 3 viruses in adult volunteers and in chimpanzees. J Clin Microbiol 29: 1175-1182.
329. Lee FE, Walsh EE, Falsey AR, Betts RF, Treanor JJ (2004) Experimental infection of humans with A2 respiratory syncytial virus. Antiviral Res 63: 191-196.
330. Even DL, Henley AM, Geraghty RJ (2006) The requirements for herpes simplex virus type 1 cell-cell spread via nectin-1 parallel those for virus entry. Virus Res 119: 195-207.
331. Coyne CB, Bergelson JM (2006) Virus-induced Abl and Fyn kinase signals permit coxsackievirus entry through epithelial tight junctions. Cell 124: 119-131.
332. King SL, Kamata T, Cunningham JA, Emsley J, Liddington RC, et al. (1997) Echovirus 1 interaction with the human very late antigen-2 (integrin alpha2beta1) I domain. Identification of two independent virus contact sites distinct from the metal ion-dependent adhesion site. J Biol Chem 272: 28518-28522.
333. Schmitt AP, Lamb RA (2004) Escaping from the cell: assembly and budding of negative-strand RNA viruses. Curr Top Microbiol Immunol 283: 145-196.
334. McDermott JE, Shankaran H, Eisfeld AJ, Belisle SE, Neuman G, et al. (2011) Conserved host response to highly pathogenic avian influenza virus infection in human cell culture, mouse and macaque model systems. BMC Syst Biol 5: 190.
335. Leyrat C, Renner M, Harlos K, Grimes JM (2013) Solution and crystallographic structures of the central region of the phosphoprotein from human metapneumovirus. PLoS One 8: e80371.
336. Karlin D, Ferron F, Canard B, Longhi S (2003) Structural disorder and modular organization in Paramyxovirinae N and P. J Gen Virol 84: 3239-3252.
337. Tyrrell DL, Ehrnst A (1979) Transmembrane communication in cells chronically infected with measles virus. J Cell Biol 81: 396-402.

338. Nagai Y (1999) Paramyxovirus replication and pathogenesis. Reverse genetics transforms understanding. Rev Med Virol 9: 83-99.
339. Ding B, Zhang G, Yang X, Zhang S, Chen L, et al. (2014) Phosphoprotein of human parainfluenza virus type 3 blocks autophagosome-lysosome fusion to increase virus production. Cell Host Microbe 15: 564-577.
340. Curran J, Pelet T, Kolakofsky D (1994) An acidic activation-like domain of the Sendai virus P protein is required for RNA synthesis and encapsidation. Virology 202: 875-884.
341. Bowman MC, Smallwood S, Moyer SA (1999) Dissection of individual functions of the Sendai virus phosphoprotein in transcription. J Virol 73: 6474-6483.
342. Ryan KW, Morgan EM, Portner A (1991) Two noncontiguous regions of Sendai virus P protein combine to form a single nucleocapsid binding domain. Virology 180: 126-134.
343. Huber M, Cattaneo R, Spielhofer P, Orvell C, Norrby E, et al. (1991) Measles virus phosphoprotein retains the nucleocapsid protein in the cytoplasm. Virology 185: 299-308.
344. Garcia-Barreno B, Delgado T, Melero JA (1996) Identification of protein regions involved in the interaction of human respiratory syncytial virus phosphoprotein and nucleoprotein: significance for nucleocapsid assembly and formation of cytoplasmic inclusions. J Virol 70: 801-808.
345. Roper RL, Wolffe EJ, Weisberg A, Moss B (1998) The envelope protein encoded by the A33R gene is required for formation of actin-containing microvilli and efficient cell-to-cell spread of vaccinia virus. J Virol 72: 4192-4204.
346. Masante C, El Najjar F, Chang A, Jones A, Moncman CL, et al. (2014) The human metapneumovirus small hydrophobic protein has properties consistent with those of a viroporin and can modulate viral fusogenic activity. J Virol 88: 6423-6433.
347. Wilson RL, Fuentes SM, Wang P, Taddeo EC, Klatt A, et al. (2006) Function of small hydrophobic proteins of paramyxovirus. J Virol 80: 1700-1709.
348. Triantafilou K, Kar S, Vakakis E, Kotecha S, Triantafilou M (2013) Human respiratory syncytial virus viroporin SH: a viral recognition pathway used by the host to signal inflammasome activation. Thorax 68: 66-75.
349. Perez M, Garcia-Barreno B, Melero JA, Carrasco L, Guinea R (1997) Membrane permeability changes induced in Escherichia coli by the SH protein of human respiratory syncytial virus. Virology 235: 342-351.
350. Gan SW, Tan E, Lin X, Yu D, Wang J, et al. (2012) The small hydrophobic protein of the human respiratory syncytial virus forms pentameric ion channels. J Biol Chem 287: 24671-24689.
351. Kochva U, Leonov H, Arkin IT (2003) Modeling the structure of the respiratory syncytial virus small hydrophobic protein by silent-mutation analysis of global searching molecular dynamics. Protein Sci 12: 2668-2674.
352. Gonzalez ME, Carrasco L (2003) Viroporins. FEBS Lett 552: 28-34.
353. de Graaf M, Herfst S, Aarbiou J, Burgers PC, Zaaraoui-Boutahar F, et al. (2013) Small hydrophobic protein of human metapneumovirus does not affect virus replication and host gene expression in vitro. PLoS One 8: e58572.

354. Ishiguro N, Ebihara T, Endo R, Ma X, Kikuta H, et al. (2004) High genetic diversity of the attachment (G) protein of human metapneumovirus. J Clin Microbiol 42: 3406-3414.
355. Bao X, Kolli D, Liu T, Shan Y, Garofalo RP, et al. (2008) Human metapneumovirus small hydrophobic protein inhibits NF-kappaB transcriptional activity. J Virol 82: 8224-8229.
356. Le Nouen C, Hillyer P, Brock LG, Winter CC, Rabin RL, et al. (2014) Human Metapneumovirus SH and G Glycoproteins Inhibit Macropinocytosis-Mediated Entry into Human Dendritic Cells and Reduce CD4+ T Cell Activation. J Virol 88: 6453-6469.
357. van den Hoogen BG, Bestebroer TM, Osterhaus AD, Fouchier RA (2002) Analysis of the genomic sequence of a human metapneumovirus. Virology 295: 119-132.
358. Cox RG, Erickson JJ, Hastings AK, Becker JC, Johnson M, et al. (2014) Human metapneumovirus virus-like particles induce protective B and T cell responses in a mouse model. J Virol 88: 6368-6379.
359. Lamb RA, Mahy BW, Choppin PW (1976) The synthesis of sendai virus polypeptides in infected cells. Virology 69: 116-131.
360. Tyrrell DL, Norrby E (1978) Structural polypeptides of measles virus. J Gen Virol 39: 219-229.
361. Giuffre RM, Tovell DR, Kay CM, Tyrrell DL (1982) Evidence for an interaction between the membrane protein of a paramyxovirus and actin. J Virol 42: 963-968.
362. Bohn W, Rutter G, Hohenberg H, Mannweiler K, Nobis P (1986) Involvement of actin filaments in budding of measles virus: studies on cytoskeletons of infected cells. Virology 149: 91-106.
363. Gosselin-Grenet AS, Marq JB, Abrami L, Garcin D, Roux L (2007) Sendai virus budding in the course of an infection does not require Alix and VPS4A host factors. Virology 365: 101-112.
364. Amorim MJ, Bruce EA, Read EK, Foeglein A, Mahen R, et al. (2011) A Rab11- and microtubule-dependent mechanism for cytoplasmic transport of influenza A virus viral RNA. J Virol 85: 4143-4156.
365. Lapierre LA, Kumar R, Hales CM, Navarre J, Bhartur SG, et al. (2001) Myosin vb is associated with plasma membrane recycling systems. Mol Biol Cell 12: 1843-1857.
366. Hales CM, Vaerman JP, Goldenring JR (2002) Rab11 family interacting protein 2 associates with Myosin Vb and regulates plasma membrane recycling. J Biol Chem 277: 50415-50421.
367. Morales I, Carbajal MA, Bohn S, Holzer D, Kato SE, et al. (2008) The vaccinia virus F11L gene product facilitates cell detachment and promotes migration. Traffic 9: 1283-1298.
368. Valderrama F, Cordeiro JV, Schleich S, Frischknecht F, Way M (2006) Vaccinia virus-induced cell motility requires F11L-mediated inhibition of RhoA signaling. Science 311: 377-381.
369. Alvarez DE, Agaisse H (2013) The formin FHOD1 and the small GTPase Rac1 promote vaccinia virus actin-based motility. J Cell Biol 202: 1075-1090.

370. Lu TC, He JC, Wang ZH, Feng X, Fukumi-Tominaga T, et al. (2008) HIV-1 Nef disrupts the podocyte actin cytoskeleton by interacting with diaphanous interacting protein. J Biol Chem 283: 8173-8182.
371. Goley ED, Ohkawa T, Mancuso J, Woodruff JB, D'Alessio JA, et al. (2006) Dynamic nuclear actin assembly by Arp2/3 complex and a baculovirus WASP-like protein. Science 314: 464-467.
372. Roper JA, Williamson RC, Bass MD (2012) Syndecan and integrin interactomes: large complexes in small spaces. Curr Opin Struct Biol 22: 583-590.
373. Bass MD, Williamson RC, Nunan RD, Humphries JD, Byron A, et al. (2011) A syndecan-4 hair trigger initiates wound healing through caveolin- and RhoG-regulated integrin endocytosis. Dev Cell 21: 681-693.
374. Chang TH, Segovia J, Sabbah A, Mgbemena V, Bose S (2012) Cholesterol-rich lipid rafts are required for release of infectious human respiratory syncytial virus particles. Virology 422: 205-213.
375. Manie SN, de Breyne S, Vincent S, Gerlier D (2000) Measles virus structural components are enriched into lipid raft microdomains: a potential cellular location for virus assembly. J Virol 74: 305-311.
376. Brown G, Aitken J, Rixon HW, Sugrue RJ (2002) Caveolin-1 is incorporated into mature respiratory syncytial virus particles during virus assembly on the surface of virus-infected cells. J Gen Virol 83: 611-621.
377. Jimenez-Baranda S, Gomez-Mouton C, Rojas A, Martinez-Prats L, Mira E, et al. (2007) Filamin-A regulates actin-dependent clustering of HIV receptors. Nat Cell Biol 9: 838-846.
378. Robinson CM, Jesudhasan PR, Pfeiffer JK (2014) Bacterial lipopolysaccharide binding enhances virion stability and promotes environmental fitness of an enteric virus. Cell Host Microbe 15: 36-46.
379. Krummenacher C, Baribaud I, Eisenberg RJ, Cohen GH (2003) Cellular localization of nectin-1 and glycoprotein D during herpes simplex virus infection. J Virol 77: 8985-8999.
380. Ireton K (2013) Molecular mechanisms of cell-cell spread of intracellular bacterial pathogens. Open Biol 3: 130079.

Vita

Farah El Najjar

Education

2003-2007	***American University of Beirut*; Lebanon** B.S. in Medical Laboratory Technology Faculty of Health Sciences American University of Beirut
2007-2010	***American University of Beirut*; Lebanon** M.S. in Biochemistry Thesis: "Regulation of BID by Protein Kinase C and the Inhibitory Role of Ceramide" Graduate Research Advisor: Ghassan Dbaibo, M.D. Department of Biochemistry American University of Beirut
2010-present	***University of Kentucky*; Lexington, KY** Ph.D. candidate in Biochemistry Graduate Research Advisor: Rebecca E. Dutch, Ph.D. Department of Molecular and Cellular Biochemistry University of Kentucky College of Medicine

Awards

2012	American Society for Biochemistry and Molecular Biology Graduate and Postdoctoral Travel Award
2012	Max Steckler Fellowship Award
2013	American Society of Virology Student Travel Award
2014	Graduate School Academic Year Fellowship
2015	FASEB Student Travel Award
2015	FASEB Student Poster Honorary Award
2015	Robert A. Lester Award

Publications

Masante C, **El Najjar F**, Chang A, Jones A, Moncman CL and Dutch RE. The human metapneumovirus small hydrophobic protein has properties consistent with those of a viroporin and can modulate viral fusogenic activity. (J Virol. 2014 Jun;88(11):6423-33). Highlighted by the editors.

El Najjar F, Schmitt AP and Dutch RE. Paramyxovirus glycoprotein incorporation,

assembly and budding: a three way dance for infectious particle production. (Viruses. 2014 Aug 7;6(8):3019-54)

El Najjar F, Lampe L, Baker ML, Wang LF and Dutch RE. Analysis of cathepsin and furin proteolytic enzymes involved in viral fusion protein activation in cells of the bat reservoir host. (*Plos one.* 2015 Feb 23;10(2)e0115736)

El Najjar F, Cifuentes-Muñoz N, Hackett B, Buchholz UJ, Moncman CL and Dutch RE. Human metapneumovirus manipulates the actin cytoskeleton to promote direct cell-to-cell transmission of virus particles. (To be submitted)

Presentations at Scientific Meetings

Oral Presentations:

Proteolytic processing of Hendra virus fusion protein in cells of the bat reservoir host. **El Najjar F**, Lampe L, Baker ML, Wang LF and Dutch RE. (**Southeastern Regional Virology Conference**, Atlanta, Georgia, March 2012).

Analysis of Cathepsin and Furin proteolytic processing of Viral Fusion Proteins in Cells of the Bat Reservoir host. **El Najjar F**, Lampe L, Baker ML, Wang LF and Dutch RE. (**American Society for Virology Meeting**. Pennsylvania, July 2013).

Role of the cytoskeleton in assembly and transmission of human metapneumovirus. **El Najjar F** and Dutch RE. (**Southeastern Regional Virology Conference**, Atlanta, Georgia, April 2014)

Role of the cytoskeleton in assembly and transmission of human metapneumovirus. **El Najjar F** and Dutch RE. (**XVIth International Congress of Virology**. Montreal, Canada, July 2014)

Role of the actin cytoskeleton in human metapneumovirus infection: Insights into particle assembly and transmission. **El Najjar F**, Carole Moncman and Dutch RE. (**Molecular Pathogenesis: Mechanisms of Infectious Disease**. Keystone, Colorado, July 2015)

Poster Presentations:

Proteolytic processing of Hendra virus fusion protein in cells of the bat reservoir host. **El Najjar F**, Lampe L, Baker ML, Wang LF and Dutch RE. (**American Society for Virology Meeting**. Minneapolis, Minnesota, July 2011)

Proteolytic processing of Hendra virus fusion protein in cells of the bat reservoir host. **El Najjar F**, Lampe L, Baker ML, Wang LF and Dutch RE. (**Experimental Biology Conference**, San Diego, California, April 2012)

Analysis of Cathepsin and Furin proteolytic processing of Viral Fusion Proteins in Cells of the Bat Reservoir host. **El Najjar F**, Lampe L, Baker ML, Wang LF and Dutch RE. (**Virus Structure & Assembly Meeting**. Vermont, June 2012)

Temporal analysis of HMPV infection reveals the interplay between viral proteins during the replication cycle. **El Najjar F**, Hackett BA and Dutch RE (**Negative Strand Assembly**

Meeting, Spain, June 2013)

Role of the actin cytoskeleton in human metapneumovirus infection: Insights into particle assembly and transmission. **El Najjar F**, Carole Moncman and Dutch RE. (**Molecular Pathogenesis: Mechanisms of Infectious Disease Meeting**. Keystone, Colorado, July 2015)

Professional Memberships

2013-2014	American Society of Virology
2012-2014	American Heart Association

Mentoring Experience

Rasha Hamra	(graduate rotation student)
Asmaa Hamze	(graduate rotation student)
Hye In Jang	(graduate rotation student)
Andrea Eastes	(undergraduate researcher)
Bushra Manzar	(undergraduate researcher)
David Henson	(MD/PhD rotation student)
Han Ly	(graduate rotation student)

Teaching Experience

2007-2008 ***American University of Beirut*, Lebanon**
Teaching Assistant

Spring 2012 ***University of Kentucky*; Lexington, KY**
Teaching Assistant

Fall 2015 ***University of Kentucky*; Lexington, KY**
Teaching Assistant